Generation of Non Classical States of Light

CARLOS SÁNCHEZ MUÑOZ

Tesis Doctoral

Memoria presentada para optar al grado de
Doctor en Ciencias Físicas

Universidad Autónoma de Madrid

Directores: Dr. Carlos Tejedor de Paz
Dr. Fabrice Pierre Laussy

Tribunal: Dr. Francisco José García Vidal
Dr. Juan José García Ripoll
Dr. Jonathan James Finley
Dr. Diego Porras Torre
Dr. Simone De Liberato

A mis padres.

ABSTRACT

This Thesis is devoted to the theoretical study of non classical features of light that arise from its interaction with matter. Matter (of an atomic, semiconductor or superconductor nature) is here described at the ultimate quantum limit, i.e., as a system that can only occupy a few discrete energy levels, finding its most fundamental representation in the case of the *two-level system*, with only two states available. Light, on the other hand, is described as a single electromagnetic mode—a resonance in an optical cavity—which behaves as a quantum harmonic oscillator. When they are coupled, the strongly nonlinear character of matter is thus translated into the light mode. This Thesis explores some of the consequences of this inheritance in the framework of quantum optics and open quantum systems.

The Jaynes-Cummings model, the most fundamental one in quantum optics, accounts for such a coupling between a single harmonic oscillator and a two-level system. In the limit in which only a few photons are present, many efforts have been dedicated to the observation of a photon being affected by another one due to the mediation of the two-level system, thus realizing the paradigm of photon-photon interaction. On the other hand, the character of the problem changes drastically when the system is taken to the opposite extreme, where the cavity does not contain only a few photos, but a large number of them. In that case, the Jaynes-Cummings model turns into the Mollow description of resonance fluorescence from the dressed two-level system, where the cavity can, in essence, be described as a classical field. In this limit, all the quantum features of the system manifest only in the emission from the two levels, whose energy structure gets strongly modified by the classical field.

The physics of the Jaynes-Cummings and the Mollow model, stand as the two fundamental pillars of quantum optics, describing, in principle, two opposite regimes of the same system. In this Thesis we show that, when these two scenarios are put together, that is, by exciting with an external laser a two-level system which is also coupled to an optical cavity, we can design sources that emit light with unprecedented properties. Namely, we achieve regimes of continuous emission from the cavity mode in which all the light is grouped in N-photon bundles, with N an integer, that can be optically tuned in real-life laboratories. In this configuration, the cavity is harvesting and enhancing the N-photon de-excitation events that otherwise take place in the dressed two-level system with a very small probability, and that are typically greatly outnumbered by 'normal' single-photon events. Through these processes, several photons are emitted with strongly correlated frequencies making these extremely rare events stand out in measurements of coincidences between the detection of photons of different color.

The first part of this Thesis addresses the study of such strong frequency correlations at the two photon level ($N = 2$). It starts with an analysis of the measurement itself: the time and frequency-resolved second-order correlation function. In a joint effort with an experimental group, we demonstrate that, even in classical systems, the map of correlations arising from all the possible combinations of two frequencies reveal non-trivial features. Such features correspond to a counter-intuitive manifestation in color space of the celebrated Hanbury Brown and Twiss effect. When bringing this quantity to the quantum domain we identify the regions of strong correlations in the emission of the dressed two-level system that violate fundamental limits imposed by classical mechanics and local hidden-variable theories. These strong correlations manifest at frequencies that can be put in resonance with a cavity mode, which allows to harvest them and exploit them in the way described before. In the rest of the Thesis, we explore the consequences of doing so, and identify different regimes of N-photon emission not only in the simplest example of a two-level system, but also in a four-level system, the biexciton, dressed by a laser via a two-photon excitation. The inclusion of extra degrees of freedom brought by the later provides another refinement for the theory, with the consequence of a better control and the possibility to generate a wider range of non-classical states, including bundles of photons that are entangled between them.

RESUMEN

El objetivo de la presente Tesis es el estudio teórico de aquellas propiedades no clásicas de la luz que emergen de su interacción con la materia. Aquí la materia está descrita en el límite cuántico, es decir, como un sistema que solo puede ocupar unos pocos niveles discretos de energía, encontrando su representación más fundamental en el caso del *sistema de dos niveles*, con solo dos estados disponibles. La luz, por otra parte, es descrita como un único modo electromagnético—una resonancia en una cavidad óptica—que se comporta como un oscilador armónico cuántico. Cuando ambos se acoplan, el caracter fuertemente no lineal de la materia es transladado al modo de luz. Esta Tesis explora algunas de las consecuencias de esta herencia, dentro del marco teórico de la óptica cuántica en sistemas abiertos.

El modelo Jaynes-Cummings, el más fundamental en óptica cuántica, describe tal acoplo entre un único oscilador armónico y un sistema de dos niveles. Muchos trabajos se han enfocado en observar, en el límite en el que solo unos pocos fotones están presentes, a un fotón siendo afectado por otro debido a la mediación del sistema de dos niveles, haciendo así realidad el paradigma de la interacción fotón-fotón. Por otro lado, el carácter del problema cambia drásticamente cuando el sistema es llevado al extremo opuesto, donde la cavidad no contiene unos pocos fotones, sino un número elevado de ellos. En ese caso, el modelo de Jaynes-Cummings se transforma en la descripción de Mollow de un 'átomo vestido', donde la cavidad puede, esencialmente, ser descrita como un camplo clásico. En este límite, todas las características cuánticas del sistema se manifiestan únicamente en la emisión del sistema de dos-niveles, cuya estructura energética se ve fuertemente modificada por el campo clásico.

La física del modelo Jaynes-Cummings con pocas excitaciones y la física de Mollow del átomo vestido se alzan como los dos pilares fundamendantales de la óptica cuántica, mientras son considerados límites opuestos del mismo sistema. En esta Tesis demostramos que, cuando juntamos estos dos escenarios, podemos diseñar fuentes de luz con propiedades sin precedentes. En concreto, describimos regímenes de emisión continua en los que toda la luz está agrupada en paquetes de N fotones, donde N es un entero que puede ser ajustado ópticamente cambiando parámetros que están bajo control en el laboratorio. La combinación de ambos escenarios puede llevarse a cabo, por ejemplo, excitando con un Íáser externo al sistema de dos niveles acoplado con una cavidad óptica. Curiosamente, la física del problema se encuentra en realidad en la dinámica del átomo de Mollow vestido por el láser. El papel de la cavidad, en este caso, está recopilando las fuertes correlaciones cuánticas ya presentes en el átomo vestido.

Estas fuertes correlationes tienen su origen en eventos de de-excitationes de dos fotones que tienen lugar en el átomo vestido con una pequeña proba-

bilidad, siendo vastamente superados por eventos de un solo fotón. Sin embargo, en aquellas ocasiones excepcionales en las que estos procesos tienen lugar, varios fotones son emitidos con frecuencias fuertemente correlacionadas. Esto hace que estos eventos de extrema rareza sobresalgan en medidas de coincidencias entre detecciones de fotones de distinto color.

La primera parte de esta Tesis se centra en el estudio de estas correlaciones entre frecuencias. Comienza con un análisis de la magnitud en si misma: la función de correlación de segundo orden resuelta en frecuencias. En un esfuerzo conjunto con un grupo experimental, hemos demostrado que, incluso en un sistema clásico, el mapa de correlaciones que se revela al considerar todas las posibles combinaciones de dos frecuencias tiene características no triviales. Dichas características se corresponden con una manifestación en el espacio de colores del conocido efecto de Hanbury Brown y Twiss.

Al llevar esta magnitud al dominio cuántico, idenfiticamos regiones de fuertes correlaciones en la emisión del sistema de dos niveles vestido que violan límites fundamentales impuestos por la mecánica clásica y las teorías locales de variables ocultas. Estas fuertes correlaciones se manifiestan a frecuencias que pueden ser puestas en resonancia con una cavidad, permitiendo que ésta recopile y explote estas correlaciones del modo que hemos descrito anteriormente. En el resto de la Tesis, exploramos las consecuencias de hacer esto, e idenfiticamos distintos regímenes de emisión de N fotones, no solo en el caso más simple de un sistema de dos niveles, sino también para un sistema de cuatro niveles, el biexcitón, vestido por un laser mediante la resonancia de dos fotones. La inclusión de nuevos grados de libertad por parte del biexcitón trae nuevos refinamientos a la teoría, con la consecuencia de un control más fino y la posibilidad de generar un rango mayor de estados no clásicos, incluyendo paquetes de fotones entralazados entre sí.

CONTENTS

ACRONYMS

HBT	Hanbury Brown and Twiss
2LS	Two-level system
HO	Harmonic Oscillator
QD	Quantum Dot
JC	Jaynes-Cummings
QED	Quantum Electrodynamics
cQED	Cavity Quantum Electrodynamics

1 INTRODUCTION

For the rest of my life I will reflect on what light is.
— Albert Einstein

1.1 MOTIVATION

On his celebrated television series *Cosmos: A Personal Voyage*, Carl Sagan famously noted:

"We are the way of the Cosmos to know itself".

Should we be considered the Universe understanding itself, *light* shall definitely be regarded as the medium it uses to do so.

378,000 years after the Big Bang, the Universe cooled enough for electrons and nuclei to recombine into neutral atoms and become transparent, allowing photons, no longer trapped in a cloud of plasma, to escape towards the Cosmos. Hundreds of millions of years later, the first stars began to glow, adding a myriad of photons to the primordial background of radiation. Ever since, these photons have permeated the Universe, travelling in straight lines with the remarkably property of not affecting each other.

Such an army of criss-crossing photons reflecting in every possible object at the maximum speed allowed in the Universe was an invaluable source of information for those blind organisms that had to make physical contact with an object in order to know that it was there. From some small patch of light-sensitive pigments, more than forty independent times did light motivate the evolution of the eye [57]; an organ so sophisticated as to make Darwin himself believe that the idea of its formation by natural selection was *"absurd in the highest possible degree"*.

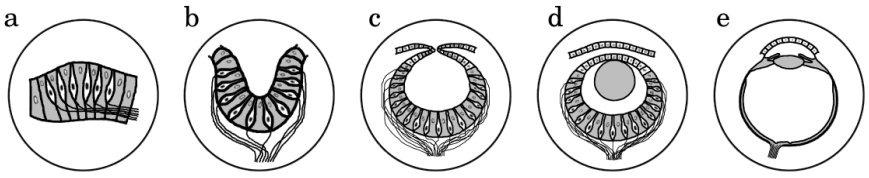

Figure 1.1: Principal stages in the evolution of the eye. a, Region of photosensive cells. **b**, Folded area for limited directional sensitivity. **c**, 'Pinhole' for finer directional sensitivity and limited imaging. **d**, Lens development. **e**, Iris and separate cornea development. Source: Wikimedia Commons.

Even after the development of the eye, light has continued assisting our particular evolution towards a higher understanding of the Universe. From those initial seeing organisms, to the first sailors guided by the Sun and the stars, light has provided us with a door to the unknown, culminating in its star role in the three last revolutions of Science: Maxwell's unification of electricity and magnetism; Einstein's special relativity; and quantum mechanics, the theory upon which this Thesis is built.

Figure 1.2: Guided by polarization. Medieval Icelandic texts mention that Viking sailors used a 'sunstone' to aid them in the navigation. It has been speculated that Vikings could have taken advantage of the *polarization* of light by making use of an Iceland spar, a natural light polariser that can be used to locate the sun in the sky in cloudy conditions [106]. Painting: *Summer in the Greenland Coast Crca Year 1000* by Jens Erik Carl Rasmussen.

Quantum mechanics was born with the problem of the ultraviolet catastrophe regarding the emission of a black body. The solution found by Planck, who assumed that energy was quantized, led Einstein to realize that light must indeed composed by particles, that we now call photons, which he introduced to account for the photoelectric effect. Photons are the elementary excitations of the electromagnetic field, in the same sense that electrons are elementary excitations of the electron field. In our current understanding of the Universe, given by quantum field theory, such fields permeate all space and are the basic substratum of reality. Our ultimate understanding of light is given by quantum electrodynamics (QED), the relativistic quantum field theory of the interaction between light and matter. This model stands as the most successful theory in History, with predictions such as the anomalous magnetic moment of the electron, measured to an outstanding precision of 11 significant figures.

While Einstein was right about the existence of photons, the **photoelectric effect** can actually be explained only with the quantization of matter only.

The new knowledge of the world brought by the theory of quantum mechanics led to very significant technological developments, such as the transistor, which is the basic component of our modern electronic technology, or the laser, with a wide range applications ranging from metrology to medicine. Nevertheless, while the working principles of the laser are quantum mechanical in nature, the light of a laser itself its not quantum, in the sense that it can perfectly be understood with Maxwell's theory of electromagnetism.

However, states of light exists that are, in essence, quantum mechanical. This has implications that could have never been envisaged in Maxwell's era, with light providing us, once again, with new, unprecedented ways to view the world and interact with it. The technological developments of the last decades make it possible to devise systems in which light and matter coexist at the ultimate quantum limit, opening exciting avenues both in the exploration of fundamental phenomena and in the design of new quantum technologies.

This Thesis is devoted to the theoretical study of systems in which the most basic building block of light, the photon, interacts with

1.2 THE DAWN OF QUANTUM TECHNOLOGIES

Due to its inherently probabilistic nature, quantum physics was at its birth a theory difficult to accept by many of the physicists of the time. Even those responsible of its development, like Planck or Einstein, did not seem ready to assimilate the implications of their own discoveries, with a reluctance commonly summarized by Einstein's words: *"God does not play dice with the Universe"*. Still today, the postulates of quantum mechanics are object of discussion, as illustrated by the ongoing debate on the meaning and interpretation of the collapse of the wavefunction [187].

Nevertheless, the quantum trauma is now long gone, and scientist have realized that, behind the apparent uncertainty of quantum mechanics, not only a world of beautiful theories and extremely precise predictions exists, but also a plethora of opportunities to be exploited. The aim of *quantum technologies* is to harness and put the exotic properties of quantum states, such as quantum superposition of states or entanglement, to use.

A prominent example is *quantum information* [173], a discipline based on the paradigm of the *qubit*, the quantum analogue of the minimum unit of information in classical physics, the bit. Contrary to its classical counterpart, the qubit can not only be in one of the two states associated to 0 and 1, but in any possible quantum superposition of them.

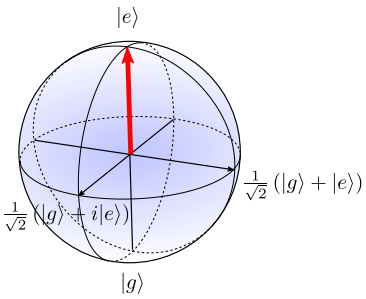

Figure 1.3: A qubit, the minimal unit of information in quantum physics. A two-level system consisting in the states $|g\rangle$ (the 0) and $|e\rangle$ (the 1), can also be in any arbitrary superposition of the two, represented as a point in the *Bloch sphere*.

With already commercial applications available such as quantum key distribution systems [90], the Holy Grail of quantum information science is the *quantum computer* [173], a device able to exploit the massive parallelization power of a quantum superpositions of qubits in order to realize calculations impossible to achieve with current technology, such as fast factorization of numbers, powerful database searching or simulation of complex quantum systems.

The photon is a privileged candidate to perform as a qubit, since this information can be encoded in many degrees of freedom such as polarization, frequency, spatial mode or time. Moreover, the maximum transmission speed offered by photons and their low noise properties make them an ideal resource in *quantum communication* [91], acting as channels that transfer information (in form of qubits) between nodes that may consist on material qubits [122]. In general, photons have been a favourite testbed for the most fundamental quantum mechanical phenomena, featuring for instance the first demonstration of entanglement [18, 83], and their quantum state can

be employed in other quantum technologies such as *quantum metrology* or *quantum lithography*. Both disciplines aim to exploit quantum correlations to perform measurements and resolve features beyond conventional bounds of precision [89]. Some of these limits are the *shot-noise*, unavoidable fluctuations in the amplitude of the electric field associated to its particle nature, or more generally, the *standard quantum limit* (SQL), a fundamental imprecision in the measurement of an observable $\mathcal{O}$ associated to the back-action perturbation associated to Heisenberg uncertainty principle:

$$\Delta\mathcal{O}\Delta\mathcal{F} \geq \hbar/2\,, \tag{1}$$

where $\mathcal{F}$ is the conjugate of $\mathcal{O}$. The shot-noise limit is then a particular case of the SQL. For instance, this can be achieved by the use of *squeezed states* [87], in which the quantum fluctuations in phase space are reduced in one direction (related to the variable chosen for the measurement) at the cost of being increased in the perpendicular one. These states have been generated in the laboratory by means of the nonlinear process of *spontaneous parametric down-conversion* (SPDC) [182], and have been used to achieved the best broadband sensitivity at LIGO [1], the observatory responsible for the recent detection of gravitational waves [2] .

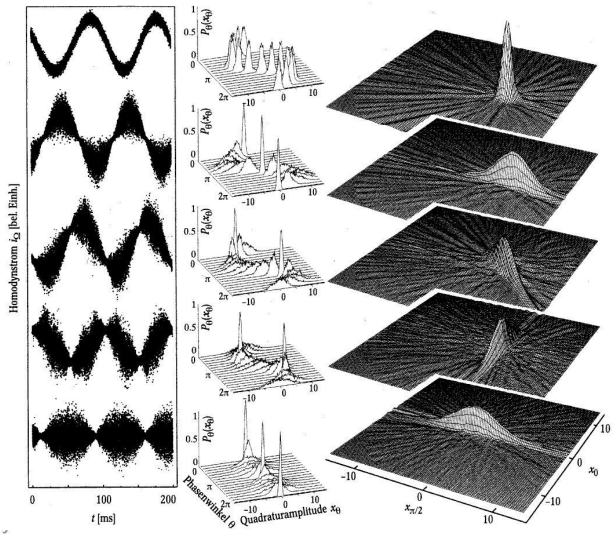

Figure 1.4: Squeezed states of light. In light, the canonical conjugate variables x and p correspond to the field 'quadratures': in-phase and out-of-phase amplitudes of the electromagnetic field. Here, the top panel features a coherent states: the most classical quantum objects, with the minimum possible uncertainty imposed by the Heisenberg limit, similar for both quadratures. The rest of the cases depict different squeezed states, where the fluctuations in on quadrature are reduced at the expense of increased fluctuations in its conjugate. Source: Wikimedia Commons.

A related approach to achieve enhanced sensitivity is the use of entangled states [89]. An important example is the case of NOON states, entangled two-modes states of N photons in a superposition where all photons are in either one mode or the other:

$$|\text{NOON}\rangle = \frac{1}{\sqrt{2}}\left(|N,0\rangle + |0,N\rangle\right)\,. \tag{2}$$

A **Mach-Zehnder interferometer** determines the relative phase change between two beams originating same source.

When these two modes correspond to the two input arms of a Mach-Zehnder interferometer, phase changes ϕ can be determined with a precision $\Delta\phi \geq 1/N$, which offers a $\sqrt{N}$ enhancement over the SQL, $\Delta\phi \geq 1/\sqrt{N}$.

These states have been generated by mixing coherent beams with light emitted from SPDC [4], and have already provided phase supersensitivity beyond the SQL in a quantum polarized microscope [117].

NONLINEARITIES AT THE SINGLE PHOTON LEVEL All the applications outlined above require some sort of interaction between the photons that has to be enabled by nonlinear optical processes [46]. The current goal is to bring these interactions to the limit in which the presence of one photon alters significantly the propagation of another one, which is a challenging task due to the small nonlinear response of light in the limit of individual photons [46, 178]. The effort, however, is worth it, since it would allow the implementation of technologies such as optical transistors with no Ohmic heating [164], logical gates between photonic qubits, protocols of quantum non-demolition measurement [177], single-photon nonlinear switches [122], or, what is the topic of this thesis, generate non-classical states of light. All the types of non-classical states that can be generated, such as squeezed states, Schrödinger kittens [54], entangled photon-pairs [84, 124, 143], or Fock states [39, 47, 55, 97, 201], share the common property of not accepting a classical interpretation, and their applications range from its said use in metrology and lithography, to its potential for quantum spectroscopy [43, 86], bioimaging of living tissues [107, 159, 242] or the direct imprinting of pure states into optical targets [42–44, 53]. Single-photon Fock states $|1\rangle$ stand out as the essential ingredient of many of these future quantum technologies [6, 44, 178]. In 2001, it was even demonstrated that scalable quantum computing is possible without any nonlinearity, just with by using optical linear elements and single photon sources [137]. The non-linearity is, of course, necessary for the generation of single photons.

Fock states $|N\rangle$ are states with a perfectly well defined number of particles.

The standard approach to overcome the problem of small nonlinear interaction at the single photon level is to interface *quantum emitters*, material dipoles with a discrete set of energy levels, to optical cavities, which are, in essence, two mirror confining light between them.

1.3 SEMICONDUCTOR CAVITY QED

Nowadays, many platforms exists that are able to implement the fundamental paradigm of the Jaynes-Cummings model [120], which the interaction between a single electromagnetic mode and a two-level system. This model is one of the pillars of quantum optics and, by extension, of the present Thesis; detailed discussions about it can be found in Section 2.2 and Chapter 5.

In the microwave regime, an architecture that has demonstrated outstanding capability to explore regimes of light matter interaction are superconducting circuits [114, 240]. In the optical domain, one approach is to use atoms trapped inside inside high-finesse optical cavities [29, 139, 141] or, in the solid state, to employ semiconductor 'artificial atoms' known as *quantum dots* and heterostructures able to confine light. This thesis is a theoretical work based on fundamental models that can be implemented in any of

these configurations, which at our level of description only corresponds to changing the parameters of the model. Nevertheless, we will consider with particular interest the case of semiconductor solid-state systems, due to its promising prospects of developing of on-chip, scalable architectures [80, 178, 194, 208]. For this reason, we offer on the following a short introduction to the physical systems that implement, in the solid state, the theoretical models that we use in the rest of this Thesis.

1.3.1 SEMICONDUCTOR QUANTUM DOTS: SINGLE PHOTON SOURCES

Quantum dots (QDs) stand out as a very promising option for the implementation of scalable, on chip architectures for photonic quantum technologies [154, 178]. QDs are 0-dimensional semiconductor structures in which the motion of charge carriers is strongly confined to regions of a nanometric size. Confinement is achieved by the modulation of the conduction and valence bands of the semiconductor, what is done by embedding the QD within a semiconductor matrix, for instance, In(Ga)As on GaAs. The QD host quasiparticles consisting on electron-hole pairs bounded by Coulomb interaction, which are known as excitons. Excitons have a discrete set of energy levels arising from the confinement potential and Coulomb interaction, which is why QDs are regarded as artificial atoms. Despite they suffer from strong dephasing mechanisms as compared to real atoms, they pose an important advantage with respect to them: their position is fixed in space. Moreover, the controlled manipulation of the structure of the surrounding material allows to embed the QDs in a field-effect device, or, as is the case of interest in this Thesis, in an optical microcavity, c.f. Fig. 1.5 a.

The **exciton** is a quasiparticle that formed from the hydrogen-like bound state of a conduction-band electrond and a valence band-hole.

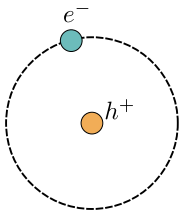

Commonly employed methods to grow semiconductor QDs are based on self-assembled growth, the Stranski-Krastanow (SK) being the most used [154]. Strain due to crystal mismatch between substrate and deposition materials gives rise to nucleation of three dimensional islands on top of a flat film known as *wetting layer* (WL). To provide confinement, quantum dots must be overgrown in a process known as *capping*. The strong changes on the morphology of the QD that take place during this process can be used to

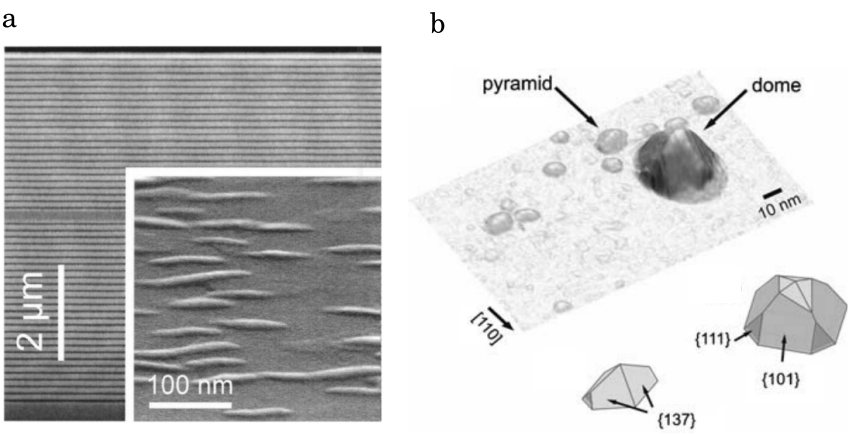

Figure 1.5: Experimental imaging of semiconductor QDs. a, $Ga_{0.7}In_{0.3}As$ quantum dots embedded in a microcavity (the inset shows a surface image of the uncapped QDs [155]. **b**, STM image showing the two kind of islands that usually appear in Stranski-Krastanow samples: pyramid and domes [136].

tune the emission properties of the QD. For instance, partial capping and annealing (PCA) processes [144], whose effect is to reduce the height of the QD, are used to blue-shift the emission from the QD.

The nonlinear, discrete energy structure of QDs allows them to act as a *two-level system*. One of the most promising prospects for QD is their performance as deterministic single photons emitters. However, although they provide excellent suppression of multi-photon emission, they emit in random directions and suffer a strong dephasing due to the interaction with the phonons, spoiling their indistinguishability [178]. As we discuss in the next Section, these problems are solved by embedding the QD in a microcavity.

1.3.2 OPTICAL MICROCAVITIES

Optical microcavities are structures able to confine an electromagnetic field in the range of the micrometers. A typical strategy used for this aim is to artificially design samples with a periodic index of refraction, yielding a band structure for light inside the material similar to the one typically studied for electrons in solids. Namely, these bands feature *bandgaps* of forbidden energies: photons of those energies impinging the material are unable to penetrate it, in a destructive interference process known as *Bragg reflection*. A defect in this periodic structure will create an *edge state* inside the gap: inside the defect, photons of the forbidden energy can live, unable to go into the bulk due to the unavailable density of states. This is the working principle behind the planar heterostructures typically used in semiconductors, in which slabs of different materials, such as gallium arsenide (GaAs) together with aluminium arsenide (AlAs), are alternated creating a pillar structure called 'distributed Bragg mirror' [115, 155, 215]. Placing these mirror one in front of each other creates a microcavity (the space inside acting as the defect mentioned earlier). Besides pillars, many other cavity structures exist, such as the already mentioned photonic crystals [108, 132, 140], nanobeam cavities [179] or microdisk cavities [13, 217]

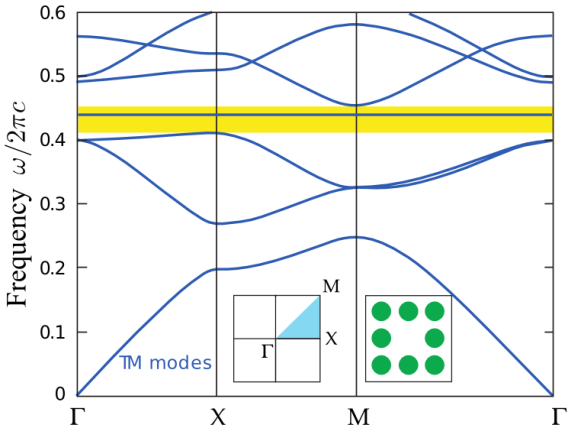

Figure 1.6: Band structure of a photonic crystal. The periodic pattern creates a band structure with a forbidden region (yellow). The inclusion of a defect (removal of a hole) creates an edge state inside the gap, corresponding to photons that resonate inside the defect and are unable to be transmitted to the bulk. Image adapted from [123].

When a quantum emitter such a QD is embedded within an optical cavity, the later alters the density of final states available for the QD to emit into. In the weak coupling regime, this affects its lifetime in accordance with Fermi's Second Golden Rule. The decrease in the lifetime of the QD due to the decay trough the cavity channel its known as *Purcell enhancement* of the emission or *Purcell effect*. The lifetime of the QD in the absence of the cavity is given by the inverse rate of the decay rate toward the vacuum or the bulk, $\tau_\sigma = \gamma_\sigma^{-1}$. The presence of the cavity decreases this lifetime by adding another decay channel with a *Purcell decay rate* κ,

Despite bearing the name of Enrico Fermi, **Fermi's Golden rule** was developed by Paul Dirac. It gaves the transition rate Γ from a initial state $|i\rangle$ to a final state $|f\rangle$: $\Gamma = \frac{2\pi}{\hbar}\rho|\langle|H|f\rangle|^2$

$$\tau_\sigma = (\gamma_\sigma + \kappa)^{-1} \tag{3}$$

which is given by:

$$\kappa = \frac{4g^2}{\gamma_a} \tag{4}$$

where γ_a is the decay rate of the cavity itself, and g the QD-cavity coupling rate (see Chapter 2). This process yields a better emission in terms of brightness, redirection of the light and indistinguishability, already showing impressing figures of merit in the solid state [215].

When $g \geq |\gamma_a - \gamma_\sigma|/4$, the coupling between light and matter is so strong as to allow light to be absorbed and re emitted several times before it is finally lost trough the imperfect mirrors. The regime of *strong coupling* is then reached; photons and material excitations do not behave as independent entities anymore, and new quasiparticles mixture of light and matter, the *polaritons*, emerge.

1.4 SUMMARY OF CONTENTS

This Thesis is structured as follows.

In Chapter 2, we provide a background of the theoretical concepts necessary to understand the rest of the Thesis. We introduce the quantization of the electromagnetic field and the interaction with matter, and discuss the physics of open quantum systems from the perspectives of both the Heisenberg and the Schrodinger equations of motion. The later yields the expression for the master equation, the central dynamical equation of this Thesis, which describes the evolution of the reduced density matrix of the system after the elimination of the degrees of freedom of the environment.

Chapter 3 discuss the generalization of the Hanbury Brow Twiss effect to the full color domain. We report results from a pioneering experiment performed at the group of Daniele Sanvitto at CNR NANOTEC, Lecce, based on a novel streak camera setup. These experimental results are described by a classical theory of an amplitude-stabilized, phase-diffusing field, and by two quantum theories: spontaneous emission from an initial state and emission from a steady-state of a two-mode condensation model. The theoretical results prove that the features observed are a fundamental behaviour of photons due to their bosonic nature, and complete the picture of the Hanbury

Brow Twiss effect by extending it to the full color space. The results of this Chapter have been accepted for publication in Scientific Reports [210].

Chapter 4 we introduce the model of two-level system strongly dressed by a laser (the Mollow regime) and analyse the the frequency-resolved correlations of photons emitted by it. We express this correlations in terms of their deviation from the boundaries imposed by the Cauchy-Schwarz inequality and Bell's inequalities. By doing so, we show that the emission with the strongest quantum character (deviating the most from the predicted classical expectations) is the one that takes place at frequencies further from real, single-photon transitions.

Chapter 5 introduces in detail the physics of the Jaynes-Cummings Hamiltonian, which describes the coupling between a cavity and a two-level system, and its extrapolation to dissipative systems. We discuss the main approaches that can be taken in order to evidence the nonlinear nature of the Jaynes Cummings ladder in observables of the light emitted by the cavity, showing that, in particular, photon statistics is extremely sensitive to the mechanism of excitation. We discuss a series of counter-intuitive resonances appearing in the statistics when the two-level system is excited directly, and show that N-photon Rabi oscillations can be achieved by tuning the laser at those precise energies.

Chapter 6 describe the dynamics of a two-level system strongly driven by a external laser and coupled to a cavity. We derive analytical expressions of effective Hamiltonian that show that N-photon coupling can be achieved between the dressed- atom and the cavity. We prove that this mechanism is associated with a regime of emission of N-photon bundles, and study in which situations it is more efficient than off-resonant, single photons mechanisms that spoil the emission. We introduce a novel quantity, the *purity* of N-photon emission, that characterizes the performance of an N-photon emitter by quantifying the percentage of light that is emitted in form of N-photon bundles, and show that it can be highly increased by filtering the emitted light. Finally, we introduce quantities that generalize the standard observables used in quantum optics to the study of the bundles of N-photons, showing that, when these bundles are regarded as the basic constituent of light in regimes of pure N-photon emission, behaviours such as antibunching are revealed.

In Chapter 7, we take the results of Chapter 6 to the next level by introducing a more complex emitter: the biexciton. We analyse the frequency-resolved correlation maps to identify different scenarios of two-photon emission, and show that these maps are dependent on the polarization of the photons, existing photons strongly correlated in frequency, only when they have opposed polarizations. This allows us to devise continuous sources of states of light entangled in polarization and frequency.

2 THEORETICAL BACKGROUND

Wisdom begins in wonder.

— Socrates

James Clerk **Maxwell** (1831-1879), born in Edinburgh, Scotland, established the foundations of classical electromagnetism, bringing together the concepts of electricity, magnetism and light. In Einstein's words, Maxwell's work was the "most profound and the most fruitful that physics has experienced since the time of Newton".

2.1 QUANTIZATION OF THE FREE ELECTROMAGNETIC FIELD

The first step for our description of light-matter interaction at the quantum limit will be the quantization of the free electromagnetic field. Here, we will outline the key elements of this procedure; a detailed derivation can be found in many textbooks on quantum optics [87, 99, 157, 229].

Maxwell's equations of motion for electromagnetic fields read, in the SI convention:

$$\nabla \mathbf{E} = \frac{1}{\varepsilon_0}\rho\,, \quad \text{(Gauss's law)} \tag{5a}$$

$$\nabla \times \mathbf{E} = -\frac{\partial \mathbf{B}}{\partial t}\,, \quad \text{(Faraday's law of induction)} \tag{5b}$$

$$\nabla \mathbf{B} = 0\,, \quad \text{(Gauss's law for the magnetic field)} \tag{5c}$$

$$\nabla \times \mathbf{B} = \mu_0 \mathbf{j} + \mu_0 \varepsilon_0 \frac{\partial \mathbf{E}}{\partial t}\,, \quad \text{(Ampère's circuital law)} \tag{5d}$$

where ρ is the electric charge density, $\mathbf{j}$ is the current density, ε_0 is vacuum permittivity and μ_0 is the magnetic constant. Note that, for notational convenience, we write the scalar product of vectors as $\mathbf{ab}$ and the vector product, as $\mathbf{a} \times \mathbf{b}$, and we omit explicit spatial and time dependence of the vectors, i.e., $\mathbf{E} \equiv \mathbf{E}(\mathbf{r}, t)$. We can express the *electric* and *magnetic field strengths*, $\mathbf{E}$ and $\mathbf{B}$, in terms of the *vector potential* $\mathbf{A}$ and the *scalar potential*, V:

$$\mathbf{E} = -\frac{\partial \mathbf{A}}{\partial t} - \nabla V, \qquad \mathbf{B} = \nabla \times \mathbf{A}\,. \tag{6}$$

By doing so, Maxwell's equations (5c) and (5d) are automatically fulfilled. Inserting Eq. (6) into Eqs. (5a) and (5b) yields:

$$\nabla(\nabla \mathbf{A}) - \nabla^2 \mathbf{A} + \frac{1}{c^2}\frac{\partial^2 \mathbf{A}}{\partial t^2} + \frac{1}{c^2}\nabla \frac{\partial V}{\partial t} = \mu_0 \mathbf{j}\,, \tag{7a}$$

$$-\varepsilon_0 \left(\nabla^2 V + \nabla \frac{\partial \mathbf{A}}{\partial t} \right) = \rho\,, \tag{7b}$$

with c the speed of light:

$$c = (\varepsilon_0 \mu_0)^{-1/2}\,, \tag{8}$$

and where we made use of the vector identity:

$$\nabla \times \nabla \mathbf{A} = \nabla(\nabla \mathbf{A}) - \nabla^2 \mathbf{A}\,. \tag{9}$$

The **vacuum permittivity** ε_0 and the **magnetic constant** or **vacuum permeability** μ_0 describe the capability of vacuum to sustain within itself an electric and a magnetic field, respectively. Their values are:

$\mu_0 = 4\pi \times 10^{-7}\,\mathrm{N\,A^{-2}}$,
$\varepsilon = 1/(\mu_0 c^2)$,
where c is the speed of light:

$c = 299\,792\,458\,\mathrm{m\,s^{-1}}$

GAUGE TRANSFORMATIONS. THE COULOMB GAUGE. The solution of these equations is simplified if we impose an additional condition on the potentials. This can be done, since $\mathbf{A}$ and V are not unique: Eq. (6) is the same for any pair of potentials $(\mathbf{A}, V)$ and $(\mathbf{A}', V')$ related by the following *gauge transformation*:

$$\mathbf{A}' = \mathbf{A} + \nabla\chi, \qquad V' = V - \frac{\partial\chi}{\partial t}, \tag{10}$$

with $\chi(\mathbf{r}, t)$ an arbitrary function of space and time. This freedom allows us to specify the following condition for the vector potential, known as the *Coulomb gauge*:

$$\nabla\mathbf{A} = 0. \tag{11}$$

This choice simplifies equations (7a) and (7b), that become:

$$\nabla^2\mathbf{A} - \frac{1}{c^2}\frac{\partial^2\mathbf{A}}{\partial t^2} = -\mu_0\mathbf{j} - \frac{1}{c^2}\nabla\frac{\partial V}{\partial t}, \tag{12a}$$

$$-\nabla^2 V = \rho/\varepsilon_0. \tag{12b}$$

Under this gauge, the scalar potential V is just the instantaneous Coulomb potential of the charged particles, since it satisfies Poisson's equation of electrostatics, Eq. (12b).

Now, according to Helmholtz's theorem, we can write the vector field $\mathbf{j}$ as a sum of a *transverse* component $\mathbf{j}_\mathrm{T}$, with zero divergence, and *longitudinal* component $\mathbf{j}_\mathrm{L}$, with zero curl:

$$\mathbf{j} = \mathbf{j}_\mathrm{T} + \mathbf{j}_\mathrm{L}, \tag{13a}$$

$$\nabla\mathbf{j}_\mathrm{T} = 0, \tag{13b}$$

$$\nabla \times \mathbf{j}L = 0. \tag{13c}$$

As $\mathbf{A}$ is transverse by definition of the Coulomb gauge (11), and $\nabla\partial V/\partial t$ is longitudinal since the curl of a gradient must be zero, we can separate Eq. (12a) into transverse and longitudinal parts:

$$\nabla^2\mathbf{A} - \frac{1}{c^2}\frac{\partial^2\mathbf{A}}{\partial t^2} = -\mu_0\mathbf{j}_\mathrm{T}, \tag{14a}$$

$$\frac{1}{c^2}\nabla\frac{\partial V}{\partial t} = \mu_0\mathbf{j}_\mathrm{L}. \tag{14b}$$

In the same way, the electric field can be divided into transverse and longitudinal components, which in this gauge are given by:

$$\mathbf{E}_\mathrm{T} = -\frac{\partial\mathbf{A}}{\partial t}, \tag{15a}$$

$$\mathbf{E}_\mathrm{L} = -\nabla V. \tag{15b}$$

One of the main advantages of the Coulomb gauge is this clear separation of Maxwell's equations into two distinct sets:

i Transverse equations that describe electromagnetic waves, influenced by transverse currents.

ii Longitudinal equations that arise from charge densities, describing the instantaneous change of the electrostatic potential when the charges move.

THE FREE CLASSICAL FIELD We consider now the case of electromagnetic waves in a region free of any charges, which leads to a wave equation for the vector potential:

$$\nabla^2 \mathbf{A} - \frac{1}{c^2}\frac{\partial^2 \mathbf{A}}{\partial t^2} = 0\,. \tag{16}$$

In order to work with a discrete set of variables, we will confine the electromagnetic field within a square box of finite size $L = V^{1/3}$, that can be taken arbitrarily large. By taking periodic boundary conditions, we can write a formal solution of the equation in terms of normal modes:

$$\mathbf{A}(\mathbf{r},t) = \sum_{\mathbf{k}} \sum_{\lambda=1,2} \mathbf{e}_{\mathbf{k},\lambda} \left[A_{\mathbf{k},\lambda} e^{-i\omega_k t + i\mathbf{kr}} + A^*_{\mathbf{k},\lambda} e^{i\omega_k t - i\mathbf{kr}} \right], \tag{17}$$

Normal mode along the x axis of an electromagnetic field confined in a box.

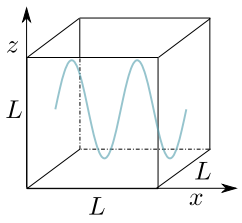

where the wavevector $\mathbf{k}$ takes the values:

$$\mathbf{k} = (k_x, k_y, k_z) = \frac{2\pi}{L}(n_1, n_2, n_3), \quad n_1, n_2, n_3 \in \mathbb{Z}\,, \tag{18}$$

$\mathbf{e}_{\mathbf{k},\lambda}$ correspond to the polarization vectors, that fulfil:

$$\mathbf{e}_{\mathbf{k},\lambda}\mathbf{k} = 0, \quad \mathbf{e}_{\mathbf{k},\lambda}\mathbf{e}_{\mathbf{k},\lambda'} = \delta_{\lambda,\lambda'}\,, \tag{19}$$

and ω_k is given by:

$$\omega_k = kc\,. \tag{20}$$

We will now quantize the electric field by turning the classical coefficients into quantum operators. This is done by the identification of the system's Hamiltonian, given by:

$$H_{\mathrm{EM}} = \frac{1}{2}\int_V \left(\varepsilon_0 \mathbf{E}^2 + \frac{1}{\mu_0}\mathbf{B}^2\right) dV\,, \tag{21}$$

with that of an harmonic oscillator. Obtaining $\mathbf{E}$ and $\mathbf{B}$ by inserting $\mathbf{A}$ from Eq. (17) into Eq. (6), and evaluating Eq. (21), one finally obtains [87, 157]:

$$H_{\mathrm{EM}} = \varepsilon_0 V \sum_{\mathbf{k}} \sum_{\lambda} \omega_k^2 (A_{\mathbf{k},\lambda} A^*_{\mathbf{k},\lambda} + A^*_{\mathbf{k},\lambda} A_{\mathbf{k},\lambda})\,. \tag{22}$$

If we define now variables $p_{\mathbf{k},\lambda}$ and $q_{\mathbf{k},\lambda}$ as fulfilling:

$$A_{\mathbf{k},\lambda} = \frac{1}{2\omega_k(\varepsilon_0 V)^{1/2}}[\omega_k q_{\mathbf{k},\lambda} + i p_{\mathbf{k},\lambda}]\,, \tag{23a}$$

$$A^*_{\mathbf{k},\lambda} = \frac{1}{2\omega_k(\varepsilon_0 V)^{1/2}}[\omega_k q_{\mathbf{k},\lambda} - i p_{\mathbf{k},\lambda}]\,, \tag{23b}$$

the Hamiltonian (21) takes the very familiar form

$$H_{\mathrm{EM}} = \frac{1}{2}\sum_{\mathbf{k}}\sum_{\lambda}(p^2_{\mathbf{k},\lambda} + \omega_k^2 q^2_{\mathbf{k},\lambda})\,. \tag{24}$$

Each term of this sum corresponds to the Hamiltonian of a simple harmonic oscillator of unit mass. Each pair of the classical quantities $(p_{\mathbf{k},\lambda}, q_{\mathbf{k},\lambda})$ are then *canonical coordinates* that satisfy the fundamental Poisson bracket relations:

$$\{q_{\mathbf{k},\lambda}, q_{\mathbf{k}',\lambda'}\} = 0\,, \quad \{p_{\mathbf{k},\lambda}, p_{\mathbf{k}',\lambda'}\} = 0\,, \quad \{q_{\mathbf{k},\lambda}, p_{\mathbf{k}',\lambda'}\} = \delta_{\mathbf{k},\mathbf{k}'}\delta_{\lambda,\lambda'}\,. \tag{25}$$

Following the canonical quantization scheme [71], the classical coordinates $(p_{\mathbf{k},\lambda}, q_{\mathbf{k},\lambda})$ can be turned into quantum operators $(\hat{p}_{\mathbf{k},\lambda}, \hat{q}_{\mathbf{k},\lambda})$, with the classical Poisson brackets being replaced by commutators multiplied by $(i\hbar)^{-1}$:

$$[\hat{q}_{\mathbf{k},\lambda}, \hat{q}_{\mathbf{k}',\lambda'}] = 0\,, \quad [\hat{p}_{\mathbf{k},\lambda}, \hat{p}_{\mathbf{k}',\lambda'}] = 0\,, \quad [\hat{q}_{\mathbf{k},\lambda}, \hat{p}_{\mathbf{k}',\lambda'}] = i\hbar\delta_{\mathbf{k},\mathbf{k}'}\delta_{\lambda,\lambda'}\,. \tag{26}$$

We can then define the quantum creation an annihilation operators as:

$$\hat{a}_{\mathbf{k},\lambda} = \frac{1}{(2\hbar\omega_k)^{1/2}}[\omega_k\hat{q}_{\mathbf{k},\lambda} + i\hat{p}_{\mathbf{k},\lambda}]\,, \tag{27a}$$

$$\hat{a}^\dagger_{\mathbf{k},\lambda} = \frac{1}{(2\hbar\omega_k)^{1/2}}[\omega_k\hat{q}_{\mathbf{k},\lambda} - i\hat{p}_{\mathbf{k},\lambda}]\,, \tag{27b}$$

satisfying the following commutation relations:

$$[\hat{a}_{\mathbf{k},\lambda}, \hat{a}_{\mathbf{k}',\lambda'}] = [\hat{a}^\dagger_{\mathbf{k},\lambda}, \hat{a}^\dagger_{\mathbf{k}',\lambda'}] = 0\,, \tag{28a}$$

$$[\hat{a}_{\mathbf{k},\lambda}, \hat{a}^\dagger_{\mathbf{k}',\lambda'}] = \delta_{\mathbf{k},\mathbf{k}'}\delta_{\lambda,\lambda'}\,. \tag{28b}$$

In terms of these operators, the quantum Hamiltonian operator can be written as:

$$\hat{H}_{\mathrm{EM}} = \sum_{\mathbf{k}}\sum_{\lambda}\hbar\omega_k\left(\hat{a}^\dagger_{\mathbf{k},\lambda}\hat{a}_{\mathbf{k},\lambda} + \frac{1}{2}\right). \tag{29}$$

The electromagnetic field is thus described as a collection of quantum harmonic oscillators of frequency ω_k. The amplitudes $A_{\mathbf{k},\lambda}$ have then become operators given by:

$$\hat{A}_{\mathbf{k},\lambda} = \left(\frac{\hbar}{2\omega_k\varepsilon_0 V}\right)^{\frac{1}{2}}\hat{a}_{\mathbf{k},\lambda}\,, \tag{30}$$

yielding quantized vector potential and electric field operators of the form:

$$\hat{\mathbf{A}} = \sum_{\mathbf{k}}\sum_{\lambda}\left(\frac{\hbar}{2\omega_k\varepsilon_0 V}\right)^{\frac{1}{2}}\mathbf{e}_{\mathbf{k},\lambda}[\hat{a}_{\mathbf{k},\lambda}e^{i(\mathbf{kr}-\omega_k t)} - \hat{a}^\dagger_{\mathbf{k},\lambda}e^{-i(\mathbf{kr}-\omega_k t)}]\,, \tag{31a}$$

$$\hat{\mathbf{E}} = i\sum_{\mathbf{k}}\sum_{\lambda}\left(\frac{\hbar\omega_k}{2\varepsilon_0 V}\right)^{\frac{1}{2}}\mathbf{e}_{\mathbf{k},\lambda}[\hat{a}_{\mathbf{k},\lambda}e^{i(\mathbf{kr}-\omega_k t)} - \hat{a}^\dagger_{\mathbf{k},\lambda}e^{-i(\mathbf{kr}-\omega_k t)}]\,. \tag{31b}$$

2.2 INTERACTION OF THE QUANTIZED ELECTROMAGNETIC FIELD WITH MATTER

We introduce here the expression of the Hamitonian for light-matter interaction at the quantum level, which is the main topic if this Thesis. We regard matter as a collection of particles of mass m_i and charge e_i. The interaction between the particles is given by the Coulomb potential:

$$U(\cdots, \mathbf{r}_i, \cdots, \mathbf{r}_j, \cdots) = \frac{1}{4\pi\varepsilon_0} \sum_{\substack{i,j \\ i \neq j}} \frac{e_i, e_j}{|\mathbf{r}_i - \mathbf{r}_j|} \,. \tag{32}$$

The Hamiltonian of the many-particle system of charges is thus given by:

$$\hat{H}_{\mathrm{E}} = \sum_i \frac{\hat{\mathbf{p}}_i^2}{2m_i} + U \tag{33}$$

where the suffix E stands for 'electronic', and where $\hat{\mathbf{p}}_i = -i\nabla_i$ is the momentum operator of the i-th particle. Let us consider now the interaction of these particles with an electromagnetic field. It has to be such that the theory is invariant under gauge transformations of the form (10), a requirement fulfilled by the so-called minimal coupling , consisting in replacing the momentum of the i-th particle by [51]:

$$\hat{\mathbf{p}}_i \to \hat{\mathbf{p}}_i - \frac{e_i}{c}\mathbf{A}(\mathbf{r}_i) \,. \tag{34}$$

For a long time, the vector potential was not believed to have a direct physical interpretation, being **E** and **B** the physical observable quantities. However, its direct appearance in the **minimal coupling** Hamiltonian allows it to affect the wavefunction and produce interference phenomena even when the fields vanish. This effect, discovered by Y. Aharonov and D. Bohm [5], revealed the fundamental role that the electromagnetic potentials play in quantum theory.

This yields a total Hamiltonian for the light-matter system:

$$\hat{H} = \sum_i \frac{(\hat{\mathbf{p}}_i - e_i\mathbf{A}(\mathbf{r}_i))^2}{2m_i} + U + \hat{H}_{\mathrm{EM}} \,, \tag{35}$$

with $\hat{H}_{\mathrm{EM}}$ given by Eq. (21). This Hamiltonian is written in a form that does not take advantage of the difference of length scale between the size of the atom and wavelength of the radiation. We can cast it into a more useful expression by applying a gauge transformation to the potentials (10) in order to obtain:

$$\hat{H} = \sum_i \left\{ \frac{[\hat{\mathbf{p}}_i - e_i(\mathbf{A}(\mathbf{r}_i) + \nabla\chi(\mathbf{r}_i))]^2}{2m_i} - e_i\frac{\partial\chi}{\partial t} \right\} + U + \hat{H}_{\mathrm{EM}} \,, \tag{36}$$

where $\chi(\mathbf{r}, t)$ is an arbitrary function of position and time. There are cases in which $\mathbf{A}$ remains approximately constant over the distribution of charges, like in the case of atoms excited by optical light, where $\mathbf{A}$ varies in a scale of hundreds of nanometers, while the typical atomic dimensions are of the range of a few Ångströms. In that situation we can consider the vector potential to be spatially uniform, $\mathbf{A}(\mathbf{r}, t) \approx \mathbf{A}(t)$, in what is called the *dipole approximation*. We can then choose the gauge function $\chi(\mathbf{r}, t) = -\mathbf{A}(t)\mathbf{r}$, which leads to the Hamiltonian:

$$\hat{H} = \sum_i \frac{\hat{\mathbf{p}}_i^2}{2m_i} - \sum_i e_i\hat{\mathbf{r}}_\mathbf{i}\mathbf{E} + U + \hat{H}_{\mathrm{EM}} = \hat{H}_{\mathrm{E}} + \hat{H}_{\mathrm{EM}} + \hat{H}_{\mathrm{I}} \,, \tag{37}$$

where $\mathbf{E} = -\partial\mathbf{A}(t)/\partial t$. This can be written in terms of the *dipole moment* $\mathbf{d}$ of the charge distribution:

$$\hat{\mathbf{d}} = \sum_i e_i \hat{\mathbf{r}}_i \,, \tag{38}$$

giving an interaction Hamiltonian:

$$\hat{H}_{\mathrm{I}} = -\hat{\mathbf{d}}\hat{\mathbf{E}} \,, \tag{39}$$

where in the last stage we used the quantized electric field $\hat{\mathbf{E}}$ given by Eq. (31b), evaluated at the position of the atom. $\hat{\mathbf{d}}$ acts on the Hilbert space of the charge system, and can be written in the basis of eigenvectors of the Hamiltonian of the charges alone, $\hat{H}_{\mathrm{E}}|i\rangle = E_i|i\rangle$:

$$\hat{\mathbf{d}} = \sum_{i,j} \mathbf{d}_{ij} \, |i\rangle\langle j| \,, \tag{40}$$

where $\mathbf{d}_{ij} \equiv \langle i|\hat{\mathbf{d}}|j\rangle$. $\hat{\mathbf{d}}$ has odd parity, and therefore, the diagonal elements of the operator in the basis of eigenfunctions vanish [157]:

$$\langle i|\hat{\mathbf{d}}|i\rangle = 0 \,. \tag{41}$$

THE JAYNES CUMMINGS HAMILTONIAN In many calculations, we are concerned just about the optical transitions between two energy levels of the matter system, $|g\rangle$ and $|e\rangle$, such that the dipole is described as a *two-level system* (2LS) and $\hat{\mathbf{d}}$ is just a 2×2 matrix, given by:

$$\hat{\mathbf{d}} = \mathbf{d}(\hat{\sigma}^\dagger + \hat{\sigma}) \,, \tag{42}$$

where $\hat{\sigma}$ and $\hat{\sigma}^\dagger$ are the annihilation and creation operator of excitations the 2LS:

$$\hat{\sigma} = |g\rangle\langle e| \,, \qquad \hat{\sigma}^\dagger = |e\rangle\langle g| \,. \tag{43}$$

In that case, the interaction of the dipole with a mode of the electric field with wavevector $\mathbf{k}$ and polarization λ (whose annihilation operator we describe just as $\hat{a} \equiv \hat{a}_{\mathbf{k},\lambda}$ to ease the notation) is:

$$\hat{H}_{\mathrm{I}} = \hbar g(\hat{\sigma}^\dagger + \hat{\sigma})(\hat{a} + \hat{a}^\dagger) \,, \tag{44}$$

where the coupling rate is given by:

$$\hbar g = i\mathbf{e}_{\mathbf{k},\lambda}\mathbf{d}\left(\frac{\hbar\omega_k}{2\varepsilon_0 V}\right)^{\frac{1}{2}} e^{i\mathbf{kr}} \,, \tag{45}$$

with $\mathbf{r}$ the position of the dipole at which $\mathbf{A}$ is considered to be approximately constant.

In the rest of this Thesis, we will typically reduce the problem to single mode interaction, i.e., we will consider the case of one resonance in a cavity mode much closer to the transition energy of the 2LS than the rest of the resonances of the cavity. Furthermore, we shall assume for simplicity that

the orientation of the dipole is such that g is purely real; we will eliminate all constant terms in the Hamiltonian that play no role in the dynamics (such as the zero-point energy of $\hat{H}_{\text{EM}}$); and finally, we will adopt the notation of natural units $\hbar = 1$. Note that, since we will take $\hbar = 1$ from now on, we will speak in terms of energy and frequency indistinctly, assuming the relationship $E = \hbar\omega$. We will also drop the $\hat{}$ notation for operators, except in those cases where it is needed to highlight the difference between them and classical quantities. Considering that the cavity has a free energy ω_a, and the energy difference between the two levels of the 2LS is ω_σ, we obtain the total Hamiltonian with notation that will be followed on the rest of the text:

$$H = \omega_a a^\dagger a + \omega_\sigma \sigma^\dagger \sigma + g(\sigma^\dagger + \sigma)(a + a^\dagger)\,. \tag{46}$$

The last step is to perform a *rotating wave approximation* that eliminates the fast-rotating terms $g\sigma^\dagger a^\dagger$ and $g\sigma a$ that do not conserve energy from the Hamiltonian, valid when $g \ll \omega_a, \omega_\sigma$. As a result, one obtains the so-called Jaynes-Cummings Hamiltonian [120]:

$$H_{\text{JC}} = \omega_a a^\dagger a + \omega_\sigma \sigma^\dagger \sigma + g(\sigma^\dagger a + \sigma a^\dagger)\,. \tag{47}$$

This Hamiltonian stands as the most basic description of light-matter interaction at the quantum level, and will be used extensively in the rest of this Thesis.

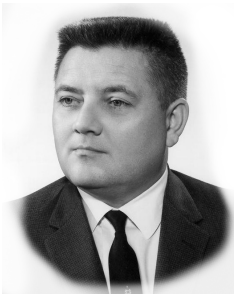

Edwin Thompson **Jaynes** (1922–1988), is known for initiating the MaxEnt (maximum entropy) interpretation of thermodynamics. Ironically, he introduced in 1963 the Jaynes-Cummings Hamiltonian, together with his student Frederick **Cummings**, as an effort to demonstrate that quantization of the electromagnetic field was unnecessary. In 1966, he bet Peter Franken 100$ whether he could, in 10 years, carry out the calculation of the Lamb shift with a classical description of the electromagnetic field [220]. Despite he was able to predict a form of spontaneous emission and Lamb shift without field quantization, the inaccuracy of the results finally gave the victory, decided by Lamb himself, to Franken.

2.3 THEORY OF OPEN QUANTUM SYSTEMS: THE LANGEVING EQUATIONS

We discuss now the theory of a quantum system interacting with a large reservoir of modes from the perspective of Heisenberg's equations of motion for the operators. Our discussions here are mainly adapted from Refs. [41, 85, 232].

2.3.1 THE QUANTUM LANGEVIN EQUATIONS

We consider a total Hamiltonian of the system S plus the reservoir R, given by:

$$H = H_{\text{S}} + H_{\text{R}} + H_{SR}\,. \tag{48}$$

Here, H_S is the free Hamiltonian of the system, about which we make no assumptions yet. H_R is the Hamiltonian of the reservoir, which we consider to be an infinite set of electromagnetic modes:

$$H_R = \sum_{\mathbf{k}} \omega_k b_{\mathbf{k}}^\dagger b_{\mathbf{k}}\,, \tag{49}$$

with $b_{\mathbf{k}}$ a bosonic annihilation operator of a photon of the bath with wavevector $\mathbf{k}$. This Hamiltonian is similar to (29), but omitting the sum in polariza-

tions; we consider for simplicity that only one polarization is relevant. Finally, the system-reservoir interaction reads:

$$H_{SR} = i\sum_{\mathbf{k}} g_{\mathbf{k}}(b_{\mathbf{k}}^\dagger c - b_{\mathbf{k}} c^\dagger)\,, \tag{50}$$

which describes the coupling between the reservoir and a mode of the system given by the annihilation operator c. We make no assumption regarding the nature of this mode; it can be bosonic if the coupling is to a cavity ($c = a$) or fermionic if the coupling is to a 2LS ($c = \sigma$). We will only assume that, under the action of H_S, it evolves with a resonant frequency ω_0 as $c(t) = e^{-i\omega_0 t}c(0)$. $g_{\mathbf{k}}$ is the coupling rate. This coupling Hamiltonian, which resembles the shape of the Jaynes-Cummings Hamiltonian (47) (but with a different phase factor) can actually be regarded as the first term of a series expansion of any possible coupling between the bath and the system.

The Heisenberg equations of motion for $b_{\mathbf{k}}$ and c are then given by:

$$\frac{\partial b_{\mathbf{k}}}{\partial t} = -i\omega_k b_{\mathbf{k}} + g_{\mathbf{k}} c\,, \tag{51a}$$

$$\frac{\partial c}{\partial t} = -i[c, H_S] - \sum_{\mathbf{k}} g_{\mathbf{k}}[c, c^\dagger] b_{\mathbf{k}}\,. \tag{51b}$$

Equation (51a) can be formally solved to obtain:

$$b_{\mathbf{k}} = e^{-i\omega_k(t-t_0)} b_{\mathbf{k}}(t_0) + g_{\mathbf{k}} \int_{t_0}^{t} e^{-i\omega_k(t-t')} c(t')\, dt'\,. \tag{52}$$

Introducing (52) into (51b), we get:

$$\frac{\partial c}{\partial t} = -i[c, H_S] - \sum_{\mathbf{k}} g_{\mathbf{k}}[c, c^\dagger] e^{-i\omega_k(t-t_0)} b_{\mathbf{k}}(t_0) - \sum_{\mathbf{k}} g_{\mathbf{k}}^2 \int_{t_0}^{t} [c, c^\dagger] e^{-i\omega_k(t-t')} c(t')\, dt'\,. \tag{53}$$

Note that, for notational convenience, we do not include explicitly the time dependence on t on the operators (i.e., $c \equiv c(t)$).

GOING TO THE CONTINUUM LIMIT At this point it is useful to perform a limit to the continuum, considering the bath is infinitely large. This is done by replacing the sums in $\mathbf{k}$ by the following integral:

$$\lim_{L\to\infty} \sum_{\mathbf{k}} = \int_0^\infty \xi(\omega) d\omega\,. \tag{54}$$

where $\xi(\omega)$ is the *mode density* counting the number of states in a given $d\omega$. We will assume a linear dispersion $\omega_k = c|\mathbf{k}|$ and a one-dimensional bath ($\mathbf{k} = k$) of length L, so that $\xi(\omega) = L/2\pi c$. In this limit, the Kronecker delta converges to the Dirac delta:

$$\lim_{L\to\infty} \delta_{k,k'} = \frac{2\pi c}{L}\delta(\omega - \omega')\,. \tag{55}$$

This leads us to the following definition of the continuous boson operators:

$$b(\omega) = \sqrt{\frac{L}{2\pi c}} b_k \,, \tag{56}$$

which satisfy commutation relations:

$$[b(\omega), b^\dagger(\omega)] = \delta(\omega - \omega') \,. \tag{57}$$

Finally, we define the *spectral density* $J(\omega)$ as:

$$J(\omega) = \xi(\omega) g_k^2 \,, \tag{58}$$

so that in the one-dimensional case we are considering, $J(\omega) = \frac{L}{2\pi c} g_k^2$. Then, we rewrite Eq. (53) in the continuous limit:

$$\begin{aligned} \frac{\partial c}{\partial t} = -i[c, H_S] - \int_{-\infty}^{\infty} \sqrt{J(\omega)}[c, c^\dagger] e^{-i\omega(t-t_0)} b_0(\omega)\, d\omega \\ - \int_{-\infty}^{\infty} J(\omega)^2\, d\omega \int_{t_0}^{t} [c, c^\dagger] e^{-i\omega(t-t')} c(t')\, dt' \,. \end{aligned} \tag{59}$$

where $b_0(\omega)$ is the value of $b(\omega)$ at $t = t_0$. The lower integration limit has been extended from 0 to $-\infty$, since only the reservoir modes of frequency ω close to the free frequency of oscillation of c will contribute significantly to the integral.

FIRST MARKOV APPROXIMATION We will now assume that $J(\omega)$ is independent of the frequency around the range of ω where the integrals are non-negligible, which is called the *first Markov approximation*. Therefore, we set:

$$J(\omega) = J(\omega_0) \equiv \gamma/2\pi \,, \tag{60}$$

and define the *input field* operator as:

$$b_{\text{in}}(t) \equiv \frac{1}{\sqrt{2\pi}} \int_{-\infty}^{\infty} e^{-i\omega(t-t_0)} b_0(\omega)\, d\omega \,. \tag{61}$$

Using the relation

$$\int_{-\infty}^{\infty} e^{-i\omega(t-t')}\, d\omega = 2\pi\delta(t - t') \,, \tag{62}$$

the input field is shown to satisfy:

$$[b_{\text{in}}(t), b_{\text{in}}^\dagger(t')] = \delta(t - t') \,. \tag{63}$$

Substituting (60) and (61) in Eq. (59), using (62) and the following relation:

$$\int_{t_0}^{t} c(t')\delta(t - t') = \frac{1}{2} c(t) \,, \tag{64}$$

Paul **Langevin** (1872-1946), born in Paris, developed the so-called Langevin dynamics, an approach to the dynamical modelling of molecular systems that accounts for the omission of external degrees of freedom by using stochastic differential equations. A public voice against fascism, he was held under house arrest by the Vichy government during World War II.

we arrive to the so-called quantum Langevin equation:

$$\frac{\partial c}{\partial t} = -i[c, H_S] - [c, c^\dagger]\left[\frac{\gamma}{2}c + \sqrt{\gamma}b_{\text{in}}(t)\right]. \tag{65}$$

In a similar manner, we could have write the formal solution of $b(\omega)$ as:

$$b(\omega) = e^{-i\omega(t-t_1)}b_1(\omega) - g(\omega)\int_t^{t_1} e^{-i\omega(t-t')}c(t')\,dt', \tag{66}$$

define the *output field* as:

$$b_{\text{out}}(t) = \frac{1}{\sqrt{2\pi}}\int_{-\infty}^{\infty} e^{-i\omega(t-t_1)}b_1(\omega)\,d\omega\,, \tag{67}$$

and obtain an analogous quantum Langevin equation in terms of the output field:

$$\frac{\partial c}{\partial t} = -i[c, H_S] + [c, c^\dagger]\left[\frac{\gamma}{2}c - \sqrt{\gamma}b_{\text{in}}(t)\right]. \tag{68}$$

We can obtain a relation between the input and output fields by substracting Eq. (68) from Eq. (65):

$$b_{\text{out}}(t) = b_{\text{in}}(t) + \sqrt{\gamma}c(t)\,, \tag{69}$$

which are the so-called *input-output relations*.

These equations allow us to determine the evolution of the system operator $c(t)$ by considering $b_{\text{in}}(t)$ as a *noise term* independent of the system. This can be done, since its definition in terms of $b_0(\omega)$ allows us to freely specify it as initial conditions assuming that, at t_0, no correlation exists between the system and the reservoir. The evolution of any system operator can then be completely specified by fixing the mean values and correlation functions of the input field. For example, in the simplest case where the external field is initially in vacuum, we have:

$$\langle b_{\text{in}}(t)\rangle = \langle b_{\text{in}}^\dagger(t)b_{\text{in}}(t')\rangle = 0\,, \tag{70a}$$

$$\langle b_{\text{in}}(t)b^\dagger(t')\rangle = \delta(t-t')\,, \tag{70b}$$

which allow us, for the case of a bosonic mode $c = a$ with $H_S = \omega_a a^\dagger a$, to readily solve the equation for $\langle a(t)\rangle$:

$$\langle a(t)\rangle = e^{-\gamma/2}\langle a(0)\rangle\,. \tag{71}$$

2.3.2 THE OUTPUT FIELD

Despite they can be used to do so, Langevin equations will not be employed in this Thesis to solve the dynamics of the system. However, they provide a key connection between the reservoir fields and the system's dynamics that justifies the approach that we will take in the rest of the Thesis to describe the light emitted by the system. In the Heisenberg picture, the vectorial component of electric field of the reservoir in the direction of the chosen polarization reads:

$$E(x,t) = E^{(+)}(x,t) + E^{(-)}(x,t)\,, \tag{72}$$

with

$$E^{(+)}(x,t) = i\sum_k \left(\frac{\omega_k}{2\varepsilon_0 AL}\right)^{\frac{1}{2}} b_k(t)e^{ikx}\,, \tag{73a}$$

$$E^{(-)} = E^{(+)}(x,t)^\dagger\,. \tag{73b}$$

where A is the cross section of the reservoir. From Eq. (52), we see that the output field is then given by a free, unperturbed part plus another term originating from the interaction with the source:

$$E(x,t) = E_f^{(+)}(x,t) + E_s^{(+)}(x,t)\,, \tag{74}$$

where

$$E_f^{(+)}(x,t) = i\sum_k \left(\frac{\omega_k}{2\varepsilon_0 AL}\right)^{\frac{1}{2}} e^{ikx - i\omega_k(t-t_0)} b_k(t_0)\,, \tag{75}$$

and

$$E_s^{(+)}(x,t) = i\sum_k \left(\frac{\omega_k}{2\varepsilon_0 AL}\right)^{\frac{1}{2}} e^{ikx} g_k \int_{t_0}^{t} e^{-i\omega_k(t-t')} c(t')\,dt\,. \tag{76}$$

We see that Eq. (74) and Eq. (69) are equivalent readings of the same fact: the output field consists on two terms; the free evolution of the initial field plus the fluorescent field emitted by the system. The integral in (76) can be simplified by taking the sum in k to the continuum. Then, if we take into account that only modes with frequency close to the resonant frequency ω_0 of the mode $c(t')$ will contribute to the integral in ω, we can use Eq. (62) to obtain:

$$E_s^{(+)}(x, t + x/c) = i\left(\frac{\omega_0}{2\varepsilon_0 Ac}\right)^{1/2} \sqrt{\gamma}\, c(t) \tag{77}$$

for $0 < x < ct$, so that:

$$\begin{aligned} &E^{(+)}(x, t + x/c) - E_f^{(+)}(x, t + x/c) \\ &= i\left(\frac{\omega_0}{2\varepsilon_0 Ac}\right)^{1/2} [b_{\text{out}}(t) - b_{\text{in}}(t)] = i\left(\frac{\omega_0}{2\varepsilon_0 Ac}\right)^{1/2} \sqrt{\gamma}\, c(t)\,. \end{aligned} \tag{78}$$

Therefore, if the input field is in vacuum, *any normal-ordered correlator of the output field depends only on the system operator* c, meaning that we can obtain direct information of the system's dynamics from the measurement of the output field. This important result allow us, from a theoretical point of view, to link the observables measured in the output electric field—which are those accessible in the laboratory—to our description of the system alone, by making the association $c \to E^{(+)}$. Then, one only needs to be able to describe the evolution of c, which we can do by means of the Langevin equation, or the master equation that we will introduce below.

The situation is more complicated if the input field is not in the vacuum state [41]. However, we can always trivially extend the derivations above to

the case of coupling to several reservoir (all of them contributing to the total value of γ), and consider one of them (in which we perform the detection) to be in vacuum. Then, the previous reasoning applies, and we can assume that the output field on that channel can be linked to the system operator c. Therefore, in the rest of this Thesis we will work under this assumption and not longer worry about the state of the output field, focusing instead on system dynamics under the assumption that normal-ordered correlators of c are mapped into normal-ordered correlators of $E^{(+)}$.

2.3.3 COHERENT EXCITATION

We discuss now a case of particular interest for the system's dynamics: the initialization of the input field as a coherent state of frequency ω_L. This coherent state fulfills:

$$\langle b_0(\omega)\rangle = \alpha\delta(\omega-\omega_L)\,, \tag{79a}$$

$$\langle b_0^\dagger(\omega)b_0(\omega')\rangle|\alpha|^2\delta(\omega-\omega_L)\delta(\omega'-\omega_L)\,, \tag{79b}$$

with α the amplitude of the coherent state. We can in this case define a new input operator

$$a_{in}(t) = b_{in}(t) - \langle b_{in}(t)\rangle\,, \tag{80}$$

where $a_{in}(t)$ is a mode in vacuum and, setting $t_0 = 0$ and using Eq. (79a), define the mean value of the input field as:

$$\langle b_{in}(t)\rangle = \frac{\alpha}{\sqrt{2\pi}}e^{-i\omega_L t}\,. \tag{81}$$

Introducing this in the Langevin equation (65), we obtain an analogous Langeving equation:

$$\frac{\partial c}{\partial t} = -i[c,H_S] - [c,c^\dagger]\left[\frac{\gamma}{2}c + \sqrt{\gamma}a_{in}(t) - i\Omega e^{-i\omega_L t}\right]\,, \tag{82}$$

with a vacuum noise term proportional to $a_{in}(t)$, and an extra term proportional to Ω, where:

$$\Omega = i\sqrt{\frac{\gamma}{2\pi}}\alpha\,. \tag{83}$$

This term can be included as a coherent driving term H_C in the Hamiltonian:

$$\frac{\partial c}{\partial t} = -i[c,H_S+H_C] - [c,c^\dagger]\left[\frac{\gamma}{2}c + \sqrt{\gamma}a_{in}(t)\right]\,, \tag{84}$$

Assuming for simplicity a phase of the input field that makes Ω real, this Hamiltonian takes the form:

$$H_C = \Omega\left(\sigma e^{i\omega_L t} + \sigma^\dagger e^{-i\omega_L t}\right)\,. \tag{85}$$

This term corresponds a continuous driving that excites the system coherently, and offer a good description of the pumping sustained by an external laser, with an intensity $I = |E|^2$ proportional to Ω^2. This is the model of a coherent driving that we will use in the rest of the Thesis.

2.4 UNITARY TRANSFORMATIONS: MOVING TO A NEW ROTATING FRAME

In the preceding Section we obtained a kind Hamiltonian that we will encounter very often

$$H = \omega_\sigma \sigma^\dagger \sigma + \Omega \left(\sigma e^{i\omega_L t} + \sigma^\dagger e^{-i\omega_L t} \right) . \tag{86}$$

and that is explicitly time-dependent. In this situation, a very convenient approach is moving to the rotating frame of the laser, where these time dependent terms disappear from the Hamiltonian. This is done by applying a unitary transformation U such that:

$$\left|\psi'\right\rangle = U \left|\psi\right\rangle , \tag{87}$$

where $\left|\psi\right\rangle$ is a state ket of the system. We will specify later which transformation is useful to eliminate the time dependence in Eq. (86), for now we leave it undefined. We want now to find the new Hamiltonian H_R (R stands for 'reference', or 'rotating') in the rotating frame, such that the time evolution of the states $\left|\psi'\right\rangle$ follow a Schrödinger equation:

$$i\partial_t \left|\psi'\right\rangle = H_R \left|\psi'\right\rangle . \tag{88}$$

By substituting (86) in (88), it is easy to obtain:

$$H_R = UHU^\dagger + i(\partial_t U)U^\dagger \tag{89}$$

Now, note that as we defined it, H_R *is not the original Schrödinger Hamiltonian transformed into the new reference frame.* Such a transformed Hamiltonias, that we will denote H', would be given directly by the *similarity transformation* $H' = UHU^\dagger$. It is defined in such a way that the measured observables are the same as in the original reference frame:

$$\left\langle\psi\right| H \left|\psi\right\rangle = \left\langle\psi'\right| H' \left|\psi'\right\rangle \tag{90}$$

so that it describes the same physical quantity. When we put ourselves on this frame, however, the laws of physics seem different and the resulting effective dynamics do not follow the Schrödinger equation for H' anymore; they do, instead, for a different Hamiltonian that we call H_R. Therefore, when referring to the Hamiltonian of the new reference frame, we must be aware of the vocabulary being used and pay attention to know whether it refers to H' or H_R.

2.4.1 THE INTERACTION PICTURE

The interaction picture is just a particular instance of the change of reference frame just discussed. In this particular case, the unitary transformation is chosen to be:

$$U = e^{iH_0 t}, \tag{91}$$

where H_0 is a part of the total Hamiltonian $H = H_0 + V$, generally, a non-interacting part whose eigenstates and eigenvalues are already known. In this case, we have:

$$\partial_t U = iH_0 U\,, \tag{92}$$

and by substitution in (89) we get:

$$H_{\mathrm{R}} = e^{iH_0 t} V e^{-iH_0 t} \equiv V_{\mathrm{I}}\,, \tag{93}$$

which gives the usual expression for the evolution of a state in the interaction picture $|\psi\rangle_{\mathrm{I}}$:

$$i\partial_t |\psi\rangle_{\mathrm{I}} = V_{\mathrm{I}} |\psi\rangle_{\mathrm{I}}\,. \tag{94}$$

Note that when discussing the interaction picture, the usual nomenclature—which is the one used in Eq. (94)—already makes clear that what we call H_{R} is in fact not the similarity-transformed Hamiltonian from the Schrödinger picture, and therefore is denoted V_{I}. We will nevertheless adopt the Hamiltonian H_{R} terminology, because, as we will see, the effect of the unitary transformation that we will typically make is just to remove the time dependence and lower the free energies by the frequency of the laser.

2.4.2 REMOVING THE TIME DEPENDENCE

Given a time dependence of the form:

$$H = \omega_b b^\dagger b + \Omega \left(b\, e^{i\omega_{\mathrm{L}} t} + b^\dagger e^{-i\omega_{\mathrm{L}} t} \right)\,, \tag{95}$$

with b a (bosonic or fermionic) system operator, the choice that we make in order to eliminate the time dependence in the Hamiltonian is:

$$U = e^{i\omega_{\mathrm{L}} t b^\dagger b}\,, \tag{96}$$

which, as one can see, is almost identical to a change to the interaction picture, but uses the frequency of the exciting field ω_{L} instead of the frequency of the mode b.

By using the commutator $\left[b^\dagger b, b\right] = -b$ (which, interestingly, is obeyed for both bosonic and fermionic operators) and the *Baker-Hausdorff lema*, that reads:

$$e^{-\theta \hat{P}} \hat{O} e^{\theta \hat{P}} = \hat{O} - \theta \left[\hat{P}, \hat{O}\right] + \frac{\theta^2}{2!} \left[\hat{P}, \left[\hat{P}, \hat{O}\right]\right] + \cdots = e^{-\theta \hat{L}_P} \hat{O}\,, \tag{97}$$

where

$$\hat{L}_P^0 \hat{O} = \hat{O}\,, \tag{98a}$$
$$\hat{L}_P \hat{O} = \left[\hat{P}, \hat{O}\right]\,, \tag{98b}$$
$$\hat{L}_P^n \hat{O} = \hat{L}_P^{n-1} \left[\hat{P}, \hat{O}\right]\,, \tag{98c}$$

one obtains:

$$UbU^\dagger = e^{i\omega_L t}\left[b - (i\omega_L t)b + \frac{(i\omega_L t)^2}{2}b + \cdots\right] = b\,, \tag{99a}$$

$$Ub^\dagger e^{-i\omega_L t}U^\dagger = b^\dagger\,, \tag{99b}$$

$$U\omega_b b^\dagger b U^\dagger = \omega_b b^\dagger b\,, \tag{99c}$$

$$i(\partial_t U)U^\dagger = -\omega_L b^\dagger b\,, \tag{99d}$$

yielding the following expression for the Hamiltonian in the rotating frame of the laser:

$$H_R = (\omega_b - \omega_L)b^\dagger b + \Omega(b + b^\dagger)\,. \tag{100}$$

in which the time dependence is removed and the free energy of mode b is substituted by its detuning to laser frequency ω_L. If the total Hamiltonian features a coupling between two modes b and c and a coherent driving of one of them:

$$H = \omega_b b^\dagger b + \omega_c c^\dagger c + g(b^\dagger c + bc^\dagger) + \Omega\left(b\,e^{i\omega_L t} + b^\dagger e^{-i\omega_L t}\right)\,, \tag{101}$$

the unitary transformation needs to be:

$$U = e^{i\omega_L t(b^\dagger b + c^\dagger c)}\,, \tag{102}$$

and the Hamiltonian in the rotating frame of the laser results in a shift of the free energy of both modes:

$$H_R = (\omega_b - \omega_L)b^\dagger b + (\omega_c - \omega_L)c^\dagger c + g(b^\dagger c + bc^\dagger) + \Omega(b + b^\dagger)\,. \tag{103}$$

2.5 THEORY OF OPEN QUANTUM SYSTEMS: THE MASTER EQUATION

In Section 2.3, we tackled the problem of describing the dynamics of a system S coupled to a revervoir R from the perspective of Heisenberg's equations of motion for the system's operators. In this section, we introduce an alternative approach based on the Schrödinger picture, i.e., in the evolution of the state vector of the system. In this description, however, the state of the system cannot be given by a pure wavefunction. Instead, it needs to be described in terms of a *density matrix*, since the basis of this approach is to trace out the reservoir's degrees of freedom, which forces us to describe the system as an statistical ensemble of quantum states.

2.5.1 THE MASTER EQUATION

Our purpose is to obtain the equations of motion for the *reduced density matrix* for the system alone:

$$\rho(t) = \mathrm{Tr}_R\{\rho_{\mathrm{tot}}(t)\}. \tag{104}$$

where Tr_R represents the partial trace over the reservoir degrees of freedom. If the density matrix ρ of a composite system $S \otimes R$ is given by: $\rho = \sum_{i,\mu,i',\mu'} \alpha_{i\mu}\alpha^*_{i'\mu'} |i_S\rangle |\mu_R\rangle \langle i'_S| \langle \mu'_R|$, the parcial trace over R is defined as:

$$\mathrm{Tr}_R\rho = \sum_{\mu''} \langle \mu''_R| \rho |\mu''_R\rangle = \sum_{i,i',\mu} |i_S\rangle \langle i'_S| \alpha_{i\mu}\alpha^*_{i'\mu} . \tag{105}$$

The evolution of the total density matrix is given by the analogue of the Schrödinger equation to mixed states, the *von Neumann equation*:

$$\frac{\partial \rho_{\mathrm{tot}}}{\partial t} = -i[H, \rho_{\mathrm{tot}}] , \tag{106}$$

where H is the total Hamiltonian of the system and reservoir, as in Eq.(48). The density matrix in the interaction picture (see Section 2.4.1) is given by:

$$\tilde{\rho}_{\mathrm{tot}} = e^{i(H_S+H_R)t}\rho_{\mathrm{tot}}e^{-i(H_S+H_R)t} , \tag{107}$$

and evolves according to:

$$\frac{\partial \tilde{\rho}_{\mathrm{tot}}}{\partial t} = -i[\tilde{H_{SR}}(t), \tilde{\rho}_{\mathrm{tot}}(t)]. \tag{108}$$

where $\tilde{H_{SR}}$ is explicitly time-dependent in the interaction picture. By formally integrating Eq.(108) and puting the solution back on the commutator, we get:

$$\frac{\partial \tilde{\rho}_{\mathrm{tot}}}{\partial t} = -i[\tilde{H}_{SR}, \rho_{\mathrm{tot}}(0)] - \int_0^t [\tilde{H}_{SR}(t), [\tilde{H}_{SR}(t'), \tilde{\rho}_{\mathrm{tot}}(t')]]dt' . \tag{109}$$

In the same way that we assumed a given initial state of the output field uncorrelated from the system for the derivation of the Langevin equations, we will now assume that at $t = 0$ the total density matrix of the system and the reservoir is factorized:

$$\rho_{\mathrm{tot}}(0) = \rho(0)\rho_R(0) , \tag{110}$$

where $\rho_R(0)$ is a reservoir density matrix and $\rho(0)$ is the initial state of the system. The partial trace over $\tilde{\rho}_{\mathrm{tot}}$ gives:

$$\mathrm{Tr}_R\{\tilde{\rho}_{\mathrm{tot}}\} = e^{iH_St}\rho e^{-iH_St} = \tilde{\rho} , \tag{111}$$

and, after tracing over the reservoir in (109), we get:

$$\frac{\partial \tilde{\rho}}{\partial t} = -\int_0^t dt' \,\mathrm{Tr}_R\{[\tilde{H}_{SR}(t), [\tilde{H}_{SR}(t'), \tilde{\rho}_{\mathrm{tot}}(t')]]\} \tag{112}$$

where for simplicity we assumed $\mathrm{Tr}_R[\tilde{H}_{SR}\rho_R(0)] = 0$ to remove the first term.

BORN APPROXIMATION We make know the so-called *Born approximation*, in which by using the fact that the system and the reservoir remain uncorrelated to zeroth order in H_{SR}:

$$\tilde{\rho}_{\text{tot}}(t) = \tilde{\rho}(t)\rho_R(0) + \mathcal{O}(H_{SR})\,. \tag{113}$$

we can write Eq. (112) to second-order in H_{SR}, obtaining the *master equation in the Born approximation*::

$$\frac{\partial\tilde{\rho}}{\partial t} = -\int_0^t dt'\,\text{Tr}_R\{[\tilde{H}_{SR}(t),[\tilde{H}_{SR}(t'),\tilde{\rho}(t')\rho_R(0)]]\}\,. \tag{114}$$

2.5.2 MARKOV APPROXIMATION AND LINDBLAD EQUATION

We will now consider a specific model for the interaction with the form of Eq. (50), as we did in Section 2.3. In the interaction picture, it reads:

$$\tilde{H}_{SR}(t) = i\sum_{\mathbf{k}} g_{\mathbf{k}}\left(b_{\mathbf{k}}^\dagger c e^{i(\omega_k-\omega_0)t} + b_{\mathbf{k}} c^\dagger e^{-i(\omega_k-\omega_0)t}\right) \equiv \tilde{\Gamma}^\dagger\tilde{c} + \tilde{\Gamma}\tilde{c}^\dagger \tag{115}$$

By substituting it in Eq. (114), we obtain:

$$\begin{aligned}\frac{\partial\tilde{\rho}}{\partial t} = -\int_0^t dt'\,\Big\{&\left[cc^\dagger\tilde{\rho}(t') - c^\dagger\tilde{\rho}(t')c\right]e^{-i\omega_0(t-t')}\langle\tilde{\Gamma}^\dagger(t)\tilde{\Gamma}(t')\rangle \\ &+\left[c^\dagger c\tilde{\rho}(t') - c\tilde{\rho}(t')c^\dagger\right]e^{i\omega_0(t-t')}\langle\tilde{\Gamma}(t)\tilde{\Gamma}^\dagger(t') + \text{h.c.}\Big\}\end{aligned} \tag{116}$$

where $\langle\tilde{\Gamma}^\dagger(t)\tilde{\Gamma}(t')\rangle \equiv \text{Tr}_R\{\Gamma^\dagger(t)\tilde{\Gamma}(t')\rho_R(0)\}$ and we have assumed the reservoir to be in a thermal state at temperature T (vacuum corresponding to the particular case of $T = 0$):

$$\langle b_{\mathbf{k}} b_{\mathbf{q}}\rangle = 0\,, \tag{117a}$$
$$\langle b_{\mathbf{k}}^\dagger b_{\mathbf{q}}\rangle = n_T(\omega_k)\delta_{\mathbf{k},\mathbf{q}}\,, \tag{117b}$$
$$n_T(\omega_k) = \frac{e^{-\omega_k/k_BT}}{1-e^{-\omega_k/k_BT}} \tag{117c}$$

yielding:

$$\langle\tilde{\Gamma}^\dagger(t)\tilde{\Gamma}^\dagger(t')\rangle = 0\,, \tag{118a}$$
$$\langle\tilde{\Gamma}(t)\tilde{\Gamma}(t')\rangle = 0\,, \tag{118b}$$
$$\langle\tilde{\Gamma}^\dagger(t)\tilde{\Gamma}(t')\rangle = \sum_{\mathbf{k}} g_{\mathbf{k}}^2 e^{i\omega_k(t-t')}n_T(\omega_k)\,, \tag{118c}$$
$$\langle\tilde{\Gamma}(t)\tilde{\Gamma}^\dagger(t')\rangle = \sum_{\mathbf{k}} g_{\mathbf{k}}^2 e^{-i\omega_k(t-t')}[n_T(\omega_k)+1]\,. \tag{118d}$$

MARKOV APPROXIMATION The second approximation that we make is the *Markov approximation*: it assumes that any change imprinted by the system into the reservoir trough the interaction H_{SR} is quickly lost, i.e., that the correlation functions of the reservoir, Eq. (118), decay very fast on time. The possibility of these changes affecting back S is what makes Eq. (114) non

Markovian, i.e., the evolution of $\rho(t)$ depends on its past values $\rho(t')$. If correlations are quickly lost, these changes cannot go back to S; mathematically, this amounts to replacing $\rho(t')$ by $\rho(t)$ in Eq. (114), since the integrand decays faster than the typical timescale in which $\rho(t)$ varies significantly. This yields the master equation in the Born-Markoff approximation:

$$\begin{aligned}\frac{\partial\tilde{\rho}}{\partial t} &= \mathrm{Re}\{A\}[2c^\dagger\tilde{\rho}c - cc^\dagger\tilde{\rho} - \tilde{\rho}cc^\dagger] + \mathrm{Re}\{B\}[2c\tilde{\rho}c^\dagger - c^\dagger c\tilde{\rho} - \tilde{\rho}c^\dagger c] \\ &\quad - i\,\mathrm{Im}\{A+B\}[c^\dagger c, \tilde{\rho}] \end{aligned} \tag{119}$$

with

$$A = \int_0^t d\tau \langle \tilde{\Gamma}^\dagger(t)\tilde{\Gamma}(t-\tau)\rangle e^{-i\omega_0\tau}\,, \tag{120a}$$

$$B = \int_0^t d\tau \langle \tilde{\Gamma}(t)\tilde{\Gamma}^\dagger(t-\tau)\rangle e^{i\omega_0\tau}\,. \tag{120b}$$

Taking the continuum limit (54) in Eq. (118), using the definition (58) of the spectral density, and the relationship:

$$\lim_{t\to\infty}\int_0^t e^{-i(\omega-\omega_0)\tau}\,d\tau = \pi\delta(\omega-\omega_0) + i\frac{\mathrm{P.V.}}{\omega_0-\omega}\,, \tag{121}$$

where P.V. indicates the Cauchy principal value, we obtain:

$$\mathrm{Re}\{A\} = \pi J(\omega_0)n_T(\omega_0) \tag{122a}$$

$$\mathrm{Re}\{B\} = \pi J(\omega_0)[n_T(\omega_0)+1] \tag{122b}$$

$$\begin{aligned}&\mathrm{Im}\{A+B\} = \Delta \\ &= \mathrm{P.V.}\int_0^\infty \frac{J(\omega)n_T(\omega)}{\omega_0-\omega}\,d\omega + \mathrm{P.V.}\int_0^\infty \frac{J(\omega)[n_T(\omega)+1]}{\omega_0-\omega}\,d\omega\end{aligned} \tag{122c}$$

We transform now back to the Schrodinger picture:

$$\frac{\partial\rho}{\partial t} = -i[H_S,\rho] + e^{-iH_St}\frac{\partial\tilde{\rho}}{\partial t}e^{iH_St}\,, \tag{123}$$

and use Eq.(122), together with the definition of γ of Eq. (60), to write the *master equation of a system in contact with a thermal reservoir*:

$$\begin{aligned}\frac{\partial\rho}{\partial t} &= -i[H_S,\rho] - i\Delta[c^\dagger c,\rho] \\ &\quad + \frac{\gamma}{2}[n_T(\omega_0)+1]\left(2c\rho c^\dagger - c^\dagger c\rho - \rho c^\dagger c\right) \\ &\quad + \frac{\gamma}{2}n_T(\omega_0)\left(2c^\dagger\rho c - cc^\dagger\rho - \rho cc^\dagger\right)\,.\end{aligned} \tag{124}$$

This master equation, with special emphasis on the case of a reservoir in vacuum, $n_T(\omega_0) = 0$, will be the central equation of motion which, in different variants, we solve in this Thesis. The term proportional to Δ is a Lamb shift, which we will always consider to be included in the definition of ω_0. In a system with several emitters coupled to the same reservoir, it would yield a coherent coupling between the modes; special attention must be taken then with the counter-rotating terms in the coupling Hamiltonian, that we did not consider here but that become relevant in that case [95].

THE LINDBLAD EQUATION Equation (124) has the form of a *Linblad master equation*:

$$\frac{\partial\rho}{\partial t} = -i[H,\rho] + \sum_O \frac{\Gamma_c}{2}\mathcal{L}_O(\rho)\,, \tag{125}$$

where the sum is over a set of operators O that form a linear basis in the system's Hilbert space, and $\mathcal{L}_O(\rho)$ are the so-called *Lindblad terms*:

$$\mathcal{L}_O(\rho) \equiv \left(2O\rho O^\dagger - O^\dagger O\rho - \rho O^\dagger O\right)\,. \tag{126}$$

Equation (125) describes a general, physical evolution of the density matrix; it is trace-preserving and completely positive for any initial condition. In physical terms, each Lindblad term $\mathcal{L}_c(\rho)$ accounts for some type of incoherent processes induced in the system due to its interaction with the reservoir. For instance, $O = c$ describes a leakage of excitations on mode c, which are transformed into photons of the output field. In the example of Eq. (124), this phenomenon occurs at a rate $\frac{\Gamma_c}{2} = \frac{\gamma}{2}[n_T(\omega_0+1)]$ and it is present as well when the reservoir is in vacuum, describing the *spontaneous emission* of photons into the environment. On the other hand, $O = c^\dagger$ describes an incoherent source of excitations into the system, it is dependent on the temperature, and we refer to it as *incoherent pumping*.

A **completely positive (CP) trace-preserving map** between spaces of operators are known in quantum information theory as a **quantum channel**.

In a general scenario, Γ_c and $\Gamma_{c^\dagger}$ do not need to be connected by the temperature T as in Eq. (124). For instance, in semiconductor QDs, which we theoretically described as a 2LS with annihilation operator σ, an incoherent pumping term can originate from the excitation of electron-hole pairs at higher energies, than then relax into the exciton level [174]. One then fixes independently $\Gamma_\sigma \equiv \gamma_\sigma$ an $\Gamma_{\sigma^\dagger} \equiv P$ [62, 149, 150]. Another typical Lindblad term arises from an interacting Hamiltonian of the type $H_{SR} = \Gamma^\dagger c^\dagger c + \text{h.c.}$, and it has the form $\frac{\gamma_\phi}{2}\mathcal{L}_{c^\dagger c}(\rho)$. This process is known as *pure dephasing*, and it has the effect of destroying coherences in the density matrix (off-diagonal elements) while keeping intact the populations. It typically originates from the coupling to a vibrational phonon bath. As an example, a semiconductor QD under incoherent pumping and pure dephasing could be described by the following master equation:

$$\frac{\partial\rho}{\partial t} = -i[H\rho] + \frac{\gamma_\sigma}{2}\mathcal{L}_\sigma(\rho) + \frac{P}{2}\mathcal{L}_{\sigma^\dagger}(\rho) + \frac{\gamma_\phi}{2}\mathcal{L}_{\sigma^\dagger\sigma}(\rho)\,. \tag{127}$$

2.6 COMPUTING OBSERVABLES

2.6.1 THE LIOUVILLIAN AND THE STEADY STATE

The general master equation (125) is usually expressed as:

$$\frac{\partial\rho}{\partial t} = \mathcal{L}\rho\,, \tag{128}$$

where $\mathcal{L}$ is the *Liouvillian superoperator*. In this form, the master equation finds a very simple, formal solution:

$$\rho(t) = e^{\mathcal{L}t}\rho(0)\,. \tag{129}$$

The easiest way to deal with the Liouvillian superoperator, both from a conceptual and a practical point of view, is to picture it simply as a matrix of dimension $h^2 \times h^2$, with h the dimension of the Hilbert space, acting on a ρ that has been 'flattened' to become a vector $\boldsymbol{\rho}$ of dimension h^2. It is easy to deduce from (129) that, in order for $\mathcal{L}$ to describe a physical evolution that brings the system towards a steady-state, all its eigenvalues λ_i must have a negative real part, except an eigenvalue which will be equal to zero, $\lambda_0 = 0$. The eigenstate of $\mathcal{L}$ with eigenvalue λ_0 (its *nullspace*) is indeed the steady-state of the system ρ_{SS}, since it will satisfy:

$$\mathcal{L}\rho_{SS} = 0\,. \tag{130}$$

Many of the calculations performed in this Thesis consist in the computation of such a steady-state. Once $\mathcal{L}$ has been written in matrix form and the elements of ρ_{SS} have been arranged in the shape of a vector, $\boldsymbol{\rho}_{SS}$, Eq. (130) takes the form of a linear system of equations which are, however, not independent. An efficient way of computing the steady state is to substitute any of these equations (we arbitrarily choose the first one) by the constraint $\mathrm{Tr}\{\rho_{SS}\} = 1$. This amount to changing the first row of $\mathcal{L}$ by another one with 1s in those entries $\mathcal{L}_{1,i}$ that multiply and element of the diagonal of ρ_{SS}, $\boldsymbol{\rho}_{SS,i} = \rho_{SS,kk}$, and 0s in the rest. This yields a matrix $\mathcal{M}$ that gives solution for $\boldsymbol{\rho}_{SS}$ in terms of a simple linear equation:

$$\boldsymbol{\rho}_{SS} = \mathcal{M}^{-1}\mathbf{c}\,, \tag{131}$$

with $\mathbf{c}$ and independent term simply given by $\mathbf{c} = (1, 0 \cdots, 0)$.

The numerical computation of the steady state will normally imply the truncation of a Hilbert space that, as in the case of a simple harmonic oscillator, is formally infinite. The numerical definition of the superoperator $\mathcal{L}$, which benefits greatly from its sparse nature, can be done very efficiently by using the following rule [171]:

$$\mathcal{K}\boldsymbol{\rho} = (\hat{A} \otimes \hat{B}^{\mathrm{T}})\boldsymbol{\rho} \leftrightarrow \mathcal{K}(\rho) = \hat{A}\rho\hat{B}\,. \tag{132}$$

This tells us the way in which the superoperator $\mathcal{K}(\rho)$ acting on ρ as $\hat{A}\rho\hat{B}$ is translated into a $h^2 \times h^2$ matrix that multiplies $\boldsymbol{\rho}$ in the 'vectorized' framework. This matrix is simply given by Kronecker product of the two operators. With this rule, every term in the Lindblad equation (125) can be immediately cast into this matrix form. Once the steady state density matrix ρ_{SS} has been determined, any steady state mean value of a system observable X can trivially be computed as:

$$\langle X\rangle_{SS} = \mathrm{Tr}\{X\rho_{SS}\}\,. \tag{133}$$

While this method to build $\mathcal{L}$ and get ρ_{SS} is efficient and fairly automatic, in order to compute steady state observables it is sometimes more convenient to write down the equations of motion of the observables themselves. For a general master equation such as Eq. (125), the equation of motion for $\langle X\rangle$ is given by:

$$\frac{\partial\langle X\rangle}{\partial t} = \mathrm{Tr}\left\{X\frac{\partial\rho}{\partial\rho}\right\} = -i\langle[X,H]\rangle + \sum_O \frac{\Gamma_O}{2}\left(\langle[O^\dagger,X]O\rangle + \langle O^\dagger[X,O]\rangle\right)\,.$$

(134)

This equation depends on the values of other observables of the system, defining a set of correlators whose equations of motion are coupled. While this set might be indeed infinite, there are occasions in which it is finite even if the dimension of the Hilbert space is not [58]. In that case, one can compute steady state observables exactly without resorting to any kind of truncation.

2.6.2 THE QUANTUM REGRESSION THEOREM

We have already encountered expectation values of the form $\langle A(t)B(t')\rangle$, featuring a product of operators evaluated at different times, c.f. Eq. (118). To compute these correlators in the framework of the master equation (i.e., Schrödinger picture) we recourse to a theorem routinely applied in quantum optics: *the quantum regression theorem*. In this Section we outline the derivation provided by K. Mølmer in [166].

If we consider an orthonormal set of states $\{|i\rangle\}$, any system operator A can be written as:

$$A = \sum_{ij} A_{ij} |i\rangle\langle j| \,. \tag{135}$$

We can see that the information about the system is then encoded in the expectation values $\langle |i\rangle\langle j|\rangle$, since the expectation values of any operator will be given by:

$$\langle A\rangle = \sum_{ij} A_{ij} \langle |i\rangle\langle j|\rangle \,. \tag{136}$$

We can then write the density matrix as:

$$\rho = \sum_{ij} \rho_{ij} |i\rangle\langle j| \,, \tag{137a}$$

$$\rho_{ij} = \langle |j\rangle\langle i|\rangle \tag{137b}$$

so that

$$\langle A\rangle = \mathrm{Tr}\{\rho A\} \,. \tag{138}$$

In this terms, if we define a matrix $\rho_A(t,\tau)$ as:

$$\rho_{A,ij}(t,\tau) \equiv \langle A(t)(|j\rangle\langle i|)(t+\tau)\rangle \,, \tag{139}$$

the two-time expectation value $\langle A(t)B(t+\tau)\rangle$ can be written as:

$$\begin{aligned}\langle A(t)B(t+\tau)\rangle &= \sum_{ij} \langle A(t)B_{ji}|(|j\rangle\langle i|)(t+\tau)\rangle \\ &= \sum_{ij} \rho_{A,ij}(t,\tau) B_{ji} = \mathrm{Tr}\{\rho_A(t,\tau)B\} \,.\end{aligned} \tag{140}$$

The problem reduces then to calculate the evolution of $\rho_A(t,\tau)$ as a function of τ, given by:

$$\frac{\partial}{\partial\tau}\langle A(t)(|j\rangle\langle i|)(t+\tau)\rangle = \langle A(t)\frac{\partial}{\partial\tau}(|j\rangle\langle i|)(t+\tau)\rangle\,. \tag{141}$$

Let us now write the evolution of the density matrix, Eq. (128), as:

$$\frac{\partial\rho_{ij}}{\partial t} = \sum_{mn}\mathcal{L}_{ij,mn}\rho_{mn}\,. \tag{142}$$

This means that, to keep consistency with Eq. (137), the evolution of the operators $(|j\rangle\langle i|)(t)$ must be:

$$\frac{\partial}{\partial t}(|j\rangle\langle i|)(t) = \sum_{mn}\mathcal{L}_{ij,mn}(|n\rangle\langle m|)(t) + F_{ji}(t)\,, \tag{143}$$

where $F_{ij}(t)$ are operators with expectation value equal to zero. The presence of these operators originates from the coupling to the reservoir, and though they do not appear in the master equation due to the zero mean, they are necessary to preserve relations between products of operators such as commutators. They are the analogue to the noise terms in the Langevin equations, and as such, are a manifestation of the fluctuation dissipation theorem.

The **fluctuation dissipation theorem** establishes that any kind of damping must also have associated some sort of diffusion.

By substituting Eq. (143) in (141), those terms involving the average of F_{ij} disappear by assuming that $\langle A(t)F_{ji}(t+\tau)\rangle = \langle A(t)\rangle\langle F_{ji}(t+\tau)\rangle = 0$, leaving:

$$\frac{\partial}{\partial\tau}\langle A(t)(|j\rangle\langle i|)(t+\tau)\rangle = \sum_{mn}\mathcal{L}_{ij,mn}\langle A(t)(|n\rangle\langle m|)(t+\tau)\rangle \quad (\tau\geq 0)\,, \tag{144}$$

or, in short:

$$\frac{\partial}{\partial\tau}\rho_{A,ij}(t,\tau) = \sum_{mn}\mathcal{L}_{ij,mn}\rho_{A,mn}(t,\tau) \quad (\tau\geq 0)\,. \tag{145}$$

This means that $\rho_A(t,\tau)$ follows the same dynamical equation as the density matrix, but starting from a different initial state, given by:

$$\rho_A(t,0) = \langle A(t)(|j\rangle\langle i|)(t)\rangle = \mathrm{Tr}\{\rho A(|j\rangle\langle i|)\} = \rho A \tag{146}$$

and, from Eq. (140), the two-time expectation value is given by:

$$\langle A(t)B(t+\tau)\rangle = \mathrm{Tr}\left\{Be^{\mathcal{L}\tau}[\rho(t)A]\right\}\,. \tag{147}$$

The two-time correlation can then be obtained form the knowledge of $\mathcal{L}$ alone, without any information on the noise operators F_{ij}. This is the Quantum Regression Theorem. It is important to note that expression (147) is for

positive τ only; for $\tau < 0$ we cannot assume that $A(t)$ and $F_{ji}(t+\tau)$ are uncorrelated. We can however repeat the argument for an analogue correlator of the form $\langle A(t+\tau)B(t)\rangle$, for $\tau > 0$, which yields:

$$\langle A(t+\tau)B(t)\rangle = \mathrm{Tr}\left\{ Ae^{\mathcal{L}\tau}[B\rho(t)]\right\} . \tag{148}$$

This argument can be extended to multiple times, giving:

$$\langle A(t_3)B(t_2)C(t_1)\rangle = \mathrm{Tr}\left\{ Ae^{\mathcal{L}(t_3-t_2)}\left[Be^{\mathcal{L}(t_2-t_1)}[C\rho(t_3)\right]\right\} \tag{149}$$

for $t_3 > t_2 > t_1$. Another type of correlator that we will usually encounter is of the form $\langle A(t)B(t+\tau)C(t)\rangle$, which applying the quantum regression theorem reads:

$$\langle A(t)B(t+\tau)C(t)\rangle = \mathrm{Tr}\left\{ Ae^{\mathcal{L}(\tau)}[C\rho(t)B]\right\} . \tag{150}$$

2.6.3 THE FLUORESCENCE SPECTRUM

One of the immediate applications of the quantum regression theorem is the calculation of the spectrum of the light emitted by the system. In 1977, Eberly and Wódziewicz considered the problem of defining a time-dependent spectrum $S(\omega,t)$ of a non-stationary field $E(t)$ [73], a subtle problem given that one aims to retain the dependence on two conjugate variables, frequency and time. In the experiment, the dependence on both time and frequency can be retained because the filter has a finite linewidth, meaning that frequency is not perfectly determined and, therefore, time is not completely undetermined. One is forced the include this indeterminacy in the theory as well, which amounts to working with a filtered version of the field. The standard choice is a Lorentzian filter, that gives, in the frequency domain, a frequency-filtered field $E_{\omega_0,\Gamma}(\omega)$:

$$E_{\omega_0,\Gamma}(\omega) \equiv H(\omega;\omega_0,\Gamma)E(\omega) , \tag{151}$$

with $H(\omega;\omega_0,\Gamma)$ the function of a filter of linewidth Γ, centered at ω_0

$$H(\omega,\omega_0,\Gamma) = \frac{(\Gamma/2)e^{i\omega_0}}{\Gamma/2 - i(\omega-\omega_0)} . \tag{152}$$

By Fourier transforming $E_{\omega_0,\Gamma}(\omega)$ back to the time domain, we get the frequency and time dependent filtered field:

$$E_{\omega_0,\Gamma}(t) = \frac{\Gamma}{2}\int_0^\infty e^{-(i\omega_0+\Gamma/2)t'}E(t-t')\,dt' , \tag{153}$$

from which the time-dependent spectrum is then obtained:

$$\begin{aligned} S_\Gamma(\omega,t) &\equiv \langle E^*_{\omega,\Gamma}(t)E_{\omega,\Gamma}(t)\rangle \\ &= \left(\frac{\Gamma}{2}\right)^2 \int_0^\infty\int_0^\infty e^{(i\omega_0-\Gamma/2)t_1}e^{(i\omega_0-\Gamma/2)t_2}\langle E^*(t-t_1)E(t-t_2)\rangle\,dt_1dt_2 . \end{aligned} \tag{154}$$

In most occasions, we will consider limit of a steady state spectrum:

$$S(\omega) \equiv \lim_{\substack{\Gamma\to 0\\ t\to\infty}} S_\Gamma(\omega, t)\,, \tag{155}$$

and by means of the association $E^+(t) \propto a(t)$ that we discussed in Section 2.3.2, we will describe the fluorescence spectrum of the light emitted by the mode a as:

$$S(\omega) = \frac{1}{\pi}\,\mathrm{Re}\int_0^\infty e^{i\omega\tau}\langle a^\dagger(0)a(\tau)\rangle d\tau\,, \tag{156}$$

which is has the form given by the *Wiener-Khinchine theorem* [73, 160, 235] and is normalized to the steady state population of the mode:

$$\int_{-\infty}^{\infty} S(\omega)\,d\omega = \langle a^\dagger a\rangle = \mathrm{Tr}\left\{a^\dagger a\rho_{\mathrm{SS}}\right\}\,. \tag{157}$$

CALCULATION OF THE SPECTRUM By means of the quantum regression theorem, Eq. (146), we can express the spectrum as:

$$S(\omega) = \frac{1}{\pi}\,\mathrm{Re}\,\mathrm{Tr}\left\{\int_0^\infty e^{i\omega\tau} a e^{\mathcal{L}\tau}[\rho_{\mathrm{SS}}a^\dagger]\right\}\,. \tag{158}$$

The evolution given by $\mathcal{L}$ is trace-preserving, so for any value of τ, we must always have

$$\mathrm{Tr}\left\{e^{\mathcal{L}\tau}[\rho_{\mathrm{SS}}a^\dagger]\right\} = \mathrm{Tr}\left\{\rho_{\mathrm{SS}}a^\dagger\right\} = \langle a^\dagger\rangle\,. \tag{159}$$

On the other side, in the limit $\tau\to\infty$, the result of the evolution of $\rho_{\mathrm{SS}}a^\dagger$ by the action of $\mathcal{L}$ must be proportional to ρ_{SS}, which is the eigenstate of $\mathcal{L}$ of eigenvalue 0. Therefore, we find:

$$\lim_{\tau\to\infty} e^{\mathcal{L}\tau}[\rho_{\mathrm{SS}}a^\dagger] = \langle a^\dagger\rangle\rho_{\mathrm{SS}}\,. \tag{160}$$

We can then formally integrate Eq. (158) to obtain:

$$S(\omega) = \frac{1}{\pi}\,\mathrm{Re}\,\mathrm{Tr}\left\{-a\frac{1}{\mathcal{L}+i\omega}\left[\rho_{\mathrm{SS}}\left(a^\dagger - \langle a^\dagger\rangle\right)\right]\right\} + S_c(\omega)\,. \tag{161}$$

where

$$S_c(\omega) = \delta(\omega)|\langle a\rangle|^2 \tag{162}$$

is the *coherent component* of the spectrum. In the following we will omit this term, since the first is the one that contains all the non-trivial information of the quantum dynamics of the system.

In this form, the calculation of $S(\omega)$ requires the evaluation of the inverse of $\mathcal{L}+i\omega$ for each ω that we choose. Since we are interested in a whole range of ω, for computational purposes it is more convenient to write the inverse in terms of the diagonalized Liouvillian $-\mathcal{D}$, which satisfies:

$$-\mathcal{D} = \mathcal{E}^{-1}\mathcal{L}\mathcal{E}\,, \tag{163}$$

where $\mathcal{E}$ is the matrix of eigenvectors of $\mathcal{L}$. One then has:

$$e^{\mathcal{L}\tau} = -\mathcal{E}e^{\mathcal{D}\tau}\mathcal{E}^{-1} \tag{164}$$

and the formal integration of the spectrum yields:

$$S(\omega) = \frac{1}{\pi}\,\mathrm{Re}\,\mathrm{Tr}\left\{a\mathcal{E}\frac{1}{\mathcal{D}-i\omega}\mathcal{E}^{-1}\left[\rho_{\mathrm{SS}}\left(a^\dagger - \langle a^\dagger\rangle\right)\right]\right\} \tag{165}$$

We have thus translated the problem to computing the eigenvectors $\mathcal{E}$, but now it needs to be done only once. In the 'vectorized' framework, we write $\rho_{\mathrm{SS}}(a^\dagger - \langle a^\dagger\rangle)$ as a vector $\boldsymbol{\rho}_A$, such that the product of a inside the trace is another vector:

$$\mathcal{E}\frac{1}{\mathcal{D}-i\omega}\mathcal{E}^{-1}\boldsymbol{\rho}_A \equiv \boldsymbol{\xi}\,. \tag{166}$$

Now, taking h as the size of the truncated Hilbert space, we can recast this vector again into matrix form:

$$M_{mn} \equiv \xi_{h(m-1)+n}\,, \tag{167}$$

and express the spectrum as:

$$S(\omega) = \frac{1}{\pi}\,\mathrm{Re}\,\mathrm{Tr}\left\{Ma\right\}\,. \tag{168}$$

It is easy to see that ξ_α is given by:

$$\xi_\alpha = \sum_\beta Q_{\alpha\beta}\frac{1}{\lambda_\beta - i\omega}\,, \tag{169}$$

with $\lambda_\beta \equiv \mathcal{D}_{\beta,\beta}$ the β-th eigenvalue of $\mathcal{L}$, and

$$Q = \mathcal{E}\,\mathrm{diag}\left(\mathcal{E}^{-1}\boldsymbol{\rho}_A\right)\,. \tag{170}$$

The spectrum is thus given by:

$$S(\omega) = \frac{1}{\pi}\,\mathrm{Re}\sum_\beta\sum_{k,n}\frac{Q_{h(k-1)+n,\beta}a_{nk}}{\lambda_\beta - i\omega}\,, \tag{171}$$

which can be written in a more illustrating way:

$$S(\omega) = \frac{1}{\pi}\sum_\beta\left[\frac{(\gamma_\beta/2)L_\beta}{(\omega-\omega_\beta)^2 + (\gamma_\beta/2)^2} - \frac{(\omega-\omega_\beta)K_\beta}{(\omega-\omega_\beta)^2 + (\gamma_\beta/2)^2}\right]\,, \tag{172a}$$

$$\omega_\beta \equiv \mathrm{Im}\{\lambda_\beta\}\,, \tag{172b}$$

$$\gamma_\beta \equiv 2\,\mathrm{Re}\{\lambda_\beta\}\,, \tag{172c}$$

$$L_\beta \equiv \mathrm{Re}\{Z_\beta\}\,, \tag{172d}$$

$$K_\beta \equiv \mathrm{Im}\{Z_\beta\}\,, \tag{172e}$$

$$Z_\beta \equiv \sum_{kn}^{h} Q_{h(k-1)+n,\beta}a_{nk}\,. \tag{172f}$$

This tells us that the fluorescence spectrum is made of a sum of Lorentzian shapes, centered at a frequency given by the imaginary part of the Liouvillian eigenvalues and with a linewidth given by their real part. The weight of each the Lorentzian is given by L_β, such that the integrated spectrum is:

$$\int S(\omega)\, d\omega = \sum_\beta L_\beta\,, \tag{173}$$

and each of them has a *dispersive term* proportional to K_β that breaks the symmetry of the Lorentzian around ω_β.

3

THE COLORED HANBURY BROWN-TWISS EFFECT

Color is my daylong obsession, joy, and torment.
— Claude Monet

3.1 INTRODUCTION

Is light ultimately a wave, or a particle? This question has been the focus of one of the longest debates in scientific history, with successive new discoveries, such as Newton's corpuscle theory, Huygens' wavefronts, Maxwell's findings on electromagnetism, Young's double slit interference, or the photoelectric effect, that seemed to balance alternatively the discussion in favour of one of the two views. The last of these discoveries was the Hanbury Brown-Twiss effect, evidenced by Robert Hanbury Brown and Richard Twiss in the late 1950s. In a time when wave-particle duality was already a well established concept, and the nature of light was apparently perfectly understood, the discovery of correlations between independently emitted photons, clear from the wave standpoint, offered a last challenge to the understanding of light as an ensemble of quantum particles. These observations kindled a discussion that would culminate with the refined development of the idea of coherence by Roy. J. Glauber and the birth of the field of quantum optics.

This Chapter focuses on the theoretical description of a pioneering experiment studying frequency-resolved correlations between photons. This experiment has revealed that, in contrast to what Hanbury Brown and Twiss observed in the 1950s, when light within a single spectral peak is frequency-filtered, photons of different frequencies show a tendency to avoid each other. The theoretical results of this Chapter evidence that this behaviour does not correspond to any particular feature of the light source but, on the contrary, constitute a fundamental phenomenon that extends the seminal observations of Hanbury Brown and Twiss to the full color domain.

The results exposed in this chapter are published Scientific Reports [211**?**].

3.1.1 THE INTENSITY INTERFEROMETER

At the end of World War II, radar technology, initially conceived for military purposes, started being applied to more pacific endeavours. In particular, the development in the detection of radio waves—originally intended to detect

Radio sources are astronomical objects that emit strong radio waves, and represent some of the most violent and energetic physical events on the universe.

reflected waves from distant, metallic objects such as planes—opened the way for the observation of previously unknown stellar objects known as radio sources, leading to the birth of radio astronomy.

The first problem faced by radio astronomers was to determine the size of the new, bright radio stars that were being discovered, such as Cassiopeia A and Cygnus A. Working on this question, Hanbury Brown made the following observation:

Robert Hanbury Brown (1916-2002) was a British scientist born in Aruvankadu, India. He played a crucial role in the development of the airbone radar. His most important contributions are the ones discussed in this section: the development of the intensity interferometer and the discovery of the Hanbury Brown-Twiss effect.

"If the radiation received at two places is mutually coherent, then the fluctuation in the intensity of the signals received at those two places is also correlated" [101].

Based on this insightful realization, and with the mathematical aid of his collegue Richard Twiss, Hanbury Brown led the development of completely new kind of interferometer: the *intensity interferometer*. In this kind of device, light coming from a given source is detected by two different detectors, and their intensities are correlated, in contrast to the Michelson interferometer, in which light is first made to interfere and then collected on a single detector.

To understand the working principle behind intensity interferometry, and the comparison with the usual phenomenon of optical interference, we will consider the case depicted in Fig. 3.1: two light sources S1 and S2 and two detectors D_1 and D_2, with d_S the distance between the sources, and d_D the distance between the detectors. We will assume that the distance between sources and detectors, L, is much larger than d_S and d_D. If the source S_i emits a spherical electromagnetic wave of amplitude a_i, wavevector k and phase ϕ_i, the total amplitude of the electric field at detector D_i is approximately given by:

$$E_i = \frac{1}{L}\left(a_1 e^{ik\,r_i + i\phi_1} + a_2 e^{ik\,r_i' + i\phi_2}\right), \tag{174}$$

where $i \in \{1,2\}$, $r_i = |\mathbf{r_i}|$, and $\mathbf{r_i}$ are the distances defined in Fig. 3.1.

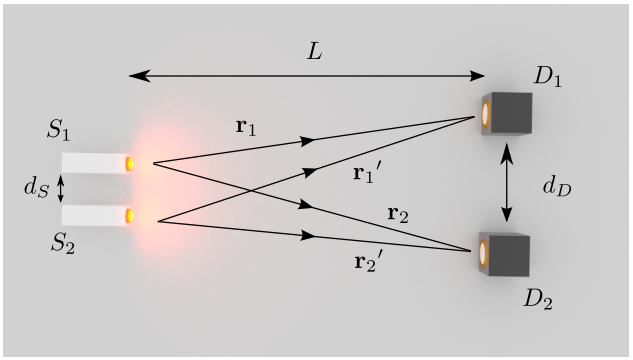

Figure 3.1: Schematic view of a Hanbury Brown and Twiss experiment. Light coming from two sources falls into two detectors D1 and D2. The intensities of the light fields detected at D1 and D2 are then correlated.

The intensity in each of the detectors will therefore be given by:

$$I_i = |E_i|^2 = \frac{1}{L^2}\left[|a_1|^2 + |a_2|^2 + \mathrm{Re}\left(a_1^* a_2 e^{ik(r_1' - r_1) + i(\phi_2 - \phi_1)}\right)\right] \tag{175}$$

This equation describes the conventional spatial interference pattern in the intensity of the light field typically discussed in classical optics. It requires a

fixed phase relationship between the two fields, which is usually achieved by splitting a quasi-monochromatic field in parts that are later recombined to interfere. Despite the theoretical simplicity of its description, the observation of this direct interference between the light coming from two *independent* sources could not be observed until the development of the laser in the 1960s, which provided for the first time a source of *coherent* light whose amplitude and phase remains constant for a time long enough to be measured.

A **laser** (acronym for "light amplification by stimulated emission of radiation") was built for the first time in 1960 by Theodore H. Maiman at Hughes Research Laboratories, based on the theoretical work of Charles Hard Townes and Arthur Leonard Schawlow.

If, on the contrary, the fields would have unstable, fluctuating phases, these interference fringes would no longer be visible. We can easily prove this by considering the phases ϕ_i as quantities that vary randomly in time, so that every physical observable of the electric field that depends on the phase $O(\phi_i)$ has to be regarded as a stochastic variable. The quantities of interest are then the expectation values $\langle O(\phi_i)\rangle$, given by averaging $O(t)$ over many stochastic realizations of the phase evolution or, in a steady state, by averaging it over time. Under a random evolution of the phase with zero mean value, $\langle \phi_i \rangle$, the averaged intensity of Eq. (175) takes the form:

$$\langle I_1 \rangle = \langle I_2 \rangle = \frac{1}{L^2}(|a_1|^2 + |a_2|^2). \tag{176}$$

Interestingly, even in situations in which no interference pattern can be observed in the intensities themselves, the measurement of intensity correlations, defined as the average of the product of intensities $\langle I_1 I_2 \rangle$, can reveal that interference has actually taken place. It is easy to demonstrate this mathematically: if we perform the average $\langle I_1 I_2 \rangle$ using Eq. (175) we are left with a non-vanishing interference term,

$$\langle I_1 I_2 \rangle = \frac{1}{L^4}\left\{|a_1|^4 + |a_2|^4 + 2|a_1|^2|a_2|^2[1 + \cos[k(r_1 - r_2 - r_1{}' + r_2{}'))]\right\}, \tag{177}$$

that depends on the separation between the two sources. This interference term, the basis of the intensity interferometer, is also of a lower frequency and more robust to atmospheric effects as compared to the Michelson interferometer [209].

The first realization of an intensity interferometer was in the early 1950s [37], when Hanbury Brown and Twiss measured the diameter of several radio sources using two radio telescopes. Radio waves coming from a star have an approximately constant amplitude and phase on a certain coherence area at a given time, and, as originally noted by Hanbury Brown, the output signal of two detectors placed within this area will be correlated, see Fig. 3.2. When the separation between the detectors increases, the signals recorded by both of them become less correlated, reaching a point, when the distance between them is larger than the *transverse coherence length*, where they fluctuate independently. From this transverse coherence length one can infer the apparent size of the star.

In the optical domain, the first evidence of the interference of light coming from independent sources was provided by Forrester, Gudmundson and

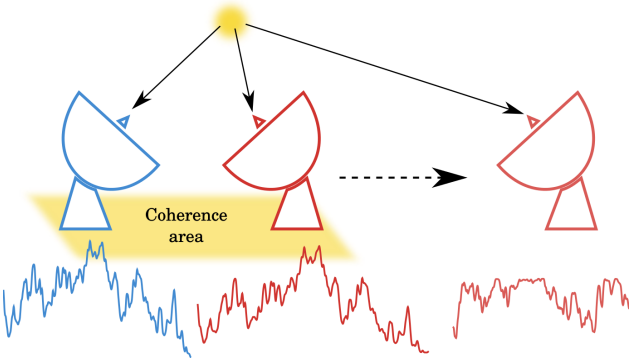

Figure 3.2: Working principle of Hanbury Brown and Twiss's stellar interferometer. The curves corresponds to the intensity measured by the detectors as a function of time: when the detectors do not fall within the same coherence area, the fluctuations of their output signals are not correlated.

Johnson in 1955, in a pioneering experiment that measured the beating between two spectral components of the light emitted from a thermal source [82]. More importantly, they demonstrated that the delay between photon absorption and electron emission in the photodetectors was small enough to follow the rapid fluctuations of the light intensity, which allowed to measure intensity correlations in the optical domain. This was precisely what Hanbury Brown and Twiss decided to do in order to test the working principle of the new interferometer with visible light. Certainly, if it worked for electromagnetic waves at radio frequency, it should work as well at optical frequencies. However, scientists had got used to think of visible light as composed of photons (contrary to the case of radio waves, that nobody regarded as an ensemble of photons, even if they are). Because of this, the idea of Hanbury Brown and Twiss found a strong opposition when it was applied to the optical domain; the principle behind their device challenged the physical understanding of some of the brightest minds of the time, who still had very present Dirac's words from his celebrated textbook on quantum mechanics:

"Each photon then interferes only with itself. Interference between different photons never occurs" [71].

Thinking in term of quantum particles, it was indeed difficult to understand that photons emitted from independent atoms of the surface of a star could show any tendency to arrive together to two photodetectors placed within a certain coherence area. The opposition that Hanbury Brown and Twiss faced was so fierce that, in the own words of Hanbury Brown: *"If science had a Pope, we would have been excommunicated"* [101]. Despite the experiment of Forrester, Gudmundson and Johnson (1955) [82] had already proved the optical mixture between independent photons, Dirac's words were definitely challenged by the experiment performed by Hanbury Brown and Twiss in 1956 [102] in which, in order to demonstrate that the working principle of their interferometer held in the visible domain, they measured the correlated arrival of photons emitted from a thermal source. They described this source as *coherent*, meaning quasi-monochromatic, since this was before the change in the terminology of coherence introduced by Glauber. The experiment they devised unveiled a fundamental phenomenon, the *Hanbury Brown-Twiss effect*, that eventually led to the birth of quantum optics, and the experimen-

tal configuration that they devised, *the Hanbury Brown and Twiss setup* (see Fig. 3.3), became an ubiquitous experiment in the field.

3.1.2 THE HBT EFFECT: PHOTON BUNCHING

The HBT experiment analyzed the intensity correlations on the light emitted by a mercury arc (that can be regarded as a thermal source). This time, the two detectors were placed at the outport ports of a beam splitter that divided a single light beam coming from the source, previously filtered to achieve a monochromatic field. If the length of the two output paths were made equal, the detected signals should be the same and the fluctuations would therefore be correlated. As the path lengths become different, one would study the correlations between the signal and itself at different times, and it would become less correlated; the experiment can indeed be equally understood by considering the time correlations of the intensity measured by a single detector. The fact that the signals are correlated when there are zero delay seemed surprising when one thought in term of photons: it implied that photons emitted from a thermal source show a tendency to arrive together to the detectors, the so called *photon bunching effect*.

This effect was again easy to understand when thinking of light in classical terms, but difficult to believe for many if one pictured it in terms of photons emitted by independent atoms. A subsequent work by Brannen and Ferguson [36] tried to disprove it with an experiment that, as later noted by HBT themselves [103], lacked the sensitivity to reveal the phenomenon. The atmosphere of confusion regarding the effect is well summarized by the following sentence from the paper of Brannen and Ferguson: *"(...) if such a correlation did exist, it would call for a major revision of some fundamental concepts in quantum mechanics"*.

THE CLASSICAL VIEW From a classical point of view, the origin of the correlations observed by HBT is clear. We can consider thermal/chaotic light as a sum of the electric fields emitted by N radiating atoms; the field $E_i(t)$ emitted by the i-th atom is written as:

$$E_i(t) = E_0 e^{i\omega_0 t + \phi_i(t)}. \tag{178}$$

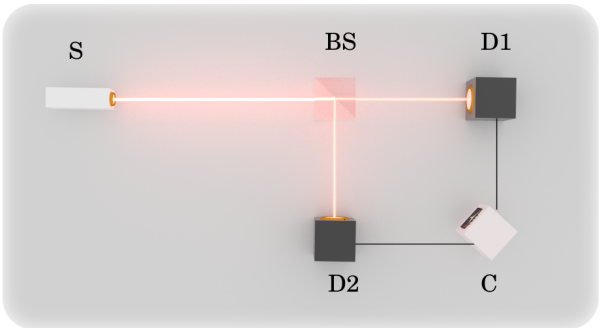

Figure 3.3: Schematic view of a typical Hanbury Brown and Twiss setup. A light beam is separated on a beam splitter (BS) and directed into two detectors D1 and D2. The intensities of the light fields detected at D1 and D2 are correlated at C.

Here, the phase $\phi_i(t)$ is a stochastic variable that changes randomly, due for instance to atomic collisions (see Fig. 3.4). The total electric field is then given by:

$$E(t) = \sum_{i=1}^{N} E_i(t) = E_0\, e^{-i\omega_0 t}\left[\sum_{i=1}^{N} e^{i\phi_i(t)}\right] = E_0\, e^{-i\omega_0 t} a(t) e^{i\psi(t)}\,. \quad (179)$$

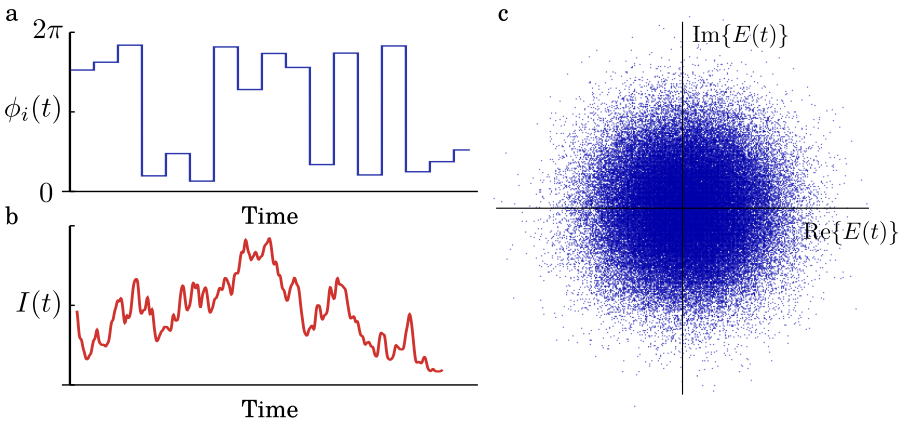

Figure 3.4: Chaotic electrif field. a, Stochastic dynamics of the phase $\phi_i(t)$ of the light emitted by an individual atom.**b**, Fluctuating intensity of a chaotic field $E(t)$. **c**, Distribution of chaotic light in phase space, each point representing the value of the electric field at a given time.

It is easy to see that the intensity of the total field $I(t) = E^*(t)E(t)$ fluctuates around the mean value $\bar{I} = N\,E_0$ as given by the stochastic amplitude term $a(t)$. The origin of this term is the interference between all the atomic contributions to the field, and the effect of this interference is to decrease the intensity of the field with respect to the mean value at some times, and increase it at other, effectively cluttering the field and originating the bunching effect.

THE QUANTUM VIEW The description of the effect from the quantum point of view was insightfully explained by Purcell [191], settling the argument that had took place during 1956. When considering Dirac's words (*"a photon interferes only with itself"*), one must bear in mind that "itself" is ill defined when the photons involved are indistinguishable. In this case, it is well known that exchange degeneracy gives rise to interference effects in which it is twice as likely to find two identical Bose particles together as it would be if we calculated that probability considering independent particles. This is the quantum-mechanical origin of the effect observed by HBT, and the fact that it can be perfectly described by classical theory shows that the principle of superposition in classical electromagnetism is ultimately a manifestation of the bosonic character of photons.

Exchange degeneracy refers to fact that all kets of the form $c_1|\phi_1,\phi_2\rangle + c_2|\phi_2,\phi_1\rangle$ give the same set of eigenvalues when measurement is performed.

3.1.3 MEASURING THE CORRELATIONS: SECOND ORDER CORRELATION FUNCTION

The calculations of Purcell indicated that the positive correlations would be clearer using a more monochromatic source (as will be discussed later). This posed the question, after the development of the laser on the 1960s, whether the correlations observed by HBT would also be present on these highly stable, monochromatic light beams, generated by strong polarization currents that were known to emit Poissonian distribution of photons (henceforth, statistically independent) [92]. In order to answer that question, in an effort that awarded him a Nobel Prize in 2005, Roy. J. Glauber formalized the theory of optical coherence by defining rigorously the quantity describing the counting measurements of HBT: the *second-order correlation function* $g^{(2)}$, defined as:

$$g^{(2)}(t,\tau) = \frac{\langle \hat{E}^-(t)\hat{E}^-(t+\tau)\hat{E}^+(t+\tau)\hat{E}^+(t)\rangle}{\langle \hat{E}^-(t)\hat{E}^+(t)\rangle\langle \hat{E}^-(t+\tau)\hat{E}^+(t+\tau)\rangle}\,, \tag{180}$$

with $\hat{E}^{\pm}(t)$ the negative/positive frequency part of the Heisenberg electric field operator at time t and τ the time delay between detections (omitting position dependence for simplicity). Now a central quantity in quantum optics, it describes the statistical distribution between photons in their stream of temporal detection. In a steady state, this quantity is independent of t:

$$g^{(2)}(t,\tau) = g^{(2)}(\tau)\,. \tag{181}$$

In that situation, we will use in this text the following terminology for its value at zero delay:

$$g^{(2)} \equiv g^{(2)}(\tau = 0)\,. \tag{182}$$

The generalization of this quantity to higher orders, $g^{(n)}$, follows straightforwardly. The work of Glauber evidenced that the condition of coherence in the usual optical sense, $g^{(1)} = 1$, which is related to the monochromaticity of the field, should extent to all orders, $g^{(n)} = 1$. When $g^{(2)}$ takes values larger than 1, it describes the tendency of photons to arrive together to the detectors, the bunching effect observed by HBT. On the other hand, values lower than 1 would indicate a tendency of photons to not arrive to the detectors at the same time, a feature arising from the particle nature of light that, as will be explained in detail in Section 4.4.1, cannot be reproduced by any classical field. The measurement of a $g^{(2)}$ lower than 1 in the resonance fluorescence of atoms can be regarded as the first direct evidence of the existence of the photon [135].

Figure 3.5: Visualization of **coherent**, **bunched** and **antibunched** light, according to the statistical distribution of photon detection times.

3.1.4 FREQUENCY-RESOLVED CORRELATIONS: THE TWO-PHOTON SPECTRUM

Some elements of the previous discussion suggest the important role that the spectral structure of light has on its own temporal correlations. Purcell already included the finite line-shape of light as a fundamental element of his description, and the implications for extremely monochromatic lasers was the motivation behind the theoretical developments of Glauber. This Chapter revolves around a quantity that explicitly takes into account the frequency of the light: the *frequency resolved correlation function*, i.e., the second order correlation between photons having two specific energies. The idea behind the measurement of this quantity is summarized in Fig. 3.6; it extends the standard HBT setup, that just provides the temporal correlations within a light beam, by placing different filters in each of the output arms of the beam splitter, measuring instead the correlations between different spectral components.

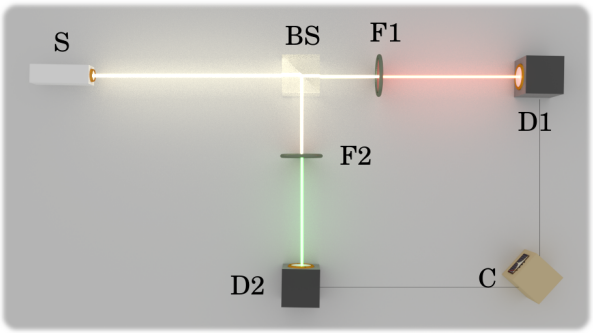

Figure 3.6: Scheme for the measurement of frequency resolved correlations: a different filter is placed in each of the arms of the HBT setup, so that correlations are measured between light of different spectral windows.

Since time and frequency are conjugate variables, by retaining the energy degree of freedom one performs a characterization of a fundamentally different type than, for instance, tracking position or polarization. If we are able to tell the precise time at which a photon has been detected, it will be impossible to specify its frequency, and viceversa. From a physical point of view, this limitation is easy to understand if one pictures a filter as an optical cavity with a certain linewidth. If the cavity is placed on the path followed by a stream of photons, only those that are resonant with it will be able to enter and eventually cross to the other side, and their frequency will be perfectly specified. However, the narrower the linewidth of the cavity is, the more time will the photon spend inside it, increasing the time uncertainty in its detection.

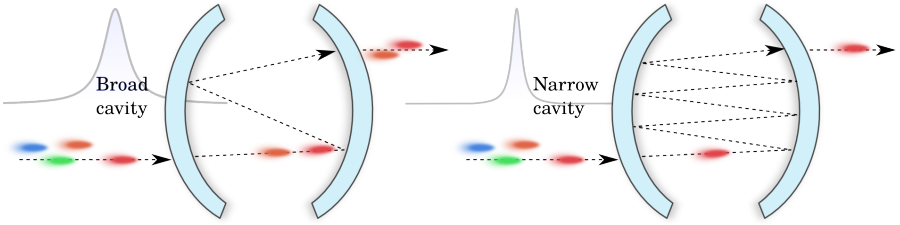

Figure 3.7: Illustration of the time-frequency uncertainty in terms of a filter made of an optical cavity.

The fundamental problem of describing a frequency and time-dependent field like the one we would obtain in front of a frequency filter was tackled by Eberly and Wódkiewicz in 1977 [73]; the solution amounts to include the filter in the description, which is both a physical and mathematical necessity to describe a frequency-time dependent field. The electric field after passing through a Lorentzian filter with frequency component ω_i and width Γ at time t_i takes the form:

$$\hat{E}_{\omega_i,\Gamma}(t_i) = \frac{\Gamma}{2}\int_0^\infty e^{-i\omega_i t} e^{-\Gamma t/2}\hat{E}(t_i - t)\, dt\,. \tag{183}$$

This expression for the field can now be used to compute the frequency-resolved correlations that we would measure with the setup of Fig. 3.6. The formal theory of time and frequency resolved correlations was established in the 80s [50, 56, 138, 176], and it upgrades Eq. (180) to the *second order frequency-resolved correlation function*:

$$g^{(2)}_\Gamma(\omega_1, t_1; \omega_2, t_2) = \frac{\langle : \mathcal{T}\left[\prod_{i=1}^2 \hat{E}_{\omega_i,\Gamma}(t_i)\hat{E}^+_{\omega_i,\Gamma}(t_i)\right] : \rangle}{\prod_{i=1}^2 \langle \hat{E}_{\omega_i,\Gamma}(t_i)\hat{E}^+_{\omega_i,\Gamma}(t_i)\rangle}\,, \tag{184}$$

now using the frequency-filtered field (183), and where $\mathcal{T}$, (resp. :) refers to time (resp. normal) ordering. Equation (184) provides the tendency of a correlated detection of one photon of frequency ω_1 at time t_1 with another photon of frequency ω_2 at time t_2. In this work, we will only consider Lorentzian filters, which in the time domain corresponds to the exponential functions of Eq. (183). However, our discussion applies to other types, such as square filters [126].

In the steady state, this quantity depends only on $\tau = t_1 - t_2$:

$$g^{(2)}_\Gamma(\omega_1, \omega_2; \tau), \tag{185}$$

and for the case of zero delay we will adopt the following notation:

$$g^{(2)}_\Gamma(\omega_1, \omega_2) \equiv g^{(2)}_\Gamma(\omega_1, \omega_2; \tau = 0)\,. \tag{186}$$

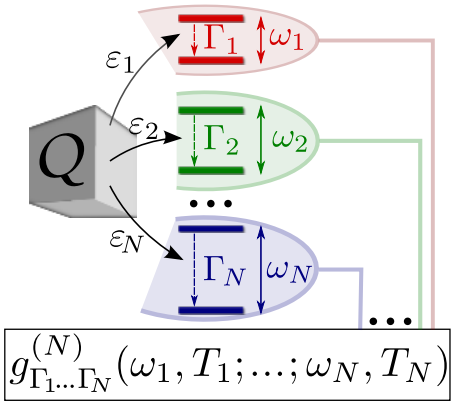

Figure 3.8: Method of sensors for the computation of frequency-resolved correlations. The system Q is weakly coupled to a set of N sensors, described as two-level systems with frequencies ω_i and decay rates Γ_i that account for the frequency and linewidth of the filters. In the limit of small coupling rates ϵ_i, their correlations allow to recover the N-th order, frequency resolved correlation function.. Image from [67].

COMPUTATION OF FREQUENCY-RESOLVED CORRELATIONS From the theoretical point of view, the calculation of this quantity and its generalization to higher orders turned out to be quite demanding. In 2012, Elena del Valle *et. al.* [67] developed a method that allow to compute it efficiently and easily for any order and time delay. This theory establishes that frequency-resolved correlations of the light emitted by any open quantum-system are the same as the correlations between "sensors" at these frequencies (see Fig. 3.8). These sensors are bosonic, commuting modes with annihilation operator ς_i, $i = 1, 2$, free energy ω_i and decay rate Γ_i—accounting for the frequency linewidth of the sensors—that are weakly coupled with a small coupling constant ε to the emitting mode, described by the annihilation operator a. They are included in the dynamics by the Hamiltonian term $H_S = \sum_i \omega_i \varsigma_i^\dagger \varsigma_i + \varepsilon(\varsigma_i^\dagger a + \varsigma_i a^\dagger)$ and Lindblad terms $\frac{\Gamma}{2}\sum_i \mathcal{L}_{\varsigma_i}\rho$. For instance, frequency-resolved correlations at zero delay are then computed as:

$$g_\Gamma^{(2)}(\omega_1, \omega_2) = \lim_{\varepsilon \to 0} \frac{\langle \varsigma_1^\dagger \varsigma_2^\dagger \varsigma_2 \varsigma_1 \rangle}{\langle \varsigma_1^\dagger \varsigma_1 \rangle \langle \varsigma_2^\dagger \varsigma_2 \rangle} \,. \tag{187}$$

In practice, since the coupling to the sensors must be very small so they do not affect the dynamics of the system, they have a negligible population and can be described as two-level systems.

Many measurements of frequency-resolved correlations have been performed for fixed sets of frequencies, merely by inserting filters in the paths of a standard Hanbury Brown–Twiss setup [7, 70, 109, 127, 199, 227]; however, this new computational technique [67] allowed to reveal the conceptual importance of this measurement by spanning over all possible combination of energies, giving rise to a so-called *two-photon correlation spectrum* (2PS) [96, 186].

Considering the most common case of coincidences—$\tau = 0$ in Eq. (180) and $t_1 = t_2$ in Eq. (184)—one elevates in this way a single number, $g^{(2)}$, to a full landscape $g_\Gamma^{(2)}(\omega_1, \omega_2)$ of correlations. The quantity defined by such

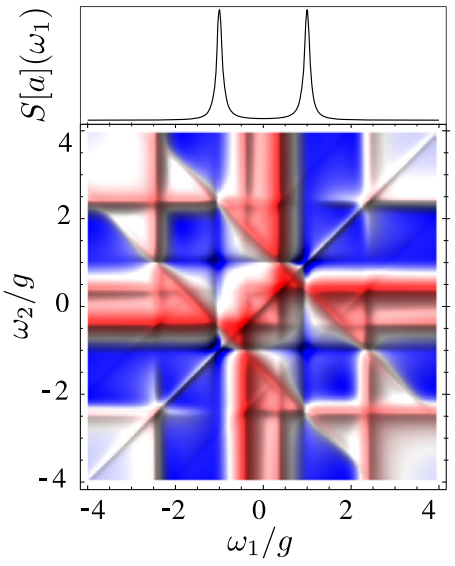

Figure 3.9: Two photon spectrum (2PS) of the Jaynes-Cummings system. Spanning the frequency-resolved correlations over all possible combinations of energies can reveal whole families of physical features, in this case related to the multi-photon transition taking place in the nonlinear ladder of energy levels. Color code: Red, larger than 1; White, 1; Blue, lower than 1. Image from [96].

a landscape (the 2PS) acquires a fundamental meaning by revealing certain physical features [96, 186], in the same way that the normal spectrum is meaningful because its an observable that spans over a frequency range. Figure 3.9 shows one of these landscapes of correlations only visible when spanning over all the frequency range , corresponding in this case to the 2PS of the light emitted by a two-level system coupled to a bosonic mode, the Jaynes-Cummings system [96]. This quantity provides a much deeper information than the standard correlation functions, since frequency–resolved correlations are observables that cannot be associated to a given quantum state, as they also bring information on the dynamics of emission.

3.2 2PS OF A POLARITON ENSEMBLE: EXPERIMENTAL RESULTS

This Chapter focuses on the theoretical description of a joint experimental-theoretical work that provided, for the first time, a full measurement of a two-photon correlation spectrum. In this Section, we offer a brief overview of the experimental methods and the results that were obtained.

3.2.1 EXPERIMENTAL SCHEME

The experiment measured, at the single photon level, frequency-resolved correlations in the light emitted from a macroscopic out-of-equilibrium ensemble of exciton-polaritons pumped around the threshold of condensation. Polaritons are strongly-coupled light-matter bosonic particles in a semiconductor microcavity [130]. Such a source is more convenient than a laser because it is, for our purposes, essentially a laser with a broad linewidth, thereby allowing the spectral filtering. Besides, polaritons have enjoyed thorough studies of their coherence properties, including at the quantum optical level [3, 20, 68]. The experiment is based on a streak camera setup that detects individual photons from the spontaneous emission of an ensemble of polaritons maintained in a non-equilibrium steady state under continuous wave (cw) excitation. This is the first time that such a technique has been used in the continuous pumping regime.

A **streak camera** measures ultrafast time variations in the intensity of a beam of light by applying a synchronized voltage that deflects photoelectrons into a spatial profile on a detector.(see Fig. 3.10).

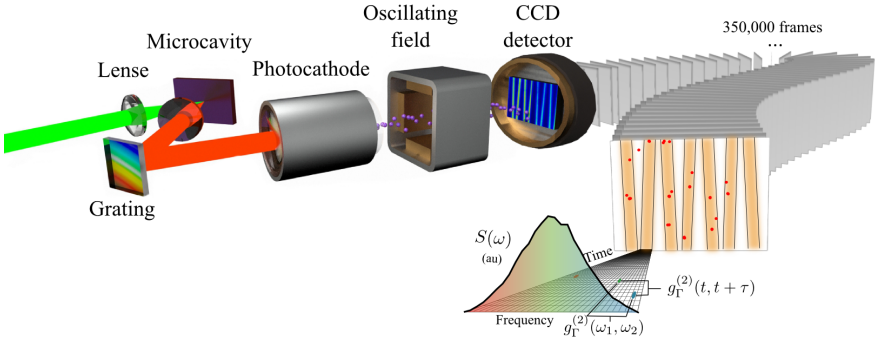

Figure 3.10: Experimental setup The reflected light from a microcavity is dispersed onto a streak camera detecting at the single-photon level and stored in individual frames, whose post-processing allows to build photon-correlation landscapes.

The setup is sketched in Fig. 3.10: light coming from the steady state of polaritons is dispersed by a spectrometer and is directed into the streak camera that is able to detect single photon events, as has already been demonstrated with standard photon correlations in time domain only, under pulsed excitation [236]. The sweeping in time and dispersion in energy allow the simultaneous recording of both the time and frequency of each detected photon in successive frames that are post-processed to calculate intensity correlations. Each frame includes several sweeps: in Fig. 3.10, 8 sweeps per frame are shown as vertical orange stripes, with red dots indicating single photon events. Within each sweep, a time of 1536 ps is spanned in the vertical direction (3.2 ps per pixel), while the photon energy, obtained by coupling a spectrometer to the streak camera, is measured as horizontal pixel positions within each sweep (each sweep covers a total energy range of 456.7 μeV, with 10.6 μeV per pixel). With the time- and energy-range used in the experiment, the overall temporal and energy resolution of the setup are of 10 ps and 70 μeV, respectively. Correlation landscapes are obtained from coincidences between these clicks, with an average of ≈ 1.69 clicks per sweep in a total of 350 000 frames. All the analysis is done with the raw data only: there is no normalisation and the correlations go to 1 at long time self-consistently.

3.2.2 EXPERIMENTAL RESULTS

Figure 3.11 shows the experimental 2PS for the polariton state at $\tau = 0$, and the temporal correlations for three points of the (ω_1, ω_2). A clear evolution of the correlations from positive ($g^{(2)}_\Gamma(\omega,\omega) \approx 1.5$ in region 1) to negative correlations ($g^{(2)}_\Gamma(-\omega,\omega) \approx 0.7$ in region 3) is observed.

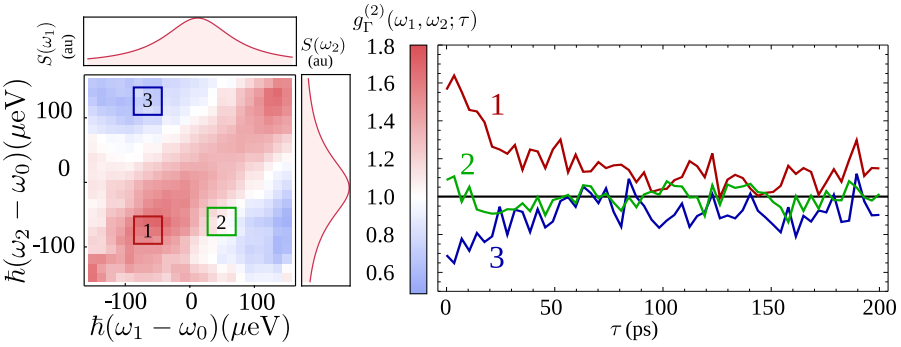

Figure 3.11: Experimental two-photon correlation spectrum. Left: Experimental observation of $g^{(2)}_\Gamma(\omega_1,\omega_2)$ for the spontaneous emission from a steady-state of polaritons. Right: Time-resolved correlation for the three regions marked in the colour map: (i) on the diagonal ($\omega_1 = \omega_2$) exhibiting bunching, (ii) in the region of transition with no correlation, (iii) correlating opposing elbows, exhibiting anticorrelations.

The anticorrelations between photons is a remarkable feature that differs significantly from the positive correlations originally observed by HBT. The purpose of the rest of this Chapter is to demonstrate that these features do not emerge as a particular property of the emitter, but are instead the manifestation of a deeper, fundamental phenomenon; they portray the first evidence of a HBT effect generalized to the full frequency-frequency domain: the *colored Hanbury Brown–Twiss effect*.

Another fundamental feature of the theory is that correlations depend on the frequency windows that select which photons are correlated. Smaller windows lead to stronger correlations but, again, at the price of a smaller

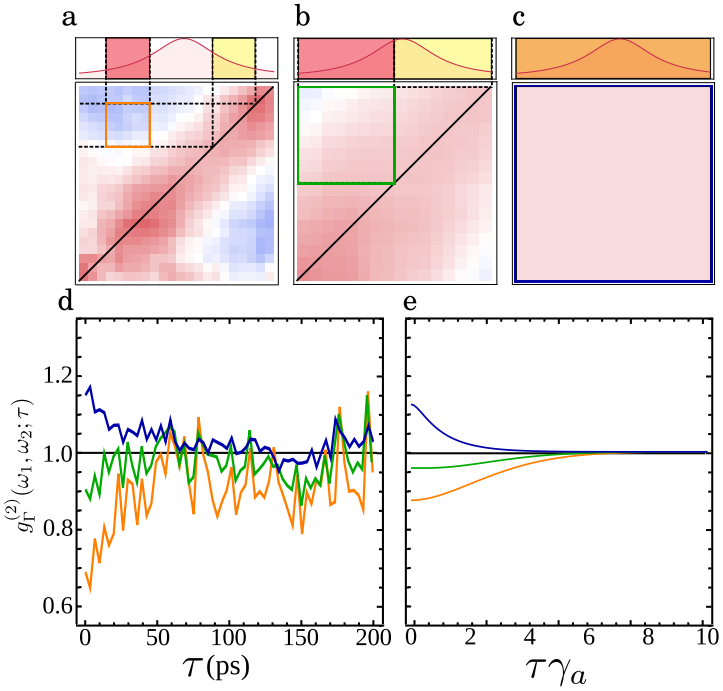

Figure 3.12: Effect of the filter width. Two-photon correlation landscapes $g_\Gamma^{(2)}(\omega_1,\omega_2;0)$ as a function of the filter width. **a** Fraction of the peak, 74.10 µeV. **b**, Roughly half-peak width, 158.80 µeV. **c**, Full-peak filtering, corresponding to standard auto-correlations. The position of the two filters is shown explicitly on the spectral line as the red and yellow windows (orange when overlapping). Colorscale as in Fig. 3.11. **d**, Time evolution, experiment. **e**, Time evolution, theory from the condensation model, see Section 3.3.3.

signal. While it does not correspond exactly to a change in the width of the filter, the effect is neatly illustrated by changing the number of pixels of the streak camera that we associate to a given frequency. In Fig. 3.12, we show the dependence of the 2PS on the size of the frequency windows for a point that features antibunching. When the frequency window is very large, $\Gamma \gg \gamma_a$, both the experimental and theoretical $g_\Gamma^{(2)}(\omega_1,\omega_2;\tau)$ recover as expected the results of standard photon correlations which have always been reported to be larger than 1 for this kind of systems [21, 128, 158]. As the size of the frequency window decreases, the system shows a transition from bunching to antibunching, demonstrating how the statistics of coloured photons can be easily tuned externally.

3.3 2PS OF A POLARITON ENSEMBLE: THEORETICAL DISCUSSION

We now analyse and discuss the experimental results from three following perspectives:

1. A general analysis of the correlations of a classical, phase diffusing field.

2. A general analysis of light spontaneously emitted from an initial quantum state.

3. A specific analysis modeling the physical system used in the experiment.

This discussion will show that the effect reported experimentally can be reproduced by both classical and quantum models of a very general nature, that provide a remarkable quantitative agreement.

3.3.1 CLASSICAL ANALYSIS: FREQUENCY CORRELATIONS OF A PHASE-DIFFUSING FIELD

We now go back to some of the concepts commented in Section 3.1. There, we discussed how Purcell had already included the linewidth of the light as an essential element of his theoretical description; we now enter in more details regarding that matter. In [191], Purcell associated the fluctuations of the intensity of the electric field to the linewidth of the light (*"whether it be set by circumstances in the source itself or by a filter"*). Such fluctuations in amplitude correspond to a "cluttering" of the field in the time domain, and are directly translated into positive correlations of the kind observed by HBT, typical of a thermal field like the one depicted in Fig. 3.4. Some fields, however, can have a finite linewidth even if they have a stable, constant amplitude corresponding to $g^{(2)} = 1$. This is the case of lasers, whose linewidth above threshold is determined by random fluctuations of the phase and indeed present a fundamental lower limit known as the Schawlow-Townes limit. It is well known that spectral filtering within the linewidth of such phase-diffused fields transforms the phase noise into intensity noise [14, 172]. This thermalization of the field is responsible for the bunching in the diagonal line (corresponding to filters of equal frequency) that we observe in the experiment; in this sense, this feature is nothing but the manifestation of the standard HBT effect: positive correlations presented by a thermal field .

The **Schawlow-Townes limit** is a minimum value for the linewidth of a laser set by quantum fluctuations, e.g., spontaneous emission. It was theoretically discovered by Schawlow and Townes in 1958 [204], before the laser was experimentally demonstrated.

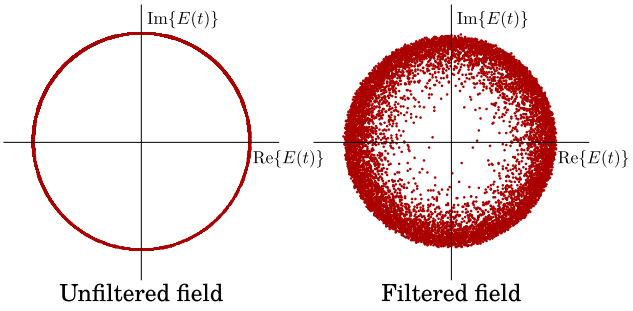

Figure 3.13: Thermalization due to frequency filtering Phase noise is converted into intensity noise after frequency filtering.

From a classical point of view, this can be understood with the particular case of a quasi-monochromatic field $E(t)$ that has a finite bandwith given by a phase diffusion process:

$$E(t) = E_0 e^{-i[\omega_0 t + \phi(t)]}, \tag{188}$$

where $\phi(t)$ is a stochastic function that evolves, for instance, according to a random walk providing the line broadening. As is clear from Eq. (183), the frequency-filtered field is obtained by summing the field to itself at different times. If phase diffusion is present, this corresponds to the superposition of fields with random phases, which is analogous to the description of a thermal

field that we showed in Eq. (179). Such a superposition of fields of equal frequency but different phase produces interferences that wildly oscillate in a chaotic intensity profile, resulting in fluctuations in the intensity of the filtered field $I_{\omega,\Gamma}$ that satisfy:

$$\frac{\langle {I_{\omega,\Gamma}}^2 \rangle}{\langle I_{\omega,\Gamma} \rangle^2} > 1\,. \tag{189}$$

This is well known textbook material [157]. Interpreted in terms of photons, the underlying particles thus tend to "clump" together, and increase the spacing between their arrival time, which gives rise to the bunching effect.

INTENSITY ANTICORRELATIONS We have just seen how phase noise is converted into intensity noise by frequency-filtering (see Fig. 3.13). In a related but subtler way—which is the novel feature reported in this experiment–such correlations can be negative when they involve different frequencies. This remains true at the single particle level, as is demonstrated by the experiment, showing anticorrelations between individual photons of different colors. Since we want to show that the effect is linked to the aforementioned conversion of phase noise into amplitude noise by filtering, we can keep the paradigmatic case of a quasi-monochromatic field, that has only phase noise, Eq. (188). On physical grounds, one expects that a field with a stabilized Poynting vector (in which the uncertainty in the number of photons detected in a certain time window is given by the shot noise) cannot yield in average more photon counting events per unit time when spectrally resolved than it does without being frequency-filtered. Therefore, the detection of a clump of photons of some frequency in a small time window—in which photons are detected as random events prior filtering—must lower the probability of detecting photons at other, different frequencies, in order for the total rate of detected photons to be preserved. The anticorrelation we observe can therefore be interpreted as a consequence of energy conservation (in the classical sense related to photon number, not frequency) acting together with the HBT effect, that yields bunching of indistinguishable photons of equal frequencies. The photons on the detector, even if unrelated in the first place, cannot afford to remain so when frequency-filtered.

This argument is verified by explicit computation of Eq. (184) applied on the field (188), assuming random walk dynamics for the phase. In that case, the phase difference $\Delta\phi(\tau) = \phi(t+\tau) - \phi(t)$ has the following properties:

$$\begin{aligned} \langle \Delta\phi(\tau) \rangle &= 0\,, \\ \langle \Delta\phi(\tau)^2 \rangle &= 2\gamma_1|\tau|\,, \\ \langle e^{i[\phi(t)-\phi(t-\tau)]} \rangle &= e^{-\gamma_1|\tau|}\,, \\ \langle e^{2i[\phi(t)-\phi(t-\tau)]} \rangle &= e^{-\gamma_2|\tau|}\,. \end{aligned} \tag{190}$$

In the case of a phase diffusing field that we consider here, the fourth orther correlation constant γ_2 is given by $\gamma_2 = 4\gamma_1$. However, we left γ_2 in the previous expressions to account for other possible models of phase noise, like the phase-jump model, in which $\gamma_2 = \gamma_1$ [45]. The numerator of Eq. (184),

that we denote $G_\Gamma^{(2)}(\omega_1,\omega_2,\tau)$ (it depends on τ since we consider a steady state), is given by the following quadruple integral:

$$\begin{aligned} G_\Gamma^{(2)}(\omega_1,\omega_2,\tau) &= \left(\frac{\Gamma}{2}\right)^4 \int_0^\infty \prod_{i=1}^4 dt_i\, e^{i\omega_1(t_2-t_1)} e^{i\omega_2(t_4-t_3)} e^{-\Gamma(t_1+t_2+t_3+t_4)/2} \\ &\times \langle E(t-t_3+\tau)E^*(t-t_4+\tau)E(t-t_1)E^*(t-t_2)\rangle \\ &= E_0^4 \left(\frac{\Gamma}{2}\right)^4 \int_0^\infty \prod_{i=1}^4 dt_i\, e^{-i\Delta_1(t_2-t_1)-i\Delta_2(t_4-t_3)} e^{-\Gamma(t_1+t_2+t_3+t_4)/2} \\ &\qquad \times \langle e^{-i[\phi(t-t_1)-\phi(t-t_2)+\phi(t-t_3+\tau)-\phi(t-t_4+\tau)]}\rangle, \end{aligned} \tag{191}$$

where $\Delta_i \equiv \omega_0 - \omega_i$. Defining $t_1' \equiv t - t_1$, $t_2' \equiv t - t_2$, $t_3' \equiv t - t_3 + \tau$ and $t_4' \equiv t - t_4 + \tau$, the statistical average in the last line of (191) takes the form $\langle e^{i[\phi(t_1')-\phi(t_2')+\phi(t_3')-\phi(t_4')]}\rangle$. The exponent can be written in term of phase differences $\Delta\phi(\tau)$ in two possible ways, $\langle e^{i[\Delta\phi(t_1'-t_2')+\Delta\phi(t_3'-t_4')]}\rangle$ or $\langle e^{i[\Delta\phi(t_1'-t_4')+\Delta\phi(t_3'-t_2')]}\rangle$. For a given set of values for t_1', t_2', t_3' and t_4', the choice between both options must be made such that the two $\Delta\phi$ are defined in non-overlapping time intervals, making them statistically independent.

This allows to factorize the exponential and use Eq. (190) to evaluate the statistical averages. Figure 3.14 depicts the three possible configurations that exist depending on the values of t_i'. Panel c shows the particular case $t_4', t_2' < t_1', t_3'$ that requires the introduction of a third time interval to avoid overlapping; this is the case that will invoke the last equation in (190), involving the fourth order correlation constant γ_2.

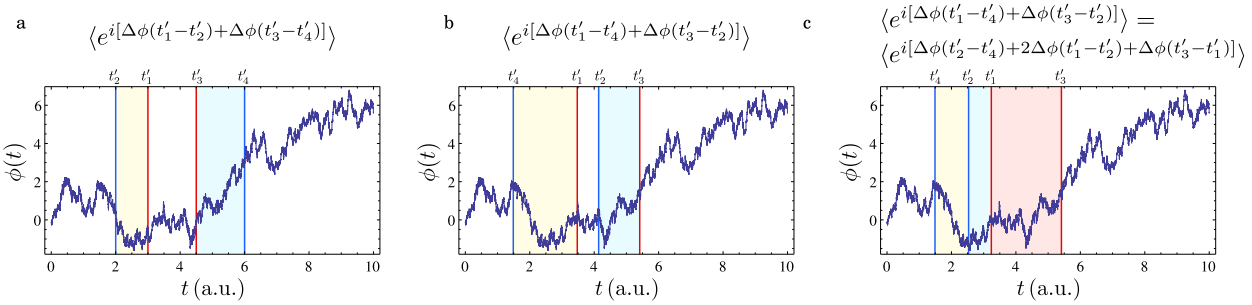

Figure 3.14: Examples of the possible integration domains for the fluctuating phase. These domains correspond to three possible exponents that appear in the integrals. **a**, Domain I, **b**, Domain VIII and **c**, Domain XI. In domains IX–XII, the exponent must be written as three phase differences to ensure they are statistically uncorrelated.

Since the integrand has to be written differently depending on the values of the t_i', one needs to split the integral in the 24 possible domains. Half of these integrals are the complex conjugate of the other half, yielding 12 independent terms, defined in the domains:

$$\begin{aligned}
\text{I}: &\quad t_2' < t_1' < t_3' < t_4' &\overset{*}{\leftrightarrow}\quad & t_1' < t_2' < t_4' < t_3', \\
\text{II}: &\quad t_2' < t_3' < t_1' < t_4' &\overset{*}{\leftrightarrow}\quad & t_1' < t_4' < t_2' < t_3', \\
\text{III}: &\quad t_4' < t_3' < t_1' < t_2' &\overset{*}{\leftrightarrow}\quad & t_3' < t_4' < t_2' < t_1', \\
\text{IV}: &\quad t_4' < t_1' < t_3' < t_2' &\overset{*}{\leftrightarrow}\quad & t_3' < t_2' < t_4' < t_1', \\
\text{V}: &\quad t_2' < t_1' < t_4' < t_3' &\overset{*}{\leftrightarrow}\quad & t_1' < t_2' < t_3' < t_4', \\
\text{VI}: &\quad t_2' < t_3' < t_4' < t_1' &\overset{*}{\leftrightarrow}\quad & t_1' < t_4' < t_3' < t_2',
\end{aligned}$$

$$
\begin{aligned}
\text{VII}: &\quad t_4' < t_3' < t_2' < t_1' &&\overset{*}{\leftrightarrow}&& t_3' < t_4' < t_1' < t_2'\,,\\
\text{VIII}: &\quad t_4' < t_1' < t_2' < t_3' &&\overset{*}{\leftrightarrow}&& t_3' < t_2' < t_1' < t_4'\,,\\
\text{IX}: &\quad t_2' < t_4' < t_1' < t_3' &&\overset{*}{\leftrightarrow}&& t_1' < t_3' < t_2' < t_4'\,,\\
\text{X}: &\quad t_2' < t_4' < t_3' < t_1' &&\overset{*}{\leftrightarrow}&& t_1' < t_3' < t_2' < t_4'\,,\\
\text{XI}: &\quad t_4' < t_2' < t_1' < t_3' &&\overset{*}{\leftrightarrow}&& t_3' < t_1' < t_2' < t_4'\,,\\
\text{XII}: &\quad t_4' < t_2' < t_3' < t_1' &&\overset{*}{\leftrightarrow}&& t_3' < t_1' < t_4' < t_2'\,. \qquad (192)
\end{aligned}
$$

By denoting the non-overlapping time differences as τ_i and making a change of variables, we obtain 12 different integrals of the form:

$$
I_{\text{I}} = C\int_0^\infty dt_2 \int_{t_2}^0 d\tau_1 \int_0^{t_2-\tau_1+\tau} dt_3 \int_{t_3}^0 d\tau_2\, e^{i(\Delta_2\tau_2-\Delta_1\tau_1)} e^{-\Gamma(2t_2+2t_3-\tau_1-\tau_2)/2-\gamma(\tau_1+\tau_2)},
$$

with $C = E_0^4\left(\frac{\Gamma}{2}\right)^4$. Here, we only show the first of them, I_{I}, for ease of reading From these integrals, that can be computed analytically, we can obtain an expression for $G_\Gamma^{(2)}(\omega_1,\omega_2,\tau)$, given by:

$$
G_\Gamma^{(2)}(\omega_1,\omega_2,\tau) = 2\text{Re}\sum_{i=\text{I}}^{\text{XII}} I_i\,, \qquad (193)
$$

whose final form is lengthy so we do not reproduce it here.

On the other hand, the denominator in Eq. (184) consists of the product of the mean intensities of the two filtered fields. This mean intensity is readily given by:

$$
\begin{aligned}
&\langle E^+_{\omega_i,\Gamma}(t) E_{\omega_i,\Gamma}(t)\rangle = \langle I_{\omega_i,\Gamma}(t)\rangle =\\
&= E_0^2\frac{\Gamma^2}{4}\left(\int_0^\infty dt_1\int_0^{t_1} dt_2\, e^{i\Delta_i(t_1-t_2)-\Gamma(t_1+t_2)/2-\gamma(t_1-t_2)}\right.\\
&\left.+\int_0^\infty dt_2\int_0^{t_2} dt_1\, e^{i\Delta_i(t_1-t_2)-\Gamma(t_1+t_2)/2-\gamma(t_2-t_1)}\right)\\
&= E_0^2\frac{\Gamma^2}{2}\text{Re}\int_0^\infty dt_1\int_0^{t_1} dt_2\, e^{(i\Delta_i-\gamma)(t_1-t_2)-\Gamma(t_1+t_2)/2}\\
&= E_0^2\frac{\Gamma}{2}\frac{\gamma+\Gamma/2}{\Delta_i^2+(\gamma+\Gamma/2)^2}\,. \qquad (194)
\end{aligned}
$$

Normalizing the expression of $G_\Gamma^{(2)}(\omega_1,\omega_2,\tau)$ resulting from Eq. (193) by the intensity from Eq. (194), we obtain the final expression for $g_\Gamma^{(2)}(\omega_1,\omega_2,\tau)$. At $\tau = 0$, this expression takes the form:

$$
\begin{aligned}
g_\Gamma^{(2)}(\Delta_1,\Delta_2) &= \frac{\left[\Delta_1^2+(\gamma+\Gamma/2)^2\right]\left[\Delta_2^2+(\gamma+\Gamma/2)^2\right]}{4(\gamma+\Gamma/2)^2}\\
&\text{Re}\left\{\frac{2(\gamma+3\Gamma/2)}{(\gamma+i\Delta_2+\Gamma/2)(\Delta_1^2+(\gamma+3\Gamma/2)^2)}+\Gamma\left[f_\Gamma(\Delta_2,\Delta_{12}^-,\Delta_2)\right.\right.\\
&+ f_\Gamma(\Delta_1,\Delta_{12}^-,-\Delta_2)+f_\Gamma(\Delta_1,\Delta_{12}^+-i\gamma_2,\Delta_1)+\\
&\left.\left.f_\Gamma(\Delta_2,\Delta_{12}^+-i\gamma_2,\Delta_1)\right]+[\Delta_1\leftrightarrow\Delta_2]\right\} \qquad (195)
\end{aligned}
$$

where $\Delta_i \equiv \omega_i - \omega_0$, $\Delta_{12}^- \equiv \Delta_2 - \Delta_1$, $\Delta_{12}^+ \equiv \Delta_2 + \Delta_1$ and:

$$f_\Gamma(\omega_1, \omega_2, \omega_3) = \frac{1}{(i\omega_1 + \gamma + \Gamma/2)(i\omega_2 + \Gamma)(i\omega_3 + \gamma + 3\Gamma/2)} \,. \quad (196)$$

This expression reflects the same structure of correlations and anticorrelations that is observed in the experiment, as depicted in Fig. 3.15, where it is shown to fit very well the experimental data. The main assumption behind this equation–that the unfiltered field has negligible amplitude fluctuations–is closely met in the experiment, in which the high coherence degree of the light emitted by the polaritons around the condensation threshold allows to unambiguously observe the anticorrelations.

PERFECT ANTICORRELATIONS An interesting effect takes place in the limit when the filter linewidth is much larger than the natural linewidth of the field, $\Gamma \gg \gamma$. The intensity of the filtered field is then given by:

$$\begin{aligned} I_{\omega_i,\Gamma}(t) &= E_0^2 \frac{\Gamma^2}{2} \mathrm{Re} \int_0^t dt_1 \int_0^{t_1} dt_2 \, e^{-\Gamma(t_1+t_2)/2} e^{i[\Delta_i(t_1-t_2)+\phi(t-t_1)-\phi(t-t_2)]} \\ &= E_0^2 \frac{\Gamma^2}{2} \int_0^t dt_1 \int_0^{t_1} dt_2 \, e^{-\Gamma(t_1+t_2)/2} \\ &\quad \cos\left[\Delta_i(t_1-t_2) + \Delta\phi(t_1,t_2,t)\right] \\ &= E_0^2 \frac{\Gamma^2}{2} \int_0^t dt_1 \int_0^{t_1} dt_2 \, e^{-\Gamma(t_1+t_2)/2} \\ &\quad \{\cos\left[\Delta_i(t_1-t_2)\right] \cos[\Delta\phi(t_1,t_2,t)] \\ &- \quad \sin[\Delta_i(t_1-t_2)] \sin[\Delta\phi(t_1,t_2,t)]\} \,, \end{aligned} \quad (197)$$

where $\Delta\phi(t_1,t_2,t) = \phi(t-t_1) - \phi(t-t_2)$. If $\Gamma \gg \gamma$, the timescale given by the filter linewidth is much shorter than the natural timescale of the phase diffusion, and we can assume $\Delta\phi(t_1,t_2,t) \ll 1$ for those values of t_1 and t_2 where the integrand is non-negligible. By expanding to first order in $\Delta\phi(t_1,t_2,t)$, we obtain:

$$\begin{aligned} I_{\omega_i,\Gamma}(t) \underset{\Gamma\gg\gamma}{\approx} E_0^2 \frac{\Gamma^2}{2} \int_0^t dt_1 \int_0^{t_1} dt_2 \, e^{-\Gamma(t_1+t_2)/2} \{\cos\left[\Delta_i(t_1-t_2)\right] - \sin[\Delta_i(t_1-t_2)] \\ \times \Delta\phi(t_1,t_2,t)\} = \langle I_{\omega_i,\Gamma}\rangle + \delta I_{\omega_i,\Gamma}(t) \,, \end{aligned} \quad (198)$$

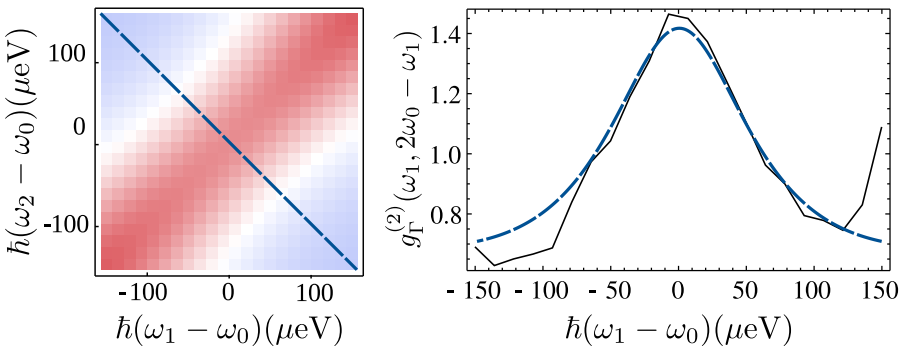

Figure 3.15: Fitting of the experimental 2PS by equation (195). **a**, Fitting of the full 2PS. The colorscale is that of Fig. 3.11. **b**, 2PS along the dashed line in a for the experiment (straight, black), and fitting for the phase diffusing field (long dashed, blue) given by Eq. (195). Fitting parameters: $\gamma \approx 193\,\mu\mathrm{eV}$, $\Gamma \approx 134\,\mu\mathrm{eV}$.

where we defined

$$\langle I_{\omega_i,\Gamma}\rangle = E_0^2\frac{\Gamma^2}{2}\int_0^t dt_1\int_0^{t_1} dt_2\, e^{-\Gamma(t_1+t_2)/2}\cos\left[\Delta_i(t_1-t_2)\right]$$
$$= E_0^2\frac{(\Gamma/2)^2}{\Delta_i^2+(\Gamma/2)^2}\,. \tag{199}$$

(in agreement with Eq. (194) in the limit $\Gamma \gg \gamma$) and

$$\delta I_{\omega_i,\Gamma}(t) = -E_0^2\frac{\Gamma^2}{2}\int_0^t dt_1\int_0^{t_1} dt_2\, e^{-\Gamma(t_1+t_2)/2}\sin[\Delta_i(t_1-t_2)]\Delta\phi(t_1,t_2,t)\,. \tag{200}$$

Since this equation changes sign when Δ_i changes sign, we observe that, in this limit, although $g_\Gamma^{(2)}(\omega_1,\omega_2)$ gets closer to one (converging to the "unfiltered" result), the fluctuations around the mean value in opposite sides of the spectrum are perfectly anticorrelated at all times:

$$\delta I_{\omega_0-\omega,\Gamma}(t) = -\delta I_{\omega_0+\omega,\Gamma}(t)\,, \tag{201}$$

and $g_\Gamma^{(2)}(\omega_0+\omega,\omega_0-\omega)$ is close, but always lower than one:

$$g_\Gamma^{(2)}(\omega_0+\omega,\omega_0-\omega) = 1+\frac{\langle\delta I_{\omega_0-\omega,\Gamma}\delta I_{\omega_0+\omega,\Gamma}\rangle}{\langle I_{\omega_0-\omega,\Gamma}\rangle\langle I_{\omega_0+\omega,\Gamma}\rangle} = 1-\frac{\langle\delta I^2_{\omega_0+\omega,\Gamma}\rangle}{\langle I_{\omega_0+\omega,\Gamma}\rangle^2} < 1\,. \tag{202}$$

Just as the autocorrelations of Hanbury Brown for radio-waves of same frequencies (with no filtering), these anticorrelations of the filtered signal are obvious even to the naked eye, as can be seen in Fig. 3.16.

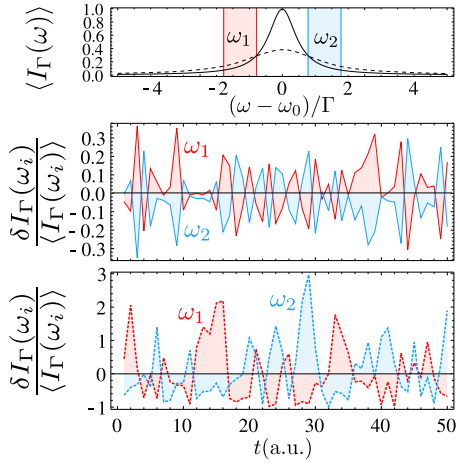

Figure 3.16: Visualization of the anticorrelations. Fluctuations in the intensity of the filtered field $I_\Gamma(\omega_i) = \langle I_\Gamma(\omega_i)\rangle + \delta I_\Gamma(\omega_i)$ for the two frequencies shown at the top panel and two values of γ, $\gamma \approx 8\times10^{-3}\Gamma$ (solid lines, middle panel), and $\gamma \approx 0.8\,\Gamma$ (dashed lines, bottom panel). The corresponding values of $g^{(2)}(\omega_1,\omega_2)$ are 0.97 and 0.65 resp. In the middle-panel case, where $\Gamma \gg \gamma$, the anticorrelations in the noise become exact.

3.3.2 QUANTUM ANALYSIS: FREQUENCY CORRELATIONS OF THE LIGHT EMITTED BY A QUANTUM STATE UNDER SPONTANEOUS EMISSION

Describing this effect from the quantum/particle point of view poses more difficulties, since the 2PS is a dynamical observable and one cannot attribute

a value of $g^{(2)}_{\Gamma}(\omega_1, \omega_2)$ with frequency-filtering to a given quantum state without also including information about the dynamics. This means that, by virtue of the quantum regression theorem, one needs to include the Liouvillian operator $\mathcal{L}$ in the calculation, contrary to the case without frequency-filtering where the knowledge of the diagonal elements of the density matrix is sufficient. This makes the formulation of a general statement a complicated task. We consider for that purpose a simple situation in which an arbitrary quantum state given by the density matrix $\rho(0)$ is left to decay from a source to a continuum of modes under spontaneous emission with a rate γ_a and also with a pure dephasing rate γ_ϕ, thus eliminating every possible dynamics except the essential one that brings photons from the source to the detector and some dephasing mechanism. This dephasing is included since, as we will show below, it is an essential ingredient of the HBT phenomenology, as it was for the classical description of the previous section. Therefore, the resulting master equation is given by $\partial_t \rho = \left[\frac{\gamma_a}{2}\mathcal{L}_a + \frac{\gamma_\phi}{2}\mathcal{L}_{a^\dagger a}\right](\rho)$, where $\mathcal{L}_{\mathcal{O}}$ denotes the Lindblad term, $\mathcal{L}_{\mathcal{O}}(\rho) = 2O\rho O^\dagger - O^\dagger O\rho - \rho O^\dagger O$.

The equation can be integrated in closed form for $\rho_{n,m} = \langle n|\rho|m\rangle$ which takes the form:

$$\dot{\rho}_{n,m} = -\frac{1}{2}\left[\gamma_a(n+m) + \gamma_\phi(n-m)^2\right]\rho_{n,m} + \gamma_a\sqrt{(m+1)(n+1)}\rho_{n+1,m+1}\,, \tag{203}$$

and that can be solved by recurrence, yielding:

$$\rho_{n,m}(t) = \sum_{k=0}^{\infty}\rho_{k,m-n+k}(0)\sqrt{\binom{k}{n}\binom{m-n+k}{m}}\left(e^{\gamma_a t}-1\right)^{k-n} \times e^{-\left[\gamma_a(2k+m-n)+\gamma_\phi(n-m)^2\right]t/2}\,. \tag{204}$$

From $\rho(t)$, one can compute all single-time observables, such as the population:

$$n(t) = \langle a^\dagger a\rangle(t) = n(0)\exp(-\gamma_a t)\,, \tag{205}$$

i.e., simple exponential decay, as expected on physical grounds and despite the complicated form of the general solution. The two-photon correlation:

$$g^{(2)}(t) = \frac{\langle a^\dagger a^\dagger a a\rangle(t)}{\langle a^\dagger a\rangle(t)^2} \tag{206}$$

provides an even simpler and stronger result:

$$g^{(2)}(t) = g^{(2)}(0)\,. \tag{207}$$

The photon-statistics is constant with time. One can also compute the two-times correlation function (Eq. (1) of the main text) through the quantum regression theorem (demonstration not given), and find a similarly constrained result:

$$g^{(2)}(t,\tau) = g^{(2)}(0,0)\,. \tag{208}$$

This implies, for instance, $\lim_{\tau\to\infty} g^{(2)}(t,\tau) \neq 1$ for most of the cases, i.e., photons are always correlated. This is reasonable since any two photons emitted by the system come from the same and only initial state which is let to evolve at precisely $t = 0$.

We now compute the two-photon correlations from an initial state when including the frequency degree of freedom. To keep the discussion as fundamental and simple as possible, we consider here the time-integrated case that disposes of time altogether:

$$\bar{g}^{(2)}_{\Gamma}(\omega_1,\omega_2) = \frac{\iint_0^\infty \langle : \mathcal{T}\left[\prod_{i=1}^2 \hat{E}_{\omega_i,\Gamma}(t_i)\hat{E}^+_{\omega_i,\Gamma}(t_i)\right] : \rangle dt_1 dt_2}{\prod_{i=1}^2 \int_0^\infty \langle \hat{E}_{\omega_i,\Gamma}(t_i)\hat{E}^+_{\omega_i,\Gamma}(t_i)\rangle dt_i}\,. \tag{209}$$

This is equivalent to letting the detectors gather statistical information from photons detected at any time, hence reconstructing the frequency of the photons with full precision. This quantity is the closest one to what an actual experiment would perform, although other configurations are possible (they would bring us to an essentially identical discussion and conclusions). Applying Eq. (209) to the case of free propagation only ($\gamma_a = 0$ and $\gamma_\phi = 0$) is pathological because the energy is then exactly determined and frequency correlations become trivial or ill-defined in terms of δ functions.

In the most general case, Eq. (209) can be analytically solved , giving the result:

$$\bar{g}^{(2)}_{\Gamma}(\omega_1,\omega_2) = g^{(2)}\mathcal{F}_{\Gamma,\gamma_a,\gamma_\phi}(\omega_1,\omega_2)\,, \tag{210}$$

with $g^{(2)}$ the standard zero-delay, second-order correlation function, Eq. (182), and $\mathcal{F}_{\Gamma,\gamma_a,\gamma_\phi}(\omega_1,\omega_2)$ a *boson form factor*, which is independent of the quantum state ρ in which the system is prepared, and depends only on the dynamics of emission and detection:

$$\begin{aligned}\mathcal{F}^{(2)}_{\Gamma,\gamma_a,\gamma_\phi}(\omega_1,\omega_2) = \mathrm{Re}\Big\{ &\frac{(\gamma^2+4\omega_1^2)(\gamma^2+4\omega_2^2)}{2\gamma^2(\gamma+2i\omega_2)}\Big[\frac{\gamma+2\gamma_a}{(\gamma+2\gamma_a)^2+4\omega_1^2}\\
&+\frac{\gamma_a}{\gamma+2\gamma_a+2i\omega_2}\times\Big(\frac{\gamma+2\gamma_a-i(\omega_1-\omega_2)}{(\gamma+2\gamma_a-2i\omega_1)(\Gamma+\gamma_a-i(\omega_1-\omega_2))}\\
&+\frac{\gamma+2\gamma_a+i(\omega_1+\omega_2)}{(\gamma+2\gamma_a+2i\omega_1)(2\gamma-\Gamma-\gamma_a+i(\omega_1+\omega_2))}\Big)\Big]\Big\}\\
&+[1\leftrightarrow 2]\,.\end{aligned} \tag{211}$$

with $\gamma = \Gamma + \gamma_a + \gamma_\phi$ and $1 \leftrightarrow 2$ means index exchange. The form factor reproduces exactly the features observed in the experiment and therefore captures the essence of this extension of the HBT effect. The wide range of frequencies used in Figure 3.17 serves to illustrate the non trivial shape of the anticorrelations along the antidiagonal line $(\omega, -\omega)$, featuring a minimum approximately at the point where the total filtered intensity is maximum without a considerable overlapping of the filters. Consistently with the classical analysis based on a stochastic field (188), the quantum calculation shows that when the unfiltered field has no intensity fluctuations $g^{(2)}_0 = 1$, the filtered field displays anticorrelations.

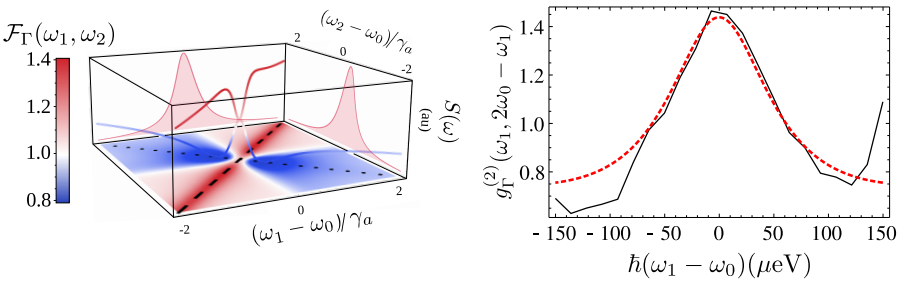

Figure 3.17: Boson form factor. Left: Bosonic form factor $\mathcal{F}_{\Gamma,\gamma_a,\gamma_\phi}(\omega_1,\omega_2)$, i.e., time-integrated 2PS for the spontaneous emission of a coherent state with $g^{(2)}=1$, providing the backbone for the experiment. The diagonal and antidiagonal exhibit bunching and antibunching, respectively. Right: Experimental curve (solid, black) along the antidiagonal, and fitting of the form factor $\mathcal{F}_{\Gamma,\gamma_a,\gamma_\phi}$ (short-dashed, red) along the same line. Despite not being an exact theoretical description for this experiment, the form factor agrees very well with the data for the parameters $\gamma \approx 99\,\mu$eV, $\gamma_\phi \approx 440\,\mu$eV, $\Gamma \approx 17\,\mu$eV.

Let us consider now one of the simplest physically sound dynamics: a free field that, at least, decays ($\gamma_a \neq 0$ and $\gamma_\phi = 0$). In this case, corresponding to spontaneous emission of the state, the result is the same for frequencies as Eq. (208):

$$\bar{g}^{(2)}_\Gamma(\omega_1,\omega_2) = g^{(2)}\,. \tag{212}$$

Eq. (212), follows from the fact that, when the dephasing rate γ_ϕ is equal to zero, $\mathcal{F}_{\Gamma,\gamma_a,\gamma_\phi}(\omega_1,\omega_2)$ is equal to one, and therefore featureless. This result highlights that some dephasing mechanism is an essential ingredient for the manifestation of the phenomenon (as it is for the standard HBT effect), consistently with the classical description of Section 3.3.1. This also explains why the coherent part of the resonance fluorescence spectrum, not subjected to dephasing, does not present this features while the incoherent part does (see Fig. 3.18).

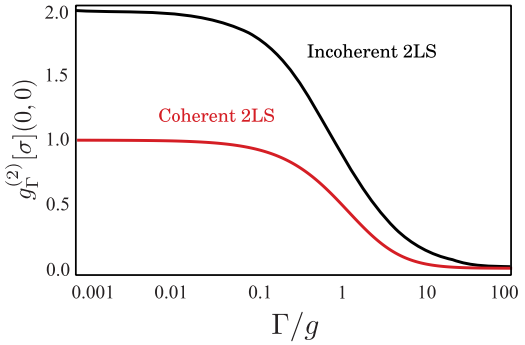

Figure 3.18: Effect of dephasing in other systems. Second order frequency-resolved correlation function at zero delay at the central frequency of emission of an incoherently (black) and coherently (red) driven two-level system, as a function of the filter linewidth. In the case of the coherent driving, the HBT effect (bunching of the filtered peak) at low filter linewidth is not present due to the lack of any dephasing mechanism. Figure adapted from [96].

3.3.3 EMISSION FROM AN OUT-OF-EQUILIBRIUM POLARITON ENSEMBLE

Our previous analysis demonstrated that excellent qualitative agreement with the experimental results can be obtained from very general models, both classical and quantum. This proves that the reported anticorrelations are, as the original HBT effect, a fundamental result connected to the bosonic nature of photons, and not an specific feature of the source. Nevertheless, in order to complete our description of the experiment with more quantitative results, we provide now a more specific analysis on the frequency-resolved

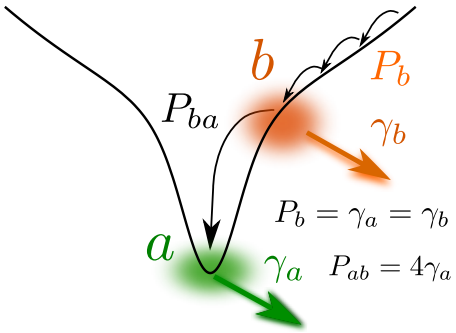

Figure 3.19: Sketch of the emitter. A laser excites non-resonantly the lower polariton dispersion, creating a reservoir of hot excitons b that condense into the ground state a at the minimum of the branch.

correlations of the steady emission of an out-of-equilibrium ensemble of polaritons.

A scheme of the emitter is shown in Fig. 3.19: polaritons relax into the ground state from a reservoir of high energy polaritons injected by a cw off-resonant laser. The constant losses through the cavity mirror allow to study the steady-state correlations. We describe our system theoretically by the following minimal model which accounts for all the key ingredients of the experiments:

$$\frac{\partial \rho}{\partial t} = \left[\frac{\gamma_a}{2}\mathcal{L}_a + \frac{\gamma_b}{2}\mathcal{L}_b + \frac{P_b}{2}\mathcal{L}_{b^\dagger} + \frac{P_{ba}}{2}\mathcal{L}_{a^\dagger b}\right](\rho)\,, \tag{213}$$

where ρ is the combined reservoir-condensate density matrix defined on the Hilbert space of two bosonic fields, since we describe both the BEC and the exciton reservoir by two harmonic modes a and b, which obey bosonic algebra $[c, c^\dagger] = 1$, with $c = a, b$. In the rotating frame of the frequency of the condensate, the dynamics is purely dissipative. Both modes lose particles, with decay rate γ_c, described by Lindblad terms: $\sum_{c=a,b} \frac{\gamma_c}{2}\mathcal{L}_c(\rho)$, where $\mathcal{L}_c(\rho) = 2c\rho c^\dagger - c^\dagger c\rho - \rho c^\dagger c$. The excitation is through the incoherent injection of reservoir excitons at a rate P_b with the accompanying Lindblad term $\frac{P_b}{2}\mathcal{L}_{b^\dagger}(\rho)$. The transfer of particles from the reservoir to the condensate, typically assumed to be phonon mediated, is described by the incoherent relaxation mechanism from a to b, described by a crossed Lindblad term $\frac{P_{ba}}{2}\mathcal{L}_{a^\dagger b}(\rho)$ [110]. In an open system, such a reduced system is enough to capture the physics of condensation that otherwise requires a macroscopic reservoir with N states and $N \to \infty$ to achieve coherence buildup [153]. This model has the minimum, but also all, ingredients to explain the core physical processes that takes place within our experimental conditions. It accounts successfully for, e.g., line narrowing and transition to lasing/condensation of the mode a when the pumping P_b is high enough, to all orders of the condensate field correlators $N_{ab}[n, 0]$, where:

$$N_{ab}[n, m] = \langle (a^\dagger)^n a^n (b^\dagger)^m b^m \rangle\,, \tag{214}$$

with $n, m \in \mathbf{N}$ form a closed set under the dynamics of Eq. (213) [63]. It is therefore also a sound model to compute theoretically the frequency-resolved correlations.

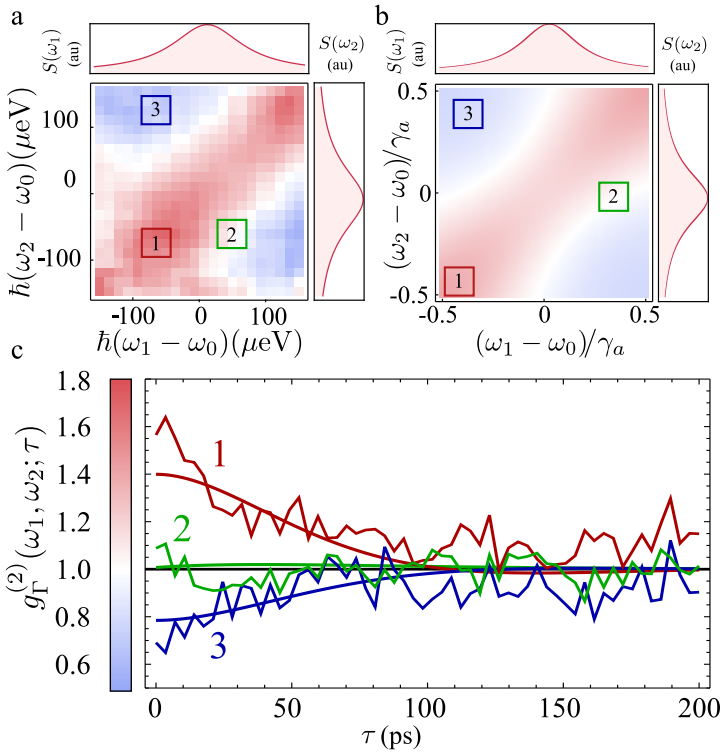

Figure 3.20: Theoretical description of the experiment based on a model of out of equilibrium emission. We show here the results of a model based on the master equation of Eq. (213), compared to the experimental results shown in Fig. 3.11.

The zero-time delay dynamics is easily obtained:

$$\dot{N}_{ab}[n,m] = -\Big[n\gamma_a + m\big(\gamma_b - P_b + P_{ba}\big) + nmP_{ba}\Big]N_{ab}[n,m] + n^2P_{ba}N_{ab}[n-1,m+1] + nP_{ba}N_{ab}[n,m+1] + P_bm^2N_{ab}[n,m-1] - mP_{ba}N_{ab}[n+1,m]\,. \quad (215)$$

Integrating these equations, it is possible to calculate, e.g., the condensate population, $n_a = N_{ab}[1,0]$, the unnormalized second order correlation function at zero delay $G^{(2)}(\tau=0) = N_{ab}[2,0]$ or any other single time correlator. In particular, the steady state is obtained by setting $\dot{N}_{ab}[n,m] = 0$ and solving the system of linear equations, which is finite when truncating to a large enough number of excitations. It is well known, and is straightforwardly shown, that $g^{(2)}$ goes from values above 1, when $P_b \ll \gamma_{b,a}$, to 1 when $P_b \gg \gamma_{b,a}$, corresponding to a coherence buildup that accompanies condensation with $n_a \gg 1$ and triggering a dynamics of relaxation dominated by stimulated emission [153]. By following the sensors method for the steady state [67] (see Section 3.1.4) and the Liouvillian of Eq. (213) we can compute (now numerically) the 2PS in this case. The result, depicted in Fig.3.20, show a remarkably agreement with the experiment.

3.4 CONCLUSIONS

In this Chapter, we have presented experimental and theoretical results reporting the anticorrelations between individual photons emitted from an ensemble of polaritons under continuous pumping. We have demonstrated

with a theoretical analysis that this phenomenon generalizes the Hanbury Brown–Twiss effect for color correlations, and is therefore a deep, fundamental result linked to the bosonic nature of photons.

The frequency-resolved second-order correlation function is an observable of increasing importance in quantum-optical technologies. In general, when the physics goes beyond that of the mere emission from a quantum state ρ, and involves virtual processes, dressing of the states, collective emission, stimulated emission and other types of likewise quantum correlations, the standard Glauber's correlation $g^{(2)}$ does not simply factorize from $g^{(2)}_{\Gamma}(\omega_1, \omega_2)$. In such cases, the 2PS offers a complex landscape of correlations with strong and characteristic features [96], that can be taken advantage of for distillation [59], strongly-correlated emission [201] and quantum information processing [200]. These strong correlations, that in many situations violate the limits imposed by classical physics, and that can be harvested to provide sources of non-classical light, will be the topic of the next Chapters of this Thesis.

4

VIOLATION OF CLASSICAL INEQUALITIES BY PHOTON FREQUENCY-FILTERING

Why, sometimes I've believed as many
as six impossible things before breakfast.

— Lewis Carroll, Alice in Wonderland

4.1 INTRODUCTION

In Chapter 3, we introduced a quantity central to this Thesis, the second-order frequency-resolved correlation function $g^{(2)}_{\Gamma}(\omega_1, \omega_2; \tau)$, and showed how by spanning over all possible combinations of frequencies—the two-photon spectrum—we can reveal features that extend the fundamental observations of Hanbury Brown and Twiss. As in the original HBT effect, this phenomenology—its most striking feature being an effective repulsion between photons of different energies—is well described both by a quantum theory and a classical description with scalar electromagnetic fields. This Chapter, while also devoted to the analysis of the two-photon spectrum, focuses on an opposite scenario: the emergence of features that are impossible to describe from a classical point of view.

Classical descriptions of the electromagnetic field [156] and local hidden variable theories [27] yield a series of inequalities that impose an upper limit to the correlations between two modes and whose violation prove unequivocally the non-classical character of quantum mechanics [192]. Among such equalities, the Cauchy–Schwarz inequality and Bell's inequalities are prominent examples that have been put to scrutiny in a large and varied set of platforms. The Cauchy–Schwarz Inequality (CSI) [104] is one of the most important relations in all of mathematics. It states that fluctuations of products of random variables are bounded by the product of autocorrelations: $|\langle XY \rangle| \leq \sqrt{\langle X^2 \rangle \langle Y^2 \rangle}$. When X and Y are quantum observables, however, this relation can be violated. That is to say, quantum correlations between two separate objects can be so strong as to overcome their individual fluctuations in a way that is unaccountable by classical physics. Bell's inequalities (BI), on the other hand, refer to the wider problem of the nonlocal character of quantum mechanics [16]. Their violation decides in favour of quantum theory over local hidden variable theories. The underlying correlations are well known to power quantum information processing [75].

The first experimental demonstrations of violation of these inequalities were realized in the 70s in the radiation of an atomic two-photon cascade

for the CSI [48] and in the early 80s for the BI [18, 19]. There has been a large body of literature confirming and documenting such violations ever since [23, 131, 142, 162, 197, 198, 222]. Most experimental realizations in both cases involve the correlation of photons of different frequencies emitted in a multi-photon process, such as atomic cascades [18] or four-wave mixing [218, 222]. In the underlying theoretical models, these photons are attributed to "decay operators" that correspond to specific optical transitions [192]. This facilitates the calculation of frequency correlations in terms of these operators. They are, however, abstract mathematical representations of the photons, the latter being the only physical reality perceived by the measuring devices. One can inquire what are the correlations between photons with a given property—typically, frequency and polarization for CSI and BI respectively—with no theoretical prejudice as to their origin in terms of underlying operators. For instance, one can ask what are the correlations from spectral windows that do not correspond to transitions that such a model can represent through suitable decay-operators. In this Chapter, we address this question in a general context for frequency correlations, but to fix ideas, we will illustrate our claims on one particular source of photons. To emphasize that the frequency-correlated photons do not need to be attached to different modes, we will consider a single-mode emitter and focus on the simplest non-trivial candidate: the emission from a coherently-driven two-level system. This model is of great intrinsic interest and has been a favourite testbed of quantum optics [134]. To make clear that this is a general theme that is not specific to this system, however, we will also discuss briefly similar results in the Jaynes–Cumming dynamics [120].

These results have been published in Physical Review A [200].

4.2 RESONANCE FLUORESCENCE: THE MOLLOW TRIPLET

In this section we introduce one of the most simple and fundamental quantum optical systems, that stands as a central concept for this Thesis: a two-level system (2LS) excited by coherent light. The light emitted by such a system is termed *resonance fluorescence* [22, 79, 154]. We denote the ground and excited state of the 2LS by $|g\rangle$ and $|e\rangle$ respectively, so that $\sigma \equiv |g\rangle\langle e|$ is the annihilation operator. The coherent driving is included in the Hamiltonian as a term given by Eq. (85), yielding a total Hamiltonian:

$$H_0 = \omega_\sigma \sigma^\dagger \sigma + \Omega(e^{-i\omega_L t}\sigma^\dagger + e^{i\omega_L t}\sigma) \tag{216}$$

with ω_σ the energy of the 2LS and Ω describes the amplitude of the field driving it with frequency ω_L. With little loss of generality we will consider resonant excitation: $\omega_L = \omega_\sigma$. Dissipation for the emitter is included in the density matrix formalism as a Lindblad term $\mathcal{L}_\sigma\rho$ with decay rate γ_σ in the master equation:

$$\frac{\partial \rho}{\partial t} = -i\,[H_0, \rho] + \frac{\gamma_\sigma}{2}\mathcal{L}_\sigma\rho \tag{217}$$

where $\mathcal{L}_\sigma\rho = 2\sigma\rho\sigma^\dagger - \sigma^\dagger\sigma\rho - \rho\sigma^\dagger\sigma$.

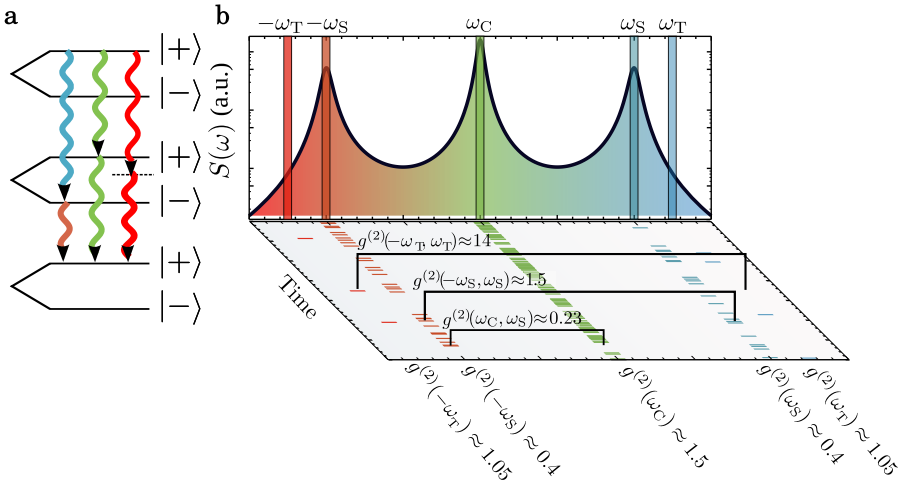

Figure 4.1: Violation of CSI and BI by frequency-resolved correlations. a, Single-photon transitions between manifolds in the ladder can have three type of energies (blue, orange and green arrows). Two-photon de-excitation between rungs of the Mollow ladder may involve an intermediate real state (blue, orange and green arrows) or a virtual state (red arrows). The latter type conveys CSI and BI violation. It is found in the flanks or between the peaks, where the signal is however weaker. **b**, Spectrum of resonance fluorescence, where filtering is illustrated in the tails (T), sidebands (S) and central peak (C) of the Mollow triplet. Parameters: $\Omega = 10\gamma_\sigma$, $\Gamma = \gamma_\sigma$, $\omega_S \approx 2\Omega$, $\omega_T = 2.5\Omega$.

The bare states of the joint 2LS-laser system are grouped into manifolds of a constant number of excitations n, consisting of the states $\{|n, g\rangle, |n-1, e\rangle\}$, where n denotes the number of photons in the exciting mode. As we will discuss in more detail in Chapter 5, when the 2LS and the light are coupled, each of the manifolds are diagonalized to yield two eigenstates $|\pm\rangle_n$, whose separation in energies is proportional to $\sqrt{n}$. However, for high values of n, sine $\partial\sqrt{n}/\partial n \sim 0$, one can drop the dependence of n in the energy separation between these states.

In our model of coherent driving, though, the electromagnetic mode is assumed to be in a coherent state and its quantum fluctuations are not explicitly included in the description. Therefore, our Hilbert space is only of dimension 2. However, we can still understand the phenomenology of this model as the limit of large n of the previous discussion [52]. We thus see that the separation between $|+\rangle_n$ and $|-\rangle_n$, which is independent of n, is given in this picture by $\omega_S \equiv 2R$, where R is the *Rabi frequency*:

$$R \equiv \sqrt{\Omega^2 + \left(\frac{\Delta}{2}\right)^2}. \tag{218}$$

Based on this, we can picture the spectrum of energy levels as a ladder of doublets $|\pm\rangle$ split by an energy ω_S, each of them defining a manifold of excitation, see Fig. 4.1 a. The separation between manifolds (i.e., between a state $|+\rangle$ and the state $|+\rangle$ one step up in the ladder) is just given by the laser energy, ω_L.

One can solve Eq. (217) to obtain an analytical expression of the spectrum of resonance fluorescence. At high pumping intensity, this spectrum develops a structure of three peaks known as the Mollow triplet, presenting a central peak at $\omega = \omega_L$ and two sidebands at $\omega = \omega_L \pm \omega_S$, see Fig. 4.1 b. These peaks are related to the four possible transitions that can take place between adjacent manifolds: two going from $|\pm\rangle$ to $|\pm\rangle$ with energy ω_L (green arrows in Fig. 4.1 a), one from $|+\rangle$ to $|-\rangle$ with energy $\omega_L + \omega_S$ (blue arrow), and one from $|-\rangle$ to $|+\rangle$ with energy $\omega_L - \omega_S$ (orange arrow).

While the emission comes from a single mode, σ, the distinctive spectral shape calls naturally to question what are the correlations of—and between—the three peaks. It has been suggested theoretically [10, 50, 176, 205] and established experimentally [17, 205, 227] that the photons from the peaks are strongly correlated. It is at this point where an ad hoc multiple-mode description is usually enforced out of the genuine single mode σ. One introduces three auxiliary decay operators associated to the three peaks, written in terms of the dressed states $|\pm\rangle$: $\sigma_1 = c^2|-\rangle\langle+|, \sigma_2 = cs\,[|+\rangle\langle+| - |-\rangle\langle-|]$ and $\sigma_3 = -s^2|+\rangle\langle-|$ with s and c two amplitudes [10, 176]. One can easily compute correlations $\langle\sigma_i^\dagger\sigma_j^\dagger\sigma_j\sigma_i\rangle$ for $1 \leq i,j \leq 3$ between these operators, that are associated in the input-output formalism to those $\langle a_i^\dagger a_j^\dagger a_j a_i\rangle$ of the detected photons with a given frequency [85]. There are various shortcomings to this approach, which is an approximation rooted in the physical picture of the dressed atom. First, the identification of each photon to a given transition based on its frequency is a simplification. Although infrequent, it happens that a photon detected at the frequency of a given peak actually originates from the transition that chiefly accounts for another peak. When considering regions of overlap, such a misattribution can become a source of large errors. Second, this approach neglects interferences between photons that truly are emitted by the same mode σ. Third, operators defined in this way are usually non-commuting, and therefore correlations at zero delay can yield different results depending on the order of the operators [205]. Last, but not least, this approach also restricts the calculation to the three operators thus defined, while one can correlate any two frequency windows, of various widths and centred at arbitrary frequencies, not compulsorily at the peak maxima.

4.3 THEORY OF FREQUENCY CORRELATIONS

To dispense from these approximations and constrains, an exact theory of frequency-resolved photon detection is required to correlate any two photons based only on their measured properties, with no assumption as to their origin or time of emission. The formal expression for the second-order correlation function between photons of two different frequencies, $g_\Gamma^{(2)}(\omega_1,\omega_2)$, was introduced in Eq. (184). We will recourse to del Valle *et al.*'s theory of frequency-resolved photon correlations [67], introduced in Section. 3.1.4, to compute exactly this measurable property. We recall that this is done by associating the frequency-resolved correlations of the light emitted by the system to the cross-correlations between sensors weakly coupled to it, giving:

$$g_\Gamma^{(2)}(\omega_1,\omega_2) = \lim_{\varepsilon\to 0} \frac{\langle\varsigma_1^\dagger\varsigma_2^\dagger\varsigma_2\varsigma_1\rangle}{\langle\varsigma_1^\dagger\varsigma_1\rangle\langle\varsigma_2^\dagger\varsigma_2\rangle}\,. \tag{219}$$

where ς_i is the annihilation operator of the i-th sensor. This method involves no intermediate, artificial decay operators associated with a given frequency,

and therefore, it takes into account all the possible interferences and indistinguishability imposed by quantum mechanics.

With such a theoretical apparatus, a full mapping of the photon correlations can be obtained. For the case of the Mollow triplet that we have chosen for illustration, the problem takes the vivid form pictured in Fig. 4.1. The spectral shape—the triplet—is represented in log scale with a choice of five frequency windows, centered at $\pm\omega_T$ (tails), $\pm\omega_S$ (sidebands) and ω_C (central peak). A quantum Monte Carlo trajectory was calculated to simulate the photon-detection events [190] for photo-detectors measuring in these windows. The emitted photons in a small fraction of the trajectory are represented with ticks on the projected plane of Fig. 4.1 b. The intensities vary in each frequency window: there is of course more signal in the central peak than in the sidebands and more so than in the tails. What is of interest in quantum optics is the statistical distribution of, and the correlation between, these photons. The auto-correlation in a given window, shown in the lower part of Fig. 4.1 b, gives the statistics of emission of the stream of photons now defined by their mean frequency and spread. While the light emitted by the two-level system overall is perfectly antibunched, one sees that by spectral filtering, one can "distill" light with different statistical properties [59], namely, i) uncorrelated in the tails, ii) antibunched in the satellite peaks and iii) bunched in the central peak. One can similarly calculate the cross-correlations between photons from two different windows, showing this time that photons from the satellites are positively correlated, $g^{(2)}_\Gamma(-\omega_S, \omega_S) \approx 1.5$, while photons from one satellite and the central peak are anti-correlated, with $g^{(2)}_\Gamma(\omega_C, \omega_S) \approx 0.23$. It is worth noting here that the stronger correlations come from the tail events, with $g^{(2)}_\Gamma(-\omega_T, \omega_T) \approx 14$ for the window chosen, and increasing with greater still separations. The price to pay for these strong correlations is a correspondingly vanishing signal. Events are more rare but the strength of their correlations is increased. This is a general trend.

4.4 CAUCHY-SCHWARZ AND BELL'S INEQUALITIES

As we will show in the next Section, these correlations can be so strong as to surpass the boundaries that would exist were this fields classical in nature. In this Section we review two of these limits, given the *Cauchy-Schwarz inequality* and *Bell's inequalities*, and discuss how these classical limits are expressed in terms of upper boundaries for the correlations of the frequency-filtered fields.

4.4.1 CAUCHY–SCHWARZ INEQUALITY

Cauchy-Schwarz inequality states that, given two vector $\mathbf{X}$ and $\mathbf{Y}$, the absolute value of their inner product $\langle \mathbf{X}, \mathbf{Y} \rangle$ is bounded as:

$$|\langle \mathbf{X}, \mathbf{Y} \rangle|^2 \leq \langle \mathbf{X}, \mathbf{X} \rangle \langle \mathbf{Y}, \mathbf{Y} \rangle. \tag{220}$$

The **Cauchy-Schwarz inequality** was published for the first time by Augustin-Louis Cauchy in 1821, in its form for sums. The inequality for integrals was derived later by Viktor Bunyakovsky in 1859, and its modern proof was obtained by Hermann Amandus Schwarz in 1888.

In the case in which the inner product is the dot product, this inequality sets a limit to its absolute value, given by the product of the absolute values of the vectors:

$$|\mathbf{X}\cdot\mathbf{Y}|^2 \leq |\mathbf{X}|^2|\mathbf{Y}|^2. \tag{221}$$

This inequality can be used to set some bounds on the correlations observed on quantities than can be described in this way, as would be a classical field. This is done by considering a stochastic variable X_i, the index i denoting the $i-$th stochastic realization. The mean value of the variable, $\langle X\rangle$, is obtained by averaging over a large ensemble of realizations:

$$\langle X\rangle = \lim_{N\to\infty}\frac{1}{N}\sum_i^N X_i\,. \tag{222}$$

For ease of notation, from now on we will not write explicitly the limit and will always consider N to be a large number. The previous definition corresponds to a classical description; in quantum mechanics, the mean value of an observable $\hat{X}$ will not necessary be described by Eq. (222), which is associated with a positive probability distribution $\rho(X)$:

$$\langle X\rangle = \int \rho(X)X\,dX\,. \tag{223}$$

In the following, we show some of the limits that this classical description imposes on different kinds of second-order correlations.

ANTIBUNCHING The first set of boundaries we consider concerns the second-order time correlations of a field. Let us consider X and Y to be the intensity of a field that undergoes stochastic evolution, at times t and $t+\tau$: $X_i = I_i(t)$, $Y_i = I_i(t+\tau)$. A first, straightforward bound for the autocorrelation of the intensity can be obtained simply by considering that I_i is a set of real numbers. In that case, the square of the sum of two members of the ensemble $I_i + I_j$ must be positive, giving:

$$2I_iI_j \leq I_i^2 + I_j^2\,. \tag{224}$$

Applying this in all the cross terms appearing in the expression of $\langle I_i\rangle^2$ resulting from Eq. (222), we can write:

$$\langle I(t)\rangle^2 = \left[\frac{\sum_i^N I_i(t)}{N}\right]^2 \leq \frac{1}{N}\sum_i^N I_i(t)^2 = \langle I(t)^2\rangle\,, \tag{225}$$

giving

$$\frac{\langle I(t)^2\rangle}{\langle I(t)\rangle^2} = g^{(2)} \geq 1\,. \tag{226}$$

This states that the second-order correlation function at zero delay must always be equal or larger than one in a field following a classical description. This can also be regarded as a consequence of the fact that a field described by a probability distribution such as (223) has a positive variance,

$\langle I(t)^2\rangle - \langle I(t)\rangle^2 \geq 0$, and is a manifestation of the "cluttering" of photons in a thermal field discussed in Section 3.1.2. The violation of this inequality is the phenomenon known as *photon antibunching*. It cannot be accounted for by a classical theory of light, and it is therefore considered as a determining evidence of its quantum character. Antibunching manifests naturally in the light emitted from quantum sources that can only accommodate and emit one photon at a time.

A bound for the *temporal* second-order correlation can also be derived from the Cauchy-Schwarz inequality of Eq. (221). If we write the ensemble $I_i(t)$ in the form of a vector, $I_i(t) = \mathbf{I}(t)$, following Eq. (222), we obtain:

$$\langle I(t)I(t+\tau)\rangle = \frac{1}{N}\sum_i^N I_i(t)I_i(t+\tau) = \frac{1}{N}\mathbf{I}(t)\cdot\mathbf{I}(t+\tau) \tag{227a}$$

$$,\langle I(t)^2\rangle = \frac{1}{N}\sum_i^N I_i(t)^2 = \frac{1}{N}\mathbf{I}(t)\cdot\mathbf{I}(t)\,. \tag{227b}$$

According to Eq. (221), the dot product between the two vectors $\mathbf{I}(t)$ and $\mathbf{I}(t+\tau)$ satisfies: $|\mathbf{I}(t)\cdot\mathbf{I}(t+\tau)|^2 \leq [\mathbf{I}(t)\cdot\mathbf{I}(t)][\mathbf{I}(t+\tau)\cdot\mathbf{I}(t+\tau)]$. Taking the square root of both sides of the inequality, and taking into account that in a steady state, mean values are independent of time:

$$\langle I(t)\rangle = \langle I(t+\tau)\rangle\,, \tag{228}$$

we obtain:

$$\langle I(t)I(t+\tau)\rangle \leq \langle I(t)\rangle^2\,, \tag{229}$$

or, equivalently,

$$g^{(2)}(\tau) \leq g^{(2)}(0)\,, \tag{230}$$

meaning that time-delayed correlations within a classical field cannot exceed the correlations at zero delay. The violation of this inequality is automatically implied in the case of antibunched light in the steady state, where inequality (226) is violated. This is due to the fact that correlations will always disappear at large delays, $g^{(2)}(\tau\to\infty) = 1$, and therefore, the $g^{(2)}(\tau)$ of any state violating inequality (226) will need to eventually acquire values larger than $g^{(2)}(0)$ to reach 1. However, it is important to notice that states that are not antibunched in the sense of inequality (226) can display a quantum character by violating inequality (230).

MULTIMODE CORRELATIONS The previous argument can be equally applied to the zero-delay correlations between two different fields with intensities $I_1(t)$ and $I_2(t)$, if we now consider X and Y to be $X_i = I_{1,i}(t)$, $Y_i = I_{2,i}(t)$. Expressing the ensemble in vectorial form, $I_{1,i}(t) = \mathbf{I}_1(t)$, $I_{2,i}(t) = \mathbf{I}_2(t)$, and making use again of the CSI (221), we obtain:

$$\langle I_1(t)I_2(t)\rangle^2 \leq \langle I_1(t)^2\rangle\langle I_2(t)^2\rangle\,, \tag{231}$$

which, dividing on both sides by $\langle I_1(t)\rangle^2\langle I_2(t)\rangle^2$ gives the CSI in terms of the multimode second-order correlation function:

$$[g_{12}^{(2)}]^2 \leq g_{11}^{(2)} g_{22}^{(2)}. \tag{232}$$

In a quantum context, this can be expressed in terms of Glauber's second-order correlation functions at zero delay [93] :

$$g_{ij}^{(2)} = \frac{\langle \varsigma_i^\dagger \varsigma_j^\dagger \varsigma_j \varsigma_i \rangle}{(\langle \varsigma_j^\dagger \varsigma_j \rangle \langle \varsigma_i^\dagger \varsigma_i \rangle)}, \tag{233}$$

where ς_1 and ς_2 correspond to the bosonic annihilation operators of mode 1 and 2. We will define a ratio R that quantifies the degree of CSI violation:

$$R = \left[g_{12}^{(2)}\right]^2 \Big/ \left[g_{11}^{(2)}\, g_{22}^{(2)}\right], \tag{234}$$

so the CSI takes the form:

$$R \leq 1\,. \tag{235}$$

In this Chapter, we analyse the case in which the two modes 1 and 2 previously discussed correspond to light filtered at frequencies ω_1 and ω_2. One can use the definition (219) for the cross correlations of Eq. (234) to obtain a degree of CSI violation for frequency filtered light, $R_\Gamma(\omega_1, \omega_2)$.

4.5 BELL'S INEQUALITY

We have seen how the classical descriptions of light are incompatible with certain results involving second-order correlations of the fields. The violation of these fundamental limits are normally interpreted as an evidence of the fact that light is ultimately quantum (and thereby, composed of photons). The discussion exists, however, whether quantum mechanics is an incomplete theory or not, with the maximum exponent of this debate being the fundamental paradox posed by Einstein-Podolsky-Rosen (EPR) [74]. The EPR paradox consisted of a mental experiment to prove that the wavefunction is not a complete description of reality, and that some *hidden variables* must exist that remove the apparent probabilistic nature of quantum mechanics. A hidden variable theory postulates the existence of unknown states $|\lambda\rangle$, so that the expectation value of any observable O is mathematically described as:

Stated in 1935, the **EPR paradox** showed that entangled particles could violate Heisenberg's uncertainty principle unless measuring one particle would instantaneously affect the other, what was considered a "spooky action at distance".

$$\langle O\rangle = \int \rho(\lambda) O(\lambda)\, d\lambda. \tag{236}$$

where $\rho(\lambda)$ corresponds to the density distribution over the states $|\lambda\rangle$. The apparent randomness of quantum mechanics would emerge from our ignorance and lack of control of the hidden variables λ, whose number is not restricted.

ENTANGLED STATES The EPR paradox emerged from the exotic properties of *entangled states*. The state of a group of particles is entangled if it cannot be decomposed as the product of individual particle states, so that the quantum state of one particle cannot be described independently of the others. This yields some counterintuitive effects, since a measurement performed on one of the particles might seem to affect the properties of the others, even if the system are separated over long distances. One of the simplest instances of an entangled state is the singlet state:

$$|\psi\rangle = \frac{1}{\sqrt{2}}(|\uparrow\downarrow\rangle + |\downarrow\uparrow\rangle) \tag{237}$$

where a measurement on the spin of one of the particles would instantly define the spin of the other, no matter how far these particles are from each other. The discussion about the necessity of hidden variables seemed a philosophical question beyond experimental testing until 1964, when John Stewart Bell derived an inequality on measurable correlations between particles that could confirm or exclude the necessity of a hidden variable theory [26].

John Stewart Bell (28 June 1928–1 October 1990) was a theoretical physicist born in Northen Ireland. He is well known for the derivation of the inequalities that we describe in this Chapter.

DERIVATION OF THE BELL'S INEQUALITY In order to derive a Bell inequality [28, 192], we consider two measuring apparatuses, A and B. In the most general case, the outputs of A and B correspond to two quantities, $\langle S_A(\theta)\rangle$ and $\langle S_B(\phi)\rangle$, that take values from -1 to 1. The outcomes depend on θ and ϕ, which are controllable parameters of the apparatuses A and B respectively. These quantities can be constructed from probabilities associated to some sort of dichotomic measurement in each apparatus, $P^A_\pm(\theta)$, $P^B_\pm(\phi)$, so that, $P^A_\pm(\theta) \geq 0$ and $P^A_+(\theta) + P^A_-(\theta) = 1$ (same for B). Then, $S_A(\theta)$ and $S_B(\phi)$ are defined as:

$$S_A(\theta) = P^A_+(\theta) - P^A_-(\theta)\,, \tag{238a}$$
$$S_B(\phi) = P^B_+(\phi) - P^B_-(\phi)\,. \tag{238b}$$

This type of output can come, for instance, from a dichotomic measurement in which, in each apparatus, a particle must select one of two possible channels, one giving a value -1 and the other 1, with probabilities $P^A_\pm(\theta)$ and $P^B_\pm(\phi)$. However, this is not the only possibility; we can equally construct the observables $\langle S_A(\theta)\rangle$ and $\langle S_B(\phi)\rangle$ from any pair of quantities $I^A_\pm(\theta)$, $I^B_\pm(\phi)$ simultaneously measured in each of the apparatuses, defining the probabilities:

$$P^A_\pm(\theta) = \frac{I^A_\pm(\theta)}{I^A_+(\theta) + I^A_-(\theta)}\,, \tag{239a}$$
$$P^B_\pm(\phi) = \frac{I^B_\pm(\phi)}{I^B_+(\phi) + I^B_-(\phi)}\,, \tag{239b}$$

without necessarily assuming pure, deterministic states that would always yield $P^A_+(\theta) = 1, 0$, $P^A_-(\theta) = 1 - P^A_+(\theta)$.

To provide a concrete example without losing generality, we will consider that $I^A_\pm(\theta)$ and $I^B_\pm(\phi)$ correspond to the field intensity measured at the output arms of a beam splitter, one labeled $+$ and the other $-$, as sketched in

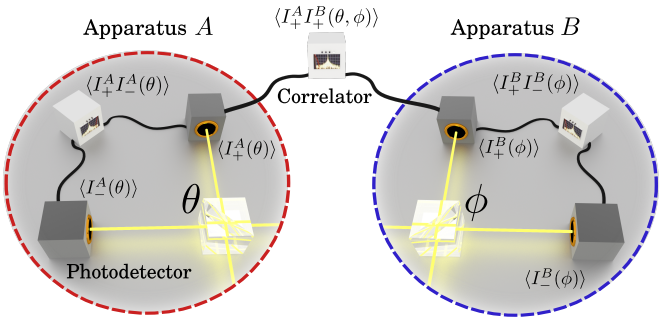

Figure 4.2: Test for the violation of the Bell inequality. Two measurement apparatus with two photodetectors each, measuring intensities $\langle I_\pm^{A_\theta}\rangle$, $\langle I_\pm^{B_\phi}\rangle$

Fig. 4.2. The parameters θ and ϕ could correspond, for instance, to the polarization angle of a polarizing beam splitter, or simply a tunable transmissivity. From the current measured by the photodectectors one can directly obtain the mean value of the intensities, $\langle I_\pm^A(\theta)\rangle$, and by means of correlators one can measure correlations of the type $\langle I_i^A I_j^B(\theta,\phi)\rangle$, where $i,j\in\{+,-\}$. In a hidden variable theory, a state $|\lambda\rangle$ characterized by the hidden variable λ would deterministically yield an expected value of the intensities, that we label as $I_\pm^A(\lambda,\theta,\phi)$. According to Eq. (236), the measured mean values would then be given by:

$$\langle I_i^A I_j^B(\theta,\phi)\rangle = \int \rho(\lambda) I_i^A(\lambda,\theta,\phi) I^B(\lambda,\theta,\phi)\, d\lambda. \tag{240}$$

We can make the reasonable assumption that, for a given λ, the results at B cannot be affected by the choice of the apparatus parameter θ made at A, and vice versa:

$$\begin{aligned} I_\pm^A(\lambda,\theta,\phi) &= I_\pm^A(\lambda,\theta),\\ I_\pm^B(\lambda,\theta,\phi) &= I_\pm^B(\lambda,\phi). \end{aligned} \tag{241}$$

A hidden variable theory satisfying these assumptions is called a *local hidden variable theory.*

Bell's inequality is constructed from the correlations between the observables $S_A(\theta)$ and $S_B(\phi)$, $E(\theta,\phi)=\langle S_A S_B(\theta,\phi)\rangle$ From equations (238) and (239), this takes the form:

$$E(\theta,\phi) = \frac{\langle (I_+^A - I_-^A)(I_+^B - I_-^B)\rangle}{\langle (I_+^A + I_-^A)(I_+^B + I_-^B)\rangle}, \tag{242}$$

where we dropped explicit dependences on θ and ϕ to lighten the notation. According to equations (236) and (241), in a local hidden variable theory this quantity would be written as:

$$E(\theta,\phi) = \frac{1}{D}\int \rho(\lambda)[I_+^A(\lambda,\theta) - I_-^A(\lambda,\theta)][I_+^B(\lambda,\theta) - I_-^B(\lambda,\theta)]\, d\lambda, \tag{243}$$

with

$$D = \int \rho(\lambda)[I_+^A(\lambda,\theta) + I_-^A(\lambda,\theta)][I_+^B(\lambda,\theta) + I_-^B(\lambda,\theta)]\, d\lambda\,. \tag{244}$$

Noting that the total intensity measured in each of the apparatuses is independent of the measurement parameters θ, ϕ:

$$I^A(\lambda) = I^A_+(\lambda,\theta) + I^A_-(\lambda,\theta)\,, \tag{245a}$$
$$I^B(\lambda) = I^B_+(\lambda,\phi) + I^B_-(\lambda,\phi)\,, \tag{245b}$$

the hidden-variable version of the most general quantities $S_A(\theta)$ and $S_B(\theta)$ reads:

$$S_A(\lambda,\theta) = \frac{I^A_+(\lambda,\theta) - I^A_-(\lambda,\theta)}{I^A(\lambda)}\,, \tag{246a}$$
$$S_B(\lambda,\phi) = \frac{I^B_+(\lambda,\phi) - I^B_-(\lambda,\phi)}{I^B(\lambda)}\,. \tag{246b}$$

We now rewrite $E(\theta,\phi)$ in terms of these quantities:

$$E(\theta,\phi) = \frac{1}{D}\int f(\lambda) S_A(\lambda,\theta) S_B(\lambda,\theta)\, d\lambda\,, \tag{247a}$$
$$D = \int f(\lambda)\, d\lambda\,, \tag{247b}$$

where $f(\lambda) = \rho(\lambda) I^A(\lambda) I^B(\lambda)$. Now, following Bell's 1971 proof (page 9 of [28]), we have:

$$\begin{aligned} &E(\theta,\phi) - E(\theta,\phi') \\ &= \frac{1}{D}\int f(\lambda) S_A(\lambda,\theta) S_B(\lambda,\phi)\, d\lambda - \frac{1}{D}\int f(\lambda) S_A(\lambda,\theta) S_B(\lambda,\phi')\, d\lambda \\ &= \frac{1}{D}\int f(\lambda) S_A(\lambda,\theta) S_B(\lambda,\phi)[1 \pm S_A(\lambda,\theta') S_B(\lambda,\phi')]\, d\lambda \\ &\quad - \frac{1}{D}\int f(\lambda) S_A(\lambda,\theta) S_B(\lambda,\phi')[1 \pm S_A(\lambda,\theta') S_B(\lambda,\phi)]\, d\lambda. \end{aligned} \tag{248}$$

Now we make use of the triangular inequality and the fact that $S_A(\lambda,\theta)$ and $S_B(\lambda,\phi)$ are bounded by construction:

$$|S_A(\lambda,\theta)| \le 1\,, \quad |S_B(\lambda,\phi)| \le 1, \tag{249}$$

The **triangular inequality** is a theorem about distances that states that, for any two vectors $\mathbf{a}$ and $\mathbf{b}$: $|\mathbf{a}+\mathbf{b}| \le |\mathbf{a}| + |\mathbf{b}|$.

and eliminate the products involving $S_A(\lambda,\theta)$ in (248):

$$\begin{aligned} &|E(\theta,\phi) - E(\theta,\phi')| \\ &\le \frac{1}{D}\int f(\lambda)[1 \pm S_A(\lambda,\theta') S_B(\lambda,\phi')]\, d\lambda + \frac{1}{D}\int f(\lambda)[1 \pm S_A(\lambda,\theta') S_B(\lambda,\phi)] \\ &= 2 \pm \frac{1}{D}\int f(\lambda)[S_A(\lambda,\theta') S_B(\lambda,\phi') + S_A(\lambda,\theta') S_B(\lambda,\phi)]\, d\lambda \\ &= 2 \pm [E(\theta',\phi') + E(\theta',\phi)], \end{aligned} \tag{250}$$

leading to the Bell inequality in the so called Clauser, Horne, Shimony, Horne (CHSH) form [49]:

$$B \le 2, \tag{251}$$

where

$$B = \left| E(\theta,\phi) - E(\theta,\phi') + E(\theta',\phi') + E(\theta',\phi) \right| . \tag{252}$$

The example of measurement that we depicted in Fig. 4.2 using polarizing beam splitters and θ, ϕ corresponding to polarization angles is one the most typical situations when measuring BI violations for states of the type:

$$|\psi\rangle = \frac{1}{\sqrt{2}}(a^\dagger_{1+}a^\dagger_{2+} + a^\dagger_{1-}a^\dagger_{2-})\,|0\rangle \ , \tag{253}$$

where $a^\dagger_{i,\pm}$ is the creation operator for a photon with polarization $\pm$ along path i, i.e., for states that are entangled. Following the previous argument, our purpose is to prove that the emission of a source displaying strong correlations between different spectral windows can show a violation of the Bell inequality. To do that, we focus on the correlations from the output of a dynamical process, that is, we do not restrict to deterministic pure states [192] but consider a steady state as an input, meaning that the intensities $I^A_\pm(\theta), I^B_\pm(\phi)$ are no restricted to unity but can take any positive value. Since we are interested in the correlations between different frequency modes, we focus on a different scenario that does not involve the polarization degree of freedom, but only two modes states of the type $|\psi\rangle = a^\dagger_1 a^\dagger_2 |0\rangle$. If disposing of an emitter that provides such a two-mode output, it is immediate to bring it into an entangled form

$$|\psi\rangle = \frac{1}{2}(a^\dagger_{1+}a^\dagger_{2+} - a^\dagger_{1-}a^\dagger_{2-} + ia^\dagger_{1-}a^\dagger_{2+} + ia^\dagger_{1+}a^\dagger_{2-})\,|0\rangle \tag{254}$$

by placing two beam splitters across paths 1 and 2. Subscripts $\pm$ then refer to path instead of polarization. By recombining the four resulting beams in two additional beam splitters with variable transmissivities belonging to the apparatuses A and B, these states can also violate the BI by following the same line of reasoning as exposed above [49, 192]. θ and ϕ represent in this case the tunable transmitivities of the two final beam splitters.

The setup implementing such a scheme of BI based on frequency filtering is sketched in Fig. 4.3, where the path degree of freedom 1, 2 is associated

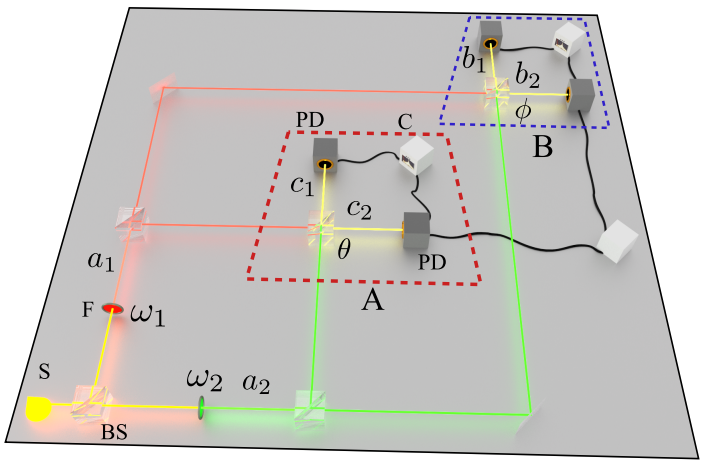

Figure 4.3: Test for the violation of Bell inequalities by frequency filtering. A source (S) emits photons in a broadband of frequencies. Frequency filters (F) select light at frequencies ω_1 and ω_2, described by the operators a_1 and a_2. Recombination at beam splitters (BS) with transmittivities given by $\sin\theta$ and $\sin\phi$ gives a total of four output beams, which are collected at the photodetectors (PD) and correlated with coincidence counters (C). Alice (A) and Bob (B) test nonlocality by independently measuring probability of detection at the output ports of the two beam splitters, $P^{A_\theta}_\pm$ and $P^{B_\phi}_\pm$.

to the energy degree of freedom ω_1, ω_2 by using frequency filters. The two possible channels of detection in each final beam splitter are then equivalent to the two output ports of the polarizing filters of the case depicted in Fig. 4.2. In a quantum-mechanical treatment, the modes at the output arms of the beam splitters are given by:

$$\begin{aligned} c_1 &= \cos\theta a_1 + \sin\theta a_2\,, \quad c_2 = -\sin\theta a_1 + \cos\theta a_2\,, \\ b_1 &= \cos\phi a_1 - \sin\phi a_2\,, \quad b_2 = \sin\phi a_1 + \cos\phi a_2\,, \end{aligned} \tag{255}$$

and $E(\theta, \phi)$ takes the form:

$$E(\theta,\phi) = \frac{\langle : (c_1^\dagger c_1 - c_2^\dagger c_2)(b_1^\dagger b_1 - b_2^\dagger b_2) : \rangle}{\langle : (c_1^\dagger c_1 + c_2^\dagger c_2)(b_1^\dagger b_1 + b_2^\dagger b_2) : \rangle}\,. \tag{256}$$

We adopt the standard choice of angles that provides the greatest violation of the inequality [192]: $\theta = 0, \phi = \pi/8, \theta' = \pi/4, \phi' = 3\pi/8$. This yields the following expression for B:

$$B = \sqrt{2}\left|\frac{\langle a_1^{\dagger 2} a_1^2\rangle + \langle a_2^{\dagger 2} a_2^2\rangle - 4\langle a_1^\dagger a_2^\dagger a_2 a_1\rangle - \langle a_1^{\dagger 2} a_2^2\rangle - \langle a_2^{\dagger 2} a_1^2\rangle}{\langle a_1^{\dagger 2} a_1^2\rangle + \langle a_2^{\dagger 2} a_2^2\rangle + 2\langle a_1^\dagger a_2^\dagger a_2 a_1\rangle}\right|. \tag{257}$$

It is equally easy to formulate these concepts in terms of frequency correlations than for the CSI. The operators a_1 and a_2 in Eq. (255) can be replaced by the sensor operators ς_1 an ς_2 previously introduced and employed into Eq. (219), thus describing the light emitted at the two frequencies ω_1 and ω_2, as shown in Fig. 4.3. Direct application of Eq. (257) with these sensors ς_i, whose finite linewidth Γ is described by their decay rate, provides $B_\Gamma(\omega_1, \omega_2)$.

4.6 CAUCHY-SCHWARZ AND BELL'S INEQUALITIES

4.6.1 RESONANCE FLUORESCENCE

At this point, we have set the stage to fully characterize the quantumness of the emission in terms of violation of the CSI and BI spanning over all the frequencies of emission and windows of detection. Note the considerable improvement as compared to the approach that assigns a decay operator to each spectral line, since a continuum of frequencies in windows of arbitrary sizes can now be investigated without assumptions on the order of emission. Figure 4.4 shows three correlation landscapes in the frequency domain depicting the value of $g_\Gamma^{(2)}(\omega_1, \omega_2)$, $R_\Gamma(\omega_1, \omega_2)$ and $B_\Gamma(\omega_1, \omega_2)$ for three different values of the detector linewidth in an otherwise identical configuration.

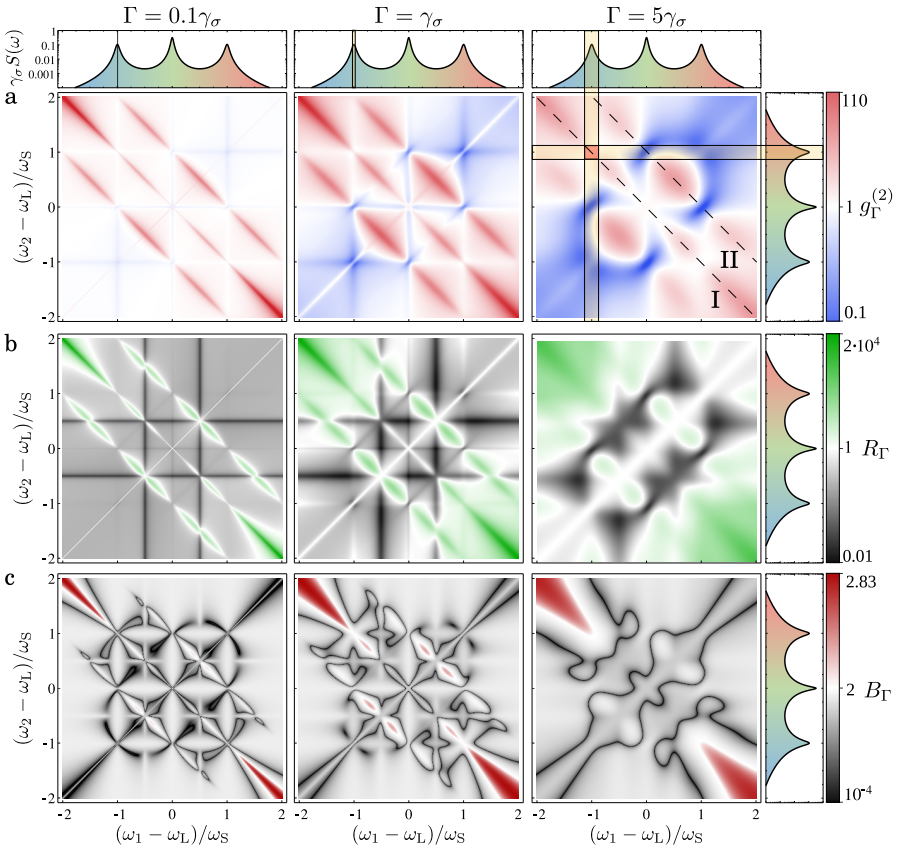

Figure 4.4: Landscapes of correlations in the frequency domain for three different filter linewidths. **a**, $g^{(2)}_\Gamma(\omega_1,\omega_2)$. **b**, $R_\Gamma(\omega_1,\omega_2)$. **c**, $B_\Gamma(\omega_1,\omega_2)$. In b [resp. c], the color code is such that green [resp. red] violates the CSI [resp. BI] and thus corresponds to genuine quantum correlations between the detected photons in the corresponding energy windows, while black and white do not (with white maximizing the inequality). The violation originates from the emission that involves virtual states. Dashed lines I and II in a are the cuts in the frequency domain along which curves in Fig. 4.5 are calculated. The spectra on the axes show which frequency windows are correlated. Parameters are the same as in Fig. 4.1.

It immediately comes across that the quantum character of the emission, where the inequalities are violated, is structured along three antidiagonals. In particular, the anticorrelation $g^{(2)}_\Gamma(\omega_1,\omega_2) < 1$ (corresponding to blue areas in Fig. 4.4 a), is a CSI violation in time when $\omega_1 = \omega_2$ and therefore corresponds to a non-classical effect [157]. It makes no such guarantee, however, of a genuine quantum nature when $\omega_1 \neq \omega_2$, and as discussed in Chapter 3, it could in fact even be produced by a classical emitter.. The corresponding CSI violation in time in this case is $\left[g^{(2)}_\Gamma(\omega_1,\omega_2,\tau)\right]^2 > g^{(2)}_\Gamma(\omega_1,\omega_1,0)g^{(2)}_\Gamma(\omega_2,\omega_2,0)$, which we study at zero time delay $\tau = 0$ in Fig. 4.4 b. Comparing these two rows, one can see that the regions of CSI violation correspond not to frequency antibunching but, on the opposite, to frequency bunching. The reason for this lies in the nature of the violation, with cross-correlations being higher with respect to auto-correlations than is permitted by classical physics.

Physically, the anti-diagonals where this happens are precisely those where two-photon emission occurs in a *leapfrog process* [96], i.e., a jump over the intermediate real state by involving a virtual state instead. This generates the state $|1,1\rangle$ that, fed to beam splitters, generates the maximally entangled state that optimizes the violation. The antidiagonal, line I, corresponds to transitions from $|+\rangle$ to $|+\rangle$ or from $|-\rangle$ to $|-\rangle$, two rungs below, as is sketched in Fig. 4.1 b, thus satisfying $\omega_1 + \omega_2 = 0$. Line II and its symmetric

correspond to transitions from $|+\rangle$ to $|-\rangle$ and from $|-\rangle$ to $|+\rangle$, respectively, satisfying $\omega_1 + \omega_2 = \pm\omega_S$.

CROSSING REAL STATES The CSI and BI are less, or are not, violated whenever the intermediate rung intersects a real state, as seen by the fact that the green (for R_Γ) and red (for B_Γ) regions are depleted or pierced when intersecting the sidebands $\pm\omega_S$. This is particularly important since previous studies focused precisely on correlations between real transitions [10, 17, 50, 176, 205, 205, 227], i.e., between peaks, such as indicated by the red square in the rightmost panel of Fig. 4.4 a. Instead, the exact treatment shows that these are detrimental to the effect, that is optimum when involving virtual states, since these are the vector of quantum correlations. It is easy to prove, from the closed form expression Eqs. (6–8) in Ref. [96], that a single-mode emitter with no dressing (here by the laser) never violates the CSI, regardless of frequencies and detection widths. The same was checked numerically for the case of BI. Notably, this is true even if the emitter is a two-level system and exhibits perfect antibunching, $g^{(2)}(\tau = 0) = 0$. All this evidence confirms that CSI and BI violations are rooted in the quantum dynamics that involves a virtual state in a collective de-excitation in the quantum ladder of the dressed states. Here, one must keep in mind that there is only one emitter, so the term collectivity does not refer to the cooperation of multiple emitters, as is usually the case with effects such as superradiance [8], but to the joint action of multiple excitations of the one emitter. In our case, indeed, two photons team-up to undergo a de-excitation that they can only realize together. Such pairs of photons are at the origin of the quantum emission: other types of de-excitation, which are not collective in this sense, do not violate the classical inequalities.

A more quantitative reading of these results is given in Fig. 4.5 a–b, that shows slices in the landscapes along lines I and II of the rightmost panel of Fig. 4.4 a. The quantum correlations violating the CSI are found in the side peaks and beyond, being larger the farther from the peaks. The same feature is present in the BI violation, which furthermore tends to the maximum value allowed $B_\Gamma = 2\sqrt{2}$.

Figure 4.5 c–d shows $g^{(2)}_\Gamma(\omega, \omega)$ and $g^{(2)}_\Gamma(\omega, -\omega)$—that can be used to derive $R_\Gamma(\omega, -\omega)$ and an approximation of $B_\Gamma(\omega, -\omega)$— as calculated exactly (solid red lines) [67, 96] and through the approximation of auxiliary decay operators used in previous works (dashed blue) [176, 205]. In such an approximation, the estimation is local around the peaks, that is, at $\omega/\omega_S = \pm 1$ and 0 (dotted vertical lines), where it is seen to be fairly accurate indeed, although not numerically exact. It can still lead to qualitative error, e.g., the autocorrelation at the sidebands is exactly zero in this approximation, predicting arbitrary violation of the CSI even when it is obeyed. A violation of the BI was also predicted [125]; however, it was considered ill-defined due to the perfect antibunching of the sidebands.

An **approximation for** $B_\Gamma(\omega, -\omega)$ can be obtained by dropping the last two terms of the numerator in Eq.(257) [9]. This approximation can be applied when there are no second-order transfer of photons between the modes, but these terms could be important in other cases. We have verified that in our case they are negligible.

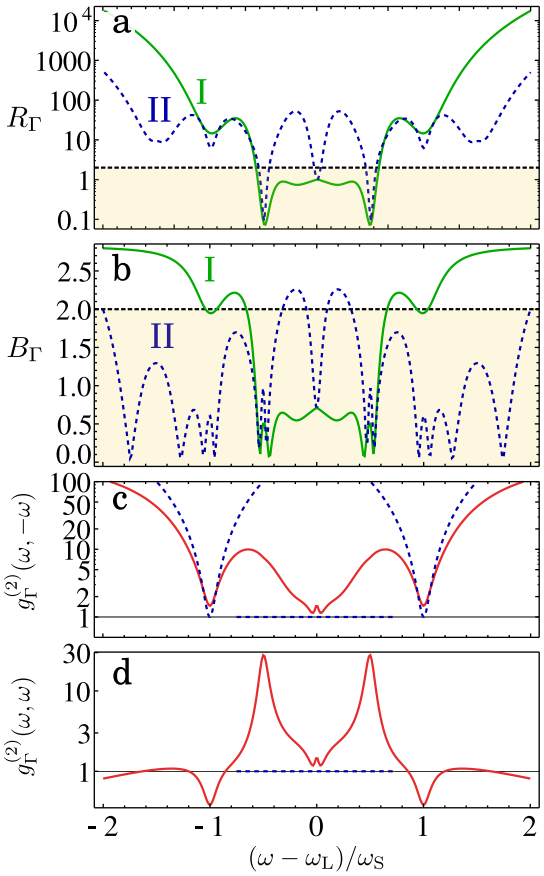

Figure 4.5: **a–b**: Cuts of R_Γ (a) and B_Γ (b) along the lines I $(\omega,-\omega)$ and II $(\omega,\omega_S-\omega)$ of Fig. 4.4 a. Parameters are the same as in Fig. 4.1, with $\Gamma=\gamma_\sigma$. **c–d**: photon-correlation $g^{(2)}_\Gamma(\omega,\pm\omega)$ computed exactly (solid red) or through the usual auxiliary operator approximation (dashed blue). In panel d, the absence of the latter curve in some domains correspond to values which are, incorrectly, exactly zero (the vertical axis is in log-scale).

An animation of the full landscapes of correlations as a function of the linewidth of filtering can be found at:

https://youtu.be/2LvUA4jDvIU

DEPENDENCE ON THE FILTER LINEWIDTH Furthermore, these expressions are found in limiting cases for the filter linewidths: either $\Gamma \ll \gamma_\sigma \ll \Omega$ or $\gamma_\sigma \ll \Gamma \ll \Omega$. Both assume that the peaks are well separated to allow for the auxiliary operator approximation. They predict no CSI or BI violation for narrow filters, which is ultimately verified, although, in the case of CSI, it is for values of the detector linewidth so small that they are unphysical. Solid lines in Fig. 4.6 a show the dependence of R_Γ and B_Γ on the detector linewidth Γ for the three sets of frequencies $(\omega_i,-\omega_i)$, $i\in 1,2,3$ depicted in Fig. 4.6 b. For the already extremely small value of frequency windows $\Gamma=0.1\gamma_\sigma$, the CSI and BI can be violated, in contradiction with the prediction of the auxiliary operator approximation.

There are mainly three regimes of frequency correlations: narrow filters, peak filtering and overlapping windows. While narrow filters better define the structure, as can be seen in Fig. 4.4, they also correspond to longer times of integration due to the time-frequency uncertainty and thus average out the correlations. A maximum is found when filtering in windows of the order of the peak linewidth or above, which is a welcomed result for an experimentalist. The overlap of the filters marks a change of trend in all the curves, due to a competition between various phenomena involving, for instance, various transitions as well as averaging over different types of interferences. Dashed lines in Fig. 4.6 a show the value of $\Gamma S_\Gamma(\omega)$ corresponding to the

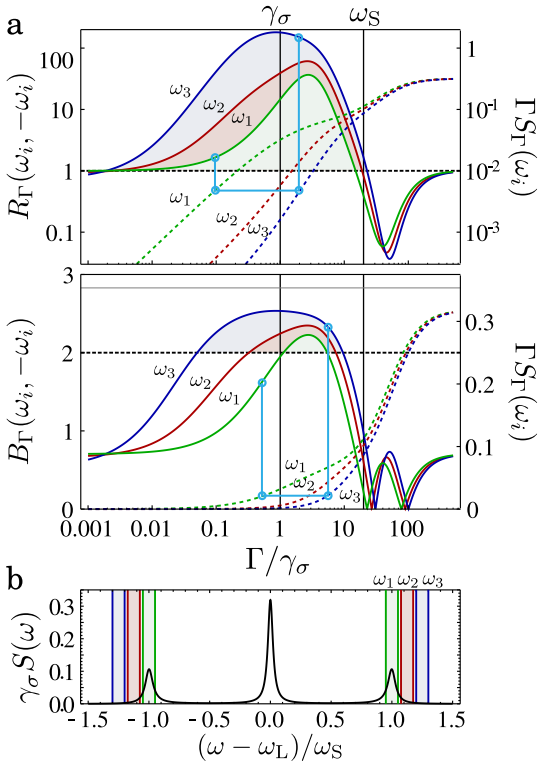

Figure 4.6: **a**, Solid lines: $R_\Gamma(\omega_i,-\omega_i)$ (top panel) and $B_\Gamma(\omega_i,-\omega_i)$ (bottom panel) as a function of the detector linewidth for the three set of frequencies $(\omega_i,-\omega_i)$, $i\in 1,2,3$ depicted in panel (b). Dashed lines: Amount of signal $\Gamma S_\Gamma(\omega)$ that can be collected for the corresponding filter linewidth. Blue points illustrate how two configurations with the same amount of collected signal can yield different degrees of violation. **b**, Resonance fluorescence spectrum, this time in linear scale, displaying the characteristic Mollow triplet and three sensors with linewidth $\Gamma = 2\gamma_\sigma$ centred at the frequencies used for panel (a): $\omega_1 = \omega_S$, $\omega_2 = 1.125\,\omega_S$ and $\omega_3 = 1.25\,\omega_S$. Parameters are the same as in Fig. 4.1.

amount of signal that can be collected with a detector of linewidth Γ at the frequency ω [67]. This way, one can easily compare, for a given amount of available signal, the different degrees of violation which are accessible simply by selecting the frequency and the window of the detector appropriately.

Since such correlations are useful for technological purposes, the ability to compute the entire landscape of frequency correlations becomes helpful for optimizing quantum information processing. Correlations along line I of the map arise from a well defined family of virtual processes, from which sideband correlations have been shown to be just a particular, and in fact also a detrimental case. By positioning the filters away from the sidebands and increasing the frequency window of detection, it is possible to extract light showing stronger quantum correlations without paying any price on the signal. This way, one can optimize quantum correlations in a distillation process in which only photons with sought correlations are retained, and the others are filtered out.

4.6.2 JAYNES-CUMMINGS

The previous results are general, as they relate to the added information one can gain from frequency filtering, rather than on the specificities of the source. While resonance fluorescence is a particular fruitful emitter where to investigate such effects, the same principles apply in any other system which emits correlated photons and that has a spectral structure. To illustrate this point, we show in Fig. 4.7 similar features observed in the case of the Jaynes-Cummings model, see Section 2.2, in which a 2LS interacts with a single

electromagnetic mode via the Hamiltonian $H = g(a^\dagger\sigma + a\sigma^\dagger)$ and with Lindblad terms to describe the incoherent pumping of the 2LS as well as decay of both the 2LS and the electromagnetic mode, leading to the master equation:

$$\frac{\partial\rho}{\partial t} = -i\,[H,\rho] + (\frac{\gamma_\sigma}{2}\mathcal{L}_\sigma + \frac{\gamma_a}{2}\mathcal{L}_a + \frac{P_\sigma}{2}\mathcal{L}_{\sigma^\dagger})\rho. \tag{258}$$

As we will discuss in detail in the next Chapter, the spectral shape of this system is the Rabi doublet at low pumping and a Jaynes–Cummings multiplet when transitions from higher rungs get activated at higher pumping. In Fig. 4.7, one can observe how, again, regions of quantum emission appear along the lines that correspond to families of virtual two-photon processes in the Jaynes-Cummings ladder [96]. There is a region of CSI violation between the Rabi peaks but it is hindered by the proximity of real states transitions. Bell's inequalities are, overall, more difficult to violate than in resonance fluorescence. At lower pumping, only the CSI violation survives and with regions of quantum emission closely associated to those of photon bunching (not shown). A full analysis would bring us to the peculiarities of the Jaynes–Cummings dynamics and therefore goes beyond the scope of this text, which focuses on the principle of frequency filtering to optimize the violation of classical inequalities.

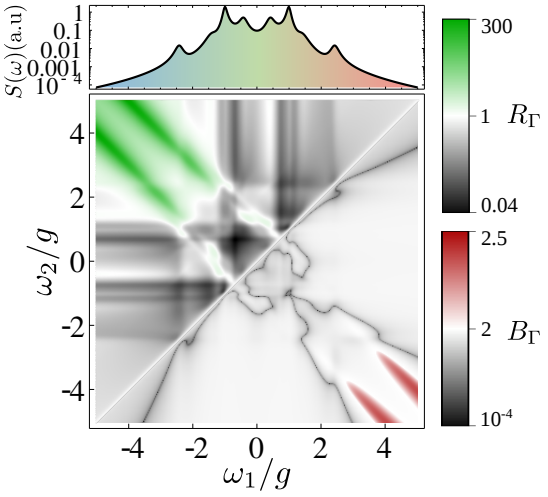

Figure 4.7: Landscapes of correlations for the Jaynes-Cummings model. These correlations violate both Cauchy-Schwarz (upper-left) and Bell's inequalities (bottom-right). The full-landscape for each case follows by symmetry. Parameters: $\gamma_\sigma = 10^{-3}g$, $\gamma_a = 0.1g$, $P_\sigma = 0.05g$, and $\Gamma = 0.1g$.

4.7 CONCLUSIONS AND PERSPECTIVES

We have shown how to evidence and optimize CSI and BI violations between photons resolved in frequency from a quantum source, with no constrains nor approximations from the theoretical description. Maximum violation is to be found not when correlating peaks in the spectrum, as previously thought, and thus linked to transitions between real states, but when involving virtual processes in the quantum dynamics. These results show the potential of frequency correlations to engineer quantum correlations and could be applied towards the design of optimum quantum information processing

devices. In particular, these correlations can be Purcell enhanced when the system is coupled to a single cavity mode, resulting in a new family of light sources that is the topic of the next Chapters.

5 CLIMBING THE JAYNES-CUMMINGS LADDER

Nature uses only the longest threads to weave her patterns, so that each small piece of her fabric reveals the organization of the entire tapestry.

— Richard P. Feynman

5.1 INTRODUCTION

This Chapter offers a review of some of the most important experimental and theoretical efforts that have attempted to reveal the strong quantum character of light matter coupling when it is brought to the ultimate limit, where single photons interact with the most elemental description of matter: a two-level system. We discuss physical phenomena that evidence this quantum character by probing the system with an external, weak laser, and show that by increasing the power of this laser, the same phenomena become a manifestation of an altogether different regime, the dressed-atom, thus bridging the two most fundamental pillars of quantum optics. This has striking physical consequences on the light emitted by the system which will be the topic of the next Chapter.

5.2 NONLINEARITIES IN THE JAYNES-CUMMINGS HAMILTONIAN

The physics of light-matter coupling reaches its most fundamental paradigm when brought to the zero dimensional case. In this limit, a single electromagnetic mode, like a resonant mode confined in an optical cavity, can interact with a quantum emitter (QE), i.e., matter that is sufficiently confined for its spectrum to be quantized in discrete energy levels. In the simplest case where the matter component can be described as a two-level system (2LS), the dynamics of the system can be described by one of the most relevant models in quantum mechanics, the Jaynes-Cummings Hamiltonian, that reads:

$$H = \omega_a a^\dagger a + \omega_\sigma \sigma^\dagger \sigma + g(\sigma^\dagger a + \sigma a^\dagger), \tag{259}$$

where a, σ are the annihilation operators of a bosonic cavity mode and a 2LS, respectively. Specifically, the operator σ is defined as $|g\rangle\langle e|$, with $|g\rangle$ and $|e\rangle$ describing the ground and excited state of the 2LS.

The first landmark of the light-matter coupling physics is the regime of *strong coupling*. When the cavity is good enough to retain a photon for a long time, this photon can be absorbed and emitted by the QE several times,

so that the character of the system oscillates between light and matter. Such an oscillation reflects that the photonic or material modes alone no longer constitute eigenstates of the system. New eigenstates consist in the quantum superposition of particles of light and matter, describing new quasiparticles with mixed properties from both components. This quasiparticles are usually termed 'polaritons'.

Strong coupling was reported for the first time for atoms in optical cavities [223], has also been demonstrated for artificial atoms in circuit quantum electrodynamics [231] and for optical QDs coupled to high-quality microcavities [189, 195, 239]. However, while the phenomenon constitutes a first manifestation of the quantum mixture between light and matter, it finds a straightforward classical analogue in the coupling between two harmonic oscillators. The latter case can also be described from a quantum point of view, this time using two bosonic operators a and b:

$$H = \omega_a a^\dagger a + \omega_b b^\dagger b + g(a^\dagger b + a b^\dagger)\,. \tag{260}$$

We can understand the similarities and differences between both models by analyzing their energy spectrum. The Hamiltonian of two coupled oscillators can be diagonalized by defining new Bose operators, $u = \cos(\theta)a + \sin(\theta)b$, $l = -\sin(\theta)a + \cos(\theta)b$, where the mixing angle is given by $\theta = \arctan\left[g/(\frac{\Delta}{2} + \mathcal{R})\right]$. We call the new modes u and l *upper* and *lower* modes. $\mathcal{R}$ is half of the *Rabi frequency*, and represents the energy splitting between the two new modes:

$$\mathcal{R} = \sqrt{g^2 + \left(\frac{\Delta}{2}\right)}, \tag{261}$$

with $\Delta = \omega_a - \omega_b$, such that the new Hamiltonian reads $H = \omega_+ u^\dagger u + \omega_- l^\dagger l$, with energies:

$$\omega_\pm = \frac{\omega_a + \omega_b}{2} \pm \mathcal{R}\,. \tag{262}$$

The resulting ladder of energies levels is depicted in panel a of Fig. 5.1. It can be divided in manifolds having the same number n of excitations, each of them consisting of n eigenstates of the form $|m, n-m\rangle$, $m \in [0, n]$, where $|m, n\rangle$ represents the state with m excitations on the lower mode, and n on the upper [129]. The multiple transitions that can take place between adjacent manifolds can only have energies ω_- or ω_+, since they imply the annihilation of an exciton from the upper or lower mode. These first-order transitions are reflected in the spectrum of emission, that features a distinct doublet of emission with two peaks centered at ω_- and ω_+. However, there is nothing inherently quantum in the underlying dynamics that gives rise to these two peaks: they just reflect the existence of two normal modes, as happens with two coupled harmonic oscillators in classical mechanics.

In the case of the JC Hamiltonian, we can as well divide the energy spectrum in manifolds with a fixed number n of excitations. However, in this case there are only two eigenstates $|n_\pm\rangle$ per manifold, belonging to the subspace

$\{|n,g\rangle, |n-1,e\rangle\}$. The Hamiltonian can be diagonalized independently in each subspace, giving, for the n-th manifold, the two eigenvalues

$$\omega_{\pm}^{(n)} = n\omega_a - \frac{\Delta}{2} \pm \sqrt{(\sqrt{n}g)^2 + \left(\frac{\Delta}{2}\right)^2}, \tag{263}$$

with $\Delta = \omega_a - \omega_\sigma$. This indicates that the coupling energy between the 2LS and a number of photons larger than one bears the signature of the quantization of light, being larger by a factor of $\sqrt{2}g$, $\sqrt{3}g$, etc. The resulting structure of energy levels can be seen in panel b of Fig. 5.1. Note that the frequency of the cavity was chosen small to aid the visualization; normally it is orders of magnitude larger than the coupling rate g (when both are indeed of the same order, the system is said to be in the *ultrastrong coupling* regime [15, 175, 196, 224], which is not described by the JC Hamiltonian since the rotating wave approximation does not hold). Due to the factor $\sqrt{n}$ in Eq. (263), the energy of the transitions going from one manifold to the next below depends on the number of excitations n that characterizes the manifold. In contrast to the case of the coupled harmonic oscillators, now there are four possible transitions between adjacent manifolds. Each of them belongs to one of three possible groups of transitions that are close in energy: we label these energies ω_R (from $+$ branch to $-$ branch), ω_0 (from $\pm$ to $\pm$) and ω_L (from $-$ to $+$). ω_R corresponds to frequencies larger than that of

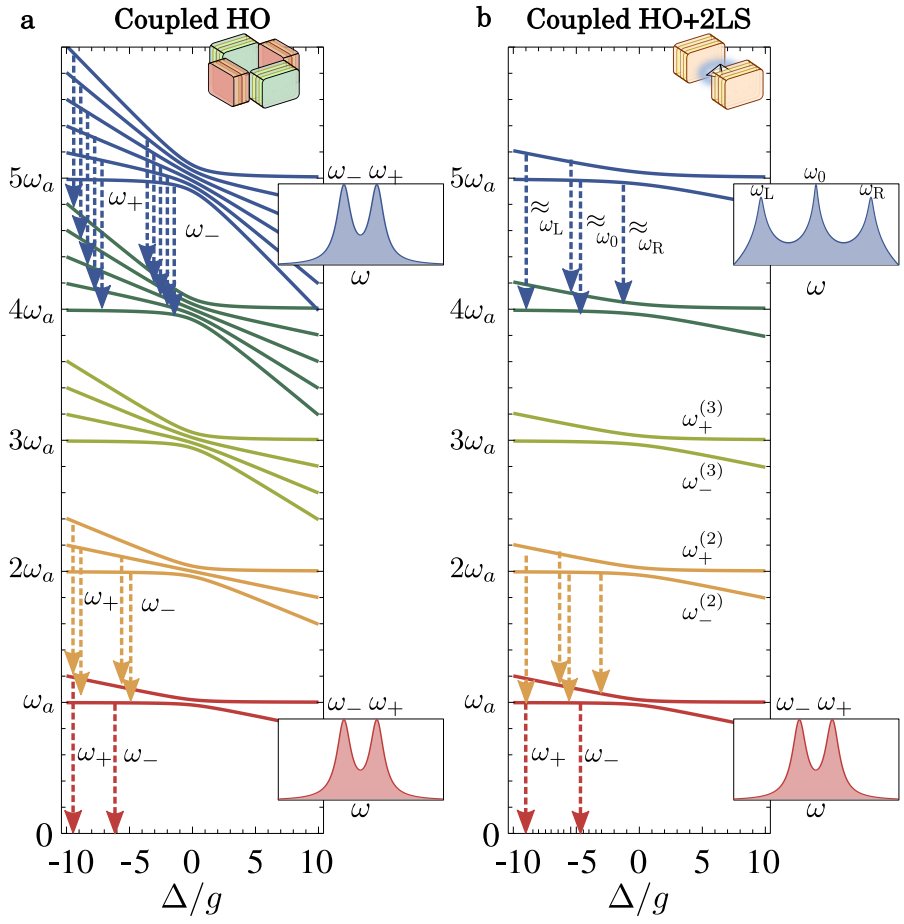

Figure 5.1: Energy spectrum of light matter systems. a, Coupled harmonic oscillators. The spectrum consists of manifolds of excitations (marked with different colors) of equally spaced energy levels. Transitions between manifolds can occur with two possible energies, ω_- and ω_+. **b**, Harmonic oscillator coupled to a two-level system. Each manifold has only two eigenstates, and there four possible transitions between consecutive manifolds with energies that depend on the number of excitations in the system.

the cavity, ω_0, around the cavity energy, and ω_L, lower. While the energy of these transitions change from one manifold to the next, at high manifold numbers, energies belonging to the same group are very close together. This manifests in the spectrum of the light emitted by the 2LS as the three distinctive peaks of the Mollow triplet at frequencies ω_L, ω_0 and ω_R [60]. The position of the sideband peaks, i.e., the values of ω_L and ω_R, depends on the mean number of photons in the cavity, that determines how high in the ladder the system is. Interestingly, this behaviour can be described by a semiclassical model that does not quantize the light field, as in the model of resonance fluorescence presented in Section 4.2. In that case, the cavity field is considered to be in a coherent state and is characterized just by a number (not an operator), with Ω in Eq. (216) determining the mean number of photons n_a as $\Omega = \gamma_a\sqrt{n_a}/2$.

The notation of the subindexes R and L in ω_R and ω_L stands for "right" and "left" sideband

This nonlinear structure of energy levels has an important consequence: the energy required for a photon to be absorbed by the system depends on whether another photon is already present or not, realizing a highly sought case of photon-photon interaction. However, as can be observed in Fig. 5.1, the two transitions that can occur between the first manifold and vacuum have the same energies than in the case of the coupled harmonic oscillators. The corresponding lines in the spectrum are therefore the same two peaks that are associated to the classical, normal mode coupling, what is known as the vacuum-Rabi spectrum. The visualization of these two peaks in the spectrum requires that their separation (given by $2g$ when the bare modes are in resonance, without dissipation) must be greater than the spectral linewidth of the modes (given by the inverse lifetime). Following the intuitive picture given before in terms of photon absorption and emission, this regime corresponds to the situation in which the period of the Rabi oscillations is smaller than the lifetime of the photon, allowing it to be reabsorbed by the emitter inside the cavity. The observation of these two well separated peaks, even in the resonant case where the bare modes have the same energy and only one peak would be expected in the uncoupled case, is known as avoided crossing or anticrossing. While the experimental observation of anticrossing has constituted the first direct indication of the strong coupling between light and matter [189, 195, 239], in order to reveal the nonlinearities of the energy level structure, and therefore the quantum character of the coupled light-matter system, further evidences beyond the observation of a doublet are needed.

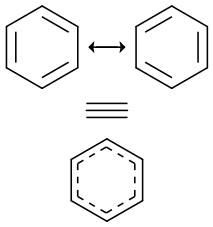

The concept of **anticrossing** is also of great importance in quantum chemistry. Anticrossing always implies the emergence of an eigenstate with lowered energy, with the corresponding increase in stability. Mixing of states to gain more stability is precisely the mechanism of **chemical bond resonance**.

5.3 THE DISSIPATIVE JC LADDER

Providing unambiguous proof of the nonlinear character of systems that seem to be described JC ladder is not an easy task. The first evidences of the $\sqrt{n}$ scaling was obtained by Fourier transform of Rabi oscillations in the time domain using Rydberg atoms [38]. However, direct spectroscopy observation of the higher rungs of the ladder faced much difficulties, the main one lying in the dissipative nature of the system. The light and matter components are both inevitably coupled to an external continuum of elec-

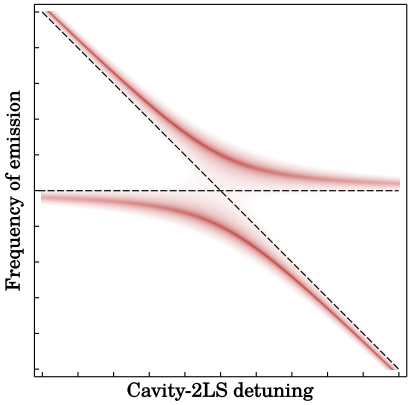

Figure 5.2: Anticrossing. The anticrossing of the energy levels as one of the bare modes crosses the other manifests in the spectrum of emission as a doublet of peaks that never cross. In the case of cavity-2LS coupling, its origin lies in the transitions from the first manifold to vacuum.

tromagnetic modes that allows them to relax by emission of a photon (see Sections 2.3 and 2.5). While the detection of the light leaked in this way is a very useful resource to retrieve information on the system, this coupling also implies a broadening of the energy levels that smears out the features of the anharmonic ladder. From the theoretical point of view, we describe the open character of the system by means of a master equation for the dynamical evolution of the density matrix:

$$\frac{d\rho}{dt} = \mathcal{L}(\rho) = -i[H,\rho] + \frac{\gamma_a}{2}\mathcal{L}_a(\rho) + \frac{\gamma_\sigma}{2}\mathcal{L}_\sigma(\rho) + \frac{P_a}{2}\mathcal{L}_{a^\dagger}(\rho) + \frac{P_\sigma}{2}\mathcal{L}_{\sigma^\dagger}(\rho) \tag{264}$$

where $\mathcal{L}_c(\rho) = 2c\rho c^\dagger - c^\dagger c\rho - \rho c^\dagger c$ (see Section 2.5). This describes the leakage of photons from the cavity and the 2LS with decay rates γ_a and γ_σ resp., and also the inverse process where an excitation is incoherently put into the system with rates P_a and P_σ [149]. From the eigenvalues of the Liouvillian superoperator $\mathcal{L}$ we can upgrade the energy spectrum given by Eq. (263) to a dissipative spectrum of complex energies [58, 152]:

$$\omega_\pm^{(n)} = n\omega_a - \frac{\Delta}{2} - i\frac{(2n-1)\gamma_a + \gamma_\sigma}{4} \pm \sqrt{(\sqrt{n}g)^2 + \left(\frac{\Delta}{2} - i\frac{\gamma_a - \gamma_\sigma}{4}\right)^2} \tag{265}$$

where the imaginary part describes the width of the broadened energy levels. The resulting dissipative JC ladder is depicted in panel a of Fig. 5.3, where the shading around the lines represents their width, according to Eq. (265). The form of this equation reflects very clearly why it is so difficult to observe the higher rungs of the JC ladder in dissipative systems: as we go high in the ladder, the splitting of the levels increase as $\sqrt{n}$, but the broadening does it as $n\gamma_a/g$. Figure 5.3 illustrates as well the different forms of excitation, and what are the resonances expected in this case. While there are numerous ways of bringing excitations into the system, most of them fall into two categories: coherent and incoherent excitation.

COHERENT EXCITATION Coherent excitation refers to the direct pumping of the system by a beam of coherent light with a specific frequency. This

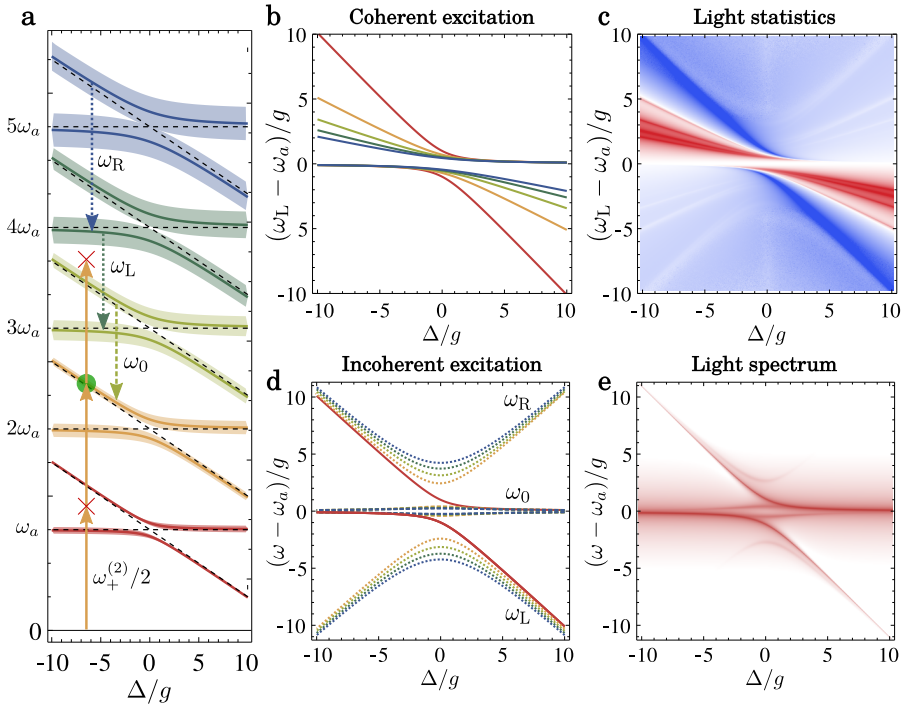

Figure 5.3: The dissipative Jaynes-Cummings system. **a**, Dissipative JC ladder. The width of the lines represent the linewidth of the levels. **b** Energy of multi-photon transitions starting from the ground state. **c**, Fifth-order correlation function under coherent excitation of the 2LS, featuring bunching peaks at the energies of the multi-photon transitions shown in b. **d**, Energy of the possible transitions between consecutive manifolds. **e**, Spectrum of the light emitted by the cavity under incoherent pumping of the 2LS.

way, one targets with the incident light a resonance of a given energy and can probe the system by changing the frequency of the excitation. Theoretically, the excitation by a laser, described as a coherent state of mean photon number $\bar{n} = \sqrt{\alpha}$ and frequency ω_L, is accounted for with the addition of an extra term H_C to the Hamiltonian (see Section 2.3.3):

$$H_C = \Omega(c\, e^{i\omega_L t} + c^\dagger e^{-i\omega_L t}), \tag{266}$$

The selective, coherent pumping of cavity or 2LS can be implemented experimentally by different methods, like a change in the orientation of the excitation or a convenient choice of polarizations. A model with coherent excitation of the 2LS only can also be derived from another with only cavity excitation by applying a displacement to the cavity mode to remove the coherent part (see Section 6.2)

where $c = a$ for cavity excitation, and $c = \sigma$ for 2LS excitation and with $\Omega = i\alpha\sqrt{\gamma_c/2\pi}$, and the phase α chosen so that $\Omega \in \mathbb{R}$. Ω is therefore a descriptor of the laser amplitude; this laser is a third external field that we describe classically, and must not be confused with the cavity, that we still describe as a quantum mode. This type of excitation will yield a family of multi-photon transitions, depicted as straight arrow lines in Fig. 5.3 a that, when the frequency of the excitation is changed to probe the system, correspond to the family of resonances depicted in panel Fig. 5.3 b. Those resonances are given by

$$\omega^*_{n,\pm} = \omega^{(n)}_\pm / n, \tag{267}$$

where $\omega^{(n)}_\pm$ are the energies of the JC ladder given by Eq. (263).

INCOHERENT EXCITATION In the case of incoherent excitation, the energy levels are populated incoherently, e.g., from the relaxation of excitations at higher energy levels. In this case, one can observe the emission corresponding to transitions between adjacent manifolds, depicted as dashed arrow lines in Fig. 5.1 b and as dashed and dotted arrow lines in Fig. 5.3 a. Their energies of emission are shown in Fig. 5.3 d. As described before, these

transitions can be divided in three groups with energies: ω_0 (dashed lines in panel a and d), ω_L and ω_R (dotted lines).

These resonances are linked to the nonlinear character of the spectrum and serve as evidence of the quantum character of the system. Both schemes present as well the two vacuum-Rabi resonances (red solid lines), that not only are common to the classical picture of coupled harmonic oscillators, but are also the most easily excited and detected and consequently always the dominant feature. Therefore, the challenge is, both from a theoretical and experimental point of view, to provide an evidence of the rest of the resonances coming from higher rungs in the ladder.

5.3.1 OBSERVABLES

The two main kinds of observables to use in order to evidence these resonances are either the intensity of emission (resolving in energies to analyse the spectrum, or studying its dependence on the frequency of a probe excitation), or photon statistics at second and higher orders.

While the latter approach is in principle more difficult—since measuring photon statistics, i.e., intensity fluctuations, is a more challenging task than measuring the intensity itself—it offered nevertheless some of the first indirect evidences of the existence of a nonlinear ladder of energy levels. In 2005, Birnbaum *et al.* [29] reported the measurement of antibunching from an atom-cavity system under coherent excitation in resonance with the vacuum-Rabi doublets. As shown in Fig. 5.4, due to the nonlinearity of the the energy levels, the absorption of a first photon at the energy of the Rabi doublet tunes the energy of the system out of resonance, blocking the absorption of a second one. This converts the poissonian stream of light used to excite the system into a sub-poissonian, antibunched one. The same kind of evidence based on photon statistics was provided in 2008 by Faraon *et al.* [76] using a semiconductor quantum dot embedded in an optical microcavity. In this case, they probed the system as a function of the laser detuning (dashed line in panel b of Fig. 5.4).

Doing so, they partially reproduced the features depicted in panel c, namely,

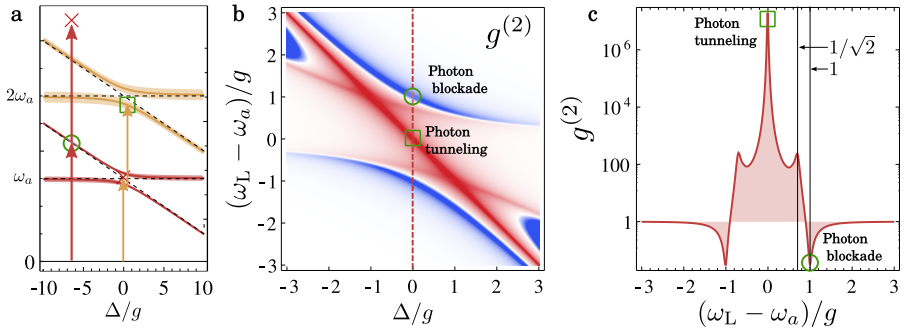

Figure 5.4: Mechanism of photon blockade. a, The absorption of a first photon blocks the absorption of a second one. **b**, Second-order correlation function $g^{(2)}$ under coherent excitation of the cavity in the limit of low pumping, as a function of laser frequency and detuning between cavity and 2LS. **c**, $g^{(2)}$ at zero detuning as a function of the laser energy. Photon blockade manifests as antibunching at energy $\omega_L - \omega_a = g$.

the already observed antibunching that evidences the photon blockade at driving frequency $\omega_L - \omega_a = g$, and a big bunching peak at the frequency resonant with the bare energy of the 2LS. In the particular configuration

of Ref. [76], cavity and 2LS were in resonance, and this bunching peak was mistakenly attributed to the bare resonance of the cavity. However, Fig. 5.4 b unambiguously shows that the peak follows the energy of the 2LS. To the best of our knowledge, this feature is still not well understood and certainly deserves further investigation. Some first results on the matter will be presented in the following discussions of this Section.

In 2008, Schuster *et al.* [207] showed the first direct spectroscopic observation of the higher rungs of the JC ladder in the transmitted field of an atom coupled to an optical cavity excited by a coherent driving. On a subsequent paper [141], they evidenced the same resonance by analysing the statistics of the emitted light, reporting the bunching peak at the two-photon resonance $\omega_L - \omega_a = g/\sqrt{2}$ shown in Fig. 5.4 c). Soon afterwards the nonlinearity was directly observed by Fink *et al.* [77] using a pump-probe measurement on a circuit QED system, in which a pump tone populated the state $|1_\pm\rangle$ and a second probe tone excited the transition $|1_\pm\rangle \to |2_\pm\rangle$. Therefore, this pump-probe measurement allows to use coherent excitation to target first-order transitions between higher manifolds in the ladder, i.e, those depicted in Fig. 5.3 d (particularly, transitions of the group ω_0, i.e., those between the Rabi doublet, were observed). The next year, Bishop *et al.* [31] observed unambiguously the multi-photon resonances up to $n = 5$ in the transmitted field of the cavity. The first direct access to the second rung in a semiconductor solid-state device was reported by Reinhard *et al.* [193] by looking at the statistics of emission and observing the bunching of the two-photon resonance under pulsed excitation. They also observed that a higher degree of antibunching was obtained when the cavity and dot were far detuned.

All these experiments rely on the capability of coherent excitation to target specific resonances of the JC ladder by changing the energy of the excitation. When trying to describe these experiments from a theoretical point of view, it is soon apparent that some differences exist between the two possible mechanisms of coherent excitation: cavity excitation and 2LS excitation. In the case of those experiments studying the transmitted field, the differences are not large; Fig 5.5 shows the steady-state cavity population, $\mathrm{Tr}\{a^\dagger a \rho_{SS}\}$, that is proportional to the intensity of the transmitted field, as a function of the 2LS-cavity detuning and the frequency of the exciting laser.

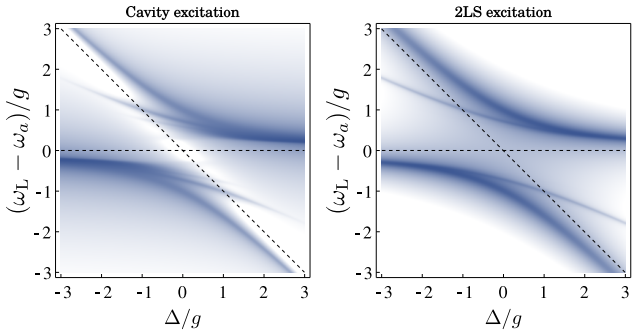

Figure 5.5: Transmitted field. Cavity population $n_a = \mathrm{Tr}\{a^\dagger a \rho_{SS}\}$ in the steady state, proportional to the intensity of the transmitted field, as a function of the frequency ω_L of the exciting laser and the detuning between cavity and 2LS, Δ. The two-photon resonance to the second rung of the JC ladder is clearly visible in both cases; higher resonances are only slightly visible in the case of cavity excitation. Parameters of the simulation: $\gamma_a = 0.1g$, $\gamma_\sigma = 0.01g$, $\Omega = 0.1g$.

We see that the multi-photon resonance to the second rung is clearly visible in both schemes, while higher resonances, as depicted in Fig. 5.3 b, do

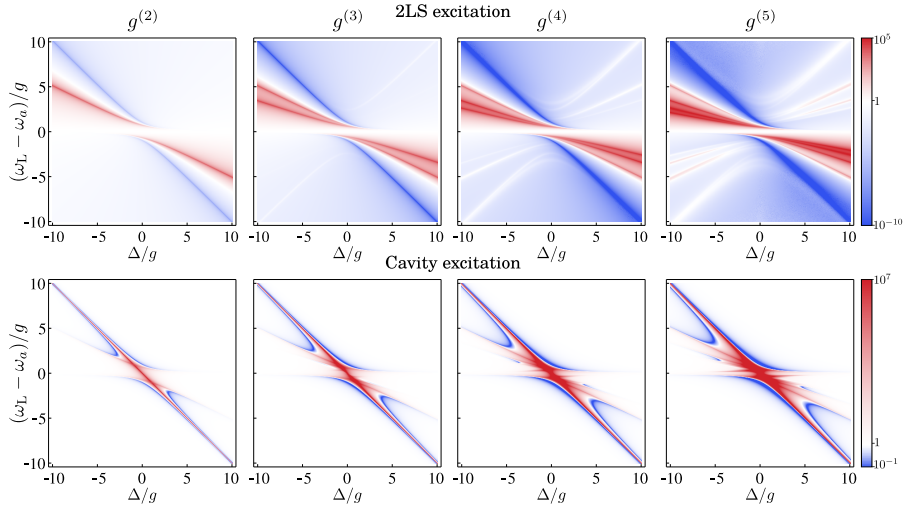

Figure 5.6: Statistics of emission. $g^{(n)}$ for $n \in [2,5]$ of the light emitted by the cavity under coherent driving of the cavity (top) and the 2LS (bottom). By varying the laser frequency ω_L and the detuning Δ between cavity and 2LS, the statistics of the emission reveals the multi-photon resonances displayed in Fig. 5.3. Strong differences exist between the two possible schemes of excitation. Parameters: $\gamma_a = 0.1g$, $\gamma_\sigma = 0.01g$, $\Omega = 0.01g$.

only manifest in the case of cavity excitation, probably too faint to be observed experimentally. While the differences between both schemes in the intensity of emission are not too large, they become dramatic for the photon statistics. We have shown already some particular cases: namely, $g^{(5)}$ under coherent excitation of the 2LS (Fig. 5.3 c) and $g^{(2)}$ under coherent excitation of the cavity (Fig. 5.2 b), both as a function of frequency of the excitation ω_L and the cavity-2LS detuning Δ. A full series of $g^{(n)}$ with $n \in [2,5]$ for both schemes of excitation is shown in Fig. 5.6, clearly manifesting the important effect that the kind of excitation has on the statistics. There are two main differences. On one hand, the bunching peak known as *photon tunneling*, is only present in the case of cavity excitation and, as we have discussed before, it always manifests at the energy of the 2LS (contrary to what is stated for instance in Ref. [76]). This is clearly seen in Fig. 5.7, that depicts two cuts of the $g^{(2)}$ maps of Fig. 5.6 at $\Delta = 0, -2g$.

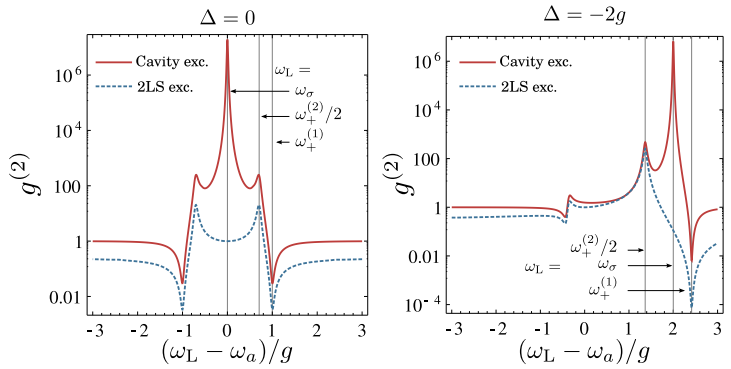

Figure 5.7: Statistics of emission. $g^{(n)}$ for $n \in [2,5]$ of the light emitted by the cavity under coherent driving of the cavity (top) and the 2LS (bottom). By varying the laser frequency ω_L and the detuning Δ between cavity and 2LS, the statistics of the emission reveal the multi-photon resonances displayed in Fig. 5.3. Strong differences exist between the two possible schemes of excitation. Parameters: $\gamma_a = 0.1g$, $\gamma_\sigma = 0.01g$, $\Omega = 0.01g$.

On the other hand, in the case of 2LS excitation, $g^{(n)}$ develops a rich structure of bunching peaks as n increases, that corresponds exactly to the n-photon resonances that were depicted in Fig. 5.3 b. These bunching peaks are also present in the case of cavity excitation, but they fade as Δ deviates from zero, while in the case of 2LS excitation they are much more resilient to detuning. Laussy *et al.* [152] reported for the first time most of these theoretical re-

sults shown here, highlighting the important role of detuning and photon statistics in the observation of the fingerprints of the JC ladder. Müller *et al.* [168] explored these ideas experimentally using semiconductor QDs. As detuning increases, so does the separation between the excitation energies of the first and higher rungs (c.f. Fig. 5.3 b); one of the consequences of this is an improvement of the mechanism of photon blockade when exciting the first rung, since the probability of exciting higher rungs is reduced. This way, by using a detuned configuration, the experiment reported antibunching with one of the smallest value of $g^{(2)}$ achieved so far in solid state.

5.4 MULTI-PHOTON RESONANCES

It is evident from the discussion above that the physics of the dissipative Jaynes Cummings ladder is extremely rich, and much room exists for further investigation. We will focus here on one of the features that we have presented: the bunching peaks appearing in $g^{(n)}$ at the frequency of the multi-photon resonances, $\omega_{\pm}^{(n)}/n$. These features can appear counterintuitive if one follows the reasoning that we used to explain photon blockade. In the case of photon blockade, i.e., a one-photon resonance with the first manifold of the JC ladder, the energy of the laser is tuned out of resonance when the system is excited to the first manifold (c.f. Fig. 5.4 a). Something similar occurs in the case of an n-photon resonance: as can be seen in Fig. 5.3 a, once the system is excited to the n-th manifold via a n-photon process, the excitation to higher rungs is blocked. Following the intuition we develop in the case of photon blockade, this would imply that the m-th photon resonance should manifest as bunching in the $g^{(n)}$ for $n \leq m$, and antibunching for $n > m$. However, contrary to this expectation, bunching peaks appear for $n \geq m$, and no particular features for $n < m$. At this point, one might wonder whether the broadening of the energy levels due to the dissipative nature of the system could explain this phenomenon. We will show now that this is not the case, and that these features can be recovered from a pure Hamiltonian dynamics.

We are concerned with the scenario of coherent excitation of the 2LS. This is described by the sum of the Hamiltonian of Eq. (259) and the coherent driving of Eq. (266) for 2LS excitation ($c = \sigma$). In a frame rotating with the frequency of the laser ω_{L} (see Section 2.4), this takes the form:

$$H = \delta_a a^\dagger a + \delta_\sigma \sigma^\dagger \sigma + g(a^\dagger \sigma + \sigma^\dagger a) + \Omega(\sigma^\dagger + \sigma)\,, \tag{268}$$

with $\delta_a \equiv \omega_a - \omega_{\mathrm{L}}$ and $\delta_\sigma = \omega_\sigma - \omega_{\mathrm{L}}$. The wavefunction of the system, $|\psi\rangle$, evolves according to Schrodinger's equation, $|\dot{\psi}\rangle = -iH|\psi\rangle$, whose formal solution in the basis of eigenstates $|\phi_i\rangle$ of H reads:

$$|\psi(t)\rangle = c_1|\phi_1\rangle e^{-iE_1 t} + c_2|\phi_2\rangle e^{-iE_2 t} + \cdots \tag{269}$$

with the coefficients $c_i = \langle\phi_i|\psi_0\rangle$ to be determined by the initial state. Using the basis of bare states,

$$\{|i\rangle\} \equiv \{|0\rangle\,, |1\rangle\,, |2\rangle\,, |3\rangle\,, \ldots\} \equiv \{|0,g\rangle\,, |0,e\rangle\,, |1,g\rangle\,, |1,e\rangle\,, \ldots\}, \tag{270}$$

one can represent the wavefunction through the probabilities p_i for the system to be in the state $|i\rangle$:

$$p_i(t) = |\langle i|\psi(t)\rangle|^2 = \sum_{j,k} c_j c_k^* \langle i|\phi_j\rangle\langle\phi_k|i\rangle e^{i(E_k - E_j)t} . \tag{271}$$

Contrary to the probabilities that one would obtain from the diagonal terms of the steady-state density matrix, $p_i \equiv \langle i|\rho_{\rm SS}|i\rangle$, these depend explicitly on time. However, we can obtain analogous time-independent probabilities by averaging the oscillations, i.e., retaining only the non-oscillating terms in Eq. (271):

$$\langle p_i\rangle = \sum_j |c_j|^2 |\langle i|\phi_j\rangle|^2 . \tag{272}$$

From this, we can compute the probability of having n photons in the cavity, given by $\langle p_n^c\rangle \equiv \langle p_{ng}\rangle + \langle p_{ne}\rangle$, and obtain the corresponding n-th order correlation function $g^{(n)}$, given by:

$$g^{(n)} = \frac{\sum_{m=1}^{\infty}\prod_{i=0}^{n-1}(m-i)\langle p_m^c\rangle}{\left(\sum_{m=1}^{\infty} m\langle p_m^c\rangle\right)^n} . \tag{273}$$

This is to be contrasted with the $g^{(n)}$ that we would obtain from the steady state density matrix, substituting $\langle p_n^c\rangle$ by p_n^c in Eq. (273), where

$$p_n^c \equiv \langle ng|\rho_{\rm SS}|ng\rangle + \langle ne|\rho_{\rm SS}|ne\rangle . \tag{274}$$

The result of both calculations is displayed in Fig. 5.8. We can clearly observe that the bunching peaks arise from a photon probability distribution that is very similar in both the dissipative and the Hamiltonian case. More

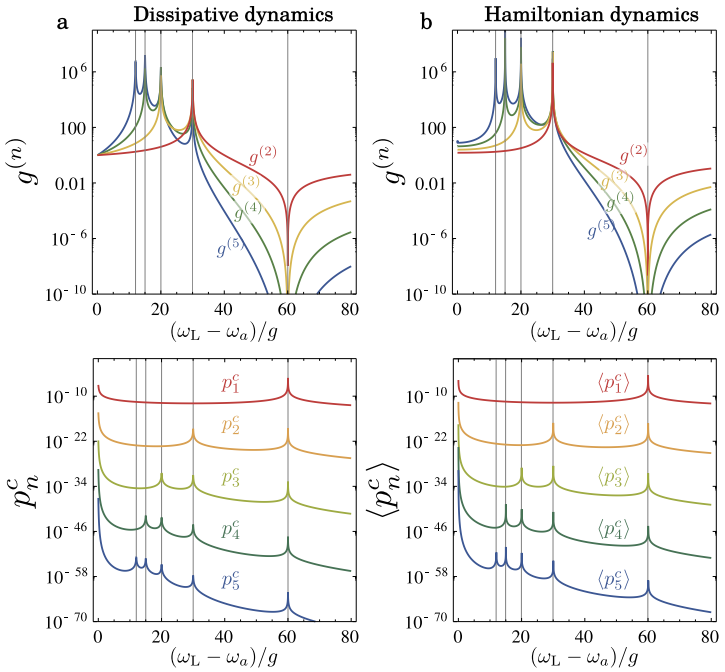

Figure 5.8: Comparison of statistics from dissipative and Hamiltonian dynamics. $g^{(n)}$ for $n \in [2,5]$ (top) and probability of having n photons in the cavity (bottom) for the case of dissipative dynamics (left) and Hamiltonian (right). The simulations are performed in a very detuned configuration, with $\Delta = -60g$, and in the low driving limit, $\Omega = 10^{-3}g$. In the dissipative case, $\gamma_a = 0.1g$, $\gamma_\sigma = 0.01g$. Vertical lines mark the n-th photon transitions given by $\omega_+^{(n)}/n$, with n going from 1 to 5, from right to left.

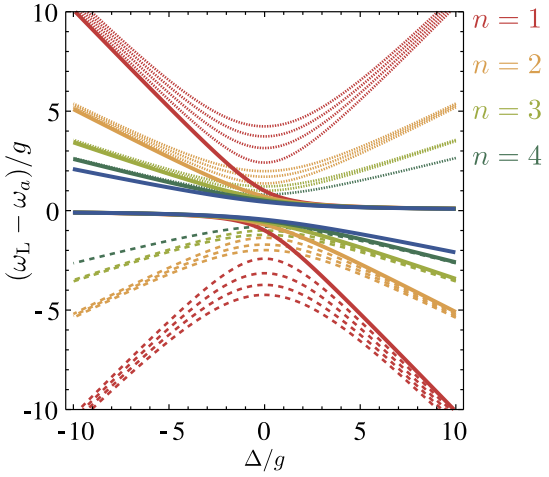

Figure 5.9: Diagram of all possible n-photon transitions. This shows the energies of the n-photon resonances that can take place with initial states higher than vacuum. The colors determine the number of photons exchanged in the transition. Dotted lines represent transitions from $-$ to $+$, and dashed, from $+$ to $-$. Straight lines correspond to the n-photon resonances that have vacuum as initial state, c.f. Fig. 5.3 b. Resonances of $n = 1$ correspond to the lines of Fig. 5.3 d. As detuning increases, n-photon resonances of equal n and same initial state clutter together. However, they cannot be concatenated, since the final and initial states are detuned.

specifically, when the laser hits the n-th photon resonance, the probability of the cavity containing m photons, with $m \geq n$, increases. These resonances on the probabilities manifest in all rungs up the JC ladder, and though they consist on small increases over a exceptionally small background (notice the range of the logarithmic scale), they are responsible of the bunching peaks observed in the set of $g^{(n)}$, which are extremely sensitive to these deviations. This rules out the possibility of the bunching peaks being due to the finite broadening of the energy levels.

To understand how these higher rungs are excited, we will consider the possible multi-photon transitions that can take place, not only starting from the ground state $|0g\rangle$, but from states higher in the ladder. In general, the energy of an n-photon transition from the eigenstate $|m_\chi\rangle$, with $\chi = \pm$, to the eigenstate $|(m+n)_{\chi'}\rangle$, n rungs above, is given by:

$$\omega^{(n)}_{m,\chi,\chi'} = (\omega^{(m+n)}_{\chi'} - \omega^{(m)}_{\chi})/n\,, \tag{275}$$

with $\omega^{(n)}_{\chi}$ corresponding to the eigenvalues of the JC Hamiltonian, Eq. (263). The energies for some of these transitions, going from $-$ to $+$ rungs, and vice-versa, are depicted in Fig. 5.9. This draws a more complete picture of the possible resonances of the system, since it extends with the n-photon transitions between higher rungs our previous description of the n-photon resonances $\omega^*_{n,\pm}$ shown in Fig. 5.3 b and Eq. (267) (those that start from vacuum) and the one-photon resonances between higher rungs depicted in Fig. 5.3 d. The transitions that go from $+$ to $+$ and from $-$ to $-$ have energies close to the cavity frequency and have not been included for clarity. From the Figure, we can see that, as the detuning Δ between cavity and 2LS increases, n-photon transitions of equal n starting from $-/+$ rungs (for negative/positive detunings) tend to clutter together. However, this cluttering does not imply that exciting resonantly a n-photon transition from the ground state would resonantly populate all the rungs, since, taking the case of negative Δ as an example, all these n-photon transitions start on a $-$ rung and finish on a $+$ rung, in such a way that they cannot occur consecutively. However, and keeping the example of negative detuning, if we are driving the state

$|n_+\rangle$ from the ground state, hitting with the laser a n-photon transition, an excitation might, with a very small probability, be off-resonantly put into the state $|n_-\rangle$. In that case, since the energies of all the n-photon transitions starting from a $-$ rung are cluttered together, the system would enter again in resonance and a higher manifold would be populated. This is the origin of the small resonances in the occupancy of higher rungs shown in Fig. 5.8, and of the consequential bunching peaks in $g^{(n)}$.

We will now focus on the mechanism of resonant, n-photon excitation of the n-th manifold in the limit of big detuning Δ, as we showed in Fig. 5.8. We will take the particular case of negative detuning, that we consider from now on for concreteness. In this case, excitation of the n-photon resonance will drive the state $|n_+\rangle$, which in this limit, it is $|n_+\rangle \approx |n-1, e\rangle$. The n-photon resonance, therefore, corresponds to driving a state with $n-1$ photons in the cavity. However, Figure 5.8 seems to describe a different picture, since at the two-photon resonance, the first peak seems to appear in $\langle p_2^c \rangle$, at the three-photon resonance, in $\langle p_3^c \rangle$, and so on. If the two-photon resonance is driving the state $|1e\rangle$, we would expect an important increase of the value of $\langle p_1^c \rangle$ which seems absent in the figure. The answer to this apparent paradox lies in the details: one has to look at the resonance really closely. The result of making such a zoom for the case of the two-photon resonance is shown in Fig. 5.10. There, we can see emerging a very thin peak in the probability of having one photon in the cavity, just too sharp to be resolved in the original figures. Other peaks are also present, corresponding to the rest of two-photon transitions with energies $\omega^{(2)}_{m,-,+}$, with $m \geq 1$. A complete zoom around the n-photon resonance reveals that the probability $\langle p_{n-1}^c \rangle$ gets to $1/2$, as shown in Fig. 5.11 for the three-photon resonance, which corresponds to a regime of full Rabi oscillation between the states $|0, g\rangle$ and $|n-1, e\rangle$. Since n can be any integer, depending on which resonance is driven, the superposition takes place between states that can differ arbitrarily in energy:

$$|\psi_N\rangle = \frac{1}{\sqrt{2}}(|0, g\rangle + |N, e\rangle). \tag{276}$$

Such a superposition has been hypothetically referred to describe "spooky" features of quantum mechanics, like non-conservation of energy (the col-

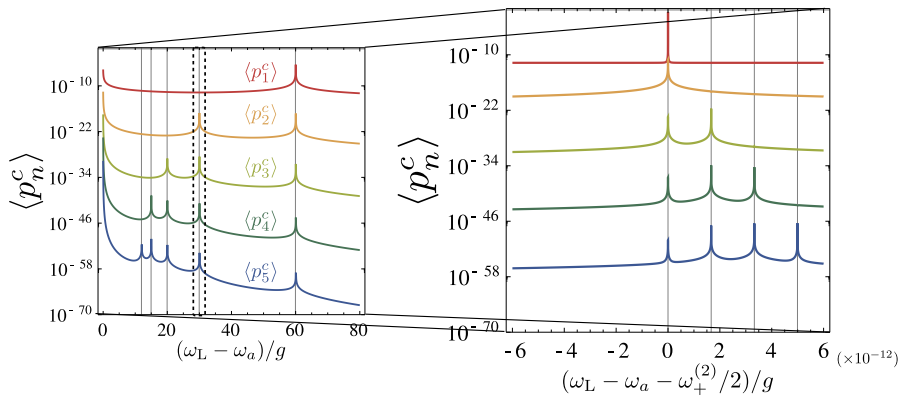

Figure 5.10: Zoom around two-photon resonance. When zooming around the two-photon resonance, we observe a sharp peak on the occupation of the states with only one photon in the cavity. This sharp peak is not responsible for the bunching peaks that we observe in the curves of $g^{(2)}$ of Figure 5.8. $\Omega/g = 10^{-3}$.

lapse of such a wavefunction suddenly provides a state that has either no energy or the huge amount $\hbar\omega_\sigma + N\hbar\omega_a$) [185, 212]. Our results show that the detuned JC Hamiltonian allows to actually realize such a superposition.

We started this Section by discussing an apparent paradox: why is the antibunching observed in the photon-blockade regime (resonance with the first manifold) not replicated at the n-photon level? Following the intuition developed in the case of photon blockade, n-photon resonances should excite a state of the n-th manifold and tune the system out of resonance, blocking any further n-photon absorption of photons from the laser. As a consequence, one should observe antibunching in $g^{(m)}$ for $m > n$. Furthermore, in the regime of large detuning, we have seen that the coupling to the n-th manifold occurs via a state with $n-1$ photons in the cavity, implying that antibunching should indeed observed in $g^{(m)}$ for $m \geq n$. On the contrary, n-photon resonances manifest as a family of bunching peaks. The paradox is solved when looking at the small frequency ranges in which we have shown that resonances manifest fully as N-photon Rabi oscillations; in those very small ranges, a dip appears in the bunching peaks of $g^{(n)}$ and they become indeed antibunched as expected, only in frequency ranges too small to be discerned in the figures displayed so far. This is observed for the three-photon resonance in Fig. 5.11 b, corresponding to a Rabi oscillation between the states $|0,g\rangle$ and $|2,e\rangle$ and is therefore antibunched for $g^{(n)}$ with $n \geq 3$.

5.5 MULTI-PHOTON RABI OSCILLATIONS

We now analyse the behaviour of the system when it undergoes N-photon Rabi oscillation. Let us consider the Hamiltonian in the rotating frame of the laser, Eq. (268), disposing of the 2LS-cavity coupling and the excitation terms:

$$H_0 = \delta_a a^\dagger a + \delta_\sigma \sigma^\dagger \sigma. \tag{277}$$

The eigenstates of this "bare" Hamiltonian H_0 consist of the basis of bare states, $\{|n,e/g\rangle\}$. The eigenvalues belonging to the states $|0,g\rangle$ and $|n-1,e\rangle$ are $\lambda_1 = 0$ and $\lambda_2 = (n-1)(\omega_a - \omega_L) + \omega_\sigma - \omega_L$, respectively. We see then that, when $\omega_L \approx [(n-1)\omega_a + \omega_\sigma]/n$, both eigenvalues are

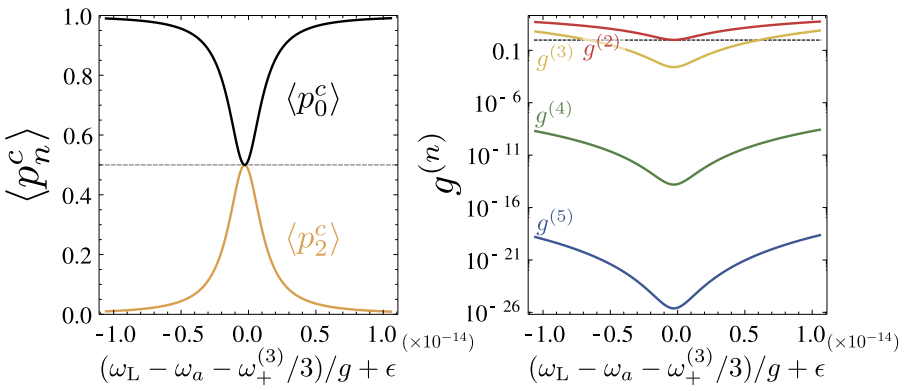

Figure 5.11: Zoom around the three-photon resonance. $\Omega/g = 10^{-3}$. ϵ represents a small Lamb shift that deviates the n-photon resonance from its original position.

almost equal, $\lambda_1 \approx \lambda_2 \approx 0$. This proximity in energies allows to define a subspace consisting only of these two states, the rest of them living in another subspace separated from the first by energies of the order of δ_a and δ_σ. Both subspaces are uncoupled in the bare Hamiltonian, but get coupled when we include as a perturbation the terms $g(a^\dagger\sigma + a\sigma^\dagger)$ and $\Omega(\sigma^\dagger + \sigma)$. However, if Ω and g satisfy $g, \Omega \ll \delta_a, \delta_\sigma$, the cluttering in energies of the bare Hamiltonian holds, and we can still define the independent subspace $\{|0,g\rangle, |n-1,e\rangle\}$. This allows us to separate the dynamics of this subspace from the rest of the states and perform an adiabatic elimination to retain only the coupling between the states inside it, obtaining an effective Hamiltonian that provides the frequency of the Rabi N-photon oscillation.

Let us use the basis $\{|i\rangle\}$ of Eq. (270) in order to write the wavefunction of the system as $|\psi(t)\rangle = \sum_i c_i(t)|i\rangle$. We consider that the system is driven at the nth-photon resonance that couples the states $|0\rangle = |0,g\rangle$ and $|2n-1\rangle = |n-1,e\rangle$, so we truncate the Hilbert space at the n-th manifold, meaning $i \in [0, 2n]$. Using the Hamiltonian (268), the dynamical evolution of the coefficients $c_i(t)$ is given by the Schrödinger equation:

$$i\dot{\mathbf{C}}(t) = \mathcal{M}\mathbf{C}\,, \tag{278}$$

where $\mathbf{C}(t) \equiv (c_0(t), c_1(t), \cdots, c_{2n}(t))^{\mathrm{T}}$, and:

$$\mathcal{M} \equiv \begin{pmatrix} 0 & \Omega & 0 & 0 & 0 & & & \\ \Omega & \delta_\sigma & g & 0 & 0 & & & \\ 0 & g & \delta_a & \Omega & 0 & & \vdots & \\ 0 & 0 & \Omega & \delta_\sigma+\delta_a & \sqrt{2}g & & & \\ 0 & 0 & 0 & \sqrt{2}g & 2\delta_a & & & \\ & & & & & (n-1)\delta_a & \Omega & 0 \\ & \cdots & & & & \Omega & (n-1)\delta_a+\delta_\sigma & \sqrt{n}g \\ & & & & & 0 & \sqrt{n}g & n\delta_a \end{pmatrix}. \tag{279}$$

The coefficients of the states in the subspace of the multi-photon Rabi oscillation are $c_0(t)$ and $c_{2n-1}(t)$. An adiabatic elimination is performed by setting the derivative of the rest of the coefficients to zero. This transforms the previous system of differential equations into another one for the reduced subspace:

$$\begin{aligned} i\dot{c_0}(t) &= \Omega c_1(t)\,, \\ i\dot{c_{2n-1}}(t) &= [(n-1)\delta_a + \delta_\sigma]c_{2n-1}(t) + \Omega\, c_{2n-2}(t) + \sqrt{n}g\, c_{2n}(t), \end{aligned} \tag{280}$$

with the rest of $2n-1$ coefficients, $\mathbf{c} = (c_1, c_2, \cdots, c_{2n-2}, c_{2n})^{\mathrm{T}}$ being determined by an algebraic equation:

$$\mathcal{H}\mathbf{c} = \mathbf{v} \tag{281}$$

where $\mathbf{v} = (-\Omega c_0, 0, \cdots, 0, -\Omega c_{2n-1}, -\sqrt{n}g\, c_{2n-1})^{\mathrm{T}}$ (we skip the time dependence for simplicity of notation) and $\mathcal{H}$ is a $(2n-1)\times(2n-1)$ symmetric, tridiagonal matrix:

$$\mathcal{H} = \begin{pmatrix} a_1 & -b_2 & 0 & & \\ -b_2 & a_2 & -b_3 & & \\ & & \ddots & & \\ & & -b_{2n-2} & a_{2n-2} & -b_{2n-1} \\ & & 0 & -b_{2n-1} & a_{2n-1} \end{pmatrix}, \tag{282}$$

with $a_{2n-1} = n\delta_a$, $b_{2n-1} = 0$, and, for $m < 2n-1$:

$$a_m = \begin{cases} \delta_\sigma + \frac{m-1}{2}\delta_a & (m = \text{odd}) \\ \frac{m}{2}\delta_a & (m = \text{even}) \end{cases} \quad \text{and} b_m = \begin{cases} -\Omega & (m = \text{odd}) \\ -\sqrt{\frac{m}{2}}g & (m = \text{even}) \end{cases} \tag{283}$$

By computing the inverse of $\mathcal{H}$ we can obtain the list of coefficients $\mathbf{c} = \mathcal{H}^{-1}\mathbf{v}$ as a function of c_0 and c_{2n-1}, so that Eq. (280) becomes a linear system of equations for the two states that can be described by an effective Hamiltonian H_{eff}:

$$i\frac{d}{dt}\begin{pmatrix} c_0 \\ c_{2n-1} \end{pmatrix} = H_{\text{eff}} \begin{pmatrix} c_0 \\ c_{2n-1} \end{pmatrix}. \tag{284}$$

The term in the equation for c_{2n-1} multiplying c_0, and viceversa, will correspond to the Rabi frequency $\Omega_{\text{eff}}^{(n)}$ of the n-photon Rabi oscillation. The equation for $\dot{c}_{2n-1}$ depends on c_{2n} and c_{2n-2}. Since $b_{2n-1} = 0$, the elements of the last row and column of $\mathcal{H}$ are zero excluding the diagonal, and therefore, the same occurs for $\mathcal{H}^{-1}$:

$$\mathcal{H} = \begin{pmatrix} & & 0 \\ & \mathcal{H}' & \vdots \\ & & 0 \\ 0 & \cdots\ 0 & a_{2n-1} \end{pmatrix} \to \mathcal{H}^{-1} = \begin{pmatrix} & & 0 \\ & \mathcal{H}'^{-1} & \vdots \\ & & 0 \\ 0 & \cdots\ 0 & 1/a_{2n-1} \end{pmatrix}. \tag{285}$$

Consequently, c_{2n} does not depend on c_0. On the other hand, c_{2n-2} depends on c_0 with a term $-\Omega\,\mathcal{H}^{-1}_{2n-2,1}c_0$ or, equivalently, $-\Omega\,\mathcal{H}'^{-1}_{2n-2,1}c_0$. Therefore, $\dot{c}_{2n-1}$ depends on c_0 as $i\dot{c}_{2n-1} = \cdots - \Omega^2\mathcal{H}'^{-1}_{2n-2,1}c_0$, giving the effective Rabi frequency:

$$\Omega_{\text{eff}}^{(n)} = -\Omega^2\mathcal{H}'^{-1}_{2n-2,1}, \tag{286}$$

Fortunately, the inverse of a symmetric, diagonal matrix is analytic [163]. It is given by (setting $m \equiv 2n-2$):

$$\mathcal{H}'^{-1} = \begin{pmatrix} u_1v_1 & u_1v_2 & u_1v_3 & \cdots & u_1v_m \\ u_1v_2 & u_2v_2 & u_2v_3 & \cdots & u_2v_m \\ u_1v_3 & u_2v_3 & u_3v_3 & \cdots & u_3v_m \\ \vdots & \vdots & \vdots & \ddots & \vdots \\ u_1v_m & u_2v_m & u_3v_m & \cdots & u_mv_m \end{pmatrix}, \tag{287}$$

with

$$u_m = \frac{1}{\delta_m v_m}, \quad u_{m-i} = \frac{b_{m-i+1}\cdots b_m}{\delta_{m-i}\cdots\delta_m v_m}, \quad i = 1, \cdots, m-1, \tag{288a}$$

$$\delta_1 = a_1, \quad \delta_i = a_i - \frac{b_i^2}{\delta_{i-1}}, \quad i = 2, \cdots, m, \tag{288b}$$

$$v_1 = \frac{1}{d_1}, \quad v_i = \frac{b_2\cdots b_i}{d_1\cdots d_{i-1}d_i}, \quad i = 2, \cdots, m, \tag{288c}$$

$$d_n = a_n, \quad d_i = a_i - \frac{b_{i+1}^2}{d_{i+1}}, \quad i = m-1, \cdots, 1. \tag{288d}$$

$\mathcal{H}'^{-1}_{2n-2,1}$ is therefore given by $u_1 v_m$, which yields:

$$\Omega_{\text{eff}}^{(n)} = -\Omega^2 \frac{b_2\cdots b_m}{\delta_1\cdots\delta_m} \tag{289}$$

Finally, by evaluating b_i and δ_i on the previous expression, we arrive to a result that shows more clearly the dependence of $\Omega_{\text{eff}}^{(n)}$ on Ω:

$$\Omega_{\text{eff}}^{(n)} = \frac{g^{n-1}\Omega^n\sqrt{(n-1)!}}{D_{2(n-1)}}, \tag{290}$$

where D_n is defined through the recurrence relation

$$D_n = a_n D_{n-1} - b_{n-1}^2 D_{n-2}, \tag{291}$$

with $D_0 = 1$, $D_1 = a_1$. This gives rise to exact expressions easily obtained but too heavy to write here. To provide an example, we show the results for the two and three-photon Rabi frequencies, the most relevant ones:

$$\Omega_{\text{eff}}^{(2)} = \frac{\Omega^2 g}{\delta_\sigma\delta_a - g^2}, \tag{292a}$$

$$\Omega_{\text{eff}}^{(3)} = \frac{g^3\Omega^3}{\sqrt{2}\{g^4 - g^2\delta_a(\delta_a + 2\delta_\sigma) + \delta_a\delta_\sigma[\delta_a(\delta_a+\delta_\sigma) - \Omega^2]\}}. \tag{292b}$$

These formulas show very clearly that the Rabi frequency of the n-photon resonance, that determines both the period of oscillation between the ground state and the $(n-1)$-photon state and the width of the resonance as a function of ω_{L}, scales as Ω^n, which explains the small width of the resonances. In the limit of small pumping intensity Ω that we have considered so far, the extremely narrow character of these resonances might leave them as a mere academic curiosity, since they are too sharp to actually be appreciable in any realistic configuration. Moreover, a small peak width is associated to very small frequency of oscillation, which, turning back to the dissipative scenario, would be overcome by decay, that would not let the population of the cavity grow before a photon is emitted and would make these resonances even dimmer and more difficult to observe. Finally, we note as well that the effective n-photon coupling that we have discussed has also associated a small renormalization of the energy levels (that we have not explicitly calculated here). This kind of Lamb shift displaces the resonance from its ideal value $\omega_{n,+}^* = \omega_+^{(n)}/n$, a displacement that we denoted ϵ in Fig. 5.11.

5.6 DRESSING THE DRESSED STATES

Because of this, it would be desirable to make these multi-photon Rabi frequency as large as possible, so they can be turned from an academic curiosity to a physical mechanism with fruitful applications. In order to do so, the obvious strategy is to increase the pumping intensity, Ω. This approach, however, has an important consequence. It eventually brings the system into a regime different from the simple probing of the JC ladder that we have discussed in this Chapter.

Under strong pumping, the level structure becomes that of a dressed atom [52] strongly detuned from a cavity mode [241], bridging the Jaynes–Cummings dynamics with another fundamental model of light-matter interaction, namely, the Mollow physics of resonance fluorescence [165], already discussed in Section 4.2 of Chapter 4. The strong coupling that was previously dominated by the interaction between the 2LS and a cavity-photon, and probed by the laser, is now dominated by the interaction of the 2LS with the laser-photons, and is probed by the cavity. In this case, n-photon resonances in the system are understood from a different perspective: they correspond to the Purcell-enhancement by the cavity of the virtual n-photon transitions taking place in the dressed Mollow ladder (see Fig. 5.12), whose effects in the frequency-resolved statistics of the light emitted was the focus of Chapter 4. These transitions occur between states $|\pm\rangle$ to states $|\mp\rangle$, n rungs below in the ladder, and therefore have an energy:

$$\omega^{(n)}_{\pm\to\mp} = n\omega_{\rm L} \pm 2R, \tag{293}$$

where $2R$ is the energy separation between the $|+\rangle$ and $|-\rangle$ states in the ladder, with:

$$R = \sqrt{\Omega^2 + \left(\frac{\omega_\sigma - \omega_{\rm L}}{2}\right)^2}. \tag{294}$$

Therefore, the resonance condition is set in terms of the cavity energy, ω_a, imposing the condition that the energy of n cavity photons matches the energy of an n-photon transition in the ladder:

$$\omega_a = \omega^{(n)}_{\pm\to\mp}/n = \omega_{\rm L} \pm \frac{2R}{n}, \tag{295}$$

In this case, the order n of the multi-photon transition matches the number of photons absorbed by the cavity in the process, that we denote N. On the other hand, in the low pumping regime, we recall that the n-photon transition creates a state with a number of photons in the cavity $N = n - 1$. To fix terminology, from now on we will use N to refer to the number of photons created in the cavity.

Let us discuss in more detail the connection between the mechanisms of N-photon absorption present in both models. Without loss of generality, we will consider here the case of negative detuning $\Delta < 0$, and the transitions

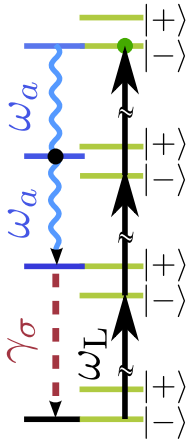

Figure 5.12: Mollow ladder. In the high excitation regime: the laser dresses the QE while the cavity Purcell-enhances a N-photon transition from $|-\rangle$ to $|+\rangle$ (here for $N = 2$). A subsequent emission from the QE brings the system back to a $|-\rangle$ state.

going from $|+\rangle$ to $|-\rangle$ in the Mollow ladder. Based on Eq. (267), when pumping is low enough as not to distort the level structure of the JC Hamiltonian, one can selectively excite a state with N photons in the cavity at the $(N+1)$th rung by adjusting the laser frequency to

$$\omega_N^{\mathrm{JC}} \approx \omega_a + \frac{\sqrt{4(N+1)g^2 + \Delta^2} - \Delta}{2(N+1)}\,. \tag{296}$$

On the other hand, resonances in the amplitude of the Rabi oscillations still appear when pumping is increased, but they occur at different energies than in the low pumping limit, due to the dressing of the states by the laser. These resonances have their origin in the mechanism outlined above, and the value of the laser frequency ω_{L} at which they appear can be obtained by solving Eq. (295) for ω_{L}, bringing the expression in Eq. (296) to the form:

$$\omega_N^{\mathrm{Mollow}}(\Omega) \approx \omega_a + \frac{\Delta + \sqrt{4(N^2-1)\Omega^2 + N^2\Delta^2}}{N^2 - 1}\,. \tag{297}$$

The actual relationship between Eqs. (296) and (297) is not evident; they correspond to apparently different multi-photon mechanisms, each of them described within the formalism of one of the two main pillars of nonlinear quantum optics: the Jaynes Cummings Hamiltonian in one case, and the Mollow physics of resonance fluorescence in the other. However, in the regime of large detuning $\Delta \gg g$ that we have considered in this Chapter, there is an elegant transition between the two mechanisms, since $\omega_N^{\mathrm{Mollow}}(\Omega)$ tends to ω_N^{JC}, when pumping intensity tends to zero:

$$\lim_{\Omega\to 0} \omega_N^{\mathrm{Mollow}}(\Omega) = \omega_N^{\mathrm{JC}} = -\frac{\Delta}{N+1}\,. \tag{298}$$

As a consequence, resonances in the amplitude of the N-photon Rabi oscillations can be adiabatically followed, from the limit of low pumping to high pumping, as they are progressively blueshifted from the initial values ω_N^{JC} along curves $\omega_N^{\mathrm{Mollow}}(\Omega)$ (see Fig. 5.13 a).
Resonances in $g^{(n)}$ also shift; this is shown for $g^{(2)}$ in Fig. 5.13 b for three values of pumping, starting with $\Omega_0 = g/10$, close to the vanishing pumping case shown in Fig. 5.13 c.

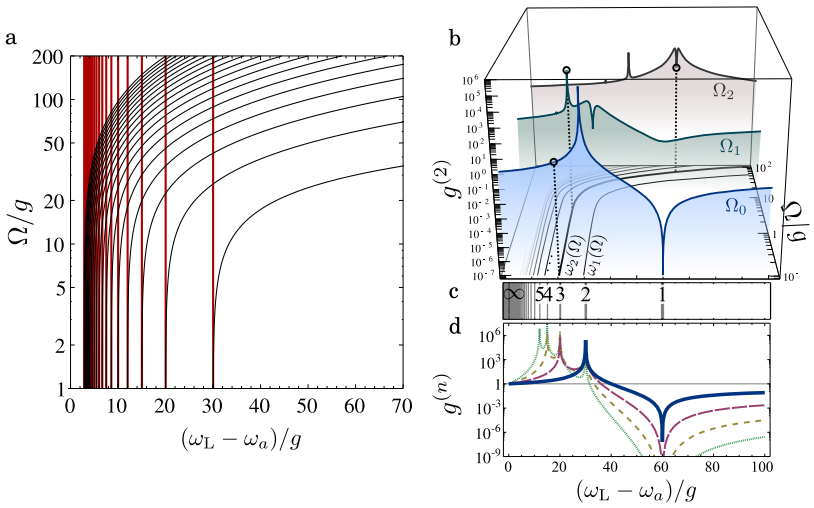

Figure 5.13: Dressing of the states. a, As the intensity of the pumping Ω increases, the multi-photon resonances ω_N^{JC} of the JC Hamiltonian given by Eq. (296) (here shown as red lines or $N \geq 2$) shift due to the dressing of the energy levels by the laser (black lines) following the curves $\omega_N^{\text{Mollow}}(\Omega)$ given by Eq. (297). **b** $g^{(2)}$ as a function of ω_L for pumping $\Omega_0 \approx 10^{-2}g$, $\Omega_1 \approx 4g$ and $\Omega_2 \approx 32g$. The resonances $\omega_N^{\text{Mollow}}(\Omega)$ are shown in the plane (ω_L, Ω). Open circles are the projection of ω_2^{Mollow} on $g^{(2)}$. **c**, Resonant energies to excite the nth rung of the ladder. **d**, $g^{(n)}$ for $n = 2$ (solid), 3 (long dash), 4 (short dash) and 5 (dotted) at vanishing pumping with $n-1$ bunching resonances matching those inc. $\Delta/g = -60$ in all the panels.

Following $g^{(2)}$ along the ω_2 resonance shows that a new peak emerges out of a uniform background, reaching a maximum $g^{(2)} \approx 3649$ at the pumping $\Omega_1 \approx 4g$ (middle trace) before a depletion of the resonance forms for higher pumping, reaching its minimum along ω_2 of $g^{(2)} \approx 17$ at $\Omega_2 \approx 32g$ (background trace).

In this last section we have discussed how an increase in the pumping intensity, that would bring the multi-photon Rabi oscillations in the Jaynes-Cummings Hamiltonian to the realm of real applications, forces a change in the model used to describe it, which brings with it obvious differences in the physical features, from a blueshift of the levels to a change in the statistics of the emission. However, deviations do not stop there; the physics of the Mollow regime coupled to a cavity is also full of quantum features that we can harness and exploit. This is the matter of study of the next chapters.

6 EMITTERS OF *N*-PHOTON BUNDLES

One of the heresiarchs of Uqbar had stated that mirrors and fatherhood are abominable, since they both multiply the number of men.

— Jorge Luis Borges, Tlön, Uqbar, Orbis Tertius

6.1 INTRODUCTION

In the previous Chapter, we have discussed some of the properties that evidence the quantum character of one of the most fundamental models of light-matter interaction: the Jaynes Cummings model. We demonstrated that the system can undergo Rabi oscillations between states with zero and N photons in the cavity, and that the associated Rabi frequency could be improved by increasing the intensity of the pumping laser. This brings the system to a regime that cannot be described within the Jaynes Cummings framework; instead, the phenomenology it displays, associated to the dressing of the 2LS by a strong driving field, is better accounted for by the Mollow physics of resonance fluorescence.

In this Chapter, we investigate from that perspective the multi-photon coupling between a dressed 2LS and a cavity. We will show how, in the strong pumping regime, these multi-photon oscillations can be used to realize a family of *N-photon emitters*, i.e., sources that release their energy exclusively in groups, or *bundles*, of N photons (for integer N) and in effect provide us with light made up from building blocks that are not single photons anymore. This ability to substitute the quantum of light by a bundle has unforeseeable consequences for both applications and fundamental physics. For instance, this renormalizes the link between the energy of the fundamental unit of excitation to its frequency through a magnified Planck constant: $E = N\hbar\nu$. The type of emission can be varied with system parameters to realize both N-photon lasers and photon guns [98] at the N-photon level. Such highly non-classical emitters should boost new generations of light sources [178, 233], be useful to produce NOON states [4], for quantum lithography and metrology [89], and also for medical applications, allowing for higher penetration lengths and increased resolution with minimum harm to the tissues [69, 113]. The recent demonstration that biological photoreceptors are sensitive to photon statistics [213] may also render such sources highly relevant for studies of biological photosystems and, potentially, of quantum biology [24]. Many of the results shown here have been published in the journal Nature Photonics [201].

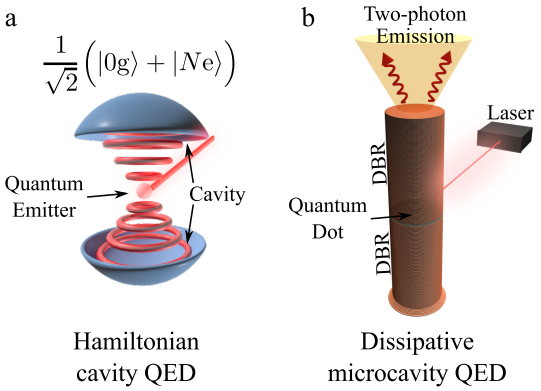

Figure 6.1: Implementations of cavity QED. a A general representation of a cavity QED scheme. In the Hamiltonian regime, the mechanisms that we report are able to create a superposition of states with 0 and N photons. **b** A possible solid-state implementation of our proposal places a quantum dot in a micropillar. With excitation from the side with a conventional laser, one can collect, in the cavity, emission as the output.

6.2 MODEL

The Hamiltonian that we will use throughout this Chapter is similar to that in Chapter 5, namely, the one that describes the coupling between a two-level system (2LS) and a quantum harmonic oscillator (corresponding to a single electromagnetic mode in a cavity), including a coherent driving of the 2LS. We will, however, adopt small changes in the notation. For reasons that will be clear in Section 6.3, we will use $\tilde{\sigma} = |g\rangle\langle e|$ instead of σ to describe the lowering operator of the 2LS. As well, we will make use of the operators $\tilde{\sigma}_z = |e\rangle\langle e| - |g\rangle\langle g|$, $\tilde{\sigma}_y = i(\tilde{\sigma} - \tilde{\sigma}^\dagger)$ and $\tilde{\sigma}_x = \tilde{\sigma} + \tilde{\sigma}^\dagger$, that fulfill the commutation relations of angular momentum. Also, in order to give more importance to the parameters that are relevant in the Mollow regime, i.e., when the 2LS is dressed by the laser, Δ will now describe the detuning between the 2LS and the laser, $\Delta \equiv \omega_\sigma - \omega_\mathrm{L}$, and we will use Δ_a to describe the detuning between the cavity and the laser, $\Delta_a \equiv \omega_a - \omega_\mathrm{L}$. Then, in a frame rotating at the frequency of the laser, ω_L, the Hamiltonian reads:

$$H = \frac{\Delta}{2} + \frac{\Delta}{2}\tilde{\sigma}_z + \Delta_a a^\dagger a + g(a^\dagger\tilde{\sigma} + a\tilde{\sigma}^\dagger) + \Omega\tilde{\sigma}_x. \tag{299}$$

Since we will be mainly concerned about the emission properties of the system, it is mandatory to consider a dissipative scenario in which excitations of both the 2LS and the cavity mode will have a finite lifetime and photons can be leaked out of the system. To do so, we describe its evolution in terms of a master equation governing the evolution of the density matrix ρ of the system (see Section 2.5):

$$\frac{d}{dt}\rho = -i[H,\rho] + \frac{\gamma_a}{2}\mathcal{L}_a(\rho) + \frac{\gamma_{\tilde{\sigma}}}{2}\mathcal{L}_{\tilde{\sigma}}(\rho) \tag{300}$$

Exciting only the 2LS without exciting the cavity, as is described by Eq. (299), might appear a challenging task in real implementations. Note however that an equivalent master equation can be obtained if one considers instead a driving of the cavity mode:

$$H' = \frac{\Delta}{2} + \frac{\Delta}{2}\tilde{\sigma}_z + \Delta_a a^\dagger a + g(a^\dagger\tilde{\sigma} + a\tilde{\sigma}^\dagger) + (i\Omega_a a^\dagger - i\Omega_a a) \tag{301}$$

with Ω_a a real number, and now one writes the quantum mode $\hat{a}$ (we use momentarily the $\hat{}$ notation to unambiguously distinguish operators from numbers) as:

$$\hat{a} = \alpha + \delta\hat{a} \tag{302}$$

where α is a complex number. This describes the quantum mode $\hat{a}$ as a quantum fluctuation $\delta\hat{a}$ on top of a classical, coherent displacement α, with $\delta\hat{a}$ inheriting the bosonic properties of $\hat{a}$, i.e., $[\delta\hat{a}, \delta\hat{a}^\dagger] = 1$. The coherent driving term of the cavity in Eq. (301) can then be eliminated from the master equation by choosing α to be:

$$\alpha = \frac{2\Omega_a}{\gamma_a}, \tag{303}$$

yielding a master equation completely analogous to Eq. (300), with a exchanged by the quantum fluctuations δa and a Hamiltonian that now has a coherent driving term for the 2LS:

$$H = \frac{\Delta}{2} + \frac{\Delta}{2}\tilde{\sigma}_z + \Delta_a \delta a^\dagger \delta a + g(\delta a^\dagger \tilde{\sigma} + \delta a \tilde{\sigma}^\dagger) + \Omega\tilde{\sigma}_x. \tag{304}$$

with

$$\Omega = g\alpha = g\frac{2\Omega_a}{\gamma_a}. \tag{305}$$

The quantum properties of a would then be completely described by its quantum fluctuations, δa, which are unaffected by the coherent component α. This component will appear in observables such as the spectrum of emission as a delta peak at the frequency of the exciting laser (see Section 2.6.3 usually termed as coherent scattering. This, as we will see in next sections, can be unimportant if our emission of interest (that arising from the quantum dynamics of a, i.e., of δa) takes place in a different spectral window out of resonance with the laser.

As we have discussed previously in this Thesis, this model can be implemented in a variety of physical systems, from atomic physics [94], to solid-state implementations in semiconductor [11, 88, 109, 147, 181, 217, 230] and superconducting samples [114, 240]. Of particular interest are those systems that are able to realize the paradigm of resonance fluorescence with a single quantum emitter—evidenced by the Mollow triplet in the fluorescence spectrum—in a cavity QED or waveguide QED setup [78, 133, 208]. One of the most remarkable examples that approaches the paradigm of our model is the observation of the coupling between the cavity and one of the sidebands of the Mollow triplet [133] on a solid-state sample. It is also worth noting the recent development on experimental techniques that are able to suppress the coherent scattering of the laser in the light emitted by cQED samples, opening new possibilities in the detection of features related to the dynamics that we discuss here.

6.3 FIRST ORDER CORRELATORS: FIRST SIGNS OF n-PHOTON COUPLING

At the end of Section 5.3, we discussed briefly the origin of the multiphoton resonances existing in the system when it is dressed by a laser, akin to those appearing in the pure JC configuration when the laser acts only as a probe. These resonances have their origin in the virtual, multi-photon transitions taking place in the Mollow ladder, that were subject of deep investigation in Chapter 4 from the perspective of frequency-resolved, second order correlation functions $g^{(2)}_{\Gamma}(\omega_1, \omega_2)$. Indeed, there is an unambiguous relationship between the features that these processes leave in the 2PS of the dressed 2LS and those that can be found in first order observables of the cavity-QED system that we discuss here.

Let us recall from Sections 4.2 and 5.3 that a 2LS under a strong coherent pumping of intensity Ω and frequency $\omega_{\rm L}$ develops a triplet structure in the spectrum of emission, corresponding to a central peak at frequency $\omega_{\rm L}$, and two sideband peaks at energies $\omega_{\rm L} \pm \omega_{\rm S}$, with $\omega_{\rm S} = 2R$ and R the Rabi frequency associated to the coupling between the 2LS and the laser photons:

$$R = \sqrt{\Omega^2 + \left(\frac{\Delta}{2}\right)^2}. \tag{306}$$

These peaks correspond to the three possible first-order transitions that can take place between consecutive rungs in the Mollow ladder, depicted as red, green and blue arrows in Fig. 6.2. Leapfrog processes correspond to the multiphoton transitions of the kind depicted by light cyan arrows in the Fig. 6.2, and for the case of photons of equal energy, n-photon processes correspond to photons of energy:

$$\omega_n = \omega_{\rm L} \pm \frac{2R}{n}. \tag{307}$$

Note that these higher-order transitions do not manifest in any first order observable of the 2LS-laser system, such as the emission spectrum, and

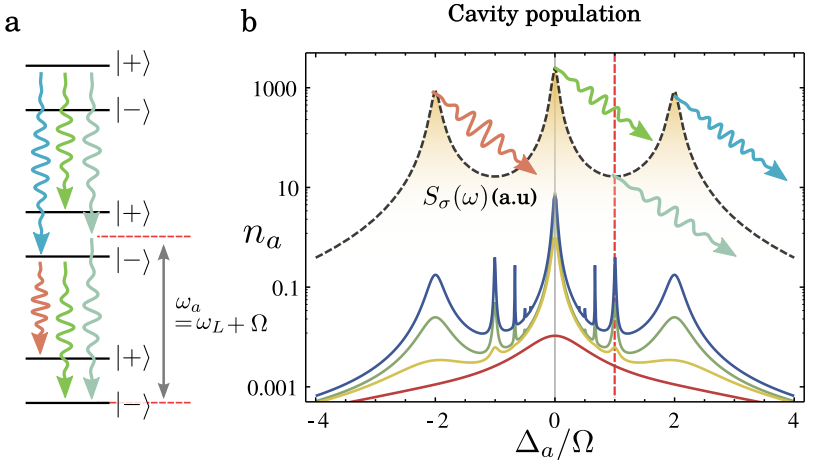

Figure 6.2: Evidences of multiphoton transitions on the cavity population. b, Simulation parameters: $\gamma_{\tilde{\sigma}} = 0.01g$, $\Delta = 0$, $\Omega = 10g$, $\gamma_a = 0.01g$ (blue), $0.1g$ (green), g (yellow) and $10g$ (red).

they must be evidenced by at least second-order observables, for instance, analyzing the frequency-resolved statistics of the light emitted by the system [96, 186], as throughly discussed in Chapter 4. This restriction can, however, be lowered in our current scenario in which the cavity can probe the dynamics of the dressed 2LS. In this case, the simplest way to evidence these transitions is to look at the intensity of emission of the cavity, proportional to the steady state cavity population $n_a = \mathrm{Tr}\{a^\dagger a \rho_{SS}\}$, as we sweep the cavity frequency across the domain of energies in which the Mollow triplet is developed. As shown in Fig. 6.2b, the cavity reflects the structure at the Mollow triplet in its population as we sweep its resonant frequency over the sidebands.

However, for cavities of good enough quality (i.e., low decay rate γ_a), a family of extra peaks can be discerned between the sidebands and the central peak, exactly at frequencies $\omega_a = \omega_n$ of Eq. (307), dimmer as n increases and with the most prominent case being $n = 2$ at $\Delta_a = \Omega$. We have in this way upgraded the signature of multi-photon physics in the dressed Mollow ladder to the realm of first-order observables.

This however, takes its most vivid manifestation when looking at the spectrum of the cavity as a function of the cavity frequency. The idea is sketched in Fig. 6.3: as the cavity detuning is changed, in this case around the two-photon resonance $\Delta_a = \Omega$, the spectrum of emission is recorded. This Figure illustrates a first fact that will be of big importance in next Sections: the cavity emits not only at its resonant frequency, but emits also at those of the Mollow triplet. However, the increase in the cavity population as it crosses the two-photon resonance manifest only on the emission peak at the resonant energy of the cavity.

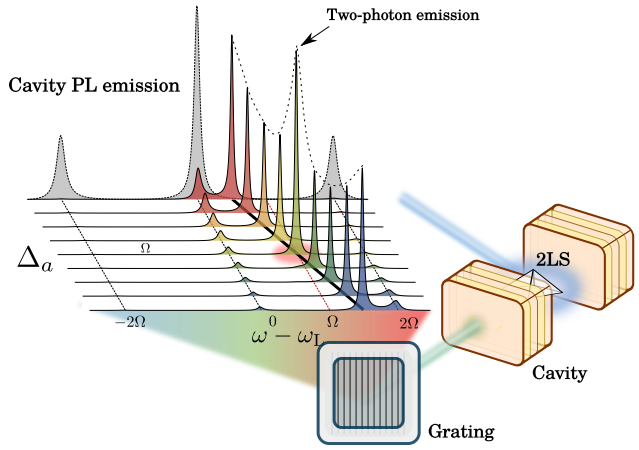

Figure 6.3: Cavity spectrum for different cavity detunings around the two-photon resonance varying ω_a. Simulation parameters: $\gamma_a = 0.5g$, $\gamma_{\bar{\sigma}} = g$, $\Omega = 10g$.

Applying this idea to the full frequency domain of the Mollow triplet allows us to generate a two-dimensional map of frequency spectra as a function of Δ_a. As we show in Fig. 6.4 a, such a map offers a beautiful, conclusive evidence of the multi-photon character of the peaks appearing in the cavity population and in the spectrum. Besides a peak in the emission at the frequency of the cavity, it shows three peaks appearing always at the frequencies of the Mollow triplet, and, interestingly, a family of another three

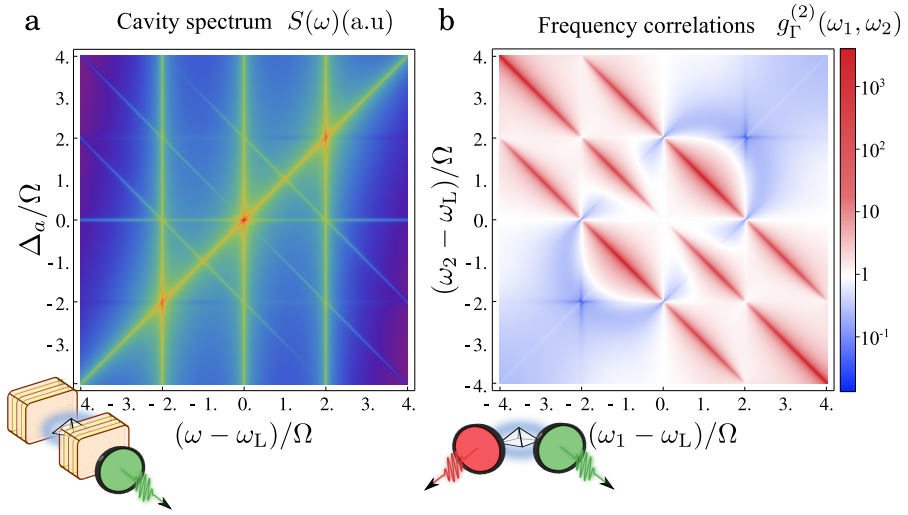

Figure 6.4: Manifestation of two-photon dynamics in a first-order cavity observable as compared to $g^{(2)}(\omega_1,\omega_2)$. Parameters: $\Omega = 30g$, $\gamma_a = 0.5g$, $\gamma_{\tilde{\sigma}} = 0.1g$, $\Gamma = g$.

small peaks at frequencies $\omega_0(\Delta_a), \omega_\pm(\Delta_a)$ defining three antidiagonal lines given by $\omega_0 = \omega_L - \Delta_a$ and $\omega_\pm = \omega_L - \Delta_a \pm 2\Omega$. These three lines are strongly reminiscent of the antidiagonal lines of strong correlations appearing in the 2PS that originate from the leapfrog processes, c.f. Fig. 6.4 b. This suggest that, due to the strong frequency correlations existing in the emission from the Mollow ladder, a Purcell-enhanced emission of a photon of frequency ω_a (resonant with the cavity) leaves the system in a state with enhanced probability of emitting a second photon at one of the frequencies strongly correlated with ω_a. This happens even if they are detuned from the cavity, thus realizing a sort of two-photon Purcell-enhancement. If these correlations already manifest in the spectrum of a single cavity mode, it is to be expected that exceedingly strong correlations, probably surpassing classical limits as studied in Chapter 4, would appear between two cavities coupled to the 2LS and detuned between each other, if their two frequencies are strongly correlated in the emission from the Mollow ladder.

6.4 n-PHOTON HAMILTONIAN

We will now undertake a more detailed analysis of the mechanism of n-photon coupling between the cavity and the dressed 2LS, starting from the Hamiltonian dynamics of the system (in the absence of dissipation). Since the results discussed so far strongly suggest that the physical features observed are well understood from a dressed-atom perspective, we will work in the dressed basis of the system of the 2LS+laser. By diagonalizing the 2×2 matrix $H_\Omega = \Delta/2 + (\Delta/2)\tilde{\sigma}_z + \Omega\tilde{\sigma}_x$, we obtain the following two eigenvectors:

$$|+\rangle = c|g\rangle + s|e\rangle \tag{308a}$$
$$|-\rangle = s|g\rangle - c|e\rangle \tag{308b}$$

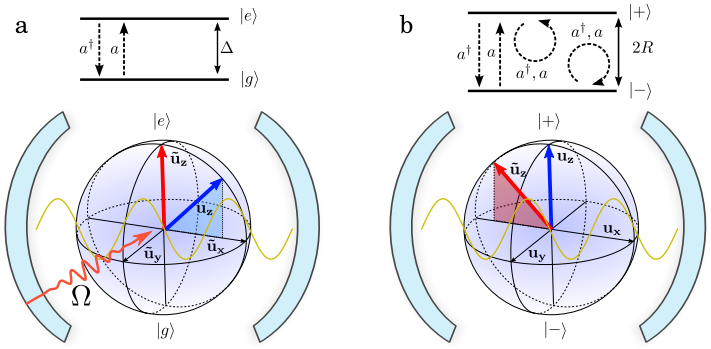

Figure 6.5: Changing to a dressed basis for the 2LS+Laser system. a, In the bare basis, Ω defines a direction $\mathbf{u}_\Omega = \mathbf{u}_\mathbf{z}$ that characterizes the Hamiltonian $H_\Omega = \Delta/2 + R\mathbf{u}_\Omega \cdot \tilde{\boldsymbol{\sigma}}$. **b**, The angular momentum operators $\boldsymbol{\sigma}$ of a rotated basis in which $\mathbf{u}_\mathbf{z} = \mathbf{u}_\Omega$ gives a diagonal Hamiltonian $H_\Omega = \Delta/2 + R\sigma_z$. In this basis, new terms appear in the total Hamiltonian of the cavity-2LS system, describing the possible transitions through the ladder of dressed states $|\pm\rangle$.

with

$$c = 1/\sqrt{1+\xi^{-2}}, \tag{309a}$$

$$s = 1/\sqrt{1+\xi^{2}}, \tag{309b}$$

$$\xi = \frac{\Omega}{\Delta/2 + R}, \tag{309c}$$

and R given by Eq. (306). c and s take their name from the fact that they correspond to the cosine and sine of a mixing angle $\theta = \arctan(\xi)$, therefore, they cannot be larger than one. This procedure gives a diagonalized Hamiltonian $H_\Omega = \Delta/2 + R\sigma_z$, where $\sigma_z \equiv |+\rangle\langle+| - |-\rangle\langle-|$. The change of basis can also be interpreted as change of coordinates in real space $(\tilde{x}, \tilde{y}, \tilde{z}) \to (x, y, z)$, more particularly, a rotation around the $\tilde{y}$-axis, such that the unitary vector $\mathbf{u}_\Omega = (\frac{\Delta}{2}\tilde{\mathbf{u}}_\mathbf{z} + \Omega\tilde{\mathbf{u}}_\mathbf{x})/R$ that defines the 2LS-laser Hamiltonian, $H_\Omega = \Delta/2 + R\mathbf{u}_\Omega \cdot \tilde{\boldsymbol{\sigma}}$ corresponds to the z-axis of the new basis, $\mathbf{u}_\Omega = \mathbf{u}_\mathbf{z}$, giving a Hamiltonian that is described by a diagonal operator $H_\Omega = \Delta/2 + R\sigma_z$. Defining the lowering operator in the dressed basis, $\sigma \equiv |-\rangle\langle+|$, we can make the substitution $\tilde{\sigma} = s^2\sigma - c^2\sigma^\dagger + cs\,\sigma_z$ in the Hamiltonian of Eq. (299) and rewrite it as:

$$H = \frac{\Delta}{2} + R\,\sigma_z + \Delta_a\, a^\dagger a + g\left\{a^\dagger(s^2\sigma - c^2\sigma^\dagger + cs\,\sigma_z) + \text{h.c.}\right\} \tag{310}$$

Note that there are now new terms on the right side of the equation: they describe the possible transitions that, mediated by the cavity, can occur between the levels of the infinite dressed atom ladder (see Fig. 6.2 a). Therefore, the coupling does not only include the familiar terms $a^\dagger\sigma$, but also the term $a^\dagger\sigma^\dagger$, that describes a decay from a state $|-\rangle$ to a state $|+\rangle$ one rung below by emitting a photon into the cavity, and $a^\dagger\sigma_z$, that describes a decay from $|\pm\rangle$ to $|\pm\rangle$.

Let us consider now the basis of bare states in the total Hamiltonian of Eq. (310), $\{|\pm, m\rangle\}$, where $\pm$ denotes the two possible states of the dressed 2LS, and m corresponds to the number of photons in the cavity. If $R \gg g$ and the cavity is close to the n-th photon transition $\Delta_a \approx \Delta_a^{(n)} \equiv \omega_n - \omega_\text{L} = \pm 2R/n$, the energy levels of the Hamiltonian are structured in manifolds $\mathcal{E}_m = \{|+, m\rangle, |-, m \pm n\rangle\}$ (where m is the number of photons in the cavity) such that the energy separation between levels inside a manifold

is much smaller than the energy separation between manifolds. This implies the existence of slow and fast degrees of freedom, which allows to perform an adiabatic approximation in order to build an effective Hamiltonian that does not couple those manifolds between them. We will obtain this Hamiltonian by using matrix perturbation theory. When the cavity is resonant with the n-th photon transition, we restrict our Hilbert space to $\{|+,0\rangle, |-,n\rangle, |+,1\rangle, |-,1\rangle, \cdots, |+,n-1\rangle|-,n-1\rangle\}$, where the Hamiltonian reads:

$$\mathcal{H}^{(n)} = \begin{pmatrix} \hat{h}^{(n)} & \vec{V}^{(n)} \\ \vec{V}^{(n)\mathrm{T}} & \hat{H}^{(n)} \end{pmatrix}. \tag{311}$$

In this way, we have divided the Hamiltonian into parts, with $\hat{h}^{(n)}$ acting on the subspace $\{|+,0\rangle, |-,n\rangle\}$, $\hat{H}^{(n)}$ acting on the rest of the Hilbert space, and $\vec{V}^{(n)}$ coupling both of them:

$$\hat{h}^{(n)} = \begin{pmatrix} R & 0 \\ 0 & -R + n\Delta_a \end{pmatrix} \tag{312a}$$

$$\vec{V}^{(n)} = \begin{pmatrix} gcs & gs^2 & \cdots & 0 & 0 \\ 0 & 0 & \cdots & \sqrt{n}gcs^2 & -\sqrt{n}gcs \end{pmatrix} \tag{312b}$$

$$\hat{H}^{(n)} = \begin{pmatrix} \hat{H}^{(n-1)} & & \vec{X}^{(n)\mathrm{T}} \\ \vec{X}^{(n)} & R + (n-1)\Delta_a & 0 \\ & 0 & -R + (n-1)\Delta_a \end{pmatrix} \tag{312c}$$

$$\vec{X}^{(n)} = \begin{pmatrix} 0 & 0 & \sqrt{n-1}gcs & -\sqrt{n-1}gc^2 \\ 0 & 0 & \sqrt{n-1}gs^2 & -\sqrt{n-1}gcs \end{pmatrix} \tag{312d}$$

Since the sign of Δ_a is irrelevant for the physics, we will consider it to be positive, $\Delta_a \approx 2R/n$. Our purpose now is to obtain an effective Hamiltonian $\hat{h}^{(n)}_{\mathrm{eff}}$ within the subspace $\{|+,0\rangle, |-,n\rangle\}$ by means of matrix perturbation theory:

$$\hat{h}^{(n)}_{\mathrm{eff}} = \hat{h}^{(n)} + \vec{V}^{(n)}(E_0 - \hat{H}^{(n)})^{-1}\vec{V}^{(n)\mathrm{T}}. \tag{313}$$

This calculation is easy to perform and allows to obtain analytic expressions for $\hat{h}^{(n)}_{\mathrm{eff}}$ that, however, are too heavy to be written here. Nevertheless, by inspecting the result of computing Eq. (313) up to $n = 6$, we obtained the off-diagonal term of $\hat{h}^{(n)}_{\mathrm{eff}}$ to lowest order in g, given by $\hat{h}_{\mathrm{eff}\,1,2} = \sqrt{n}g^{(n_{\mathrm{p}})}$, where $g^{(n_{\mathrm{p}})}$ is an effective n-photon coupling rate given by:

$$g^{(n_{\mathrm{p}})} = \frac{g^n}{R^{n-1}}\left(\frac{n^2}{2}\right)^{(n-1)}\frac{c^{n-1}s^{n+1}}{(n-1)!^2} + \mathcal{O}(g^{n+1}). \tag{314}$$

Figure 6.6: When the cavity frequency is close to a N-photon transition, the energy levels of the bare Hamiltonian ($g = 0$) is grouped into doublets. This defines subspaces of slow dynamics that allow to perform an adiabatic approximation.

Based on this result, when the cavity is in resonance with the n-th photon transition, $\Delta_a \approx \Delta_a^{(n)} = 2R/n$, we can describe the dynamics of the system by an effective n-photon Hamiltonian:

$$H_{\text{eff}}^{(n)} = \frac{\Delta}{2} + R\sigma_z + \Delta_a a^\dagger a + g^{(n_\text{P})}\left(\sigma^\dagger a^n + \sigma a^{\dagger n}\right), \tag{315}$$

which generates n-photon Rabi oscillations between the states $|+,m\rangle$ and $|-,m+n\rangle$ (see Fig. 6.7). These Rabi oscillations are the high-pumping counterpart of the n-photon Rabi oscillations that we described in Chapter 5 for the low pumping limit, and, consequently, they are associated to much higher Rabi frequencies that makes them more suitable for applications. In

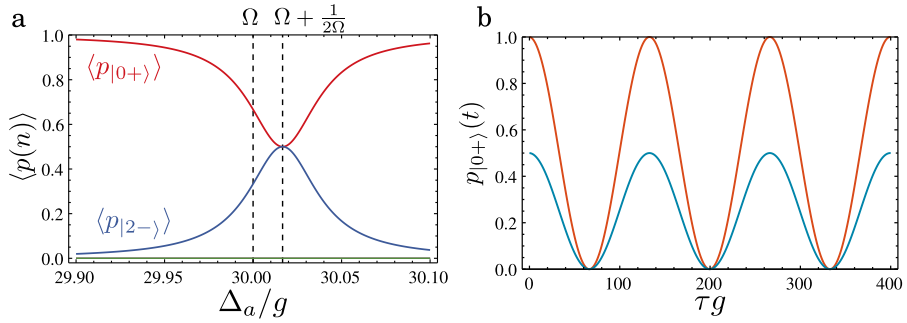

Figure 6.7: Multiphoton Rabi oscillations in the dressed atom-cavity picture. a, Time averages of the populations of the lower manifold as a function of the cavity detuning. **b**, Full Rabi oscillations when the initial state of the 2LS is $|+\rangle$ (red), and half-Rabi oscillations when the initial state is $|g\rangle$.

the derivation of an effective Hamiltonian, one also finds small renormalizations of the free energies of the 2LS and cavity that shift the n-photon resonance from the ideal values $\Delta_a^{(n)} = \pm 2R/n$. For simplicity, we will omit these renormalizations in the following descriptions, and our calculations in which the cavity is said to be in the n-th photon resonance will be assumed to have this small shift into account. The n-photon coupling rate $g^{(n_\text{P})}$ depends in a non-trivial way on Ω and Δ trough R and ξ. It is clear, though, that an increase in R will always reduce the value of $g^{(n_\text{P})}$. Therefore, there is a compromise between having $R \gg g$, such that the condition for the adiabatic approximation holds, but small enough for $g^{(n_\text{P})}$ to be significant. It is more complicated, however, to find from Eq. (314) a clear answer to what

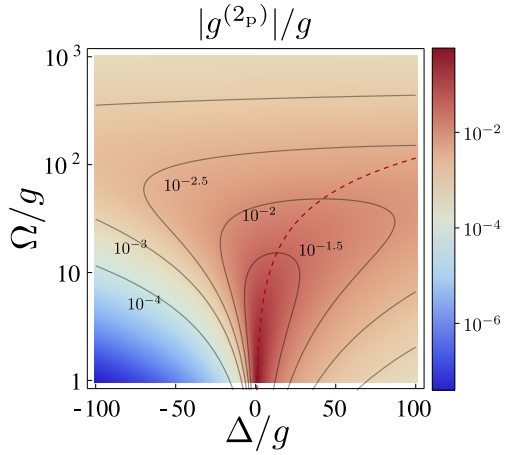

Figure 6.8: Two-photon coupling constant. The red-dashed line marks the curve of optimum Δ for a given Ω, $\Delta_{\text{opt}} = \Omega/\sqrt{2}$. This value is positive since we chose the two-photon resonance of positive detuning $\Delta_a \approx R$.

is the detuning Δ that maximizes the coupling rate for a given Ω. We will here analyse the particular, simpler case of $n = 2$, where the two-photon coupling rate reads:

$$g^{(2_P)} \approx \frac{2g^2 cs^3}{R} = \frac{4g^2\Omega(2R+\Delta)^3}{[(2R+\Delta)^2+4\Omega^2]^2 R}. \tag{316}$$

By direct differentiation of Eq. (316) we can obtain the optimum Δ that maximizes $|g^{(2_P)}|$ for a fixed Ω:

$$\Delta_{\text{opt}} = \frac{\Omega}{\sqrt{2}} \tag{317}$$

which is positive since the expressions we used have been derived for $\Delta_a > 0$ (it would have been negative in the case $\Delta_a < 0$). We will not analyse further the role of the detuning Δ in maximizing the n-photon coupling rate; as we will see in the next section, its relevance is reduced when one considers a dissipative scenario and, more particularly, the potential of the Hamiltonian n-photon coupling to grow a sizable steady state population of photons inside the cavity.

6.5 STEADY-STATE OBSERVABLES

In the context of open quantum systems, the Hamiltonian dynamics must be supplemented by the master equation Eq. (300) in order to account for the coupling to an external reservoir and the consequent photon leakage from both the cavity and the 2LS.

We will now express this master equation in terms of the dressed 2LS operator σ, instead of $\tilde{\sigma}$. By making the substitutions $\tilde{\sigma} = s^2\sigma - c^2\sigma^\dagger + cs\,\sigma_z$, we can write the Lindblad term for the 2LS a:

$$\frac{\gamma_{\tilde{\sigma}}}{2}\mathcal{L}_{\tilde{\sigma}}(\rho) \approx \frac{\gamma_{\tilde{\sigma}}}{2}s^4\mathcal{L}_{\sigma}(\rho) + \frac{\gamma_{\tilde{\sigma}}}{2}c^4\mathcal{L}_{\sigma^\dagger}(\rho) + 2cs\gamma_{\tilde{\sigma}}\,\mathcal{L}_{\sigma^\dagger\sigma}(\rho) \tag{318}$$

where extra, rotating terms are eliminated under the assumption $R \gg \gamma_{\tilde{\sigma}}$ (an assumption that must be satisfied in any case in order to develop a Mollow triplet). This allows us to write a master equation in terms of the dressed 2LS of the form:

$$\frac{d\rho}{dt} = -i\,[H,\rho] + \frac{\gamma_\sigma}{2}\mathcal{L}_{\sigma}(\rho) + \frac{P}{2}\mathcal{L}_{\sigma^\dagger}(\rho) + \frac{\gamma_\phi}{2}\mathcal{L}_{\sigma^\dagger\sigma}(\rho) + \frac{\gamma_a}{2}\mathcal{L}_{a}(\rho) \tag{319}$$

meaning that a 2LS under strong coherent excitation and decay rate $\gamma_{\tilde{\sigma}}$ is equivalent to another 2LS incoherently pumped, with decay, pumping and dephasing rates equal to γ_σ, P and γ_ϕ respectively (see Fig. 6.9), where:

$$\gamma_\sigma = s^4\,\gamma_{\tilde{\sigma}}\,, \tag{320a}$$

$$P = c^4\,\gamma_{\tilde{\sigma}} \tag{320b}$$

$$\gamma_\phi = 4(cs)^2\,\gamma_{\tilde{\sigma}}\,. \tag{320c}$$

Remarkably, these parameters can be easily tuned optically by changing

the frequency and intensity of the exciting laser. The incoherent pumping accounts for the fact that the states $\{|\pm\rangle\}$ actually form an infinite ladder of energy levels, and a system in the state $|-\rangle$ can decay to a state $|+\rangle$ of a lower rung, which in our framework corresponds to a "jump" upwards in the dressed 2LS induced by the external, effective pumping P_σ. Note that the appearance of similar terms was also discussed when we introduced the Hamiltonian of Eq. (310).

6.5.1 PHOTON POPULATION GROWN BY n-PHOTON PROCESSES

Using the master equation (319), we now proceed to evaluate the steady state population that can be grown into the cavity via the multi-photon Hamiltonian $H_{\rm eff}^{(n)}$ By using Eq. (134), and under the approximation $g^{(n_{\rm P})} \ll \gamma_a$ and $P \ll \gamma_a$, we can obtain a closed set of differential equations for the correlators $\langle a^n \sigma^\dagger \rangle$, $\langle \sigma^\dagger \sigma \rangle$ and $\langle a^\dagger a \rangle$:

$$\frac{d}{dt}\langle a^n \sigma^\dagger \rangle \approx \left(2iR - ni\Delta_a - \frac{n\gamma_a + P + \gamma_\sigma + \gamma_\phi}{2} \right) \langle a^n \sigma^\dagger \rangle \, , \\ -in!\, g^{(n_{\rm P})} \langle \sigma^\dagger \sigma \rangle \tag{321}$$

$$\frac{d}{dt}\langle \sigma^\dagger \sigma \rangle = -(\gamma_\sigma + P)\langle \sigma^\dagger \sigma \rangle + 2g^{(n_{\rm P})}\, {\rm Im}\left\{ \langle a^n \sigma^\dagger \rangle \right\} , \tag{322}$$

$$\frac{d}{dt}\langle a^\dagger a \rangle = -\gamma_a \langle a^\dagger a \rangle - 2ng^{(n_{\rm P})}\, {\rm Im}\left\{ \langle a^n \sigma^\dagger \rangle \right\} . \tag{323}$$

The steady state population of the cavity $n_a = \langle a^\dagger a \rangle_{\rm SS} = {\rm Tr}\{a^\dagger a \rho_{\rm SS}\}$ is then easily obtained by setting these derivatives to zero. This way, we obtain the following expression for the population grown in a cavity by the action of an n-photon Hamiltonian:

$$n_a^{(n_{\rm P})} = \frac{nP\kappa^{(n_{\rm P})}}{\Gamma\left(n\gamma_a + \Gamma + \gamma_\phi\right)/n! + \kappa^{(n_{\rm P})}\gamma_a} \tag{324}$$

where $\Gamma \equiv P + \gamma_\sigma$ and $\kappa^{(n_{\rm P})}$ is a generalized n-photon Purcell rate:

$$\kappa^{(n_{\rm P})} \equiv \frac{4{g^{(n_{\rm P})}}^2}{\gamma_a} \, . \tag{325}$$

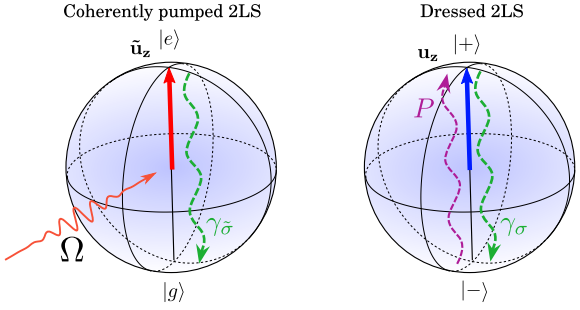

Figure 6.9: Performing a change to the basis of dressed states, a 2LS under coherent excitation and decay can alternatively be described as a 2LS experiencing decay, incoherent pumping and pure dephasing, with rates that can be manipulated with the intensity and frequency of the exciting laser.

For the case of zero detuning, the formula has a closed-form expression in terms of Ω, $\gamma_{\tilde{\sigma}}$ and γ_a:

$$n_a^{(n_\mathrm{p})}|_{\Delta=0} = \left[\frac{4\gamma_a}{n\gamma_{\tilde{\sigma}}} + \frac{\gamma_a \Omega^{2(n-1)}}{g^{2n}}(2n\gamma_a + 3\gamma_{\tilde{\sigma}})n^{2(1-2n)}16^{n-1}\right]^{-1}. \tag{326}$$

As an example, the dependence of $n_a^{(2_\mathrm{p})}$ on Δ and Ω is depicted in Fig. 6.10 c. Whereas the two photon coupling rate $g^{(2_\mathrm{p})}$ is clearly increased by choosing positive detunings (or negative if the cavity were around $\Delta_a \approx -R$), the detuning that maximizes the population is negative and close to zero (blue, dashed line in Fig. 6.10 b). This is due to the fact that the effective pumping rate P of the dressed 2LS is maximized for large, negative detuning (Fig. 6.10 a), and therefore the optimum detuning comes as a compromise between a high coupling with the cavity and a high effective pumping rate.

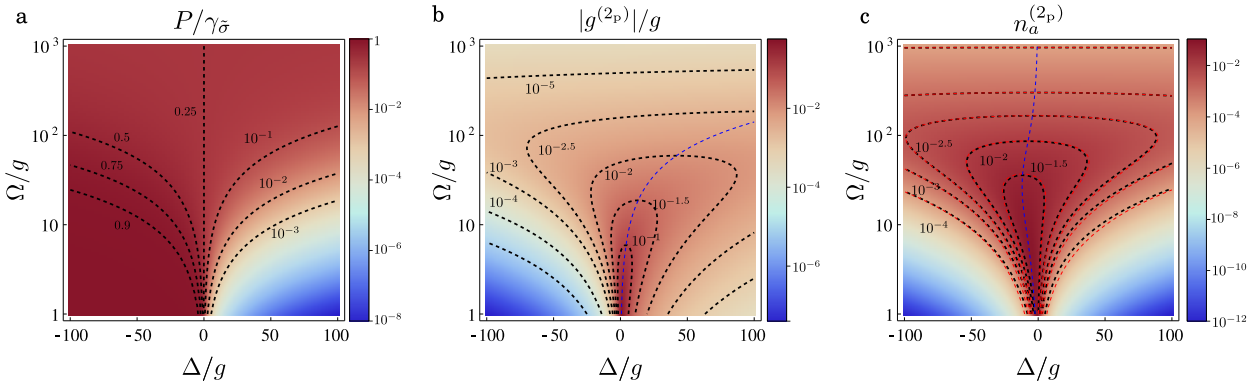

Figure 6.10: Efficiency of the two-photon process to populate the cavity. a, The effective incoherent pumping rate P of the dressed 2LS increases with Ω up to its maximum value $P_{\max} = \gamma_{\tilde{\sigma}}$, and it is always bigger for negative detuning Δ. **b**, Contrary to the effective pumping, the two-photon coupling rate increases with positive detuning. **c**, The population grown in the cavity under the action of the two-photon Hamiltonian $H^{(2)}$ comes as a compromise between having a strong coupling rate $g^{(2_\mathrm{p})}$ between the cavity and the dressed 2LS, and having an efficient pumping of the dressed 2LS, giving an optimum detuning Δ close to 0 (blue, dashed). Color plot and black-dashed lines are a numerical calculation of $\mathrm{Tr}\{a^\dagger a \rho_{\mathrm{SS}}\}$ for the master equation (319) and Hamiltonian $H^{(2)}$, red-dashed lines correspond to $n_a^{(2_\mathrm{p})}$ as

ROLE OF 2LS-LASER DETUNING Unfortunately, the dependence of Eq. (324) on Δ is too complicated to yield, from direct differentiation, a closed expression of the optimum Δ for a given γ_a, $\gamma_{\tilde{\sigma}}$ and Ω. We can, however, describe the problem in terms of R instead of Ω, and define the following adimensional variables:

$$\alpha_n = \frac{\gamma_a R^{n-1}}{g^n}, \quad \text{and} \beta_n = \frac{\gamma_{\tilde{\sigma}} R^{n-1}}{g^n} \tag{327}$$

that allows us, for a given γ_a, $\gamma_{\tilde{\sigma}}$ and R, to obtain the optimum detuning $\Delta_{\mathrm{opt}}^{(n)}$ that maximizes $n_a^{(n_\mathrm{p})}$ as:

$$\Delta_{\mathrm{opt}}^{(n)} = 2R\frac{1-\xi_{\mathrm{opt}}^2(\alpha_n,\beta_n)}{1+\xi_{\mathrm{opt}}^2(\alpha_n,\beta_n)}, \tag{328}$$

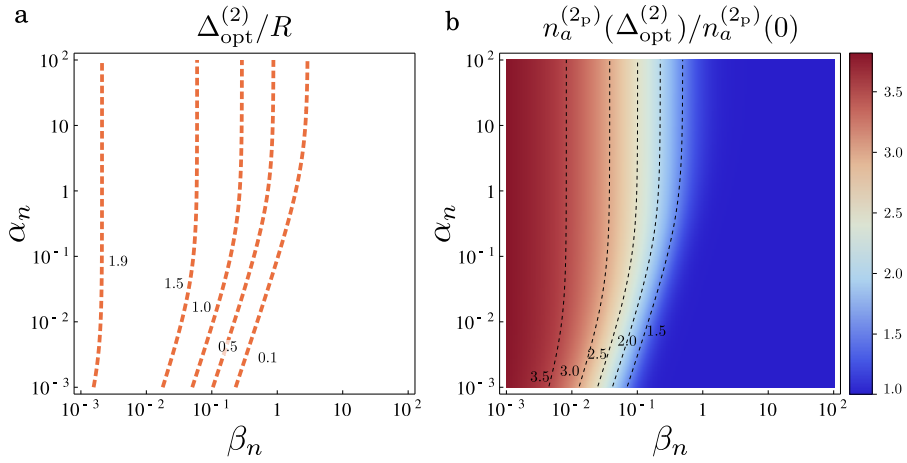

Figure 6.11: Effect of the 2LS-laser detuning Δ on the cavity population grown via two-photon processes, $n_a^{(2_{\rm P})}$. **a**, The optimum detuning divided by the Rabi coupling R speaks of the relative importance that the detuning should have in the total value of R (given by Δ and Ω, Eq. (306)) for a given (α_n, β_n). **b**, Factor of increase of $n_a^{(2_{\rm P})}$ obtained by choosing the optimum detuning, compared to its value at $\Delta = 0$.

where $\xi_{\rm opt}(\alpha_n, \beta_n)$ is the value of ξ that maximizes $n_a^{(n_{\rm P})}$:

$$n_a^{(n_{\rm P})} = \left\{ \frac{\alpha_n/\beta_n}{nc^4} + \frac{2^{2(n-1)}(c^4+s^4)(n-1)!^4}{4nc^4c^{2(n-1)}s^{2(n+1)}n!n^{4(n-1)}}[n\alpha_n^2 + \alpha_n\beta_n(c^4+s^4+4c^2s^2)] \right\}^{-1}, \tag{329}$$

with $c = 1/\sqrt{1+\xi_{\rm opt}(\alpha_n,\beta_n)^{-2}}$, $s = 1/\sqrt{1+\xi_{\rm opt}(\alpha_n,\beta_n)^2}$. While the minimization problem can yield analytical expressions for $\xi_{\rm opt}(\alpha_n, \beta_n)$, they are too cumbersome to be practical. Instead, it is more convenient to explore numerically the values of $\Delta^{(n)}_{\rm opt}/R$ and $n^{(n_{\rm P})}(\Delta^{(n)}_{\rm opt})/n^{(n_{\rm P})}(0)$ for a range of cases in (α_n, β_n) space. This allow us to appreciate the actual relevance of finding the best detuning in each case, by seeing how important this optimum detuning is as compared to the total Rabi frequency R, and how much the cavity population is actually increased as compared to its value in the resonant case $\Delta = 0$. Figure 6.11 depicts the results for $n = 2$, showing that, for $\alpha_n \gtrapprox 0.1$, the choice of the optimum detuning depends approximately on β_n only, i.e., on $\gamma_{\tilde{\sigma}}$ and R. It also shows that the change in $n_a^{(2_{\rm P})}$ that we can expect from a proper choice of Δ is significant but not of orders of magnitude, being a most a factor 4 (and a factor 2 in the range of parameters that we will typically consider in more realistic scenarios). Because of this, in the following Sections, some results will be given for $\Delta = 0$ for simplicity. The calculation for $n > 2$, not depicted here, yields similar results.

6.5.2 PHOTON POPULATION GROWN BY FIRST-ORDER PROCESSES

The expression for the cavity population (324) that we obtained in the previous Section accounted for photons that were introduced in the cavity via a n-photon coupling term. This was using Hamiltonian (315), which described

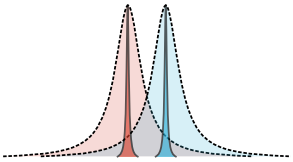

This contribution is easily pictured if one considers two detuned energy levels that broaden in a dissipative scenario, acquiring overlapping lineshapes.

an effective coupling given by a resonant n-th order process, neglecting the first order, off-resonant coupling. While this is correct in a purely Hamiltonian context, where the n-photon coupling overcomes the dynamics (as the rest of processes can be adiabatically eliminated), the situation is not necessarily the same in a dissipative scenario. In open systems, the broadening of the energy levels can yield a non-negligible contribution from the off-resonant, first-order coupling to the growth of cavity population. These mechanisms are not described by the n-photon Hamiltonian used to obtain Eq. (324). Instead, the population obtained from first-order processes can be computed, in the limit of low cavity occupation, by using the original Hamiltonian (299) in the master equation of Eq. (300) and restricting the space of correlators to the subspace with a single cavity photon. This excludes those n-th order processes responsible for the growth of photon population accounted by $n_a^{(n_\mathrm{p})}$.

From the master equation (300) and the Hamiltonian (299) we get the following set of equations:

$$\frac{d\langle a^\dagger a\rangle}{dt} = -\gamma_a\langle a^\dagger a\rangle - 2g\,\mathrm{Im}\Big\{\langle\tilde{\sigma}^\dagger a\rangle\Big\} \tag{330a}$$

$$\frac{d\langle\tilde{\sigma}^\dagger\tilde{\sigma}\rangle}{dt} = -\gamma_{\tilde{\sigma}}\langle\tilde{\sigma}^\dagger\tilde{\sigma}\rangle - 2\Omega\,\mathrm{Im}\{\langle\tilde{\sigma}\rangle\} - 2g\,\mathrm{Im}\Big\{\langle a^\dagger\tilde{\sigma}\rangle\Big\} \tag{330b}$$

$$\frac{d\langle\tilde{\sigma}\rangle}{dt} = -\left(i\Delta+\frac{\gamma_{\tilde{\sigma}}}{2}\right)\langle\tilde{\sigma}\rangle + 2i\Omega\langle\tilde{\sigma}^\dagger\tilde{\sigma}\rangle - ig\langle a\rangle + 2ig\langle a\tilde{\sigma}^\dagger\tilde{\sigma}\rangle - i\Omega \tag{330c}$$

$$\frac{d\langle a\rangle}{dt} = -\left(i\Delta_a+\frac{\gamma_a}{2}\right)\langle a\rangle - ig\langle\tilde{\sigma}\rangle + 2ig\langle\tilde{\sigma}a^\dagger a\rangle \tag{330d}$$

$$\frac{d\langle\tilde{\sigma}^\dagger a\rangle}{dt} = -\left[i(\Delta+\Delta_a)+\frac{\gamma_{\tilde{\sigma}}+\gamma_a}{2}\right]\langle\tilde{\sigma}^\dagger a\rangle - 2i\Omega\langle a\tilde{\sigma}^\dagger\tilde{\sigma}\rangle + i\Omega\langle a\rangle - 2ig\langle a^\dagger a\tilde{\sigma}^\dagger\tilde{\sigma}\rangle - ig\langle\tilde{\sigma}^\dagger\tilde{\sigma}\rangle + ig\langle a^\dagger a\rangle \tag{330e}$$

$$\frac{d\langle a\tilde{\sigma}^\dagger\tilde{\sigma}\rangle}{dt} = -\left(i\Delta_a+\frac{\gamma_a}{2}+\gamma_{\tilde{\sigma}}\right)\langle a\tilde{\sigma}^\dagger\tilde{\sigma}\rangle + ig\langle a^\dagger a\tilde{\sigma}\rangle - i\Omega\langle a\tilde{\sigma}^\dagger\rangle + i\Omega\langle a\tilde{\sigma}\rangle \tag{330f}$$

$$\frac{d\langle a\tilde{\sigma}\rangle}{dt} = -\left[i(\Delta+\Delta_a)+\frac{\gamma_{\tilde{\sigma}}+\gamma_a}{2}\right]\langle a\tilde{\sigma}\rangle - i\Omega\langle a\rangle + 2i\Omega\langle a\tilde{\sigma}^\dagger\tilde{\sigma}\rangle \tag{330g}$$

Under the approximation $\Omega \gg g, \gamma_a, \gamma_\sigma$, we can eliminate the terms proportional to $g\langle a^\dagger\tilde{\sigma}\rangle$ in Eq. (330b), to $ig\langle a\rangle$ and $ig\langle a\tilde{\sigma}^\dagger\tilde{\sigma}\rangle$ in Eq. (330c), to $g\langle\tilde{\sigma}a^\dagger a\rangle$ in Eq. (330d), to $g\langle a^\dagger a\tilde{\sigma}^\dagger\tilde{\sigma}\rangle$ and $g\langle a^\dagger a\rangle$ in Eq. (330e) and to $g\langle a^\dagger a\tilde{\sigma}\rangle$ in Eq. (330f). This leaves us, setting the derivatives to zero, with the following set of equations for the steady state observables:

$$\langle a^\dagger a\rangle_{SS} = -\frac{1}{\gamma_a}2g\,\mathrm{Im}\Big\{\langle\tilde{\sigma}^\dagger a\rangle_{SS}\Big\} \tag{331a}$$

$$\langle\tilde{\sigma}^\dagger\tilde{\sigma}\rangle_{SS} \approx -\frac{1}{\gamma_{\tilde{\sigma}}}2\Omega\,\mathrm{Im}\{\langle\tilde{\sigma}\rangle_{SS}\} \tag{331b}$$

$$\langle\tilde{\sigma}\rangle_{SS} \approx \frac{i\Omega}{i\Delta+\frac{\gamma_{\tilde{\sigma}}}{2}}(2\langle\tilde{\sigma}^\dagger\tilde{\sigma}\rangle_{SS}-1) \tag{331c}$$

$$\langle a\rangle_{SS} \approx -\frac{g}{\Delta_a - i\frac{\gamma_a}{2}}\langle\tilde{\sigma}\rangle_{SS} \tag{331d}$$

$$\langle\tilde{\sigma}^\dagger a\rangle_{SS} \approx i\frac{-2\Omega\langle a\tilde{\sigma}^\dagger\tilde{\sigma}\rangle_{SS} + \Omega\langle a\rangle_{SS} - g\langle\tilde{\sigma}^\dagger\tilde{\sigma}\rangle_{SS}}{i(\Delta+\Delta_a) + \frac{\gamma_a+\gamma_{\tilde{\sigma}}}{2}} \tag{331e}$$

$$\langle a\tilde{\sigma}^\dagger\tilde{\sigma}\rangle_{SS} \approx \frac{i\Omega(\langle a\tilde{\sigma}\rangle_{SS} - \langle\tilde{\sigma}^\dagger a\rangle_{SS})}{\frac{\gamma_a}{2} + \gamma_{\tilde{\sigma}} + i\Delta_a} \tag{331f}$$

$$\langle a\tilde{\sigma}\rangle_{SS} = \frac{-i\Omega(2\langle a\tilde{\sigma}^\dagger\tilde{\sigma}\rangle_{SS} - \langle a\rangle_{SS})}{i(\Delta+\Delta_a) + \frac{\gamma_a+\gamma_{\tilde{\sigma}}}{2}} \tag{331g}$$

This is a closed system of equations that can be readily solved. From it, we can obtain the population $n_a^{(1_P)} \equiv \langle a^\dagger a\rangle_{SS}$, which reads:

$$n_a^{(1_P)} = -\frac{1}{\gamma_a}2g\,\mathrm{Im}\left\{\frac{8g^2\Omega^2\left[-i8\Omega^2(\gamma_a+2i\Delta_a) - i\lambda(\Delta_+)\lambda(-\Delta_-)\lambda_2(\Delta_a)\right]}{(\gamma_a+2i\Delta_a)\lambda(\Delta_+)(8\Omega^2+4\Delta^2+\gamma_{\tilde{\sigma}}^2)(\lambda(\Delta_+)\lambda_2(\Delta_a)+16\Omega^2)}\right\} \tag{332}$$

where: $\lambda(\Delta) \equiv \gamma_a + \gamma_{\tilde{\sigma}} + 2i\Delta$; $\lambda_2(\Delta) \equiv \gamma_a + 2\gamma_{\tilde{\sigma}} + 2i\Delta$; $\Delta_+ \equiv \Delta + \Delta_a$; and $\Delta_- \equiv \Delta - \Delta_a$. For the case $\Delta = 0$ and $\Delta_a = \Delta_a^{(2)} \approx R$, the expansion to first order in $\gamma_{\tilde{\sigma}}$, which is a good approximation when $R \gg \gamma_{\tilde{\sigma}}$, reads:

$$n_a^{(1_P)} \approx \frac{2g^2(\gamma_a^2+28\Omega^2)}{(\gamma_a^2+4\Omega^2)(\gamma_a^2+36\Omega^2)} + \frac{32g^2\Omega^2(\gamma_a^4+432\Omega^4)\gamma_\sigma}{\gamma_a(\gamma_a^2+4\Omega^2)^2(\gamma_a^2+36\Omega^2)^2} + O[\gamma_\sigma^2] \tag{333}$$

6.6 UNVEILING N-PHOTON EMISSION

In the two previous Sections we obtained analytical expressions for the mean number of photons that the cavity is able to grow and sustain via two different mechanisms: off-resonant, first order coupling and n-photon coupling to the 2LS. These two mechanisms yield populations $n_a^{(1_P)}$ and $n_a^{(n_P)}$, respectively. Of course, the definition of two types populations in the cavity is somewhat artificial; solving the master equation of Eq. (300), using the Hamiltonian Eq. (299) with no restriction on the size the Hilbert space, will yield a total cavity population n_a that accounts for all the possible coupling mechanisms and that is the real observable quantity.

Nevertheless, the comparison between $n_a^{(1_P)}$ and $n_a^{(n_P)}$ provides invaluable information, since it tells us which of the processes is more efficient in populating the cavity. It is to be expected that, in a situation in which $n_a^{(n_P)} \gg n_a^{(1_P)}$, the total cavity population must be made up of photons that were transferred via a n-photon coupling, $n_a \approx n^{(n_P)}$. As we will see, this has enormous consequences on the properties of the light emitted by the system.

This comparison is shown in Figure 6.13. It depicts, for a fixed Ω, the values of $\gamma_a n_a^{(n_P)}$ and $\gamma_a n_a^{(1_P)}$, plotted together by superimposing their two colormaps (red for $n^{(n_P)}$, blue for $n_a^{(1_P)}$). These maps are defined in the

$(\gamma_a, \gamma_{\tilde{\sigma}})$ space for the cases $n = 2, 3, 4$. We analyse $\gamma_a n_a$ instead of n_a since the former describes the actual photon emission rate, which is the observable of practical interest. Figure 6.13 also includes two superimposed contourplots for $\gamma_a n_a$ (solid lines) and $\gamma_a (n_a^{(1_P)} + n_a^{(n_P)})$ (dashed lines), showing that the total cavity population is actually well approximated by:

$$n_a \approx n_a^{(1_P)} + n_a^{(n_P)} . \tag{334}$$

This Figure reveals that there are domains in $(\gamma_a, \gamma_{\tilde{\sigma}})$ space where the n-photon mechanism is indeed more efficient in populating the cavity, which is evidenced by the separation of red and blue colors in the 2D-plot. Those regions where $n_a \approx n_a^{(n_P)}$ define a special kind of regime, where all photons have been introduced in the cavity as an *n-photon bundle* via the n-photon coupling term of Eq. (315), and, as we will show, they are emitted as such, turning the 2LS-cavity system into a *continuous emitter of n-photon bundles*.

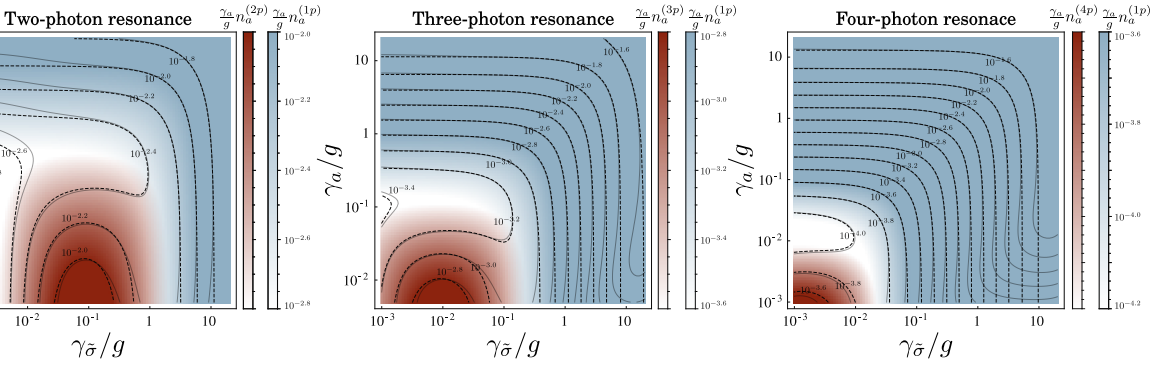

Figure 6.13: Competition between single and n-photon processes to populate the cavity. Emission rate, $\gamma_a n_a$ divided into the bundle component (red) and single-photon component (blue). Dashed lines: Analytical formulas for the total emision rate, with $n_a = n_a^{(1_p)} + n_a^{(n_p)}$. Solid lines: Numerical result for the total emission rate. $\Omega = 20g$.

INDIVIDUAL QUANTUM TRAJECTORIES An insightful view of the dynamics of emission in such a regime is provided by the quantum Monte Carlo approach [190], where one follows individual trajectories of the system and records photon clicks whenever the system undergoes a quantum jump. A tiny fraction of such a trajectory is presented in Fig. 6.13 b. This shows the probabilities of the system to be in the states $|n, g/e\rangle$ for n up to 2 (probabilities in higher rungs are included in the numerical simulation but not shown in the plot). Until time $t \approx 0.8$ (in units of $1/\gamma_a$), the QE essentially undergoes fast Rabi flopping (in an empty cavity) under the action of the laser, corresponding to the Mollow regime. At the same time, the driving of the third rung makes the probability to have two photons in the cavity sizable, as seen in bottom panel of Fig. 6.13 c, where the combined probability reaches over 1%, while the probability to have one photon is more than one order of magnitude smaller. This relatively high probability of the two-photon state, given the time available to realize it, eventually results in its occurrence. This causes the emission of a first cavity photon (indicated by a red triangle at the top of the figure) that collapses the wavefunction into the one-photon state, which is now the state with almost unit probability. The system is now expected to emit a second photon within the cavity lifetime (second red triangle in Fig.6.13 c). There is a jitter in the emission of the two-photon state due to the cavity, but this does not destroy their correlation. After the two-photon emission, the system is left in a vacuum state but

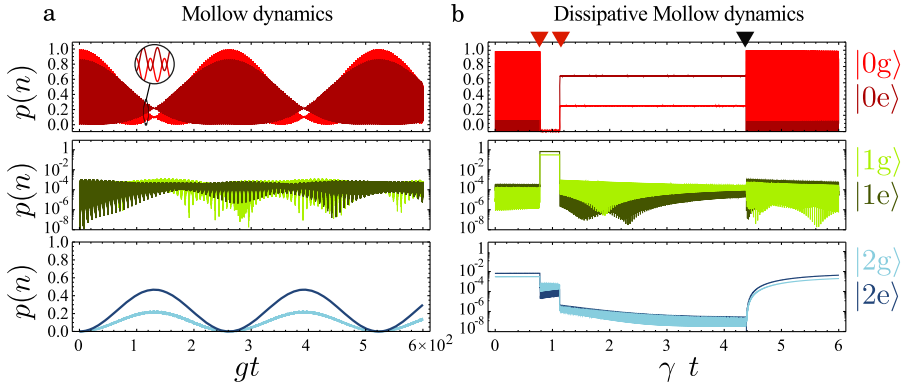

Figure 6.13: Wavefunction evolution at the two-photon resonance pictured through the probability of the system to be in any of the states $|n, g/e\rangle$. **a**, Hamiltonian evolution in the Mollow regime (high pumping). **b**, Quantum trajectory during a two-photon emission in the same regime as in **a**, but in the presence of dissipation.

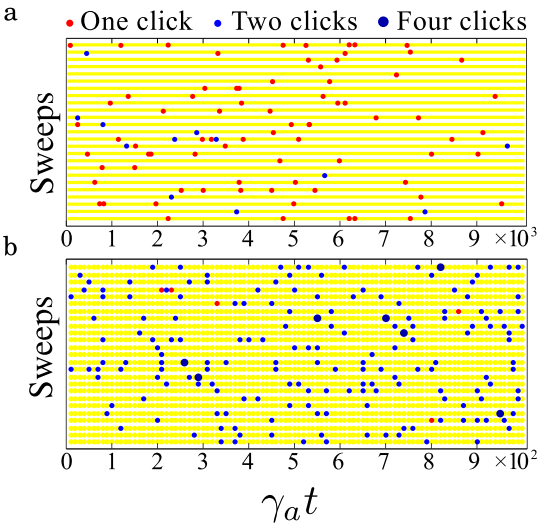

Figure 6.14: Cavity-photon clicks as they would be recorded by a streak camera (25 sweeps shown) for the pumping values Ω_1 in d and Ω_2 in e at ω_2. In a the emission is highly bunched although it largely consists of single clicks, $g^{(2)} = 3649$ with a fraction of 'two-clicks' over the total given by $\pi_2 = 16\%$. On the other hand, for b, $g^{(2)} = 17$ with $\pi_2 = 98.8\%$.

without Rabi flopping, that is restored after a direct emission from the QE (black triangle) and a two-photon state is again constructed, preparing for the next emission of a correlated photon pair. The system is then brought back to its starting point. Although one photon coming from the QE decay is emitted per two-photon emission cycle, it is at another frequency and in a different solid angle. The two-photon emission is through the cavity mode, being therefore unspoiled and strongly focused.

PHOTODETECTION EVENTS The precise times at which the jumps occur in the individual Monte Carlo trajectories can be interpreted as photodetection events, as would be recorded by perfect detector able to collect all the photons emitted by the system [237]. Figure 6.14 presents a series of such detection events, in the form in which they would be recorded by a streak camera photodetector [236] for the pumping values Ω_1 and Ω_2 of Fig. 5.13 b at $\omega_2(\Omega)$. The horizontal axis represents time and each point denotes a detection event as the detection spot is raster scanned across the image. The strong bunching at Ω_1 in Fig. 5.13 b conveys that the number of correlated two-photon events (blue points) in Fig. 6.14 a is much larger than would be expected for a coherent source. The emission remains nevertheless predominantly in terms of single photons (red points). Whilst the resonances in statistics are strong, they are therefore not meaningful for applications. On the other hand, at Ω_2, when the $g^{(2)}$ resonance is depleted, the emission now consists almost exclusively of correlated photon pairs, as can be seen by the dominance of blue points in Fig. 6.14 b.

6.7 CHARACTERIZING AN N-PHOTON EMITTER

We have introduced the concept of a continuous n-photon emitter, and shown that a dressed 2LS-cavity system has a regime in which it behaves as such. Our next aim is to analyse the configurations in which the system offers the best performance as an emitter of n-photon bundles.

Based on the analysis made so far, it is clear that the properties that define quality of n-photon emission must be the following:

- Intensity of emission of n-photon bundles. This is related to $\gamma_a n_a^{(n_\mathrm{p})}$.
- Purity of bundle emission. This tells to which extent the emission is constituted only by photon bundles, and is related to the relative value of $n_a^{(1_\mathrm{p})}$ with respect to $n_a^{(n_\mathrm{p})}$.

Based on these criteria, we will analyse the performance of the system as a function of its three most important parameters, namely, Ω, γ_a and $\gamma_{\tilde{\sigma}}$.

6.7.1 BUNDLE EMISSION RATE

Since we have shown that the dominance $n_a^{(n_\mathrm{p})}$ over $n_a^{(1_\mathrm{p})}$ corresponds to the the regime of n-photon emission, it is compelling to associate the rate of bundle emission with $\gamma_a n_a^{(n_\mathrm{p})}$. This quantity was already shown for the case of $n = 2,3,4$ in Fig. 6.13 as a function of γ_a and $\gamma_{\tilde{\sigma}}$. From there, we can observe that the bundle emission rate always decreases as γ_a increases, making the cavity decay rate always detrimental. The dependence on $\gamma_{\tilde{\sigma}}$ is less trivial. Both small values and big values of $\gamma_{\tilde{\sigma}}$ are detrimental to the bundle emission rate, and an optimum can be found by the differentiation of Eq. (324):

$$\gamma_{\tilde{\sigma}}^{(\mathrm{opt})} = g^n \frac{\sqrt{2}(n^2\Omega)^{n-1}(\Delta^2+4\Omega^2)^{\frac{3}{2}-n}}{n!^2\sqrt{\frac{(\Delta^2+2\Omega^2)(\Delta^2+6\Omega^2)}{n![2\Omega^2+\Delta(\Delta+\sqrt{\Delta^2+4\Omega^2})]}}} \tag{335}$$

which depends on Δ, Ω and n. For $\Delta = 0$ and $n = 2,3,4$, this optimum rate takes the form:

$$\gamma_{\tilde{\sigma},n=2}^{(\mathrm{opt})} = 2\sqrt{\frac{2}{3}}\left(\frac{g^2}{\Omega}\right), \quad \gamma_{\tilde{\sigma},n=3}^{(\mathrm{opt})} = \frac{81}{16\sqrt{2}}\left(\frac{g^3}{\Omega^2}\right), \quad \gamma_{\tilde{\sigma},n=4}^{(\mathrm{opt})} = \frac{64\sqrt{2}}{9}\left(\frac{g^4}{\Omega^3}\right). \tag{336}$$

The spoiling of the mechanism for low enough $\gamma_{\tilde{\sigma}}$ can be understood if we take into account that the effective pumping term P of the dressed 2LS is

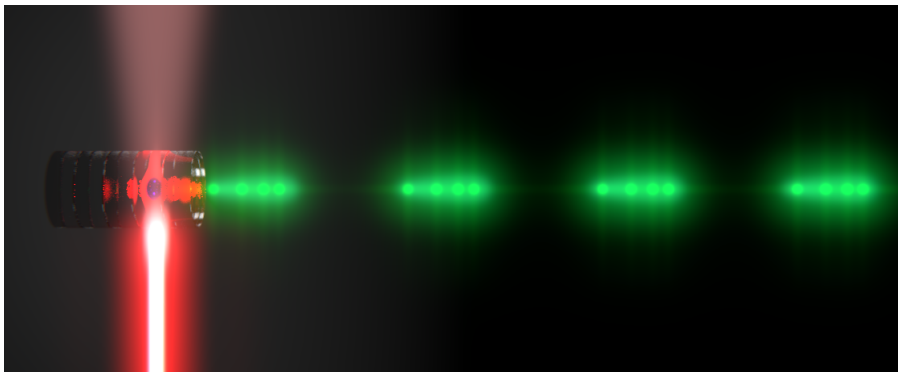

Figure 6.15: Artistic representation of an emitter of N-photon bundles. The system emits a continuous stream of light composed of bundles of a fixed number N of photons. This number can be chosen by a proper detuning between the exciting laser and the cavity. Image created by www.scixel.es.

not independent, but is also given by $\gamma_{\tilde{\sigma}}$. Therefore, as $\gamma_{\tilde{\sigma}}$ decreases, the time needed to reload the 2LS increases, while the time needed to decay does not, due to the extra decay channel provided by the cavity. This asymmetry between the reloading time and the decay time with decreasing $\gamma_{\tilde{\sigma}}$ makes the mechanism inefficient, and ultimately spoils it. The reason why the mechanism is also inefficient for big $\gamma_{\tilde{\sigma}}$ is more clear: as $\gamma_{\tilde{\sigma}}$ increases, so does the probability of having emissions to the free space instead of through the cavity channel, therefore spoiling the process. From the perspective of a cavity that acts as a filter and provides a Purcell-enhancement of the n-photon leapfrog processes, this is alternatively understood as a spoiling of the Mollow triplet structure that sustains these n-photon transitions due to the broadening of the energy levels.

Finally, we consider how the efficiency of the mechanism depends on Ω, which is the parameter of greatest practical interest since is the one most easily tuned experimentally, corresponding to the intensity of the exciting laser. From Eq. (324), we can verify that the bundle emission rate always decreases when Ω increases. This is shown in Fig. 6.15, where we display, for the two and three-photon resonance, both $n_a^{(n_\mathrm{p})}$, $n_a^{(1_\mathrm{p})}$, and the total cavity population n_a, as a function of Ω, keeping ω_a at the n-photon resonance as Ω changes. We consider, without loss of generality, the case of zero detuning $\Delta = 0$.

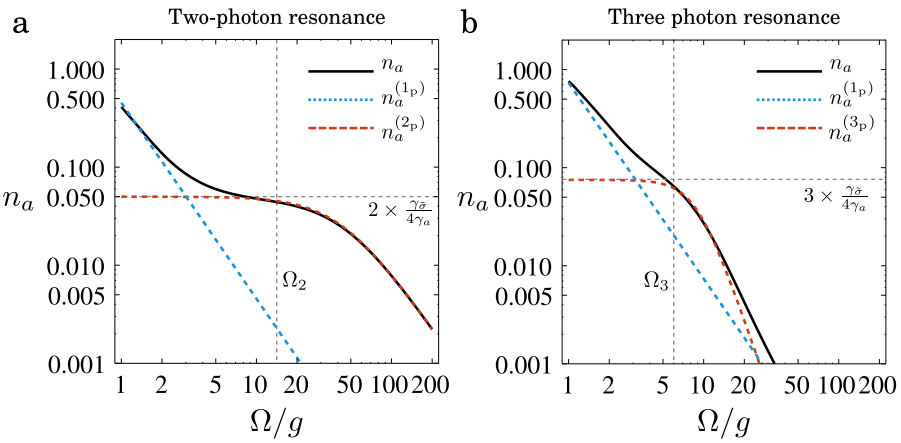

Figure 6.15: Cavity population as a function of laser intensity at the two and three-photon resonance. As Ω increases, both the bundle population $n_a^{(n_\mathrm{p})}$ and the background population $n_a^{1_\mathrm{p}}$ decrease. At low pumping, the bundle population tends to $n\gamma_{\tilde{\sigma}}/4\gamma_a$. Ω_2 and Ω_3 mark optimum pumping intensities at which the bundle population is close to its maximum value and it makes up for most of the cavity population. Parameters: $\gamma_a = 0.1g$, $\gamma_\sigma = 0.01g$.

Figure 6.15 shows that both $n_a^{(n_\mathrm{p})}$ and $n_a^{(1_\mathrm{p})}$ decrease with increasing Ω. For the case of $n_a^{(n_\mathrm{p})}$, this is due to the fact that the n-photon coupling rate $g^{(n_\mathrm{p})}$ depends on Ω as $\propto 1/\Omega^{n-1}$ (see Eq. (314) and Figs. 6.8 and 6.10).

In the case of $n_a^{(1_\mathrm{p})}$, first-order processes are more detuned as Ω increases, since $\Delta_a^{(n)} \approx 2\Omega/n$ (at $\Delta = 0$). The limits of low and high pumping for $n_a^{(n_\mathrm{p})}$ can readily be obtained from Eq. (324), giving:

$$n_a^{(n_\mathrm{p})} \sim \frac{n}{4}\frac{\gamma_{\tilde{\sigma}}}{\gamma_a}, \quad (\Omega \to 0); \tag{337a}$$

$$n_a^{(n_\mathrm{p})} \sim \frac{g^{2n}}{\Omega^{2(n-1)}} A_n, \quad (\Omega \to \infty); \tag{337b}$$

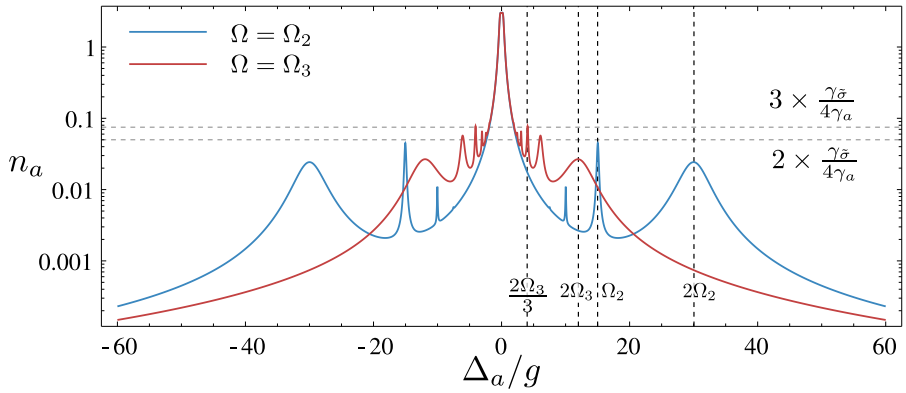

Figure 6.17: Profile of the cavity population as its frequency is detuned along the Mollow triplet. This is done for two values of Ω, Ω_2 and Ω_3, that maximize the bundle population at the two and three-photon resonance, respectively.

where

$$A_n = \frac{(n/2)^{4n-2}}{(n-1)!^3 \gamma_a (n\gamma_a/4 + 6\gamma_{\tilde{\sigma}})}. \tag{338}$$

On the other hand, the high pumping limit of $n_a^{(1_P)}$ is given by:

$$n_a^{(1_P)} \sim \left(\frac{g^2}{\Omega^2}\right) \frac{n^3(2+n^2)\gamma_{\tilde{\sigma}} + n(n^4 - n^2 + 2)\gamma_a}{16(n^2-1)^2\gamma_a}, \quad (\Omega \to \infty). \tag{339}$$

In the case of $n_a^{(n_P)}$, this limit is reached when $\kappa^{(n)} \ll \gamma_{\tilde{\sigma}}$, or equivalently, when $(\Omega/g)^{2(n-1)} \gg C$, where C is the *cooperativity* $C \equiv g^2/\gamma_a\gamma_{\tilde{\sigma}}$. For $n_a^{(1_P)}$, this limit is reached sooner, since Ω only needs to satisfy $\Omega \gg \gamma_a, \gamma_{\tilde{\sigma}}$. In fact, the curves for $n^{(1_P)}$ shown in Fig. 6.15 are already well described by Eq. (339).

The **cooperativity** C is a very popular figure of merit in quantum optics. In systems irreversibly coupled to an optical channel (i.e., below strong-coupling), it is proportional to the number of photons emitted trough the optical channel divided by the number of photons emitted to free space.

Interestingly, we find that the low-pumping limit of $n_a^{(n_P)}$, which determines the maximum value that it can take for a given $(\gamma_a, \gamma_{\tilde{\sigma}})$, increases with n. This might lead one to think that n-photon resonances of higher order are easier to evidence than those of lower orders, since they induce larger cavity populations. However, as we see clearly in Fig. 6.17, in order to observe these maximum values of $n_a^{(n_P)}$, one needs to use lower pumping intensity Ω as n increases. This leads to less-resolved resonances, and, more importantly, to a more important background contribution from the central Mollow peak.

This brings us directly to the issue of comparing the "bundle population", $n_a^{(n_P)}$, with the "background population", $n_a^{(1_P)}$. We can see from these equations, and observe in Fig. 6.15, that in the high pumping limit, only $n_a^{(2_P)}$ can remain bigger than $n_a^{(1_P)}$, since both decrease as $1/\Omega^2$. For $n > 2$, $n^{(n_P)}$ decreases with Ω faster than the background population. Figure 6.15 also shows that, as Ω approaches zero, the value of $n_a^{(1_P)}$ overcomes $n_a^{(n_P)}$ and makes up for the total population n_a. However, for $n > 2$, an intermediate pumping intensity exists where $n_a^{(nP)}$ is comparable or bigger than $n_a^{(1_P)}$, contributing significantly to the total cavity population. This is the case, for the case of the three-photon resonance, of the point labelled Ω_3 in Fig. 6.15 and used in Fig. 6.17. This kind of analysis brings us to the next criterion

to characterize the quality of the n-photon emitter: the purity of n-photon emission.

6.7.2 PURITY OF n-PHOTON EMISSION

It is clear from the results shown in Figs. 6.13 and 6.15 that we can, to a good degree of accuracy, describe the total cavity population n_a as a sum of two components. One of this components is the "bundle" contribution $n_a^{(n_\mathrm{P})}$, consisting of photons that were introduced in the cavity as a n-photon bundle via the n-photon coupling term $g^{(n_\mathrm{P})}(a^n\sigma^\dagger + \mathrm{h.c})$. The other is a "background" contribution, $n^{(1_\mathrm{P})}$, consisting on individual photons (individual not in the sense of antibunched, but in the sense of being transferred to the cavity by a term of the type $a^\dagger\sigma + \mathrm{h.c.}$). We shall adopt the terminology of "bundle" and "background" populations from now on to refer to $n_a^{(n_\mathrm{P})}$ and $n_a^{(1_\mathrm{P})}$ respectively.

In this sense, it is clear that the n-photon emission will be contaminated by individual photons emitted from the background population if this one is comparable to the bundle population. Following this argument, we will define a quantitative measure of the *purity* π_n *of* n*-photon emission* as:

$$\pi_n \equiv \frac{n^{(n_\mathrm{P})}}{n_a^{(n_\mathrm{P})} + n_a^{(1_\mathrm{P})}} \tag{340}$$

i.e., the ratio between the bundle population and the total population, which is by definition a quantity bounded by one.

Before discussing in detail the values taken by π_n in the parameter phase space, we discuss a particular feature of n-photon emitters that can be used to determine the purity of n-photon emission. This feature manifests in the *photon counting distribution* [180, 216, 243], and is related to the fact that, by definition, an ideal n-photon emitter will never produce a number of photons that is not a multiple of n. This yields, in the distribution $p(m)$ of photons counted in any time window T, a strongly suppressed probability of detecting any number of photons not given by $m = kn$, with $k \in 0, 1, 2, 3, \cdots$ (see Fig. 6.18). However, a non-ideal n-photon emitter occasionally emits individual photons that spoil these distributions. To describe this situation, one needs to consider the combination of several discrete random processes, some of them accounting for the emission of individual photons, and others, for the n-photon bundles.

For a given discrete random process X, we can define the generating function $\Pi_X = \langle s^X \rangle$, from which the probability distribution for X is given by $P(X = m) = \frac{1}{m!}\partial^m / \partial s^m \Pi_X|_{s=0}$. Probability generating functions are particularly useful when dealing with functions of independent random variables. This is precisely our case, since we are interested in the total number of counted photons X_T, given by the sum of X_1 (photons coming from the background and therefore emitted individually) and X_n (photons emitted as a bundle):

$$X_T = X_1 + X_n\,. \tag{341}$$

The probability generating function is then $\Pi_{X_T} = \Pi_{X_1}\Pi_{X_t}$. As we will see, the final generating functions that we will encounter will usually have the exponential form: $\Pi_{X_T} = e^{g(s)}$. In this case, making use of Faà di Bruno's formula for the generalized chain rule, expressed in terms of the Bell polynomials $B_{n,k}(x_1, \cdots, x_{n-k+1})$:

$$\frac{d^n}{dx^n} f(g(x)) = \sum_{k=1}^{n} f^{(k)}(g(x)) B_{n,k}\left(g'(x), g''(x), \cdots, g^{(n-k+1)}(x)\right), \tag{342}$$

we find that the total photon counting distribution of the composite random process is given by:

$$P(X_T = m) = \frac{e^{g(0)}}{m!} B_m(a_1, \cdots, a_n), \tag{343}$$

which is written in terms of the complete Bell polynomial,

$$B_n(a_1, \cdots, a_n) = \sum_{k=1}^{n} B_{n,k}(a_1, \cdots, a_{n-k+1}) \tag{344}$$

and where $a_n = \partial^n g / \partial x^n|_{x=0}$ and $B_0(\{\}) = 1$. This way, the problem of obtaining the photon counting distribution for a combination of random processes is reduced to expressing the generating function as a single exponential $e^{g(s)}$ and computing the n-th derivative of the exponent $\partial^n g / \partial x^n|_{x=0}$.

At this point, we need to make an ansatz on the photon counting distribution of individual photons and bundles. We observe that for time windows T larger than the coherence time, counting of the photon bundles becomes Poisson distributed, as short time correlations are lost [157], and the same occurs for the individual photons. The random variable X_n that counts the photons emitted in n-photon bundles will then follow the Poissonian distribution:

$$P(X_n = m) = \begin{cases} e^{-\lambda_n T} \frac{(\lambda_n T)^{m/n}}{(m/n)!} & \text{if} \quad m = 0, n, 2n, 3n, \cdots \\ 0 \quad \text{if} \quad m \neq 0, n, 2n, 3n, \cdots \end{cases} \tag{345}$$

where $n\lambda_n$ is the mean number of photons counted per unit time, yielding a generating function:

$$\Pi_{X_n}(s) = e^{-\lambda_n (1 - s^n)}. \tag{346}$$

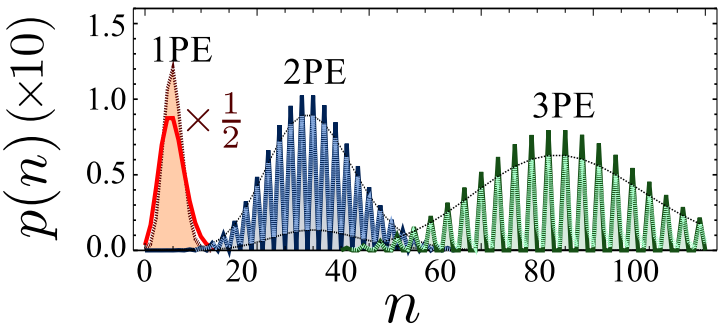

Figure 6.18: Ideal NPE (N-Photon Emission) in thick lines and 99% NPE in translucid lines with an envelope to guide the eye.

The total generating function of the composite process is then given by:

$$\Pi_{X_T}(s) = e^{-\lambda_1(1-s)-\lambda_n(1-s^n)} \tag{347}$$

and, using the results above, the distribution of counting m photons in a time window T when the system is emitting n-photon bundles with emission rate $n\lambda_n$ and single photons with rate λ_1, is given by:

$$P_n(X_T = m) = e^{-(\lambda_1+\lambda_n)T} \sum_{k=0}^{m} \frac{n!(\lambda_1 T)^{m-nk}(\lambda_n T)^k}{k!(m-nk)!}\,. \tag{348}$$

This distribution is shown in Fig. 6.18 for the cases of ideal two-photon (2PE) and three-photon (3PE) emission. In a general situation, λ_1 and λ_n would be associated respectively with $\gamma_a n_a^{(1_P)}$ and $\gamma_a n_a^{(n_P)}/n$. Consequently, we can obtain an estimation of these quantities by fitting the observed photon counting distribution to Eq. (348), with fitting parameters λ_1 and λ_n. We can then define the purity of n-photon emission obtained by photon counting π_n^{PC} as:

$$\pi_n^{(\mathrm{PC})} \equiv \frac{n\lambda_n}{\lambda_1 + n\lambda_n}\,. \tag{349}$$

From a theoretical point of view, this estimation for the purity of n-photon emission is obtained by fitting the λ_1 and λ_n parameters from a photon counting distribution, which can computed by the Monte Carlo method of quantum trajectories.

6.7.3 CHARACTERIZATION OF THE EMITTER IN TERMS OF THE PURITY

We will discuss now the dependence of the purity on the system parameters. Figure 6.20 shows the purity of two-photon emission for the same Ω and range of γ_a, $\gamma_{\tilde{\sigma}}$ shown in Fig. 6.13, computed both by using the analytical expressions of $n_a^{(n_P)}$ (324) and $n_a^{(1_P)}$ (332) and by the fitting of photon counting distributions obtained from Monte Carlo trajectories. We see that the photon counting method, while not exact, offers a fairly good perspective of the values taken by this quantity. In the range of parameters shown, which is enough to account for all current practical applications, π_n is well described by the following expression, obtained from the expansion (333) of $n_a^{(1_P)}$ and from Eq. (326):

$$\pi_n \approx \left\{1 + \left[\frac{4g(\gamma_a^2+28\Omega^2)}{(\gamma_a^2+4\Omega^2)(\gamma_a^2+36\Omega^2)} + \frac{32g^2\Omega^2(\gamma_a^4+432\Omega^4)\gamma_\sigma}{\gamma_a(\gamma_a^2+4\Omega^2)^2(\gamma_a^2+36\Omega^2)^2}\right] \times \left[\frac{4\gamma_a}{n\gamma_{\tilde{\sigma}}} + \frac{\gamma_a\Omega^{2(n-1)}}{g^{2n}}(2n\gamma_a+3\gamma_{\tilde{\sigma}})n^{2(1-2n)}16^{n-1}\right]\right\}^{-1} \tag{350}$$

By inspection of Eq. (350) and discussed in Section 6.7.1, it is easy to see that π_2 has the high pumping asymptotic limit:

$$\pi_2 \sim 1 \quad (\Omega \to \infty)\,, \tag{351}$$

whereas, for $n > 2$, we see that it decreases with Ω as:

$$\pi_n \sim \frac{A}{\Omega^{2(n-2)}} \quad (\Omega \to \infty)\,, \tag{352}$$

where A is a function of n, γ_a and $\gamma_{\tilde{\sigma}}$ that can be obtained by dividing Eq. (337a) by Eq. (339). Therefore, while for $n = 2$ we can assure a maximum purity just by increasing the pumping, in the case $n > 2$ we need to find an optimum choice of Ω that makes the fraction of bundle population significant. The analytical expression for the optimum Ω obtained by differentiating Eq. (350) is too complicated to be useful, so it is more practical to recourse to a numerical minimization for each case. However, we can approximately locate this value close to the point where the two asymptotic values of $n_a^{n_\mathrm{P}}$, given by Eqs. (337a) and (337b), meet. This gives the following expression for the optimum pumping:

$$\Omega_{\mathrm{opt}}^{(n)} \approx \left(\frac{4\gamma_a A_n}{n\gamma_{\tilde{\sigma}}}\right)^{\frac{1}{2(n-1)}}\,, \tag{353}$$

where A_n is given by Eq. (338).

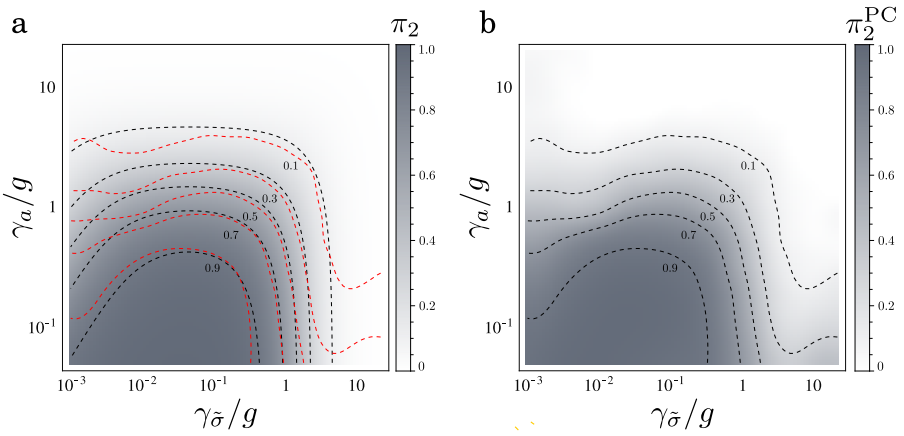

Figure 6.20: Purity of two-photon emission. **a**, Purity of two-photon emission obtained from Eqs. (324) and (332). In the ranges shown, it is perfectly described by Eq. (350). Dashed, black lines are contour lines of π_2; red dashed lines are contour lines of the π_2^{PC} shown in panel b, overlapped here for comparison. **b**, Purity obtained by fitting photon counting distributions from Monte Carlo calculations. Parameters: same as in Fig. 6.13.

6.8 FILTERING OUT THE BACKGROUND

The results that we showed in Figs. 6.3 and 6.4 for the cavity spectrum as a function of the its frequency seem to suggest that, when frequency resolved, the peak in the total emission observed when crossing the two-photon resonance manifests as an increase in the emission at the frequency of the cavity. This peak in the emission is found together with other three peaks that are independent of the cavity frequency and that correspond to the peaks of the Mollow triplet.

In our discussion so far about the performance of the system as an n-photon emitter we have not taken into account the energy degree of freedom of the emission. However, the notion of spectral components that are independent of the cavity frequency and that correspond to the peaks in the

spectrum of the 2LS seem to fit well with our description of the purity of emission, based on the existence of a "background" population of photons coming from detuned, first order processes (precisely those that manifest in the spectrum) that competes with a "bundle" population, transferred to the cavity via a resonant, n-photon process. To a good degree of accuracy, these two populations coexist as independent components of the total cavity population. Could it be that these different components emit at different spectral windows? If that were the case, most of the photons emitted by the background population could just be disregarded by frequency filtering, only selecting those photons emitted at the frequency of the cavity.

To answer this question, we can resort to the formal expression of the spectrum (see Section 2.6.3), that allow us to write it as a sum of Lorentzians plus a dispersive part:

$$S(\omega) = \frac{1}{\pi}\sum_{\beta}\left[\frac{(\gamma_\beta/2)L_\beta}{(\omega-\omega_\beta)^2+(\gamma_\beta/2)^2} - \frac{(\omega-\omega_\beta)K_\beta}{(\omega-\omega_\beta)^2+(\gamma_\beta/2)^2}\right] \tag{354}$$

where $\omega_\beta \equiv \mathrm{Im}\{\lambda_\beta\}$, $\gamma_\beta \equiv 2\,\mathrm{Re}\{\lambda_\beta\}$, λ_β is the vector of eigenvalues of the Liouvillian, $L_\beta \equiv \mathrm{Re}\{Q_\beta\}$, $K_\beta \equiv \mathrm{Im}\{Q_\beta\}$, and Q is a function of the matrix of eigenvectors of the Liouvillian and the steady state density matrix, ρ_{SS}, defined in Eq. (172). These values can be obtained by diagonalizing the Liouvillian numerically. In principle, the index β runs up to infinity; in practice, it runs up to h^2, where h is the size of the truncated Hilbert space. Each of the peaks composing the spectrum is centred at the frequency ω_β and has a weight of L_β that, when summed, yields the total population of the cavity:

$$\sum_{\beta} L_\beta = n_a\,. \tag{355}$$

After inspection of the spectrum obtained in our system, c.f. Fig. 6.4 a, it is safe to assume that, at the two-photon resonance, the sets of frequencies ω_β with a relevant contribution to the spectrum could be classified in four classes: $\omega_\beta = \omega_0, \pm\omega_{\mathrm{S}}, \omega_a$, i.e., the central and two sideband peaks of the Mollow triplet, and a peak at the cavity frequency, which is at the two-photon resonance. If we define the intensity of emission at the frequency $\omega_a = \omega_2$ as:

$$I_{\omega_a} \equiv \sum_{\substack{\beta \\ \omega_\beta = \omega_2}} L_\beta \tag{356}$$

we can verify whether bundle emission can be spectrally resolved or not by testing if the following equality is true:

$$I_{\omega_a} = n_a^{(2_{\mathrm{P}})}. \tag{357}$$

Figure 6.20 b shows the purity π_2 as given by Eq. (350), together with the purity that would be obtained by assuming Eq. (357) is true, i.e.:

$$\pi_2^{\mathrm{Sp}} \equiv \frac{I_{\omega_a}}{n_a} \tag{358}$$

which is depicted as green contour lines. The purity obtained under the assumption of Eq. (357) describes correctly the real value of π_2 up to a given point, in the range of high values of $\gamma_{\tilde{\sigma}}$, in which it deviates from the correct result, meaning that photons from the background population start being emitted at the cavity frequency. This promising result—more so if one considers that the regime of low $\gamma_{\tilde{\sigma}}$ is easily found experimentally—suggest that a great enhancement of the purity would be found if we disregarded those photons emitted at frequencies other than that of the cavity.

6.8.1 SPECTRUM OF THE BACKGROUND EMISSION

Since we have proven that the background population of photons is well described with a formalism in which the cavity is truncated at one excitation, allowing us to obtain analytical expressions that exclude the population grown by n-photon processes, we will use the same model to describe the spectrum of emission of the background photons. By doing so, we will be able to neglect the fraction of background photons that are not emitted at the frequency of the cavity.

In this case it is convenient to calculate the spectrum using the quantum regression theorem for the evolution of a vector of correlators, instead of the Liouvillian form. Let us assume that the dynamics of the mean value $\langle a \rangle$ is coupled to a set of correlators that we write in a vector $\mathbf{u}$, a being the first element, $\mathbf{u}_1 = a$. In our case, the vector is $\mathbf{u} = (a, \tilde{\sigma}, \tilde{\sigma}^\dagger, \tilde{\sigma}^\dagger\tilde{\sigma})^{\mathrm{T}}$, and the dynamics of the mean values follows the equation:

$$\frac{d}{dt}\langle \mathbf{u} \rangle = M\langle \mathbf{u} \rangle + \mathbf{c} \tag{359}$$

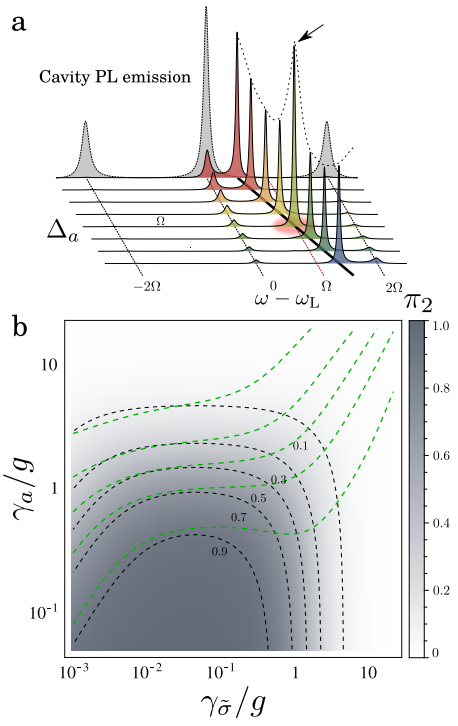

Figure 6.20: Weight of the spectral peaks as a measure of the purity if n-photon emission. a, A signature of the two-photon emission is the increase in the population of the cavity when its frequency crosses the two-photon resonance. When the emission is frequency resolved, this increase manifests in the peak resonant with the cavity frequency. **b**, Under the assumption that all the individual photons from the background population are emitted at the frequency of the Mollow peaks, the purity of n-photon emission is estimated as the fraction of light emitted trough the cavity peak with respect to the total emission. When this is done, a correct measure of the purity is recovered for values of $\gamma_{\tilde{\sigma}}$ approximately smaller than $0.1g$. For greater values, this estimation deviates from the real π_n, indicating that the assumption is not valid, and consequently, evidencing a background emission of individual photons at the frequency of the cavity.

with

$$M = \begin{pmatrix} -\frac{\gamma_a}{2} - i\Delta_a & -ig & 0 & 0 \\ 0 & -\frac{\gamma_{\tilde{\sigma}}}{2} - i\Delta & 0 & 2i\Omega \\ 0 & 0 & -\frac{\gamma_{\tilde{\sigma}}}{2} + i\Delta & -2i\Omega \\ 0 & i\Omega & -i\Omega & -i\gamma_{\tilde{\sigma}} \end{pmatrix}, \quad \mathbf{c} = \begin{pmatrix} 0 \\ -i\Omega \\ i\Omega \\ 0 \end{pmatrix} \tag{360}$$

In order to obtain an homogeneous equation, we define a vector $\mathbf{v}$ given by $\mathbf{v} = \mathbf{u} - \mathbf{u}_{\mathrm{SS}}$, where $\mathbf{u}_{\mathrm{SS}}$ are the steady state solutions of Eq. (359), giving the equation:

$$\frac{d}{dt}\langle \mathbf{v} \rangle = M \langle \mathbf{v} \rangle \,. \tag{361}$$

We can now apply the quantum regression theorem and write the dynamics of the set of two-time correlators:

$$\frac{d}{d\tau}\langle a^\dagger(t)\mathbf{v}(t+\tau)\rangle = M\langle a^\dagger(t)\mathbf{v}(t+\tau)\rangle. \tag{362}$$

Defining $\mathbf{w}(\tau) = \langle a^\dagger(t)\mathbf{v}(t+\tau)\rangle$, the spectrum is then given by:

$$S(\omega) = \frac{1}{\pi}\,\mathrm{Re}\int_0^\infty \mathbf{w}_1(\tau)e^{i\omega\tau}d\tau. \tag{363}$$

$\mathbf{w}(\tau)$ has the formal solution $\mathbf{w}(\tau) = e^{M\tau}\mathbf{w}(0)$, which, considering the diagonalized form of M:

$$-D = E^{-1}ME \tag{364}$$

where E is the matrix of normalized eigenvectors of M, reads $\mathbf{w}(\tau) = Ee^{-D\tau}E^{-1}\mathbf{w}(0)$. This allow us to integrate formally Eq. (363) and find an expression for the spectrum analogous to Eq. (354), with $D_\beta = \gamma_\beta/2 + i\omega_\beta$, and:

$$L_\beta \equiv \mathrm{Re}\{E_{1,\beta}[E^{-1}\mathbf{w}(0)]_\beta\}. \tag{365}$$

We are of course interested in $I^{(1)}_{\omega_a}$, defined as in Eq. (356); we use the superscript 1 to indicate that it corresponds to the model of a cavity truncated at one excitation. From it, we can define the part of the background population of photons that are emitted at the cavity frequency:

$$n^{(1_{\mathrm{p}})}_{a,\mathrm{f}} \equiv I_{\omega_a} \,. \tag{366}$$

This corresponds to the number of background photons that cannot be spectrally separated, since they are emitted at the cavity frequency. Accounting only for this population of photons that contaminate the n-photon emission, we can adopt a new definition of the purity that assumes that we have performed frequency filtering of the emission, giving:

$$\pi^{\mathrm{f}}_n \equiv \frac{n^{(n_{\mathrm{p}})}_a}{n^{(n_{\mathrm{p}})}_a + n^{(1_{\mathrm{p}})}_{a,\mathrm{f}}} \tag{367}$$

Thanks to the small size of the matrix M, we can obtain approximate analytical expressions for $n_{a,\mathrm{f}}^{(1_\mathrm{p})}$ based on the same approximations used to obtain Eq. (333), yielding, for the case of the two-photon resonance and $\Delta = 0$,

$$n_{a,\mathrm{f}}^{(1_\mathrm{p})} \approx \frac{32g^2\Omega^2(\gamma_a^4 + 432\Omega^4)\gamma_\sigma}{\gamma_a(\gamma_a^2 + 4\Omega^2)^2(\gamma_a^2 + 36\Omega^2)^2}. \tag{368}$$

Interestingly, this expression already appeared naturally as an independent term in Eq. (333). For the most general case of arbitrary cavity detuning, we find:

$$n_{a,\mathrm{f}}^{(1_\mathrm{p})} \approx \mathrm{Re}\left\{\frac{32g^2(\gamma_a^2\Omega^2 + 4i\gamma_a\Delta_a\Omega^2 - 4\Delta_a^2\Omega^2 - 8\Omega^4)\gamma_\sigma}{\gamma_a(\gamma_a + 2i\Delta_a)^2(\gamma_a + 2i\Delta_a - 4i\Omega)^2(\gamma_a + 2i\Delta_a + 4i\Omega)^2}\right\}. \tag{369}$$

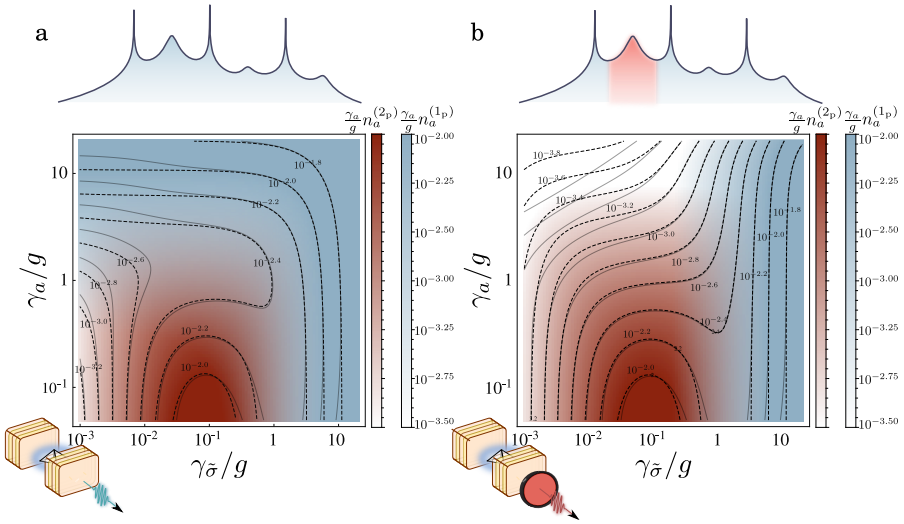

Figure 6.21: Effect of filtering the cavity peak. **a**, Bundle ($\gamma_a n_a^{(2_\mathrm{p})}$, red) and background ($\gamma_a n_a^{(1_\mathrm{p})}$, blue) emission rates, as shown in Fig. 6.13 a, but with a more saturated colorscale. 2D plots for both components are superimposed. **b**, Same as in a, but with the filtered background population $n_{a,\mathrm{f}}^{(1_\mathrm{p})}$. When filtering, the background population is greatly reduced. Straight lines: numerical calculation of total emission rate. Dashed lines: estimations by analytical formulas usings Eqs. (332) and (324) in a, and, for the expression of $n_{a,\mathrm{f}}^{(1_\mathrm{p})}$, an equation that to first order in $\gamma_{\tilde{\sigma}}$ is given by Eq. (368). Parameters: $\Omega = 20g$.

The effect of filtering the cavity peak is clearly seen in Fig.6.21, which depicts the same kind of plot shown in Fig. 6.13: background and bundle populations are plotted together by superimposing their two corresponding colormaps, of colors blue and red, respectively. It is evident how the filtering allows to reduce the background population in a big region of the parameter phase space. From Eq. (324) for $n_a^{(n_\mathrm{p})}$ and Eq. (369) for $n_{a,\mathrm{f}}^{(1_\mathrm{p})}$ we can compute, using Eq. (367), the purity of n-photon emission π_n^f when frequency-filtering is applied. This can be contrasted with the result of dividing the bundle population by the total intensity of emission at the cavity peak, given by Eq. (356), in order to verify the validity of Eq. (369). These results are shown in Figs. 6.22 and 6.23. They show a significant improvement of the purity if compared to the unfiltered results shown previously, that is well described by our analytical equations. Remarkably, we can achieve a very significant purity of emission of n-photon bundles well within the weak coupling regime, $\gamma_a > 4g$. This opens the possibility of applying this approach in irreversible systems, in which the coupling to the single cavity mode could represent an effective description of the coupling to a photonic

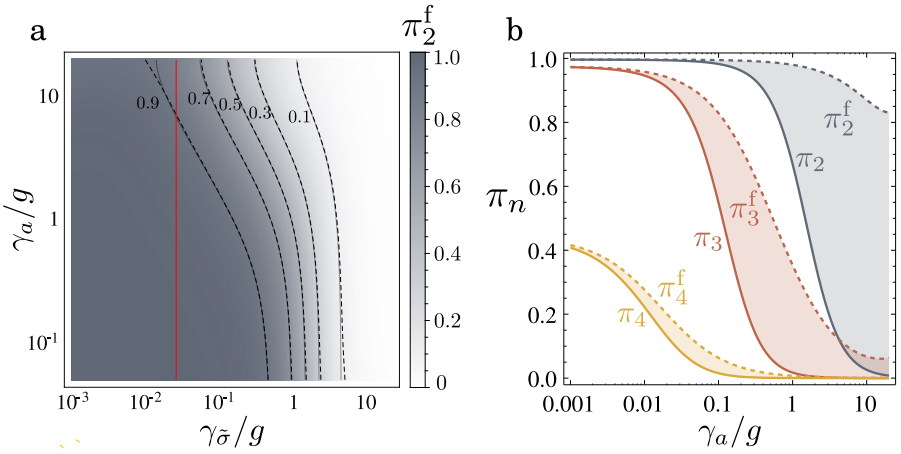

Figure 6.22: Effect of frequency filtering in the purity of n-photon emission. a, Purity calculated from $n_a^{(2_p)}$, and $n_{a,\mathrm{f}}^{(1_p)}$ given by numerical computation (solid line) and Eq. (368) (dashed lines). **b**, Purity of n-photon emission with (dashed) and without (solid) frequency filtering, along the red line in a. Parameters: $\Omega = 20g$.

density of states that Purcell-enhances the emission from the 2LS, as could be a photonic-crystal waveguide [80, 194, 208]. As mentioned earlier, a typical figure of merit in these systems is the *cooperativity* C, which is proportional to the ratio between the decay rate trough the cavity mode, given by the Purcell factor $\kappa = 4g^2/\gamma_a$, and trough other channels (typically, free space), given in our case by $\gamma_{\tilde{\sigma}}$:

$$C \equiv \frac{g^2}{\gamma_a \gamma_{\tilde{\sigma}}}. \tag{370}$$

In fact, we can obtain an asymptotic expression for the purity of two-photon emission that depends only on the cooperativity. As has been done before, we will consider $\Delta = 0$ for simplicity, since this does not alter the general

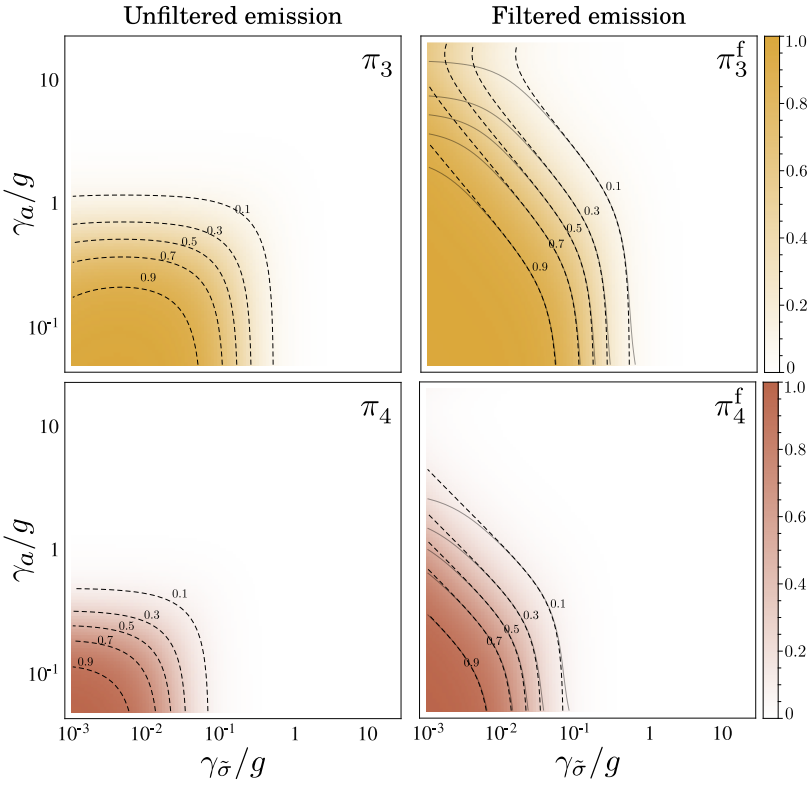

Figure 6.23: Purity of three and four photon emission for filtered and unfiltered emission.. Solid lines correspond to the numerical computation of $n_{a,\mathrm{f}}^{(1_p)}$, and dashed lines, to the estimation based on the analytical expression (369). Parameters: $\Omega = 20g$.

conclusions. We start from the expression for $n_a^{(2_P)}$ that comes directly from Eq. (326):

$$n_a^{(2_P)} = \left[\frac{2\gamma_a}{\gamma_{\tilde{\sigma}}} + \frac{\Omega^2\gamma_a}{g^4}\left(\frac{3}{4}\gamma_{\tilde{\sigma}} + \gamma_a\right)\right]^{-1}. \tag{371}$$

In terms of the cooperativity, this reads:

$$n_a^{(2_P)} = \left[2C\frac{\gamma_a^2}{g^2} + \frac{3}{4}\frac{\Omega^2}{g^2 C} + \frac{\gamma_a^2\Omega^2}{g^4} + 1\right]^{-1}. \tag{372}$$

Now we write the expression for the filtered purity $\pi_2^{(f)} = n_a^{(2_P)}/(n_a^{(2_P)} + n_{a,f}^{(1_P)})$ using Eqs. (368) and (372), and use the approximations $\Omega \gg \gamma_a, \gamma_a \gg g$ and $C \gg 1$ to obtain

$$\pi_2^f \approx \left[1 + \frac{2}{3}\left(\frac{2}{\Omega/g} + \frac{1}{C} + \frac{1}{C(\Omega/g)^2}\right)\right]^{-1}. \tag{373}$$

In the limit $\Omega/g \gg C$, this expression becomes dependent only on C:

$$\pi_2^f \approx \left(1 + \frac{2}{3C}\right)^{-1}. \tag{374}$$

To gain some insight into the dependence of the purity on such a relevant parameter, we show, in Fig. 6.24 a, π_2^f as a function of γ_a and C. This figure confirms the result stated above, since for high values of γ_a, π_2^f becomes dependent only on C. The Figure is supplemented with points that represent some state of the art parameters for semiconductor samples (shown in Table 1), demonstrating that regimes of high purity of two-photon emission are well within reach of current solid state systems, opening the exciting possibility of on-chip implementations of routed two-photon emission protocols in the solid state [80, 194].

Figure 6.24 b represents a cut of the purity along the red line in panel b ($\gamma_a = 5g$), confirming the validity of Eq. (374). It also depicts the expected emission rate of photon bundles for a sample having $\gamma_a = 5g$ with g =30 μeV. It shows that these values, well below the best figures of merit

Reference	g	γ_a/g	$\gamma_{\tilde{\sigma}}$	C
Arakawa *et al.* (2012) [11]	80 μeV	0.16 − 0.3	0.13 μeV	1970
Volz *et al.* (2012) [230]	141 μeV	0.37	(∼0.20 μeV)	1900
Giesz *et al.* (2016) [88]	21 μeV	4.28	0.30 μeV	12
Laucht *et al.* (2009) [147]	60 μeV	1.6	40 μeV	0.9
Hennessy *et al.* (2007) [109]	90 μeV	0.5	0.40 μeV	440
Ota *et al.* (2011) [181]	51 μeV	0.5	0.13 μeV	833
Srinivasan *et al.* (2007) [217]	12 μeV	0.33	2.48 μeV	15
Laucht *et al.* (2012) [148]	-	-	0.20 μeV	2.5

Table 1: Table of state of the art paramaters in semiconductor QDs. All correspond to QD-cavity systems except the last one, which is a QD-waveguide system.

achieved in the community, are enough to achieve a rate of emission of MHz and a high purity provided $C \geq 10$. These rates are similar to the best rates achieved in two-photon emission protocols based on a cascaded emission in the biexcition operating in pulsed regime [72], and they could be greatly enhanced by using the best samples, as the ones shown in Fig. 6.24. This demonstrates the great potential of working with protocols of two-photon emission based on a ladder of dressed energy levels, since their shift by the laser is not detrimental but, on the contrary, beneficial, allowing to operate in a strong pumping regime and yield high purity and emission rates.

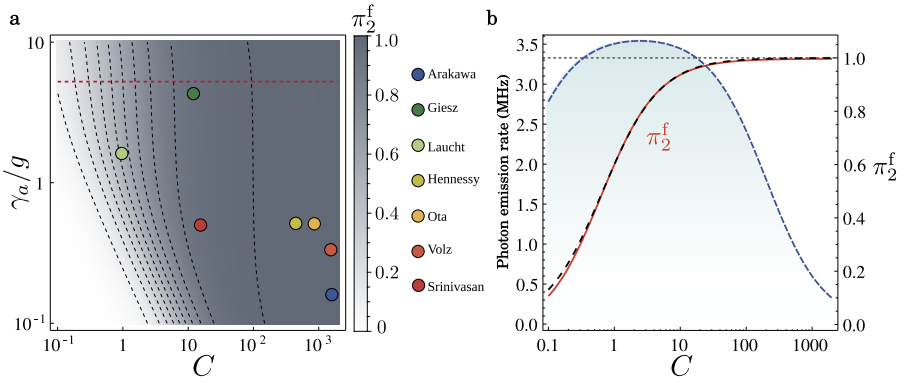

Figure 6.24: Performance of the n-photon emitter as a function of the cooperativity. a, Purity calculated as in Fig. 6.22, as a function of γ_a and C. For $\gamma_a > 1$, the purity becomes only dependent on the cooperativity. Colored points represent values of real experimental samples in semiconductor QDs, shown in Table 1. **b** Emission rate of photons emitted as a two-photon bundle, $\gamma_a n_a^{(2_p)}$, and purity π_2^f along the red line in a ($\gamma_a = 5g$). The emission rate was computed for $g = 30\,\mu$eV. The purity (solid,red) is compared to the asymptotic limit of Eq. (374) (dashed,black). Parameters: $\Omega = 20g$.

6.9 STATISTIC OF N-PHOTON EMISSION

Now that we have engineered N-photon emitters, we have to ask the same questions than those put by Glauber [93] at the birth of quantum optics, on the nature of quantum optical coherence for these sources. We can find the answer by regarding N-photon emitters as the exact counterpart of conventional emitters, but replacing the unit of emission—the photon—by a bundle of N of them. We now show that our class of emitters can operate in the same regimes, lasing or photon guns, but with bundles. To do so, we describe the statistics of the bundles when considered as single entities, by introducing the generalized correlation functions $g_N^{(n)}$:

$$g_N^{(n)}(t_1,\ldots,t_n) = \frac{\langle \mathcal{T}_-\{\prod_{i=1}^n a^{\dagger N}(t_i)\}\mathcal{T}_+\{\prod_{i=1}^n a^N(t_i)\}\rangle}{\prod_{i=1}^n \langle a^{\dagger N} a^N\rangle(t_i)} \tag{375}$$

with $\mathcal{T}_\pm$ the time ordering operators. This upgrades the concept of the nth order correlation function for isolated photons to bundles of N photons by making the replacement $a \to a^N$ in the standard definition of Glauber's correlators. The case $N = 1$ recovers the definition of the standard $g^{(n)}$, but for $N \geq 2$, the normalization to the bundle density makes Eq. (375) essentially different from the standard correlation functions $g^{(n\times N)}$. Similarly to the single-photon case, the two-bundle statistics

$$g_N^{(2)}(\tau) = \frac{\langle a^{\dagger N}(0)\, a^{\dagger N}(\tau)\, a^N(\tau)\, a^N(0)\rangle}{\langle (a^{\dagger N} a^N)(0)\rangle \langle (a^{\dagger N} a^N)(\tau)\rangle} \tag{376}$$

is the most important one. The validity of this definition for $g_2^{(2)}$ is confirmed in Fig. 6.25, where it is plotted (smooth curve) along with direct coincidences between clicks from the Monte Carlo simulation (data). Such $g_2^{(2)}$ correlations can be measured directly thanks to recent developments in two-photon detection [32]. For the Monte Carlo computation, all events are considered as single photons for the standard $g^{(2)}$ calculation (red curve in Fig. 6.25), and only two-photon events are considered as the basic unit of emission for $g_2^{(2)}$ (blue curve).

6.9.1 DIFFERENT BUNDLE STATICS

Remarkably, while $g^{(2)}$ always shows a bunching behaviour, the analysis of bundle statistics given by $g_2^{(2)}$ reveals a full gamut of regimes, from anti-bunching to bunching of bundles, that remain hidden if one considers only the standard Glauber's correlation function. This change in the bundle statistics is well understood by working in the basis of eigenstates $|\pm\rangle$ of the dressed 2LS. As discussed in Section. 6.5, this allows to describe the system as an incoherently pumped 2LS coupled to a cavity via a two-photon coupling term.

Let us analyze in which sense this picture can shed some light on the statistical properties of the emission of bundles. In order to do so, we will restrict ourselves for simplicity to the case of two-photon emission, $N = 2$, and assume strong pumping intensity Ω. This ensures a maximum purity of two-photon emission according to Eq. (351) and isolates the dynamics from the effect of any background population. In this regime, the two photon coupling constant $g^{(2_P)}$ is small, and the system is therefore in the weak coupling regime. In this situation, the system undergoes an irreversible evolution in which the cavity acts just as an extra decay channel for the dressed 2LS $|\mp\rangle$, whose dynamics is fully described by an incoherent pumping term with rate P given by Eq. (320c) and a decay term $\gamma_\sigma^{\text{eff}} = \gamma_\sigma + \kappa^{(2)}$. This decay rate is the sum of the effective decay rate of the dressed 2LS, γ_σ (320b), and $\kappa^{(2)}$, the two-photon Purcell rate (325) that describe the losses trough the cavity

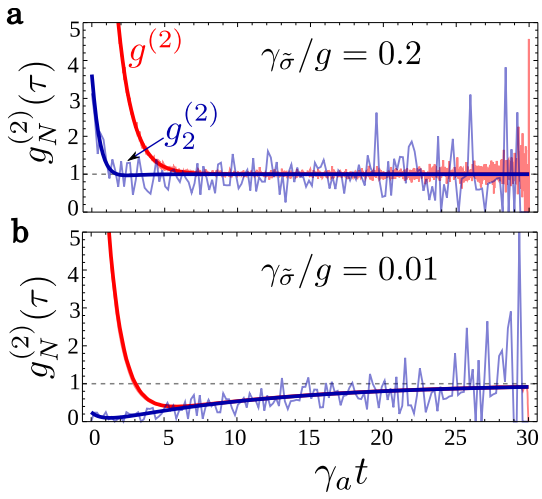

Figure 6.25: Second order correlations for photons and bundles. Eq. (376). Smooth curves are given by Eq. (376), and data curves obtained from Monte Carlo clicks (data). While the standard $g^{(2)}$ always shows bunched behaviour, panels a and b show the dependence of the bundle statistics on the decay rate of the 2LS, $\gamma_{\tilde{\sigma}}$, which reveals different regimes going from bunching of the bundles, **a**, to non-classical,**b**, antibunched statistics.

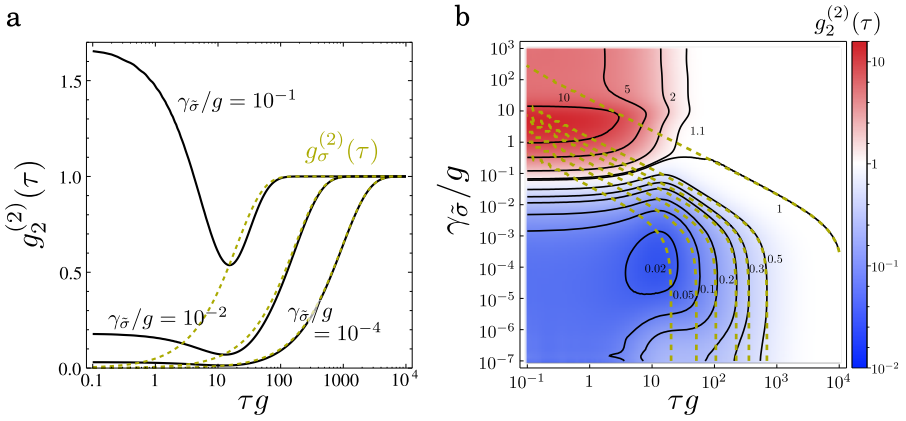

Figure 6.26: Time resolved statistics of the bundles, $g_2^{(2)}(\tau)$. Yellow, dashed lines correspond to the second order correlation function of the effective 2LS, given by Eq.(378). $\Omega = 100g$.

channel. This simple description has an analytical treatment, in which the second order correlation function of the dressed 2LS takes the form:

$$g_\sigma^{(2)}(\tau) = 1 - \exp\left[-(\gamma_\sigma^{\text{eff}} + P)\tau\right]. \tag{377}$$

In terms of the decay rate of the bare 2LS and at $\Delta = 0$, this reads as:

$$g_\sigma^{(2)}(\tau) = 1 - \exp\left[-\left(\frac{\gamma_{\tilde{\sigma}}}{2} + \kappa^{(2)}\right)\tau\right] \tag{378}$$

When the inherent 2LS lifetime $\gamma_{\tilde{\sigma}}^{-1}$ is the longest timescale in the system, its main mechanism of decay is through the coupling to the cavity channel, with a rate given by $\kappa^{(2)}$. In this case, the two-photon emission process can be pictured as a jump in the 2LS going from $|+\rangle$ to $|-\rangle$ assisted by the two-photon coupling to the cavity, which gains two-photons from the de-excitation of the 2LS. As a consequence, a single quantum jump in the 2LS will ultimately lead to two consecutive jumps in the cavity, or equivalently, a single two-photon quantum jump, which is what we identify as the emission of a bundle. In order to provide an insight into the bundle statistics, we can, based on this picture, associate the jump operator of the dressed 2LS, σ, with the bundle jump operator a^2. In this way, the statistics of the bundles would be equivalent to the statistics of the dressed 2LS:

$$g_2^{(2)}(\tau) = g_\sigma^{(2)}(\tau) \tag{379}$$

where the subindex σ indicates correlations of the operator σ. A vivid image of this mechanism linking the jumps of σ and a^2 was offered by the quantum trajectories displayed in Fig. 6.13 b, where one could clearly observe how a bundle emission (two jumps in the cavity) is associated with a jump in the 2LS.

The validity of the assumption in Eq. (378), that relates this quantity to the statistics of the bundles, can be contrasted in Fig. 6.26, that compares $g_2^{(2)}(\tau)$ and $g_\sigma^{(2)}(\tau)$ as a function of $\gamma_{\tilde{\sigma}}$. For small values of $\gamma_{\tilde{\sigma}}$ (long-lived 2LS), the long-time behaviour of $g^{(2)}(\tau)$ is indeed well described by $g_\sigma^{(2)}(\tau)$. In that regime, the bundles show antibunching behaviour, a nonclassical feature that evidences the transfer of the quantum statistics of the 2LS to the

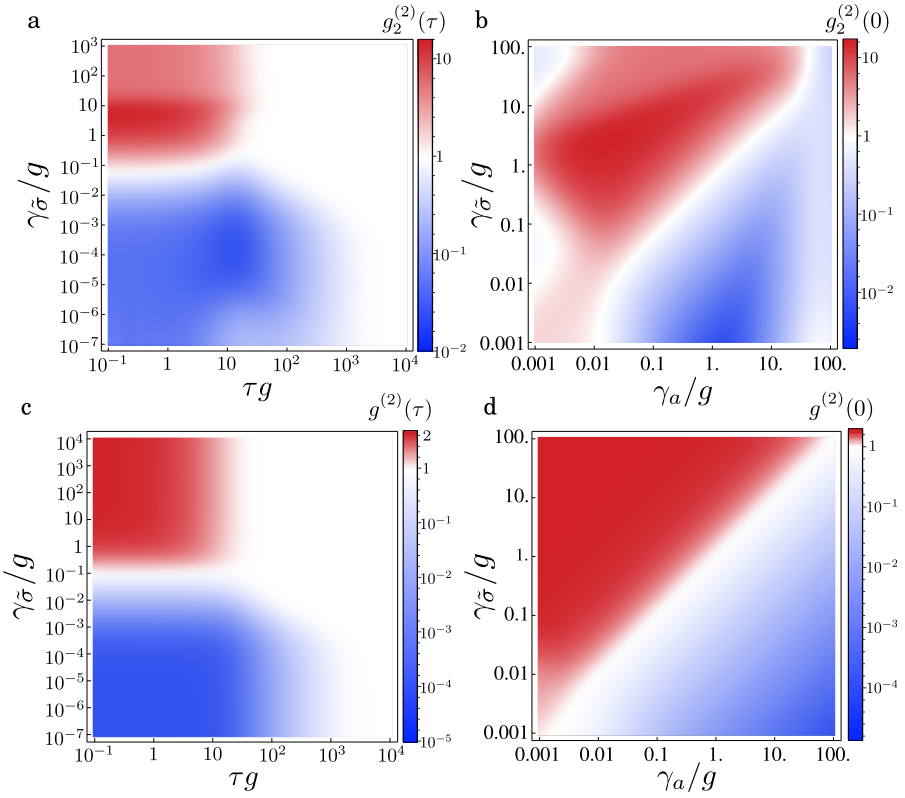

Figure 6.27: Comparison between bundle statistics and the standard statistics of the one-atom laser model. The generalized $g_N^{(2)}(\tau)$ of the model giving bundle emission (with a cavity-2LS coupling rate g in the bare basis) shows features that resemble the standard correlations $g^{(2)}(\tau)$ in the one-atom laser model. Parameters: $\Omega = 100g$. For the one-atom laser model, we use a 2LS cavity coupling $\tilde{g} = g^{(2_p)}$ as in Eq. (314), and $P = \gamma_{\tilde{\sigma}}$.

bundles emitted by the cavity, due to the irreversible two-photon coupling between them.

However, as we discussed at the beginning of this Section, the statistics of the bundles become bunched or even coherent when $\gamma_{\tilde{\sigma}}$ gets more significant. To account for this change, one needs to consider a more general case in which the cavity does not act as a mere decay channel and needs to be explicitly included in the dynamics. In that situation, our dressed-2LS model becomes a two-photon analogue of the celebrated *one-atom laser* [61], which consists on the JC Hamiltonian plus decay and incoherent pumping of the 2LS.

The phenomenology of the one-atom laser model is extremely rich [151], and its extension to a Hamiltonian with N-photon coupling certainly deserves furtheinvestigation. We do not provide such a detailed analysis here, but limit ourselves to expose the similarities between the standard second-order correlation function $g^{(2)}(\tau)$ of the one atom laser model, and the generalized second-order, N-photon correlation function $g_N^{(2)}(\tau)$ of its generalization to N-photon coupling. This comparison is provided in Fig. 6.27, which provides unambiguous evidence of the similarities in the time-resolved behaviour of these two quantities and in its dependence with the system decay rates. Interestingly, in complete analogy to the one-atom laser model, a change in the system decay rates can bring the bundles from antibunching to bunching, passing through a regime of coherent bundle emission.

True coherent bundle emission satisfies $g_N^{(n)} = 1$ at all orders.

In general, the effect the 2LS lifetime has on the statistics of the bundles can be understood as a consequence of the key role the 2LS emission plays to

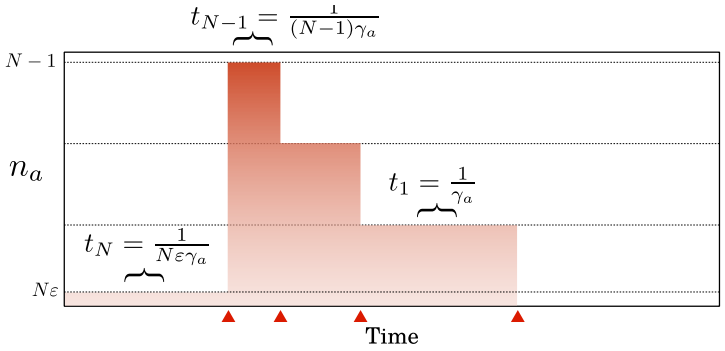

Figure 6.28: Dynamics of emission of a bundle. Until the emission of a first photon, the cavity sustains in average N photons with a small probability ε for a time $1/N\varepsilon\gamma_a$. This is followed by a cascade that transit over states with exactly $m = N-1, N-2, \cdots$ photons, each for a time $1/m\gamma_a$.

restore the construction of a N-photon state, as discussed in Section 6.6. At the single-photon level, the standard $g^{(2)}(\tau)$ fails to capture this fundamental dynamics of emission. All this confirms the emergence of a new physics at the two-photon level, that also hold for higher N.

6.10 THE INTERNAL STRUCTURE OF THE BUNDLE: RELATIONSHIP WITH FOCK STATES

We have described the emission of our system in terms of "bundles" of photons, introducing a terminology that needs to be justified. In quantum theory, a state of the field with exactly N quanta of excitation is a Fock state $|N\rangle$ and it is natural to question whether these sources are not precisely "emitters of Fock states $|N\rangle$".

There are subtle links and departures between the two concepts. The Fock state $|N\rangle$ is a well-defined state that can be prepared and maintained exactly. It has no further structure and each of the N photons that compose it is fully indistinguishable from the others. The bundle, on the other hand, arises in a dynamical process of emission, describing the energy released from the cavity QED setup to the outside world. The cavity itself is not in the Fock

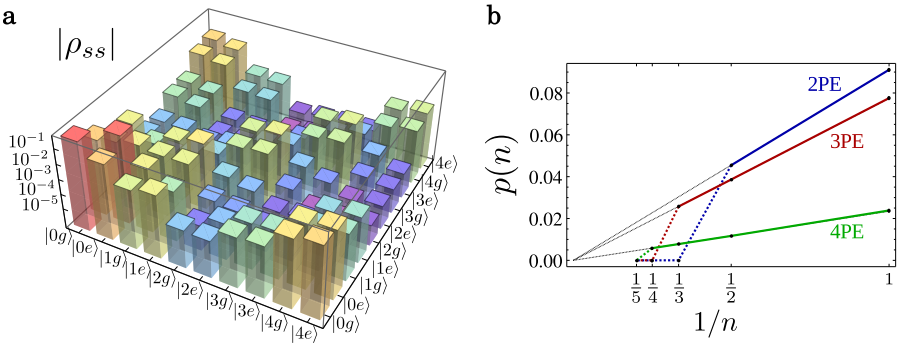

Figure 6.29: State of the system in the regime of N-photon emission (NPE). a, Full density matrix of the system in the regime of 4PE, showing the predominance of the vacuum and the strong coherence between the 2×2 sub-blocks of 0 and 4 photons and the $1/n$ cascade along the diagonal b, Diagonal elements of the cavity density matrix $p(n) = \langle n|\rho|n\rangle$. As function of $1/n$, it yields a line with a slope equal to the bundle population n_a/N and extent equal to the number N of photons per bundle, according to Eq. (380).

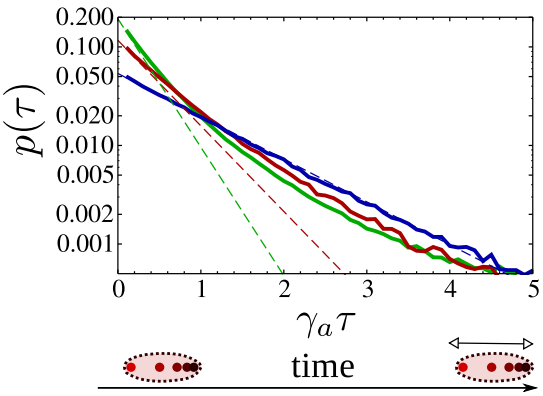

Figure 6.30: Distribution of time intervals τ between successive photons of a bundler, in the regimes of two (blue), three (red) and four (green) photon emission. The distributions are $(N-1)$-exponential for N-photon emission, i.e., exponential for $N = 2$, bi-exponential for $N = 3$, etc. This confirms the time-distribution of the photons within the bundles sketched at the bottom, arising from the process outlined in Fig. 6.28. Thin lines show the $\exp(-(N-1)\tau)$ decay, to which the distributions get parallel to. The distribution of four-photon emission (green), for instance, gets parallel to all three lines in successive intervals.

state $|N\rangle$, being, to begin with, in the vacuum most of the time, and only in very short temporal windows does it undergo a cascade that sees in rapid successions the field transit through the various Fock states $|n\rangle$, with $0 \leq n \leq N$, for a time $1/\gamma_a n$ in each of them (see Fig. 6.28). Since the system has a small probability ε to be in the state $|N\rangle$ before the emission and probability close to one to transit through each of the intermediate states during the cascade, one obtains the steady state probability:

$$p(n) = \frac{n_a}{N}\frac{1}{n}, \qquad \text{for } 1 \leq n \leq N\,. \tag{380}$$

A snapshot of the full density matrix in the regime of four-photon emission is given in Fig. 6.29 a. This shows the breakdown of the matrix into clusters of 2×2 blocks corresponding to the subspaces of the QE with n-photons. The vacuum largely predominates (the probabilities are shown in log-scale), followed by the blocks on the diagonal which provide $p(n)$ as given by Eq. (380), and blocks of coherence between the various manifolds, which are small although nonzero, except the coherence elements $|0\mu\rangle\langle 4\nu|$ with $\mu, \nu \in \{g, e\}$ which are large. This confirms the direct manifestation, also in the dissipative regime, of the quantum superposition of the type $(|0+\rangle \pm |N-\rangle)/\sqrt{2}$ induced by the N-photon coupling.

There remains a trace of this intra-cavity dynamics in the photodetection. The bundles are strongly correlated in two senses: first extrinsically, the emission comes in groups of N photons, suppressing the release of packets with other numbers of photons. Second, intrinsically, with different time intervals separating successive photons: the first photon is more closely followed by the second one than the second is by the third, and so on till the last photon that comes within $1/\gamma_a$ of the penultimate (see Fig. 6.30). Clearly, the bundle is a strongly-correlated group of closely-spaced photons that has a structure which is not described by the abstract object $|N\rangle$ alone.

However, regardless of the internal structure of the bundle, it would appear as a Fock state in a measurement integrated over a small time window.

6.11 CONCLUSIONS

In this Section, we have introduced a cavity-QED scheme that realizes a family of sources that release their energy in groups (or "bundles") of N photons (where N is an integer). These source are based on the most fundamental description of light-matter interaction, a 2LS coupled to a single electromagnetic mode (an harmonic oscillator), and the mechanism relies in the strong dressing of the 2LS by an external classical field. We have shown that this scheme, which could be implemented in any of the current cQED platforms, shows regimes of high and pure emission of N-photon bundles, and that its most straightforward realization of $N = 2$ is currently within reach of semiconductor cQED samples with modest light-matter coupling rates, well below the current state of the art. Frequency filtering of the emitted light allows to further purify the emission of N-photon bundles, eliminating any background of undesired single-photon events, allowing to implement the scheme in irreversible systems, such as QDs coupled to slow-modes of light in waveguides. This opens the exciting possibility of implementing sources of N-photon bundles that can be routed and manipulated on a chip.

7

TWO-PHOTON EMISSION FROM A DRESSED BIEXCITON

7.1 INTRODUCTION

In the previous Chapter, we discussed how a strongly driven 2LS coupled to an optical microcavity can be brought to regimes where it emits light composed of bundles of a fixed number N of photons. In this Chapter, we focus on the most straightforward implementation, the case of two-photon emission $N = 2$, which already presents a wide range of applications in quantum information and quantum communications [184]. Photon pairs are an important resource to generate heralded single photons [111] and are also used as a key element for quantum key distribution [121, 170], quantum teleportation [35, 161] or to implement entanglement swapping and quantum repeaters [183, 214, 225]. Numerous other examples, like quantum lithography [89], the absorption rate increase from organic molecules in two-photon microscopy [86, 228], quantum walks of correlated photons [188] or the quantum computation of molecular properties [146], illustrate the rich variety of applications that these non-classical states of light can find.

However, the main purpose of this Chapter is to show that the approach taken in Chapter 6 can also be applied to systems with a more complex internal structure. This provides a wider range of possibilities in the design of N-photon sources, allowing for instance to devise smarter excitation schemes or to achieve richer regimes of bundle emission, tuning their statistics or the quantum correlations between the photons inside a bundle. We will focus on the particular case of a biexciton, a molecule formed by two excitons with opposed spin. The biexciton, that we label as $|\mathrm{B}\rangle$, stands as an excellent candidate to perform as a source of photon pairs, since it naturally emits two entangled photons in a radiative cascade. This has been demonstrated for its implementation in semiconductor quantum dots in recent years [7, 72, 100, 169, 219]. Contrary to the sources of photon pairs based on parametric down-conversion, which are the ones most commonly used [33, 35, 40, 112, 143, 145, 146, 184] , schemes based on cascaded emission [18] do not present the drawback of having Poissonian statistics for the number of photon pairs generated in each process, with a non-zero probability of having zero or more than one pair [203].

The **biexciton** is a quasi-particle composed of two excitons with spins up and down, corresponding to two electrons and two holes. The Coulomb interaction of the four-particle system gives a ground-state energy ω_B lower than the energy of two separated excitons, $2\omega_X$. The difference $\chi \equiv 2\omega_X - \omega_B$ is the **biexciton binding energy**.

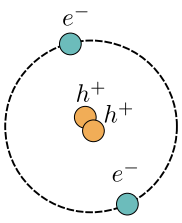

As an alternative to off-resonant excitation, it is possible to initialize the biexcitonic state by coherent two-photon excitation (TPE) [81, 116, 119, 169, 221], which increases the coherence and indistinguishability of the emitted photons as compared to non-resonant pumping. The generation efficiency and the indistinguishability of the photons can also be improved by bringing a cavity in resonance with the biexcitonic transition [72] to enhance the

emission thanks to the Purcell effect [30]. A particularly interesting possibility is to place the cavity in resonance with half the energy of the biexciton to enhance the rate of spontaneous two-photon emission, such that two photons are emitted simultaneously into the cavity mode [64, 181, 206]. The joint implementation of coherent excitation and Purcell enhancement via cavity modes has already been discussed in the literature and shown to be promising [169, 181].

Under coherent excitation, the intensity of the pumping sets a limit to the repetition rate of two-photon generation, since strong driving fields dress the excitons and spoil the biexcitonic structure [52, 167]. On the other hand, we have shown in Chapter 6 how to take advantage of such a dressing to achieve a continuous source of N-photon states. This is done by harvesting with a cavity, due to the Purcell effect, photons coming from N-photon transitions in the ladder of energy levels of the emitter dressed by the laser. These photons, as shown in Chapter 4, feature giant correlations violating classical inequalities, something that has already been demonstrated experimentally for the case of a dressed 2LS [186].

In this Chapter, we bring together the three main ideas outlined above: i) TPE from the biexciton, ii) cavity Purcell-enhancement of virtual processes and iii) multiphoton emission from a dressed system. This realizes a versatile two-photon source operating in the continuous regime with a high repetition rate. In comparison with the case of a single dressed 2LS discussed in Chapter 6, the biexciton introduces an extra degree of freedom, the polarization, that provides a richer set of physical regimes. In particular, we demonstrate the emission of degenerate photon pairs with polarization orthogonal to the laser—therefore suppressing the laser background and undesired excitation of the cavity—and different two-photon counting statistics, as well as emission of polarization-entangled photons. All these different regimes can be accessed optically with the same sample just by changing the intensity and polarization of the excitation. This unprecedented versatility has the potential of pushing forward the generation and use of photon pairs in the laboratory. Even more importantly, it evidences that the fundamental concepts are susceptible to be applied in different platforms, such as superconducting circuits [25], and that new regimes of non-classical light emission are within reach with variations of the design.

Our analysis starts with a general introduction of the model and follows with a detailed description of the features of the dressed biexciton alone, to finally move to the complete picture with the inclusion of a cavity that probes and enhances the single and two-photon transitions present in the dressed system.

The results shown here have been published in the journal New Journal of Physics [202].

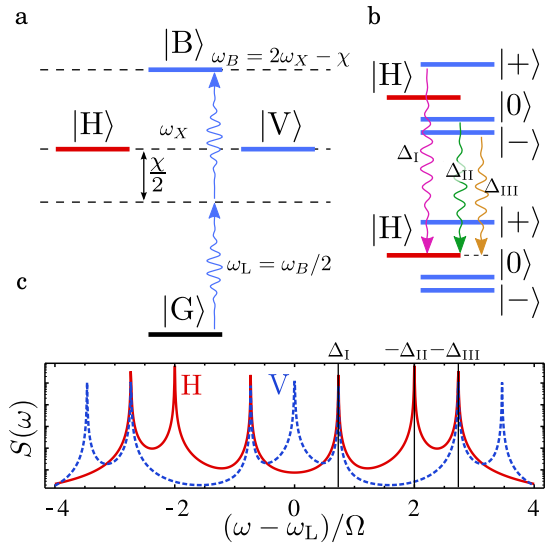

Figure 7.1: Energy levels in the bare and dressed biexciton. a, Biexcitonic level system in the linear polarization basis (Horizontal-Vertical states). The two-photon laser excitation is represented with two curly blue arrows, at half the biexciton energy $\omega_L = \omega_X - \chi/2$. **b**, Dressed state picture at strong laser pumping, where the vertical polarization states (blue) transform into the new states $|\pm\rangle, |0\rangle\}$. The three possible horizontally polarised transitions from these states to the $|H\rangle$, appear with curly arrows. **c**, Spectrum of emission in the two polarizations, horizontal (solid red) and vertical (dashed blue), and the three horizontally polarised transitions marked with vertical lines. Parameters: $\Omega = 5 \times 10^2 \gamma_\sigma$, $\chi = 2 \times 10^3 \gamma_\sigma$ and $g = 0$.

7.2 MODEL AND DRESSED STATE PICTURE

The system under consideration is a semiconductor quantum dot with a biexcitonic structure, as depicted in Fig. 7.1 a. It can host two excitons, or electron-hole pairs, with third component of the total angular momentum equal to +1 or -1, usually labelled as "spin states". Symmetric and antisymmetric combinations of these states couple to one of the two orthogonal linearly polarised light modes ("vertical" and "horizontal"). The biexciton state corresponds to the occupation of both spin states in the dot. The Hamiltonian of this system is given by:

$$H_X = \omega_X(\sigma_\uparrow{}^\dagger\sigma_\uparrow + \sigma_\downarrow{}^\dagger\sigma_\downarrow) - \chi(\sigma_\uparrow{}^\dagger\sigma_\uparrow\sigma_\downarrow{}^\dagger\sigma_\downarrow), \tag{381}$$

where $\{\sigma_\uparrow, \sigma_\downarrow\}$ are the annihilation operators of the excitons with spin $\{\uparrow, \downarrow\}$, ω_X is the excitonic energy (we consider degenerate excitons) and χ is the biexcitonic binding energy. The biexciton frequency is, therefore, $\omega_B = 2\omega_X - \chi$. In order to separate the four-level system into two different polarization cascades we change to the linear polarization basis:

$$|H\rangle = \frac{1}{\sqrt{2}}(|\uparrow\rangle + |\downarrow\rangle), \quad |V\rangle = \frac{1}{\sqrt{2}}(|\uparrow\rangle - |\downarrow\rangle) \tag{382}$$

with the annihilation operators

$$\sigma_H = \frac{1}{\sqrt{2}}(\sigma_\uparrow + \sigma_\downarrow), \quad \sigma_V = \frac{1}{\sqrt{2}}(\sigma_\uparrow - \sigma_\downarrow). \tag{383}$$

These operators describe transitions from the biexciton to an excitonic state or from an exciton to the ground state by emission of photons with the corresponding horizontal or vertical polarization (red and blue colors in Fig. 7.1). We will neglect the small fine structure splitting in frequency that is usually found between the two different excitonic states, since it has no impact in our scheme and only complicates the algebra. It can be trivially added if needed.

We implement a continuous resonant excitation of this level structure that affects only one of the polarizations (chosen to be the vertical one without loss of generalization). This is accounted for by a coherent driving term in the Hamiltonian:

$$H_\Omega = \Omega\left(\sigma_V^\dagger e^{-i\omega_L t} + \sigma_V e^{i\omega_L t}\right) \tag{384}$$

where the intensity of the laser is proportional to $|\Omega|^2$. In order to drive the biexciton state directly, the laser frequency is set at the two-photon resonance, $\omega_L = \omega_B/2$. This results in a two-photon excitation (TPE) to the biexciton level [81, 116, 119, 169, 221]. On the other hand, we gather and enhance the emission in the perpendicular polarization (horizontal) through the coupling to a cavity mode with the same linear polarization. This way, we completely separate in polarization the excitation and emission channels and do not need to worry about the elastically scattered light from the laser. The coupling to the cavity mode is given by the Hamiltonian term:

$$H_C = \omega_C a^\dagger a + g(a^\dagger \sigma_H + a\,\sigma_H^\dagger) \tag{385}$$

We write the total Hamiltonian in the rotating frame of the exciting laser:

$$\begin{aligned} H = H_X + H_\Omega + H_C = \\ \Delta_X(\sigma_H^\dagger\sigma_H + \sigma_V^\dagger\sigma_V) - \chi\sigma_H^\dagger\sigma_H\sigma_V^\dagger\sigma_V + \Omega(\sigma_V^\dagger + \sigma_V) \\ + \Delta_C a^\dagger a + g(a^\dagger\sigma_H + a\sigma_H^\dagger) \end{aligned} \tag{386}$$

where $\Delta_X = \omega_X - \omega_L$ and $\Delta_C = \omega_C - \omega_L$. The dynamics of the whole system is described by a density matrix which follows the master equation:

$$\dot\rho = -i\left[H,\rho\right] + \frac{\gamma_a}{2}\mathcal{L}_a\rho + \frac{\gamma_\sigma}{2}\sum_{X=H,V}\left[\mathcal{L}_{|X\rangle\langle B|} + \mathcal{L}_{|G\rangle\langle X|}\right]\rho \tag{387}$$

where the excitonic and cavity lifetimes are given by γ_σ and γ_a respectively. We study the steady state of the system defined by $\dot\rho = 0$.

Under TPE ($\Delta_X = \chi/2$), the energy of the photons from the laser matches half the biexciton energy, c.f. Fig. 7.1 a. To understand the spectral features of the system before coupling it to the cavity ($g = 0$), we derive a dressed state picture for the biexciton [52]. The starting point is the set of bare states with n excitations, $\{|G\rangle|n\rangle, |V\rangle|n-1\rangle, |H\rangle|n-1\rangle, |B\rangle|n-2\rangle\}$, where $|n\rangle$ describes the state of the driving field with n photons. Since the laser is polarized in the vertical direction, the state $|H\rangle$ is not dressed by it, while the rest of the excitonic states are. The new eigenstates are obtained by diagonalising the coupling Hamiltonian H_Ω (in the rotating frame of the laser) in the reduced basis $\{|G\rangle|n\rangle, |V\rangle|n-1\rangle, |B\rangle|n-2\rangle\}$, that is, the matrix:

$$H_{TPE} = \begin{pmatrix} 0 & \Omega & 0 \\ \Omega & \chi/2 & \Omega \\ 0 & \Omega & 0 \end{pmatrix}. \tag{388}$$

We do not include dissipation in this procedure since we consider it small as compared to Ω. This gives rise to the three new eigenvectors $\{|+\rangle, |0\rangle, |-\rangle\}$ in each rung with the corresponding eigenenergies:

$$\Delta_+ = \frac{1}{4}\left(\sqrt{\chi^2 + 32\Omega^2} + \chi\right), \tag{389a}$$

$$\Delta_0 = 0, \tag{389b}$$

$$\Delta_- = -\frac{1}{4}\left(\sqrt{\chi^2 + 32\Omega^2} - \chi\right), \tag{389c}$$

where the eigenvectors, dropping the photonic component from the notation, are given by $|+\rangle \propto |\mathrm{G}\rangle + \Delta_+/\Omega\,|\mathrm{V}\rangle + |\mathrm{B}\rangle$, $|0\rangle = (|\mathrm{B}\rangle - |\mathrm{V}\rangle)/\sqrt{2}$ and $|-\rangle \propto |\mathrm{G}\rangle + \Delta_-/\Omega\,|\mathrm{V}\rangle + |\mathrm{B}\rangle$. Figure 7.1 b depicts two successive rungs of excitation, including the state $|\mathrm{H}\rangle$ which, as we said, remains bare.

7.3 SINGLE PHOTON TRANSITION AND SPECTRUM

The spectrum of emission of the system in each polarization in the steady state, $S_\mathrm{X}(\omega)$, with X=H, V, is defined as $S_\mathrm{X}(\omega) = \mathrm{Re}\int_0^\infty \langle\sigma_\mathrm{X}^\dagger(0)\sigma_\mathrm{X}(\tau)\rangle e^{i\omega\tau}d\tau$. Both polarizations are plotted in Fig. 7.1 c for comparison. The number of peaks appearing and their positions can be explained in each polarization X by the allowed single photon transitions under the operator σ_X. In the case of H polarization, only transitions between $|\mathrm{H}\rangle$ and the dressed states $i = +, 0, -$ are allowed: $|\langle\mathrm{H}|\sigma_\mathrm{H}|i\rangle|^2 \neq 0$ or $|\langle i|\sigma_\mathrm{H}|\mathrm{H}\rangle|^2 \neq 0$. The transition $|\mathrm{H}\rangle \to |\mathrm{H}\rangle$ or between dressed states $|i\rangle \to |j\rangle$ are forbidden in H polarization, since $|\langle\mathrm{H}|\sigma_\mathrm{H}|\mathrm{H}\rangle| = 0$ and $|\langle i|\sigma_\mathrm{H}|j\rangle| = 0$ for all $i, j = +, 0, -$. The three possible transitions that can take place from the dressed states to $|\mathrm{H}\rangle$, occur respectively at the following detunings from the laser (see Fig. 7.1 b):

$$|+\rangle \to |\mathrm{H}\rangle: \quad \Delta_\mathrm{I} = \frac{1}{4}\left(\sqrt{\chi^2 + 32\Omega^2} - \chi\right), \tag{390a}$$

$$|0\rangle \to |\mathrm{H}\rangle: \quad \Delta_\mathrm{II} = -\chi/2, \tag{390b}$$

$$|-\rangle \to |\mathrm{H}\rangle: \quad \Delta_\mathrm{III} = -\frac{1}{4}\left(\sqrt{\chi^2 + 32\Omega^2} + \chi\right). \tag{390c}$$

The other three possible H-polarised transitions take place from $|\mathrm{H}\rangle$ to the dressed states, at opposite detunings $-\Delta_\mathrm{I}$, $-\Delta_\mathrm{II}$ and $-\Delta_\mathrm{III}$. Remarkably, $S_\mathrm{H}(\omega)$ does not present any resonance at the laser energy.

On the other hand, the spectrum in V polarization, $S_\mathrm{V}(\omega)$, plotted with a dashed blue line in Fig. 7.1 c, contains seven peaks corresponding to the nine possible transitions between dressed states, $|i\rangle \to |j\rangle$, with those three between the same dressed states, $|i\rangle \to |i\rangle$, degenerate in energy at ω_L.

These features have been confirmed by recent experiments [12, 34, 105] that demonstrated the possibility of dressing under TPE and the validity of the model discussed in Section 7.2.

7.4 TWO-PHOTON TRANSITIONS AND SPECTRUM

The next step in the characterization of the system is the calculation of the frequency-resolved second order correlation function or two-photon spectrum at zero delay, $g^{(2)}_{\Gamma}(\omega_1, \omega_2)$ [67, 96], first introduced in Chapter 3 and given by Eq. (184) with $t_1 = t_2 = 0$, that conveys how likely is to detect two photons with frequencies ω_1, ω_1 simultaneously. For that purpose we use the method of sensors [67] introduced in SECTION SENSORS, that makes the calculation of this quantity computationally accessible. The parameter Γ is the inverse response time of the detector, and provides the frequency window in which photons are detected around ω_1, ω_2. We fix it to an intermediate value $\Gamma = 10\gamma_\sigma$, so that the detectors can resolve full spectral peaks (with width of the order of γ_σ) without resulting in superimposed signals, $\gamma_\sigma < \Gamma \ll \Omega$.

Figure 7.2 a shows the H-polarized two-photon spectrum from the light emitted by the dressed biexciton system. This map features seven antidiagonal red lines of super Poissonian correlations with $g^{(2)}_{\Gamma} \gg 1$ (hyperbunching) that correspond to a family of virtual two-photon processes that go from one state in a rung to another state two rungs below, jumping over any states from the rung in between (whence the denomination of *leapfrog* processes).

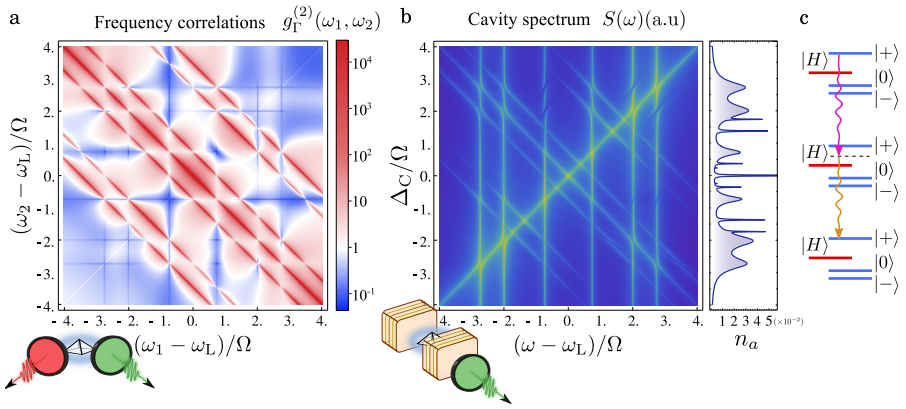

Figure 7.2: Evidences of multi-photon transitions in the ladder of dressed energy levels.. a, Two-photon spectrum in H polarization for the TPE. In blue, sub-Poissonian statistics (antibunching), in red, super-Poissonian statistics (bunching) and in white, Poissonian statistics (uncorrelated). Parameters: $\chi = 4 \times 10^3 \gamma_\sigma$, $\Omega = 10^3 \gamma_\sigma$, $\Gamma = 10\gamma_\sigma$ and $g = 0$. **b**, Cavity spectrum of emission as a function of the cavity frequency ω_a in the strong coupling regime, $g = 10^2 \gamma_\sigma$, $\gamma_a = 10\gamma_\sigma$. The plot on the right hand side shows the integrated signal, i.e., the cavity population n_a. **c**, Example of the two-photon transition $|+\rangle \rightarrow\!\!\rightarrow |+\rangle$ in the H polarization.

As shown in Chapter 4, we have demonstrated [200] that this virtual character provides such strong quantum correlations that photon pairs can violate classical inequalities such as the Cauchy-Schwarz inequality. Whenever any two of the frequencies involved correspond to transitions between real states, these correlations change character and the violation of Cauchy-Schwarz inequalities is spoiled. This can be seen in Fig. 7.2 a as a piercing in the bunching lines whenever they intersect the vertical or horizontal ones, appearing at $\omega_{1,2} - \omega_L = \pm\Delta_I, \pm\Delta_{II}, \pm\Delta_{III}$.

Since the leapfrog lines originate from two-photon transitions, we can understand them in terms of the two-photon operator $\sigma_H \sigma_H$. Transitions starting or ending at $|H\rangle$ are not allowed, since $|\langle H| \sigma_H \sigma_H |i\rangle| = 0$ and $|\langle i| \sigma_H \sigma_H |H\rangle| = 0$. All other nine two-photon transitions, $|i\rangle \rightarrow\!\!\rightarrow |j\rangle$,

occur, since $|\langle j|\sigma_{\rm H}\sigma_{\rm H}|i\rangle| \neq 0$ for all $i,j = +,0,-$, and give rise to seven lines which follow the general equation $\omega_1 + \omega_2 - 2\omega_{\rm L} = \Delta^{\rm 2P}$ with:

$$|i\rangle \rightarrow\!\rightarrow |i\rangle \quad \text{with} \quad i = +,0,- : \quad \Delta^{\rm 2P}_{\rm I} = 0\,, \tag{391a}$$

$$|+\rangle \rightarrow\!\rightarrow |0\rangle : \quad \Delta^{\rm 2P}_{\rm II} = \frac{1}{8}\left(\sqrt{\chi^2+32\Omega^2}+\chi\right), \tag{391b}$$

$$|0\rangle \rightarrow\!\rightarrow |-\rangle : \quad \Delta^{\rm 2P}_{\rm III} = \frac{1}{8}\left(\sqrt{\chi^2+32\Omega^2}-\chi\right), \tag{391c}$$

$$|+\rangle \rightarrow\!\rightarrow |-\rangle : \quad \Delta^{\rm 2P}_{\rm IV} = \frac{1}{4}\sqrt{\chi^2+32\Omega^2}\,. \tag{391d}$$

The remaining three lines are described by inverting the order of the three last transitions and changing the sign of the corresponding $\Delta^{\rm 2P}$. Figure 7.2 c shows an example of a two-photon transition, $|+\rangle \rightarrow\!\rightarrow |+\rangle$.

Figure 7.3 offers another view of these leapfrog resonances, selecting the diagonal of the two-photon spectrum in Figure 7.2 a, that is, for $\omega = \omega_1 = \omega_2$. The leapfrog processes appear as seven lines around $\Omega/\chi \approx 10^{-1}$ and spread as Ω is increased. The blue lines correspond to the single-photon resonances that are also apparent in the spectrum of emission, c.f. Fig. 7.1 c. Reducing Ω below the dissipation levels (bottom part of the plot), the system experiences a transition into the spontaneous emission regime where there is no dressing of the levels and the spectral structures are much simpler: only two peaks for the spectrum of emission and a single leapfrog peak at $\omega = \omega_{\rm L}$ in the two-photon spectrum. This regime has already been extensively investigated under incoherent excitation [59]. In the present work, where it appears as the low pumping limit, it will be used only for comparison with the high pumping regime.

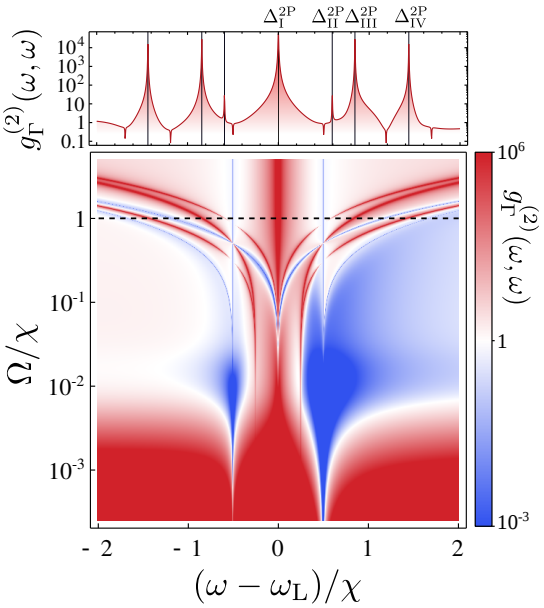

Figure 7.3: Diagonal of the two-photon spectrum ($\omega = \omega_1 = \omega_2$) of the biexciton system as a function of the driving field intensity Ω. Top panel shows a cut along the dashed line in the bottom panel. Blue colors in the map represent sub-Poissonian statistics (antibunching), red, super-Poissonian statistics (bunching) and white, Poissonian statistics (uncorrelated). The physics changes from that of the biexciton spontaneous emission regime (bottom part), with a single leapfrog peak, to that of the dressed biexciton system (top part), with seven leapfrog peaks. Parameters: $\chi = 4\times10^3\gamma_\sigma$, $\Gamma = 10\gamma_\sigma$ and $g = 0$.

7.5 PURCELL ENHANCEMENT OF TWO-PHOTON TRANSITIONS BY A CAVITY MODE

In the spirit of the results presented in Chapter 6, we can turn these virtual leapfrog transitions into real processes by coupling the system to a cavity (we switch on $g \neq 0$) in resonance with at least one of the two frequencies involved. If γ_a is sufficiently small as compared to g, the two-photon emission can be Purcell-enchanced. We can observe this in the cavity spectrum of emission, given by $S_a(\omega) = \mathrm{Re}\int_0^\infty \langle a^\dagger(0)a(\tau)\rangle e^{i\omega\tau}d\tau$ and plotted in Fig. 7.2 b. In analogy to the results presented in Fig. 6.4, due to the strong correlations between the two frequencies, the cavity Purcell-enhancement of one of the two photons of a bunching line triggers the emission of the second photon, even if this one is not in resonance with the cavity. This phenomenon leaves traces in the spectrum that help reconstruct the bunching lines when the spectrum is plotted as a function of the cavity frequency. In this sense, the cavity is acting as one of the filters necessary to perform frequency correlations.

As discussed throughly in the previous Chapter, useful two-photon emission can be obtained by using this approach to Purcell-enhance two photons of the same frequency. This is evidenced by sharp peaks in the cavity population whenever it crosses one of the two-photon resonances (Eqs. (391) with $\omega_a = \omega_1 = \omega_2$), as can be seen in the right panel of Fig. 7.2 b. The single photon resonances appear as broad peaks and are detrimental for the two-photon emission. In contrast to the case of a dressed 2LS, now there are several leapfrog resonances that can be enhanced in order to yield two-photon emission. The best candidates for pure two-photon emission are those leapfrogs far in energy from other processes, that is, the sharp peaks with small overlap with the (one-photon) broad ones and that are further from other (two-photon) sharp ones. Logically, it is also desirable that they are intense. The central peak, labeled I, at $\omega_a = \omega_\mathrm{L}$ is the best candidate for that since it is the most isolated one and is degenerate, with contributions from three different leapfrog processes. As we will discuss, this has consequences on the statistics of the emitted pairs. An accurate quantity to determine the quality of a two-photon resonance for two-photon emission is the *purity*, π_2, introduced in Section 6.7.2, Eq. (340), and defined as the fraction of photons emitted in pairs from the total emission (including single photons). Note that the purity being a probability, it is, unlike $g^{(2)}$, bounded: $0 \leq \pi_2 \leq 1$. We discussed in Section 6.7.2 how this quantity can be inferred from photon counting distributions—see Fig.6.20 and Eq. 349—due to the fact that the photon counting distribution of a perfect two-photon emitter shows a suppressed probability of counting an odd number of photons.

In order to compute the purity, we simulated the actual emission of the system in the steady state via a quantum Monte-Carlo method [190] and fitted the results with the formula given by Eq. (343). In the case of a dressed 2LS of Chapter 6, the photon counting distribution was correctly fitted by assuming that the total number came from a Poissonian distribution of sin-

gle photons plus a Poissonian distribution of bundles. Here, in contrast, the different character of the several leapfrog lines yield, as we will see, different bundle statistics in each case, thus affect the photon counting distribution. This force us to use a more general ansatz, consisting on a Poissonian one-photon distribution, a Poissonian two-photon distribution, and a thermal two-photon distribution. The thermal component is essential to describe the photon counting distribution for the leapfrog line $\Delta_{\mathrm{I}}^{2\mathrm{P}}$, i.e., the central peak, which as commented above is degenerated, originating from three different leapfrog processes. The generating functions for a coherent one-photon process (λ_1), a coherent two-photon process (λ_2) and a thermal two-photon process (θ_2) are given by:

$$\Pi_{\lambda_1} = e^{-\lambda_1(1-s)} \tag{392}$$

$$\Pi_{\lambda_2} = e^{-\lambda_1(1-s^2)} \tag{393}$$

$$\Pi_{\theta_2} = \frac{1-\theta_2}{1-s^2\theta_2} = e^{\log\left(\frac{1-\theta_2}{1-s^2\theta_2}\right)} \tag{394}$$

This gives the total generating function $\Pi_{\lambda_1,\lambda_2,\theta_2} = \Pi_{\lambda_1}\Pi_{\lambda_2}\Pi_{\theta_2} = e^{g(s)}$, with

$$g(s) = -\lambda_1(1-s) - \lambda_2(1-s^2) + \log\left(\frac{1-\theta_2}{1-s^2\theta_2}\right) \tag{395}$$

whose n-th derivatives are:

$$g^{(n)}(0) = \delta_{n,1}\,\lambda_1 + \delta_{n,2}\,2\lambda_2 + \begin{cases} \theta_2^{n/2} 2[(n-1)!] & n \text{ even} \\ 0 & n \text{ odd} \end{cases} \tag{396}$$

This is all the information one needs to construct the photon counting probability given by Eq. (349). By fitting Monte Carlo photon counting curves to this formula, one can obtain values for the parameters λ_1, λ_2 and θ_2. The mean values associated with each of the three processes are $n_1 = \lambda_1$, $n_2 = 2\lambda_2$, $n_{\theta_2} = 2\theta_2(1-\theta_2)$. The purity can then be defined as:

$$\pi_2^{(\mathrm{PC})} = \frac{n_2 + n_{\theta_2}}{n_1 + n_2 + n_{\theta_2}} = \frac{\theta_2/(1-\theta_2) + \lambda_2}{\lambda_1/2 + \lambda_2 + \theta_2/(1-\theta_2)}. \tag{397}$$

The result is plotted in Fig. 7.4 d for a cavity on resonance with each of the leapfrog peaks in the two-photon spectrum: I, II, III and IV, whose positions shift with Ω as plotted in panel e. The corresponding cavity population $n_a = \langle a^\dagger a\rangle$, second order correlation function $g^{(2)}(0) = \langle a^{\dagger 2}a^2\rangle / n_a^2$ and the two-photon second order correlation function $g_2^{(2)}(0) = \langle a^{\dagger 4}a^4\rangle / \langle a^{\dagger 2}a^2\rangle^2$, appear in a, b and c respectively.

On the low driving regime, we can see that resonances I and II converge to the same point at $\omega = \omega_{\mathrm{L}}$ and show very high purity: this is the usual regime of two-photon emission in the (undressed) biexciton, that has been studied extensively before [65, 66]. Note, however, that this high purity comes at the expense of the amount of signal (low n_a). As Fig. 7.4 shows, this signal can

The N-photon, n-th order correlation function was introduced in Section 6.9. For $n = N = 2$, $g_2^{(2)}(0)$ takes the meaning of a standard *second order correlation function for photon pairs* when these pairs dominate the emission ($\pi_2 \approx 1$).

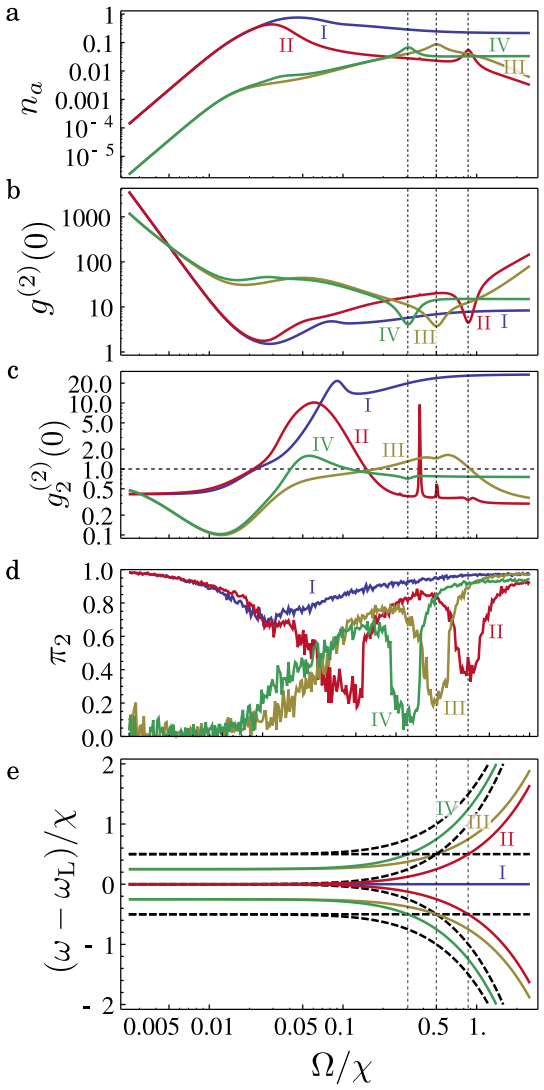

Figure 7.4: **Steady state observables as a function of the pumping intensity** Ω Parameters: $\chi = 4 \times 10^3 \gamma_\sigma$, $g = 10^2 \gamma_\sigma$, $\gamma_a = 10\gamma_\sigma$, $\Delta_X = \chi/2$ and $\Delta_C = \Delta_I^{2P}$ (blue), Δ_{II}^{2P} (red), Δ_{III}^{2P} (yellow) and Δ_{IV}^{2P} (green). The gridlines mark the three points where leapfrog processes intersect with real transitions—dashed lines in e—, which spoils the purity.

be enhanced by orders of magnitude if we increase the pumping intensity Ω in order to bring the biexciton to the dressed regime. In this regime, all the resonances start being resolved and the four of them present a sizable purity. In the case of resonances II, III and IV, the purity goes down whenever they cross a single-photon resonance (dashed, vertical lines in Fig 7.4). At very high intensity, $\Omega > \chi$, all of them reach almost 100% of pair emission.

In this limit of high pumping, we observe a bunching behaviour $g^{(2)}(0) > 1$ for all the leapfrog resonances, which is an expected result for two-photon emission. The statistics of the photons, however, hides a non-classical behaviour if one regards the pairs as the basic entity of emission and consider the pair-pair coincidences as described by the $g_2^{(2)}(0)$. In this case, we obtain *antibunched photon pairs* in resonances II, III and IV, giving the possibility

of implementing an on-demand source of single photon-pairs, and bunched photon pairs in resonance I. This is not the only difference between resonance I (blue) and the others. The position of this resonance is independent of the pumping intensity, and the emission at this frequency is order of magnitudes more intense than at the other resonances. These differences are explained by the fact that three different transitions contribute to the photon pair emission at line I, and that the starting and ending state of the transition are always the same, as can be seen in Eq. (391a). Because of this, no reloading time to go back to the initial state is needed, which is the origin of the antibunching on all the other cases. All these features are a sample of the rich set of physical regimes that can be explored when the proposed method of multi-photon Purcell enhancement in dressed states systems is applied in non-trivial configurations.

We will now compare the emission rates that can be obtained through this mechanism with other approaches in similar systems. The most straightforward comparison is with the undressed regime [181]. For the parameters used in Fig. 7.4 b, for the minimum (undressed regime) and maximum (dressed regime) values of Ω shown on the figure, we obtain $n_a = 2 \times 10^{-4}$ and $n_a = 0.25$, respectively, which for $g = 51\,\mu\text{eV}$ [181] gives pair generation rates of $r = 0.12\,\text{MHz}$ and $r = 151\,\text{MHz}$, that is, over three orders of magnitude enhancement. While this comparison is illustrative of the gain brought by our paradigm, it does not represent an exhaustive study of the space of parameters. For instance, resonances II, III and IV benefit from higher values of γ_σ than those studied here, leading to faster reloading times that increase the value of n_a. For a fixed g, changes in χ, γ_a or γ_σ can optimize the generation rates of either regime, although the dressed case should typically outperform the undressed one. A comparison can also be made with proposals in the pulsed excitation regime, although the juxtaposition with our continuous-wave excitation case is less direct. We will compare with the rates obtained in Refs. [72, 169], since both works use the biexcitonic cascade to generate photon pairs. For this analysis, since we compare with existing experiments, we use parameters of systems available in the laboratory, namely $g = 51\,\mu\text{eV}$, $\gamma_a = 24\,\mu\text{eV}$ and $\gamma_\sigma = 0.13\,\mu\text{eV}$ [181], along with $\chi = 2\,\text{meV}$ [169]. Doing so is detrimental to our proposal that exploits the strong-coupling regime [201] and performs better with figures of merit not yet available in the laboratory, but remain realistic in the light of the technological progress in growth and material science. Still, in units normalized to g, this choice of today's parameters for our mechanism yield $\gamma_a \approx 0.5g$, $\gamma_\sigma \approx 0.002g$ and $\chi \approx 40g$. We will focus on the resonance I, which is the brightest. For these parameters and high values of the pumping, $\Omega \approx 2.5\chi$, the cavity acquires a population $n_a \approx 0.01$ and a top purity of pair emission, $\pi_2 \approx 1$, with a photon pair generation rate of $r = n_a\gamma_a/2 \approx 29\,\text{MHz}$. This is superior to both the values obtained in Ref. [72], with $r = 10\,\text{MHz}$, where a Purcell enhancement through cavity modes is also used, and in Ref. [169], with $r = 0.30\,\text{MHz}$. The last work actually reports a higher generation rate but correcting for their collection efficiency of $\approx 0.4\%$, since light is emitted

isotropically from a quantum dot. In contrast, our proposal, like the one in Ref. [72], collects the light trough the cavity channel, therefore solving this problem. Notice as well that said collection through the cavity mode is done by Purcell-enhancing a two-photon process of photons with equal energy, that in consequence will be indistinguishable. This represents another advantage with respect to the conventional approach based on emission from the bare biexcitonic states, that might suffer from fine-structure splitting, spoiling indistinguishability.

7.6 EMISSION OF ENTANGLED PHOTONS

Many practical applications in quantum computing and quantum communication require emission of entangled photon pairs [35, 121, 161, 170, 183, 184, 214, 225]. So far, we have only considered the case in which the emission was filtered by a single cavity with a fixed polarization. Therefore, changing the frequency of the cavity corresponds to moving along the diagonal of Fig. 7.2 a, and all photons extracted by the cavity will tend to be indistinguishable. However, the results for the spectrum of the cavity emission depicted in Fig. 7.2 b show that correlated photons of different frequencies can be Purcell enhanced with a single cavity, so that the spectrum as a function of the cavity detuning follows the trend of the two-photon frequency correlation map of the biexciton, Fig. 7.2 a. It is therefore expected that a bimodal cavity in resonance with two different, correlated frequencies—showing bunching in the map of Fig. 7.2 a—will show strongly correlated emission. The biexcitonic scheme allows also to introduce an extra degree of freedom, the polarization, such that two-photon emission takes place in a reduced Hilbert space of polarization and frequency:

$$\{|\mathrm{H},\omega_1;\mathrm{H},\omega_2\rangle\,,|\mathrm{H},\omega_1;\mathrm{V},\omega_2\rangle\,,|\mathrm{V},\omega_1;\mathrm{H},\omega_2\rangle\,,|\mathrm{V},\omega_1;\mathrm{V},\omega_2\rangle\}. \quad (398)$$

We will now show how the mechanism of two-photon emission described above can be extended to yield emission of entangled photons of the kind $|\psi\rangle = (|\mathrm{H},\omega_1;\mathrm{V},\omega_2\rangle + |\mathrm{V},\omega_1;\mathrm{H},\omega_2\rangle)/\sqrt{2}$ when the enhancement of the light emitted by the dressed biexciton is done by a bimodal cavity, with each of the modes having two degenerate polarizations.

The system, already implemented experimentally [72, 140] is theoretically described in the same way as before, but now including including four cavity modes with annihilation operator $a_{i,X}$, $i \in \{1,2\}$, $X \in \{H,V\}$, describing the two possible polarizations of the two modes of the bimodal cavity. The part of the Hamiltonian that describes the cavity modes and their coupling to the biexciton is then given by:

$$\begin{aligned} H_{\mathrm{C}} &= \omega_{\mathrm{C}_1}(a^\dagger_{1,\mathrm{H}}a_{1,\mathrm{H}} + a^\dagger_{1,\mathrm{V}}a_{1,\mathrm{V}}) \\ &+ \omega_{\mathrm{C}_2}(a^\dagger_{2,\mathrm{H}}a_{2,\mathrm{H}} + a^\dagger_{2,\mathrm{V}}a_{2,\mathrm{V}}) \\ &+ g[(a^\dagger_{1,\mathrm{H}} + a^\dagger_{2,\mathrm{H}})\sigma_{\mathrm{H}} + (a_{1,\mathrm{H}} + a_{2,\mathrm{H}})\,\sigma^\dagger_{\mathrm{H}}] \\ &+ g[(a^\dagger_{1,\mathrm{V}} + a^\dagger_{2,\mathrm{V}})\sigma_{\mathrm{V}} + (a_{1,\mathrm{V}} + a_{2,\mathrm{V}})\,\sigma^\dagger_{\mathrm{V}}] \end{aligned} \quad (399)$$

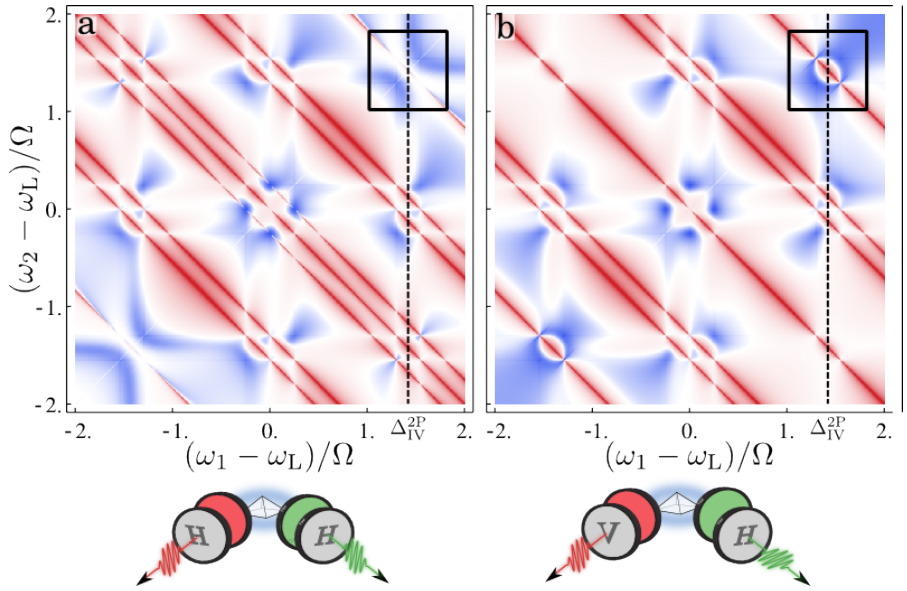

Figure 7.5: Two-photon spectra of the dressed biexciton. a, Correlations between photons with the same polarization. **b**, Correlations between photos with perpendicular polarizations. The black square highlights a zone where the correlations between photons of different polarizations are stronger than between photons with the same polarization.

The vertically polarized driving term given by (384) leads to different probability of emission in horizontal or vertical polarization. Since we now want that probability to be equal, we use a circularly-polarized driving laser:

$$H_\Omega = \Omega\,(\sigma_{\circlearrowleft}^\dagger e^{-i\omega_L t} + \sigma_{\circlearrowleft} e^{i\omega_L t}) \tag{400}$$

with $\sigma_{\circlearrowleft} = (\sigma_H + i\sigma_V)/\sqrt{2}$. We will not discuss in detail the possible single and two-photon transitions that arise in the dressed biexciton under this driving, since the physics and derivation are similar to the results exposed above for the linearly polarized pumping. However, it is interesting to analyze the frequency-resolved, cross polarized second order correlation function $g^{(2)}_{\Gamma,HV}(\omega_1,\omega_2)$ of the dressed biexcitonic system alone ($g = 0$), which is a cross-correlation function between photons emitted at frequency ω_1 and polarization H and photons emitted at frequencies ω_2 and polarization V. This correlation function can be compared with the frequency-resolved correlation functions for a fixed polarization that we have been considering so far, that we now term $g^{(2)}_{\Gamma,HH}(\omega_1,\omega_2)$. Due to the circular polarized pumping, the system is symmetric under the exchange H $\leftrightarrow$ V, so $g^{(2)}_{\Gamma,HH}(\omega_1,\omega_2) = g^{(2)}_{\Gamma,VV}(\omega_1,\omega_2)$ and $g^{(2)}_{\Gamma,HV}(\omega_1,\omega_2) = g^{(2)}_{\Gamma,VH}(\omega_1,\omega_2)$.

Figure 7.5 shows the comparison between these two quantities. While $g^{(2)}_{\Gamma,HH}$ displays the same features than in the case of linearly polarized pumping (Fig. 7.2 a), the cross-polarized correlation function $g^{(2)}_{\Gamma,HV}$ presents a leapfrog line Δ^{2P}_{IV} where correlations are much stronger than in the case of photons emitted with the same polarization. The region where this happens is highlighted with a black square on the map.

Figure 7.6 a shows a cut of both $g^{(2)}_{\Gamma,HH}$ and $g^{(2)}_{\Gamma,HV}$ on the diagonal (ω,ω) of the black square and the antidiagonal $(\omega, 2\Delta^{2P}_{IV} - \omega)$, corresponding to said leapfrog line of strong correlations. This curves show clearly that, when the light is filtered at two frequencies along this line, emission of photons of different polarization is clearly dominant over the emission of photons of equal

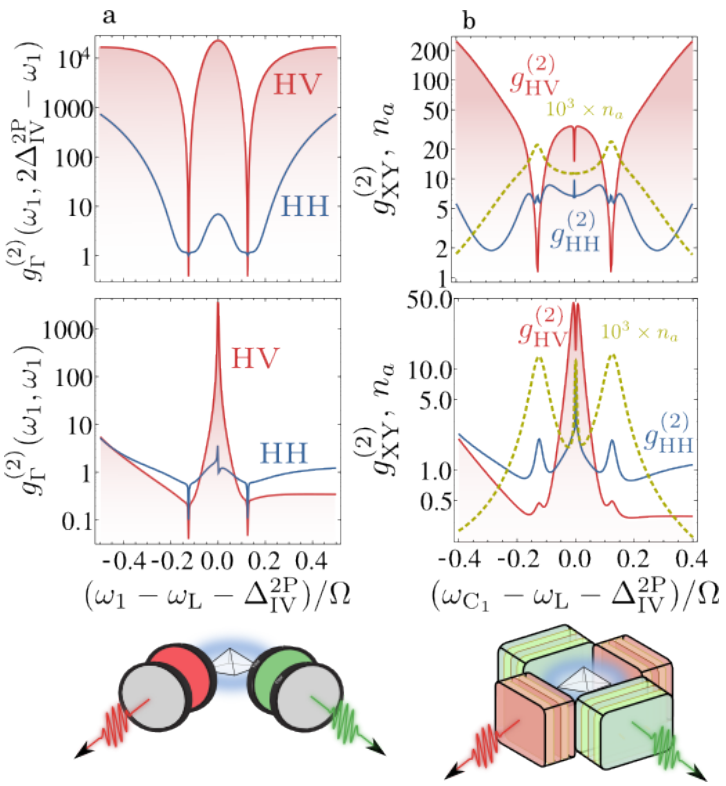

Figure 7.6: Mapping between the frequency resolved correlations of the biexciton and the statistics of the cavities. **a**, Cuts of the two-photon spectra along the antidiagonal $(\omega_1 - \omega_L, \omega_2 - \omega_L) = (\omega_1 - \omega_L, 2\Delta_{IV}^{2P} - \omega_1 + \omega_L)$ and diagonal $(\omega_1, \omega_2) = (\omega_1, \omega_1)$ of the black square in Fig 7.5 for equal (blue) and perpendicular (red) polarizations. **b**, Autocorrelations and cross-correlations between two cavity modes coupled to the biexciton that have orthogonal polarizations and whose energies are equivalent to the frequency filters of panel a. The statistics of the cavities as a function of their frequency follow the trend observed in the frequency resolved statistics of the biexciton.

polarization. The dip in the correlations corresponds to the crossing with a single-photon transition. This behaviour is mapped into the emission of the bimodal cavity when the frequencies of the modes correspond to those of the filters, as is shown in Fig. 7.6 b, which depicts the correlations between the two modes (for the same and different polarizations) when their frequencies are the same as those of the frequency filters of panel a. The population of the modes is also shown, featuring in the bottom panel a sharp resonance when the two modes have equal frequency and the two-photon resonance is crossed. The top panel shows how, as the separation in frequency between the modes increases (always maintained in the line of strong correlations), the population decreases after crossing the single photon resonance. However, a strong difference on the correlations between similar and different polarizations can be achieved without paying too much price on the signal, yielding much better entanglement, as we show below.

Quantum tomography [59, 72, 118, 226] allows us to reconstruct the density matrix of the emitted photon pairs in the basis

$$\{|\mathrm{H},\omega_1;\mathrm{H},\omega_2\rangle, |\mathrm{H},\omega_1;\mathrm{V},\omega_2\rangle, |\mathrm{V},\omega_1;\mathrm{H},\omega_2\rangle, |\mathrm{V},\omega_1;\mathrm{V},\omega_2\rangle\} \quad (401)$$

from second order correlation functions corresponding to photon coincidence measurements. We define the (unnormalized) density matrix:

$$\theta_{\mathrm{AB,CD}} = \langle a_{\mathrm{A}}^\dagger a_{\mathrm{B}}^\dagger a_{\mathrm{D}} a_{\mathrm{C}} \rangle \quad (402)$$

with $\{\mathrm{A},\mathrm{C}\} \equiv \{\mathrm{A},\omega_1;\mathrm{C},\omega_1\}$, $\{\mathrm{B},\mathrm{D}\} \equiv \{\mathrm{B},\omega_2;\mathrm{D},\omega_2\}$ and $\mathrm{A},\mathrm{B},\mathrm{C},\mathrm{D} \in \{\mathrm{H},\mathrm{V}\}$. The corresponding normalized density matrix is $\tilde{\theta} = \theta / \mathrm{Tr}[\theta]$. The

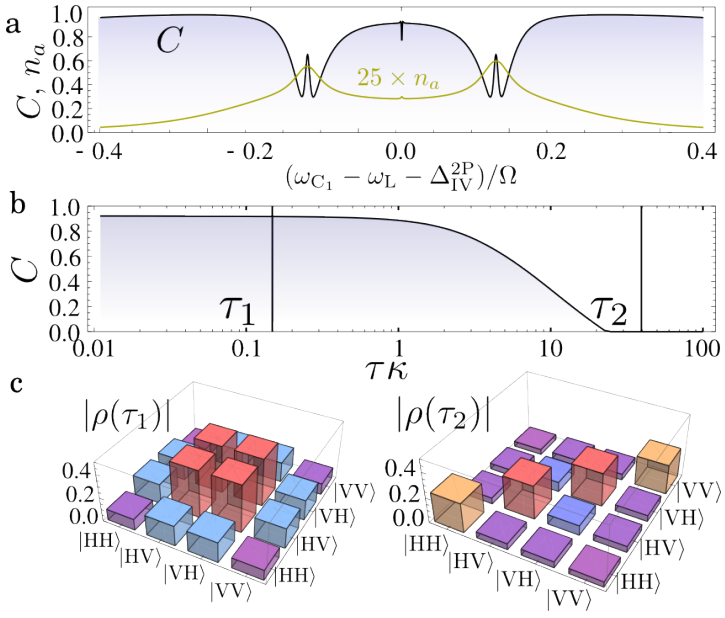

Figure 7.7: Emission of entangled photon pairs. **a**, Concurrence of the emitted photons from the bimodal cavity and population of the cavity modes when the energy of the modes is equivalent to that of the frequency filters of top panel of Fig. 7.6 b. **b**, Concurrence of the emitted photon-pair state from a single cavity with two polarizations as a function of the total measurement time. **c**, Density matrix of the emitted state for two different total measurement times denoted as τ_1 and τ_2. Parameters: $\Omega = 8 \times 10^3 \gamma_a$, all the rest same as in Fig. 7.4.

degree of entanglement of this emitted bipartite state can be quantified by the concurrence C , that in the case of pure states ranges from 0 (separable states) to 1 (maximally entangled states) [238]. Figure 7.7 a depicts the concurrence of the emitted states as the frequencies of the modes move along the leapfrog line of strong correlations, $(\omega_{C_1} - \omega_L, \omega_{C_2} - \omega_L) = (\omega_{C_1} - \omega_L, 2\Delta_{IV}^{2P} - \omega_{C_1} + \omega_L)$, corresponding to the same points shown in Fig. 7.6 b, top. A region of concurrence $C \approx 0.9$ exists for small detuning between the two modes, while another region where $C \approx 1$ can be reached for higher energy differences without a dramatic decrease in the rate of emission, as can be seen in the behaviour of n_a (which is the population of one of the modes, all of them being equally populated). These high values of the concurrence correspond to the emission of photons in a pure entangled Bell state $|\psi\rangle = (|\mathrm{H}, \omega_1; \mathrm{V}, \omega_2\rangle + |\mathrm{V}, \omega_1; \mathrm{H}, \omega_2\rangle)/\sqrt{2}$.

The **concurrence** is defined as $C = \max\{0, \sqrt{\lambda_1} - \sqrt{\lambda_2} - \sqrt{\lambda_3} - \sqrt{\lambda_4}\}$, where $\{\lambda_1, \lambda_2, \lambda_3, \lambda_4\}$ are the eigenvalues in decreasing order of the matrix $\rho T \rho^* T$, with T a diagonal matrix with diagonal $\{-1, 1, 1, -1\}$.

Entanglement can also be studied for a single cavity mode with two polarizations, with time of emission being the extra degree of freedom instead of frequency. In that case, the states of the Hilbert space are of the form $|\mathrm{XY}\rangle \equiv |\mathrm{X}, \text{early}; \mathrm{Y}, \text{late}\rangle$, with $\mathrm{X}, \mathrm{Y} \in \{\mathrm{X}, \mathrm{Y}\}$. The density matrix is then defined as [59, 226]

$$\theta_{\mathrm{AB,CD}}(\tau) = \int_0^\tau \langle a_\mathrm{A}^\dagger(0) a_\mathrm{B}^\dagger(\tau') a_\mathrm{D}(\tau') a_\mathrm{C}(0)\rangle d\tau' \tag{403}$$

with $\mathrm{A}, \mathrm{B}, \mathrm{C}, \mathrm{D} \in \{\mathrm{H}, \mathrm{V}\}$, and two-time correlation functions are calculated from the steady state of the system using the quantum regression theorem. Therefore, τ corresponds to the time of measurement that begins with the emission of the first photon, and for each τ we define the normalized density matrix $\tilde{\theta}(\tau) = \theta(\tau)/\mathrm{Tr}[\theta(\tau)]$. This analysis reveals, for short measurement times, a highly pure density matrix, $\mathrm{Tr}[\tilde{\theta}^2] \approx 0.92$ consisting of the entangled Bell state $|\psi\rangle = (|\mathrm{HV}\rangle + |\mathrm{VH}\rangle)/\sqrt{2}$ with fidelity $F \approx 0.9$, shown in Fig. 7.7 b. Beyond a certain time of measurement $1/\gamma_a$, the density matrix

loses purity due to the contributions from subsequent emissions. In our configuration, the concurrence takes a value $C \approx 0.92$ for short measurement times. However, one must bear in mind that the maximum concurrence for a mixed state is lower than one [234] and $\tilde{\theta}$ is a mixed state with linear entropy $S_L(\theta) = 4/3[1 - \mathrm{Tr}(\theta^2)] \approx 0.11$, which brings this value of C closer to that of a maximally entangled mixed state. These results, that come from an specific choice of parameters and therefore do not represent an exhaustive study of all the scenarios available, prove unambiguously that the mechanism of two-photon emission analyzed in this text can be easily extended to include new degrees of freedom—like color or polarization—and provide entangled two-photon emission.

7.7 CONCLUSIONS

We have shown how Purcell enhancement of multi-photon resonances in the dressed ladder of a strongly driven biexciton can yield regimes of bright continuous two-photon emission. Thanks to the strong driving, the emission of photon pairs occurs at a much higher rate than it would in the approach that combines standard TPE (without dressing the system) and two-photon Purcell enhancement. The richness of the dressed biexcitonic structure allows to reach different two photon regimes like antibunched two-photon emission or entangled photon pairs. These results suggest that the fundamental ideas behind this particular proposal are susceptible to be applied in a variety of platforms.

8 CONCLUSIONS

8.1 ENGLISH

In this Thesis, we have studied several regimes of light-matter interaction at the quantum level, with the aim of unveiling, enhancing and harvesting quantum correlations for the generation of states of light with novel non-classical features. The basic configuration brings together a two-level system (2LS) and an harmonic mode. This formalizes the typical configuration of a quantum emitter (say, a quantum dot) embedded in a single-mode cavity. The interaction of the combined system yields the rich dynamics of cavity QED. Most of the different scenarios that we have considered in this Thesis follow a common theme: the 2LS provides the quantum character while the harmonic mode provides the classical one. This obvious observation provides a guiding line that has seldom been followed in the experimental implementations. Illustratively, the ideal configuration to exploit the quantum features of the interacting light-matter system is to drive the 2LS and to detect the cavity. The QD—highly nonlinear—generates a strong quantum response to an impinging classical excitation, while the cavity—that can host a large number of excitations—is an ideal cast where to imprint complicated quantum states. Bringing these together is therefore a promising configuration to mold interesting quantum states of light. Much of the literature is concerned instead on the cavity QED as a system in itself, to be probed as a whole, typically by driving the cavity. Here, the paradigm is a driven 2LS brought in contact with the cavity. This conceptual variation, however innocent looking, powers breakthroughs from the previous results such as the "detuned photon blockade". There, one drives the 2LS far from the cavity, allowing to efficiently and selectively target states ultimately allowed by the presence of the cavity, even though far-detuned, namely: quantum superpositions of, on the one hand, the excited 2LS in the vacuum of the cavity with, on the other hand, the ground state of the 2LS in presence of N photons. These states are the simplest manifestation of the type of quantum dynamics that this Thesis has identified, unraveled, optimized and put to use for practical applications.

Our first step towards the quantum begins, interestingly, with a classical system: recent developments in the efficiency of the computation of frequency-resolved correlations allowed to revisit from that perspective the most common systems in quantum optics. This exercise revealed a whole zoo of correlations and features that only appear when one takes into account the energy degree of freedom and spans the measurement over all possible combinations of frequencies, yielding a 'two-photon correlation spectrum' (2PS). This has put the 2PS in the spotlight as an observable of enormous funda-

mental and practical interest, since it brings information not only about the quantum state of a system, but also of its underlying dynamics, which can me much richer and complex than suggested only by the steady state. We investigates the most fundamental features of this observable in a system that does not present many features itself: a non-equilibrium polariton ensemble in the verge of condensation. To all effects, we can regard the emission of such a state as a conventional laser with a broad linewidth, emitting uncorrelated photons at random times. Both the theory and measurement of frequency-resolved correlations in this system yield the same result; apart from the well known bunching of photons of equal frequencies, corresponding to the celebrated Hanbury Brown and Twiss (HBT) effect, we report anticorrelations between photons of opposite frequencies with respect to the center of the emission peak. This is a robust feature replicated by our three theoretical approaches to describe the system: the steady state of a classical, phase-diffusing field, the steady state of a quantum model of two-mode condensation, and the spontaneous emission of an arbitrary quantum state. These anticorrelations can be understood as a conservation of the number of photons in a stream, together with the already known HBT effect, that tends to clutter indistinguishable photons. The net result is an effective repulsion between photons of different color (that are distinguishable). It is striking that such anticorrelatiosn are, in fact, dictated by their bosonic statistics. Interestingly, as in the case of the standard HBT, this phenomenon needs some dephasing mechanism to manifest itself, even for states (such a Fock states) that have no phase in the first place. This highlights once again the power of frequency-resolved correlations to provide information about the dynamics of a system, not only about the state itself.

With the backbone of every experiment of this kind now understood, we put this quantity to scrutiny with cavity QED systems in the crucial configuration where the 2LS is driven and the cavity is observed. Alternatively, such a configuration can be seen as the Purcell-enhancement of a dressed two-level system. Under strong coherent pumping, it has long been known that a two-level system develops a ladder of energy levels consisting of doublets, that feature multiple transitions between them at different energies. To first order, four types of transitions occuring at three different energies are allowed, leading to the celebrated Mollow triplet of resonance fluorescence. However, many higher order processes are accessible by looking at the frequency-resolved correlation function of the system. For instance, two-photon cascades in the infinite ladder of energy levels give rise to another set of transitions, that are not directly visible in the single-photon spectrum. The correlations of these transitions are however so strong as to surpass the limits imposed by the Cauchy-Schwarz inequality and Bell inequalities, whereas direct one-photon transitions between the ladders are found to be classically correlated. We found for instance that the more separated are the intermediate states of a two-photon cascade from the real states of the system, the stronger is the quantum character of the emitted photons. That is to say, these transitions that avoid real states are the valuable ones insofar

as the generation of quantum states is concerned, and a quantum-optician engineer should focus on these rather than on the other, obvious, spectral features. This is one of the important results of this Thesis, that should leave a long-standing trace in the design of tomorrow's quantum optical devices.

Applying these principles to practical effects culminates with the concept of a "bundler", a configuration of the cavity QED system that drives it into a new regime of emission, whereby all the light is emitted in groups (or 'bundles') of N photons, for a tunable integer N. The underlying physical mechanism is to Purcell-enhance the strongly-correlated processes previously identified with the photon-correlation spectrum, to give rise to new types of light emitters. This provides a considerable generalization of the one-photon emitter $N = 1$ and the emerging two-photon emitter $N = 2$. Our scheme is able to provide, in principle, emitters with an arbitrary N and we have shown that sizable four-photon emitters are well within the state of the art. We have also explored variations of this theme, for instance in the dynamics of a bi-exciton coupled to two polarized cavities, and found similar possibilities to engineer usefully and boost the quantum features of such systems. This Thesis therefore finds that its concluding point is a good one to leave it to experimentalists to bring these results to the laboratory, and to usher the next generation of quantum light sources.

In conclusions, at a fundamental level, we have provided a cornerstone for two pillars of quantum optics: the Jaynes-Cummings Hamiltonian and the Mollow triplet. We have seen how the physical picture of one or the other is more suitable to understand and describe the complicated dynamics that takes place in a driven 2LS in a cavity. The concept of the two-photon correlation spectrum serves as a support for these two pillars, allowing in particular to identify the ranges of genuine quantum emission, to be found in innocuous frequency windows where nothing striking appear to the naked eye (i.e, at the one-photon level). At a practical level, we have proposed a new type of quantum light, along with the prospective device to generate it and the theoretical tools to characterize it. The light-source itself, the bundler, should serve as an archetype for future generations of quantum light emitters.

8.2 ESPAÑOL

Es esta Tesis hemos estudiado diversos regímenes de la interacción luz materia en la escala cuántica, con el objetivo de revelar, potenciar y recopilar correlaciones cuántias para la generación de estados de luz con nuevas características no clásicas. La configuración básica combina un sistema de dos niveles (2LS) y un modo armónico. Esto formaliza la típica configuración de un emisor cuántico (por ejemplo, un punto cuántico) embebido en una cavidad de un solo modo. La interacción del sistema combinado da lugar a la riqueza dinámica de la electrodinámica cuántica de cavidades (cQED). La mayoría de los diferentes escenarios que hemos considerado en esta tesis siguen un tema común: el 2LS provee el caracter cuántico, mientras que el modo armónico provee el clásico. Esta observación tan obvia proporciona

una guía que pocas veces se ha seguido en implementaciones experimentales. Como ejemplo, la configuración ideal para explotar características cuánticas de la interacción luz-materia es excitar un 2LS y detectar por la cavidad. El punto cuántico—extremádamente no lineal—genera una respuesta muy fuerte frente a una bombardeao de una excitación clásiac, mientras que la cavidad—que puede almacenar un gran número de excitaciones—es un lienzo ideal sobre el que imprimir complicados estados cuánticos. Unir estos dos aspectos es por lo tanto una prometedora configuración para moldear interesantes estados de luz. Mucha de la literatura se preocupa en vez de eso sobre el sistema en su conjunto, para ser sondeado como un todo, normalmente bombeando la cavidad. Aquí, el paradigma es un ya 2LS excitado, que es entonces puesto en contacto con la cavidad. Esta variación conceptual, por muy inocente que parezca, da lugar a grandes avances con respecto a otros resultados previos tales como el 'detuned photon blockade'. En este ejemlo, uno bombea el 2LS lejos de la cavidad, permitiendo acceder de modo selectivo a estados que solo están permitidos gracias a la presencia de la cavidad, incluso si están muy detuneados: en concreto, superposiciones cuánticas de, por un lado, el 2LS excitado en el vacío de la cavidad, y en el otro, el estado fundamental del 2LS en presencia de N fotones. Estos estados son la manifestación más simple del tipo de dinámica cuántica que en esta Tesis hemos idenfiticado y optimizado para su uso en aplicaciones prácticas.

Nuestro primer paso hacia lo cuántico comienza, curiosamente, en un sistema clásico. Recientes progresos en la eficiencia de cómputo de funciones de correlacion resueltas en frecuencias han permitido revisitar, desde la perspectiva de este observable, los sistemas mś comunes de la óptica cuántica. Este ejercicio ha revelado un completo zoo de correlaciones y patrones que solo aparecen cuando uno tiene en cuenta el grado de libertad de la energía y extiende la medida sobre todas las posibles combinaciones de frecuencias, dando lugar al 'espectro de correlaciones de dos fotones' (2PS). Esto ha colocado al 2PS en el punto de mira, como un observable de enorme interés tanto fundamental como aplicado, ya que proporciona información no solo sobre el estado cuántico del sistema, sino también sobre su dinámica subyacenete, que puede ser mucho más rica y compleja de lo que sugiere simplemente el estado estacionario. Hemos investigado los aspectos más fundamentales de este observable en un sistema que no presenta ninguna característica particular por sí mismo: un colectivo de polaritones fuera del equilibrio, al borde de la condensación. A todos los efectos, podemos considerar la emisión de este sistema como un laser convencional con un gran ancho de banda, emitiendo fotones descorrelacionados a tiempos aleatorios. Tanto la teoría como la medida de las correlaciones resueltas en frecuencias nos arrojan el mismo resultado; aparte del bien conocido 'amontonamiento' de fotones de iguales frecuencias, correspondiente con el bien conocido efecto de Hanbury Brown y Twiss (HBT), hemos reportado anticorrelaciones entre fotones con frecuencias opuestas respecto al centro del pico de emisión. Esta es una característica robusta que ha sido replicada por nuestros tres aproximamientos teóricos al problema: el estudio del estado estacionario de un campo clásico con difusión

de fase, el análisis del estado estacionario de un model cuántico de condensación de dos modos, y la emisión espontánea desde un estado cuántico arbitrario. Estas anticorrelacioes pueden entenderse como la conservación del número de fotones en el haz, junto con el ya conocido efecto de HBT, que tiene a agrupar a los fotones indistinguibles. El ersultado neto es una repulsión efectiva entre fotones de colores diferentes (que son distinguibles). Es sorprendente cómo estas anticorrelaciones son, de hecho, dictadas por la estadística bosónica de los fotones. Curiosamente, como en el caso del estándar efecto de HBT, este fenómeno necesita de algún mecanismo de desfase para manifestarse, incluso para estados (como los estados de Fock) que no tienen fase en sí mismos. Esto destaca de neuvo el poder que las funciones de correlación resueltas en frecuencias tienen para proveernos de información sobre la dinámica del sistema, y no solo sobre el estado en sí mismo.

Con la columna vertebral de todos los experimentos de este tipo ya entendida, hemos puesto a diversos sistemas de cQED bajo el escrutinio de este observable, en la configuración fundamental en la que el 2LS es excitado y la cavidad observada. Alternativamente, esta configuración puede verse como el Purcell-enhancement de un sistema de dos niveles vestido por el láser. Bajo un bombeo coherent muy fuerte, es de hace tiempo sabido que un sistema de dos niveles desarrolla una escalera de niveles de energía consistente en dobletes, manifestando multiples transiciones entre ellos a diferentes energías. A primer order, solo cuatro tipos de transiciones ocurriendo a tres distintas energías están permitidas, dando lugar al famoso triplete de Mollow en el espectro de fluorescencia. Sin embargo, muchos otros procesos de orden más alto son accesibles si miramos a las funciones de correlación resueltas en frecuencias. Por ejemplo, cascadas de dos fotones en la escalera 'infinita' de niveles de energía dan lugar a otro conjunto de transiciones que no son directamente visibles en el espectro. Las correlaciones entre los fotones emitidos en estas transiciones son, sin embargo, tan fuertes que puede sobrepasar los límites impuestos por la desigualdad de Cauchy-Schwarz y las desigualdades de Bell, mientras que las transiciones directas de un solo fotón resultan tener correlaciones clásicas. En esta Tesis hemos encontrado que cuanto más separados estén los estados intermedios de la cascada de un estado real del sistema, más fuerte es el caracter cuántico de las correlaciones entre los fotones emitidos. Dicho de otro modo, aquellas transciones que evitan a los estados reales son las más valiosas en lo que se refiere a la generación de estados cuánticos, y un ingeniero cuántico debería enfocarse en ellas antes que aquellas que se manifiestan evidentemente en el espectro. Éste es uno de los resultados importantes de esta Tesis.

La aplicación de estos principios para utilidades prácticas culmina con el concepto del 'bundler' (empaquetador), una configuración del sistema de electrodinámica cuántica de cavidades que lo conduce a un nuevo regimen de emisión donde toda la luz se emite en paquetes (en inglés, 'bundles') de N-fotones, donde N es un número que podemos seleccionar. El mecanismo subyacente es el Purcell-enhancement (emisión estimulada) de aquellos procesos fuertemente correlacionados idenfiticados previamente medi-

ante el espectro de correlaciones de dos fotones, dando lugar a nuevos tipos de emisores de luz. Esto proporciona una generalización considerable del emisor de un solo fotón $N = 1$ y del emergente emisor de dos fotones $N = 2$. Nuestro esquema es capaz de proveer, en principio, emisores con un arbitrario N. También hemos explorado variaciones de este principio, como por ejemplo en la dinámica del biexcitión acoplado a dos cavidades polarizadas, encontrando posibilidades similares para explotar las correlaciones cuánticas de estos sistemas. El punto de conclusión de esta Tesis es por lo tanto un buen lugar para que los experimentales recojan este trabajo en su laboratorio, con el objetivo de dar nacimiento a una nueva generación de fuentes de luz.

En conclusión, a un nivel fundamental, hemos proporcionado un punto de encuentro para dos pilares de la óptica cuántica: el Hamiltoniano de Jaynes-Cummings y el triplete de Mollow. Hemos visto cómo la imagen física de uno u otro es más adecuada para describir las compicadas dinámicas que tienen lugar en un 2LS en una cavidad. El concepto de espectro de correlaciones de dos fotones sirve como soporte para estos pilares, permitiendo en particular identificar los rangos de emisión cuántica genuina. En la práctica, hemos propuesto un nuevo tipo de luz cuántica, junto con dispositivos candidatos para generarla y las herramientas teóricas para caracterizarla. La fuente de luz en si mismo, el 'bundler', debería servir de arquetipo para nuevas generaciones de emisores de luz.

PUBLICATIONS

Works published during the realization of this Thesis (2013-2016).
Publications featured in this Thesis are marked by ⇒.

Peer-reviewed journals

⇒ *The colored Hanbury Brown–Twiss effect.*
B. Silva, C. Sánchez Muñoz, A. González Tudela, D. Ballarini, G. Gigli, K. W. West, L. Pfeiffer, E. del Valle, D. Sanvitto, F. P. Laussy. **Sci. Rep. 6, 37980**

Deterministic Down-Converter and Continuous Photon-Pair Source within the Bad-Cavity Limit
Y. Chang, A. González-Tudela, C. Sánchez Muñoz, C. Navarrete-Benlloch, T. Shi. **Phys. Rev. Lett. 117, 203502**

Degenerate parametric oscillation in quantum membrane optomechanics.
M. Benito*, C. Sánchez Muñoz*, C. Navarrete-Benlloch. (* Equal contributors). **Phys. Rev. A 93, 023846 (2016)**

Exciting Polaritons with Quantum Light.
J. C. López Carreño, C. Sánchez Muñoz, D. Savitto, E. del Valle, F. P. Laussy **Phys. Rev. Lett. 115, 196402 (2015)**

⇒ *Coherent generation of nonclassical light on chip via detuned photon blockade.*
K. Müller, A. Rundquist, K. A. Fischer, T. Sarmiento, K. G. Lagoudakis, Y. A. Kelaita, C. Sánchez Muñoz, E. del Valle, F. P. Laussy, J. Vučković. **Phys. Rev. Lett. 114, 233601 (2015)**

⇒ *Enhanced two-photon emission from a dressed biexciton.*
C. Sánchez Muñoz, C. Tejedor, F. P. Laussy, E. del Valle. **New Journal of Physics 17, 123021 (2015)**

⇒ *Violation of classical inequalities by frequency filtering.*
C. Sánchez Muñoz, E. del Valle, C. Tejedor, F. P. Laussy. **Phys. Rev. A 90, 052111 (2014)**

⇒ *Emitters of N-photon bundles.*
C. Sánchez Muñoz, E. del Valle, A. González-Tudela, S. Lichtmannecker, K. Müller, M. Kaniber, C. Tejedor, J. J. Finley, F. P. Laussy. **Nature Photonics 8, 550–555 (2014)**

Bichromatic dressing of a quantum dot detected by a remote second quantum dot.
M. Maragkou, C. Sánchez Muñoz, S. Lazić, E. Chernysheva, H. P. van der Meulen, A. González-Tudela, C. Tejedor, L. J. Martínez, I. Prieto, P. A. Postigo, J. M. Calleja. **Physical Review B 88, 075309, (2013)**

Plasmon-polariton emission from a coherently p-excited quantum dot near a metal interface.
C. Sánchez Muñoz, A. Gonzalez-Tudela, C. Tejedor, **Physical Review B 85, 125301 (2012)**

Preprints

Entangling a polariton with one photon: effect of interactions at the single-particle level
A. Cuevas, B. Silva, J. C. López Carreño, M. de Giorgi, C. Sánchez Muñoz, A. Fieramosca, D. G. Suárez Forero, F. Cardano, L. Marrucci, V. Tasco, G: Biasiol, E. del Valle, L. Dominici, D. Ballarini, G. Gigli, P. Mataloni, F. P. Laussy, F. Sciarrino and D. Sanvitto. **arXiv:1609.01244 (2016)** (Submitted to Nature Physics)

Exciting with Quantum Light. II. Exciting a two-level system
J. C. López Carreño,C. Sánchez Muñoz, E. del Valle and F. P. Laussy. **arXiv:1609.00857 (2016)** (Accepted by PRB)

BIBLIOGRAPHY

[1] J. Aasi, J. Abadie, B. P. Abbott, R. Abbott, T. D. Abbott, M. R. Abernathy, C. Adams, T. Adams, P. Addesso, R. X. Adhikari, et al. Enhanced sensitivity of the ligo gravitational wave detector by using squeezed states of light. *Nat. Photon.*, 7:613, 2013.

[2] B. P. Abbott, R. Abbott, T. D. Abbott, M. R. Abernathy, C. Adams, T. Adams, P. Addesso, R. X. Adhikari, et al. Observation of gravitational waves from a binary black hole merger. *Phys. Rev. Lett.*, 116: 061102, 2016.

[3] A. F. Adiyatullin, M. D. Anderson, P. V. Busi, H. Abbaspour, R. André, M. T. Portella-Oberli, and B. Deveaud. Temporally resolved second-order photon correlations of exciton-polariton Bose-Einstein condensate formation. *Appl. Phys. Lett.*, 107, 2015.

[4] I. Afek, O. Ambar, and Y. Silberberg. High-NOON states by mixing quantum and classical light. *Science*, 328:879, 2010.

[5] Y. Aharonov and D. Bohm. Significance of electromagnetic potentials in the quantum theory. *Phys. Rev.*, 115:485, 1959.

[6] I. Aharonovich, D. Englund, and M. Toth. Solid-state single-photon emitters. *Nat. Photon.*, 10:631, 2016.

[7] N. Akopian, N. H. Lindner, E. Poem, Y. Berlatzky, J. Avron, D. Gershoni, B. D. Gerardot, and P. M. Petroff. Entangled photon pairs from semiconductor quantum dots. *Phys. Rev. Lett.*, 96:130501, 2006.

[8] A. V. Andreev, V. I. Emel'yanov, and Yu. A. Il'inskiĭ. Collective spontaneous emission (dicke superradiance). 23:493, 1980.

[9] N. A. Ansari. Violation of Bell's inequality in a driven three-level cascade atomic system. *Phys. Rev. A*, 55:1639, 1997.

[10] P. A. Apanasevich and S. Ya. Kilin. Photon bunching and antibunching in resonance fluorescence. *J. Phys. B.: At. Mol. Phys.*, 12:L83, 1979.

[11] Y. Arakawa, S. Iwamoto, M. Nomura, A. Tandaechanurat, and Y. Ota. Cavity quantum electrodynamics and lasing oscillation in single quantum dot-photonic crystal nanocavity coupled systems. *IEEE Journal of Selected Topics in Quantum Electronics*, 18:1818, 2012.

[12] P-L. Ardelt, M. Koller, T. Simmet, L. Hanschke, A. Bechtold, A. Regler, J. Wierzbowski, H. Riedl, J. J. Finley, and K. Müller. Optical control of nonlinearly dressed states in an individual quantum dot. *Phys. Rev. B*, 93:165305, 2016.

[13] D. K. Armani, T. J. Kippenberg, S. M. Spillane, and K. J. Vahala. Ultra-high-Q toroid microcavity on a chip. *Nature*, 421:925, 2003.

[14] J. A. Armstrong. Theory of interferometric analysis of laser phase noise. *J. Opt. Soc. Am.*, 56:1024, 1966.

[15] S. Ashhab and F. Nori. Qubit-oscillator systems in the ultrastrong-coupling regime and their potential for preparing nonclassical states. *Phys. Rev. A*, 81:042311, 2010.

[16] A. Aspect. From Einstein, Bohr, Schrödinger to Bell and Feynman: a new quantum revolution? *Séminaire Poincaré*, XVII:99, 2013.

[17] A. Aspect, G. Roger, S. Reynaud, J. Dalibard, and C. Cohen-Tannoudji. Time correlations between the two sidebands of the resonance fluorescence triplet. *Phys. Rev. Lett.*, 45:617, 1980.

[18] A. Aspect, P. Grangier, and G. Roger. Experimental tests of realistic local theories via bell's theorem. *Phys. Rev. Lett.*, 47:460, 1981.

[19] A. Aspect, J. Dalibard, and G. Roger. Experimental test of bell's inequalities using time-varying analyzers. *Phys. Rev. Lett.*, 49:1804, 1982.

[20] M. Aßmann, F. Veit, M. Bayer, M. van der Poel, and J. M. Hvam. Higher-order photon bunching in a semiconductor microcavity. *Science*, 325: 297, 2009.

[21] M. Aßmann, J.-S. Tempel, F. Veita, M. Bayer, A. Rahimi-Iman, A. Löffler, S. Höfling, S. Reitzenstein, L. Worschech, and A. Forchel. From polariton condensates to highly photonic quantum degenerate states of bosonic matter. *Proc. Natl. Acad. Sci.*, 108:1804, 2011.

[22] O. Astafiev, A. M. Zagoskin, A. A. Abdumalikov Jr., Yu. A. Pashkin, T. Yamamoto, K. Inomata, Y. Nakamura, and J. S. Tsai. Resonance fluorescence of a single artificial atom. *Science*, 327:840, 2010.

[23] V. Balić, D. A. Braje, P. Kolchin, G. Y. Yin, and S. E. Harris. Generation of paired photons with controllable waveforms. *Phys. Rev. Lett.*, 94: 183601, 2005.

[24] P. Ball. Physics of life: The dawn of quantum biology. *Nature*, 474:272, 2011.

[25] M. Baur, S. Filipp, R. Bianchetti, J. M. Fink, M. Göppl, L. Steffen, P. J. Leek, A. Blais, and A. Wallraff. Measurement of autler-townes and mollow transitions in a strongly driven superconducting qubit. *Phys. Rev. Lett.*, 102:243602, 2009.

[26] J. S. Bell. On the Einstein podolsky rosen paradox. *Physics*, 1:195, 1964.

[27] J. S. Bell. On the problem of hidden variables in quantum mechanics. *Rev. Mod. Phys.*, 38:447, 1966.

[28] J.S. Bell. *Speakable and Unspeakable in Quantum Mechanics*. Cambridge Univ. Press, 2004.

[29] K.M. Birnbaum, A. Boca, R. Miller, A.D. Boozer, T.E. Northup, and H.J. Kimble. Photon blockade in an optical cavity with one trapped atom. *Nature*, 436:87, 2005.

[30] M. D. Birowosuto, H. Sumikura, S. Matsuo, H. Taniyama, P. J. van Veldhoven, R. Nötzel, and M. Notomi. Fast purcell-enhanced single photon source in 1,550-nm telecom band from a resonant quantum dot-cavity coupling. *Scientific Report*, 2, 2012.

[31] L. S. Bishop, J. M. Chow, J. Koch, A. A. Houck, M. H. Devoret, E. Thuneberg, S. M. Girvin, and R. J. Schoelkopf. Nonlinear response of the vacuum Rabi resonance. *Nat. Phys.*, 5:105, 2009.

[32] F. Boitier, A. Godard, E. Rosencher, and C. Fabre. Measuring photon bunching at ultrashort timescale by two-photon absorption in semiconductors. *Nat. Phys.*, 5:267, 2009.

[33] F. Boitier, A. Orieux, C. Autebert, A. Lemaître, E. Galopin, C. Manquest, C. Sirtori, I. Favero, G. Leo, and S. Ducci. Electrically injected photon-pair source at room temperature. *Phys. Rev. Lett.*, 112:183901, 2014.

[34] S. Bounouar, M. Strauss, A. Carmele, P. Schnauber, A. Thoma, M. Gschrey, J-H. Schulze, A. Strittmatter, S. Rodt, A. Knorr, and S. Reitzenstein. Time reordering of paired photons in a dressed three-level cascade. *arXiv:1610.08268*, 2016.

[35] D. Bouwmeester, J.-W. Pan, K. Mattle, M. Eibl, H. Weinfurter, and A. Zeilinger. Experimental quantum teleportation. *Nature*, 390:575, 1997.

[36] E. Brannen and H. I. S. Ferguson. The question of correlation between photons in coherent light rays. *Nature*, 178:481, 1956.

[37] R. Hanbury Brown, R. C. Jennison, and M. K. D. Gupta. Apparent angular sizes of discrete radio sources: Observations at Jodrell Bank, Manchester. *Nature*, 170, 1952.

[38] M. Brune, F. Schmidt-Kaler, A. Maali, J. Dreyer, E. Hagley, J. M. Raimond, and S. Haroche. Quantum Rabi oscillation: A direct test of field quantization in a cavity. *Phys. Rev. Lett.*, 76:1800, 1996.

[39] N. Bruno, A. Martin, T. Guerreiro, B. Sanguinetti, and R. T. Thew. Pulsed source of spectrally uncorrelated and indistinguishable photons at telecom wavelengths. *Opt. Express*, 22:17246, 2014.

[40] D. C. Burnham and D. L. Weinberg. Observation of simultaneity in parametric production of optical photon pairs. *Phys. Rev. Lett.*, 25:84, 1970.

[41] H. J. Carmichael. *An Open Systems Approach to Quantum Optics*. Springer-Verlag, 1 edition, 1991.

[42] J. C. López Carreño and F. P. Laussy. Exciting with quantum light. i. exciting an harmonic oscillator. *arXiv:1601.06187*, 2016. URL http://arxiv.org/abs/1601.06187.

[43] J. C. López Carreño, C. Sánchez Muñoz, D. Sanvitto, E. del Valle, and F. P. Laussy. Exciting polaritons with quantum light. *Phys. Rev. Lett.*, 115:196402, 2015.

[44] J. C. López Carreño, C. Sánchez Muñoz, and E. del Valle F. P. Laussy. Exciting with quantum light. ii. exciting a two-level system. *arXiv:1609.00857*, 2016. URL http://arxiv.org/abs/1609.00857.

[45] R. Centeno Neelen, D. M. Boersma, M. P. van Exter, G. Nienhuis, and J. P. Woerdman. Spectral filtering within the Schawlow–Townes linewidth as a diagnostic tool for studying laser phase noise. *Opt. Commun.*, 100:289, 1993.

[46] D. E. Chang, V. Vuletić, and M. D. Lukin. Quantum nonlinear optics – photon by photon. *Nat. Photon.*, 8:685, 2014.

[47] Y. Chang, A. González-Tudela, C. Sánchez Muñoz, C. Navarrete-Benlloch, and T. Shi. Deterministic down-converter and continuous photon-pair source within the bad-cavity limit. *Phys. Rev. Lett.*, 117: 203602, 2016.

[48] J. F. Clauser. Experimental distinction between the quantum and classical field-theoretic predictions for the photoelectric effect. *Phys. Rev. D*, 9:853, 1974.

[49] J. F. Clauser, M. A. Horne, A. Shimony, and R. A. Holt. Proposed experiment to test local hidden-variable theories. *Phys. Rev. Lett.*, 23:880, 1969.

[50] C. Cohen-Tannoudji and S. Reynaud. Atoms in strong light-fields: Photon antibunching in single atom fluorescence. *Phil. Trans. R. Soc. Lond. A*, 293:223, 1979.

[51] C. Cohen-Tannoudji, J Dupont-Roc, and G. Grynberg. *Photons and Atoms: Introduction to Quantum Electrodynamcis*. Wiley-Interscience, New York, 1989.

[52] C. N. Cohen-Tannoudji and S. Reynaud. Dressed-atom description of resonance fluorescence and absorption spectra of a multi-level atom in an intense laser beam. *J. Phys. B.: At. Mol. Phys.*, 10:345, 1977.

[53] Á. Cuevas, B. Silva, J. C. López Carreño, M. de Giorgi, C. Sánchez Muñoz, A. Fieramosca, D. G. Suárez Forero, F. Cardano, L. Marrucci,

Vittorianna Tasco, G. Biasol, E. del Valle, L. Dominici, D. Ballarini, G. Gigli, Paolo Mataloni, F. P. Laussy, F. Sciarrino, and D. Sanvitto. Entangling a polariton with one photon: effect of interactions at the single-particle level. *arXiv:1609.01244*, 2016.

[54] M. Dakna, T. Anhut, T. Opatrnỳ, L. Knöll, and D-G. Welsch. Generating schrödinger-cat-like states by means of conditional measurements on a beam splitter. *Phys. Rev. A*, 55:3184, 1997.

[55] M. Dakna, J. Clausen, L. Knöll, and D-G. Welsch. Generation of arbitrary quantum states of traveling fields. *Phys. Rev. A*, 59:1658, 1999.

[56] J. Dalibard and S. Reynaud. Correlation signals in resonance fluorescence : interpretation via photon scattering amplitudes. *J. Phys. France*, 44:1337, 1983.

[57] R. Dawkins. *Climbing Mount Improbable*. WW Norton & Company, 1997.

[58] E. del Valle. *Microcavity Quantum Electrodynamics*. VDM Verlag, 2010.

[59] E. del Valle. Distilling one, two and entangled pairs of photons from a quantum dot with cavity QED effects and spectral filtering. *New J. Phys.*, 15:025019, 2013.

[60] E. del Valle and F. P. Laussy. Mollow triplet under incoherent pumping. *Phys. Rev. Lett.*, 105:233601, 2010.

[61] E. del Valle and F. P. Laussy. Regimes of strong light-matter coupling under incoherent excitation. *Phys. Rev. A*, 84:043816, 2011.

[62] E. del Valle, F. P. Laussy, and C. Tejedor. Quantum regression formula and luminescence spectra of two coupled modes under incoherent continuous pumping. *AIP Conf. Proc.*, 1147:238, 2009.

[63] E. del Valle, D. Sanvitto, A. Amo, F. P. Laussy, R. André, C. Tejedor, and L. Viña. Dynamics of the formation and decay of coherence in a polariton condensate. *Phys. Rev. Lett.*, 103:096404, 2009.

[64] E. del Valle, S. Zippilli, F. P. Laussy, A. Gonzalez-Tudela, G. Morigi, and C. Tejedor. Two-photon lasing by a single quantum dot in a high-Q microcavity. *Phys. Rev. B*, 81:035302, 2010.

[65] E. del Valle, A. Gonzalez-Tudela, E. Cancellieri, F. P. Laussy, and C. Tejedor. Generation of a two-photon state from a quantum dot in a microcavity. *New J. Phys.*, 13:113014, 2011.

[66] E. del Valle, A. Gonzalez-Tudela, and F. P. Laussy. Generation of a two-photon state from a quantum dot in a microcavity under incoherent and coherent continuous excitation. *Proc. SPIE*, 8255:825505, 2012.

[67] E. del Valle, A. Gonzalez-Tudela, F. P. Laussy, C. Tejedor, and M. J. Hartmann. Theory of frequency-filtered and time-resolved n-photon correlations. *Phys. Rev. Lett.*, 109:183601, 2012.

[68] H. Deng, G. Weihs, C. Santori, J. Bloch, and Y. Yamamoto. Condensation of semiconductor microcavity exciton polaritons. *Science*, 298: 199, 2002. doi: doi:10.1126/science.1074464.

[69] W. Denk, J.H. Strickler, and W.W. Webb. Two-photon laser scanning fluorescence microscopy. *Science*, 248:73, 1990.

[70] Z. Deutsch, O. Schwartz, R. Tenne, R. Popovitz-Biro, and D. Oron. Two-color antibunching from band-gap engineered colloidal semiconductor nanocrystals. *Nano Lett.*, 12:2948, 2012.

[71] P. A. M. Dirac. *The principles of quantum mechanics.* Oxford Science Publications, 1930.

[72] A. Dousse, J. Suffczyński, A. Beveratos, O. Krebs, A. Lemaître, I. Sagnes, J. Bloch, P. Voisin, and P. Senellart. Ultrabright source of entangled photon pairs. *Nature*, 466:217, 2010.

[73] J.H. Eberly and K. Wódkiewicz. The time-dependent physical spectrum of light. *J. Opt. Soc. Am.*, 67:1252, 1977.

[74] A. Einstein, B. Podolsky, and N. Rosen. Can quantum-mechanical description of physical reality be considered complete? *Phys. Rev.*, 47: 777, 1935.

[75] A. K. Ekert. Quantum cryptography based on bell's theorem. *Phys. Rev. Lett.*, 67:661, 1991.

[76] A. Faraon, I. Fushman, D. Englund, N. Stoltz, P. Petroff, and J. Vuckovic. Coherent generation of non-classical light on a chip via photon-induced tunnelling and blockade. *Nat. Phys.*, 4:859, 2008.

[77] J. M. Fink, M. Göppl, M. Baur, R. Bianchetti, P. J. Leek, A. Blais, and A. Wallraff. Climbing the Jaynes–Cummings ladder and observing its $\sqrt{n}$ nonlinearity in a cavity QED system. *Nature*, 454:315, 2008.

[78] K. A. Fischer, K. Müller, A. Rundquist, T. Sarmiento, A. Y. Piggott, Y. Kelaita, C. Dory, and K. G. Lagoudakis J. Vuckovic. Self-homodyne measurement of a dynamic mollow triplet in the solid state. *Nat. Photon.*, 10:163, 2016.

[79] E. B. Flagg, A. Muller, J. W. Robertson, S. Founta, D. G. Deppe, M. Xiao, W. Ma, G. J. Salamo, and C. K. Shih. Resonantly driven coherent oscillations in a solid-state quantum emitter. *Nat. Phys.*, 5:203, 2009.

[80] F .Flassig, M. Kaniber, G. Reithmaier, K. Müller, A. Andrejew, R. Gross, J. Vuçkovic, and J. J. Finley. Towards on-chip generation, routing and detection of non-classical light. *Proc. SPIE*, 9373:937305, 2015.

[81] T. Flissikowski, A. Betke, I. A. Akimov, and F. Henneberger. Two-photon coherent control of a single quantum dot. *Phys. Rev. Lett.*, 92: 227401, 2004.

[82] A. T. Forrester, R. A. Gudmundsen, and P. O. Johnson. Photoelectric mixing of incoherent light. *Phys. Rev.*, 99:1691, 1955.

[83] S. J. Freedman and J. F. Clauser. Experimental test of local hidden-variable theories. *Phys. Rev. Lett.*, 28:938, 1972.

[84] J. Fulconis, O. Alibart, J. L. O'Brien, W. J. Wadsworth, and J. G. Rarity. Nonclassical interference and entanglement generation using a photonic crystal fiber pair photon source. *Phys. Rev. Lett.*, 99:120501, 2007.

[85] G. W. Gardiner and P. Zoller. *Quantum Noise.* Springer-Verlag, Berlin, 2nd edition, 2000.

[86] J. Gea-Banacloche. Two-photon absorption of nonclassical light. *Phys. Rev. Lett.*, 62:1603, 1989.

[87] C. C. Gerry and P. L. Knight. *Introductory Quantum Optics.* Cambridge University Press, 2005.

[88] V. Giesz, N. Somaschi, G. Hornecker, T. Grange, B. Reznychenko, L. De Santis, J. Demory, C. Gomez, I. Sagnes, A. Lemaitre, O. Krebs, N. D. Lanzillotti-Kimura, L. Lanco, A. Auffeves, and P. Senellart. Coherent manipulation of a solid-state artificial atom with few photons. *Nat. Comm.*, 7, 2016.

[89] V. Giovannetti, S. Lloyd, and L. Maccone. Quantum-enhanced measurements: Beating the standard quantum limit. *Science*, 306:1330, 2004.

[90] N. Gisin and R. Thew. Quantum communication. *Nat. Photon.*, 1:165, 2007.

[91] N. Gisin, G. Ribordy, W. Tittel, and H. Zbinden. Quantum cryptography. *Rev. Mod. Phys.*, 74:145, 2002.

[92] R. J. Glauber. Some notes on multiple-boson processes. *Phys. Rev. A*, 84:395, 1951.

[93] R. J. Glauber. The quantum theory of optical coherence. *Phys. Rev.*, 130:2529, 1963.

[94] S. Gleyzes, S. Kuhr, C. Guerlin, J. Bernu, S. Deléglise, U. Busk Hoff, M. Brune, J.-M. Raimond, and S. Haroche. Quantum jumps of light recording the birth and death of a photon in a cavity. *Nature*, 446:297, 2007.

[95] A. Gonzalez-Tudela and D. Porras. Mesoscopic entanglement induced by spontaneous emission in solid-state quantum optics. *Phys. Rev. Lett.*, 110:080502, 2013.

[96] A. Gonzalez-Tudela, F. P. Laussy, C. Tejedor, M. J Hartmann, and E. del Valle. Two-photon spectra of quantum emitters. *New J. Phys.*, 15: 033036, 2013.

[97] A. Gonzalez-Tudela, V. Paulisch, D. E. Chang, H. J. Kimle, and J. I. Cirac. Deterministic generation of arbitrary photonic states assisted by dissipation. *Phys. Rev. Lett.*, 115:163603, 2015.

[98] P. Grangier, B. Sanders, and J. Vuckovic. Focus on single photons on demand. *New J. Phys.*, 6, 2004.

[99] W. Greiner. *Quantum Mechanics. Special Chapters.* Springer, 1998.

[100] R. Hafenbrak, S. M. Ulrich, P. Michler, L. Wang, A. Rastelli, and O. G. Schmidt. Triggered polarization-entangled photon pairs from a single quantum dot up to 30K. *New J. Phys.*, 9:315, 2007.

[101] R. Hanbury Brown. *Boffin : A Personal Story of the Early Days of Radar, Radio Astronomy and Quantum Optics.* CRC Press, 1991.

[102] R. Hanbury Brown and R. Q. Twiss. Correlation between photons in two coherent beams of light. *Nature*, 177:27, 1956.

[103] R. Hanbury Brown and R. Q. Twiss. The question of correlation between photons in coherent light rays. *Nature*, 178:1447, 1956.

[104] G. Hardy, J.E. Littlewood, and G. Pólya. *Inequalities.* Cambridge Mathematical Library, 2nd edition, 1952.

[105] F. Hargart, M. Müller, K. Roy-Choudhury, S. L. Portalupi, C. Schneider, S. Höfling, M. Kamp, S. Hughes, and P. Michler. Cavity-enhanced simultaneous dressing of quantum dot exciton and biexciton states. *Phys. Rev. B*, 93:115308, 2016.

[106] R. Hegedüs, S. Åkesson, R. Wehner, and G. Horváth. Could vikings have navigated under foggy and cloudy conditions by skylight polarization? on the atmospheric optical prerequisites of polarimetric viking navigation under foggy and cloudy skies. *Proceedings of the Royal Society of London A: Mathematical, Physical and Engineering Sciences*, 463:1081, 2007.

[107] S. W. Hell. Toward fluorescence nanoscopy. *Nature Biotechnology*, 21: 1347, 2003.

[108] K. Hennessy, A. Badolato, P.M. Petroff, and E. Hu. Positioning photonic crystal cavities to single InAs quantum dots. *Photonics and Nanostructures*, 2:65, 2004.

[109] K. Hennessy, A. Badolato, M. Winger, D. Gerace, M. Atature, S. Gulde, S. Fält, E. L. Hu, and A. Ĭmamoğlu. Quantum nature of a strongly coupled single quantum dot–cavity system. *Nature*, 445:896, 2007.

[110] M. Holland, K. Burnett, C. Gardiner, J. I. Cirac, and P. Zoller. Theory of an atom laser. *Phys. Rev. A*, 54:R1757, 1996.

[111] C. K. Hong and L. Mandel. Experimental realization of a localized one-photon state. *Phys. Rev. Lett.*, 56:58, 1986.

[112] R. Horn, P. Abolghasem, B. J. Bijlani, D. Kang, A. S. Helmy, and G. Weihs. Monolithic source of photon pairs. *Phys. Rev. Lett.*, 108: 153605, 2012.

[113] N.G.K. Horton, D. Wang, C. Kobat, F. Clark, C. Wise, and C. Xu C. Schaffer. In vivo three-photon microscopy of subcortical structures of an intact mouse brain. *Nat. Photon.*, 7:205, 2013.

[114] A. A. Houck, H. E. Türeci, and J. Koch. On-chip quantum simulation with superconducting circuits. *Nat. Phys.*, 8:292, 2012.

[115] R. Houdré, C. Weisbuch, R. P. Stanley, U. Oesterle, P. Pellandin, and M. Ilegems. Measurement of cavity-polariton dispersion curve from angle-resolved photoluminescence experiments. *Phys. Rev. Lett.*, 73: 2043, 1994.

[116] T. Huber, L. Ostermann, M. Prilmüller, G. S. Solomon, H. Ritsch, G. Weihs, and A. Predojevic. Coherence and degree of time-bin entanglement from quantum dots. *Phys. Rev. B*, 93:201301, 2016.

[117] Y. Israel, S. Rosen, and Y. Silberberg. Supersensitive polarization microscopy using NOON states of light. *Phys. Rev. Lett.*, 112:103604, 2014.

[118] D. F. V. James, P. G. Kwiat, W. J. Munro, and A. G. White. Measurement of qubits. *Phys. Rev. A*, 64:52312, 2001.

[119] H. Jayakumar, A. Predojevic, T. Huber, T. Kauten, G. S. Solomon, and G. Weihs. Deterministic photon pairs and coherent optical control of a single quantum dot. *Phys. Rev. Lett.*, 110:135505, 2013.

[120] E.T. Jaynes and F.W. Cummings. Comparison of quantum and semiclassical radiation theory with application to the beam maser. *Proc. IEEE*, 51:89, 1963.

[121] T. Jennewein, C. Simon, G. Weihs, H. Weinfurter, and A. Zeilinger. Quantum cryptography with entangled photons. *Phys. Rev. Lett.*, 84: 4729, 2000.

[122] H. J.Kimble. The quantum internet. *Nature*, 453:1023, 2008.

[123] J. D. Joannopoulos, R. D. Meade, and J. N. Winn. *Photonic Crystals: Molding the Flow of Light.* Princeton University Press, 1995.

[124] R. Johne, N. A. Gippius, G. Pavlovic, D. D. Solnyshkov, I. A. Shelykh, and G. Malpuech. Entangled photon pairs produced by a quantum dot strongly coupled to a microcavity. *Phys. Rev. Lett.*, 100:240404, 2008.

[125] A. Joshi and S. V. Lawande. Violation of bell's inequality in the resonance fluorescence of two strongly driven two-level atoms. *Phys. Rev. A*, 44:716, 1991.

[126] K. Kamide, S. Iwamoto, and Y. Arakawa. Eigenvalue decomposition method for photon statistics of frequency-filtered fields and its application to quantum dot emitters. *Phys. Rev. A*, 92:033833, 2015.

[127] M. Kaniber, A. Laucht, A. Neumann, J. M. Villas-Bôas, M. Bichler, M.-C. Amann, and J. J. Finley. Investigation of the nonresonant dot-cavity coupling in two-dimensional photonic crystal nanocavities. *Phys. Rev. B*, 77:161303(R), 2008.

[128] J. Kasprzak, M. Richard, A. Baas, B. Deveaud, R. André, J.-Ph. Poizat, and Le Si Dang. Second-order time correlations within a polariton Bose–Einstein condensate in a CdTe microcavity. *Phys. Rev. Lett.*, 100: 067402, 2008.

[129] A. Kavokin, J. J. Baumberg, G. Malpuech, and F. P. Laussy. *Microcavities.* Oxford Univ. Press, 2007.

[130] A. Kavokin, J. J. Baumberg, G. Malpuech, and F. P. Laussy. *Microcavities.* Oxford Univ. Press, 2011.

[131] K. V. Kheruntsyan, J.-C. Jaskula, P. Deuar, M. Bonneau, G. B. Partridge, J. Ruaudel, R. Lopes, D. Boiron, and C. I Westbrook. Violation of the Cauchy–Schwarz inequality with matter waves. *Phys. Rev. Lett.*, 108: 260401, 2012.

[132] H. Kim, S. M. Thon, P. M. Petroff, and D. Bouwmeester. Independent tuning of quantum dots in a photonic crystal cavity. *Appl. Phys. Lett.*, 95:243107, 2009.

[133] H. Kim, T. C. Shen, K. Roy-Choudhury, G. S. Solomon, and E. Waks. Resonant interactions between a mollow triplet sideband and a strongly coupled cavity. *Phys. Rev. Lett.*, 113:027403, 2014.

[134] H. J. Kimble and L. Mandel. Theory of resonance fluorescence. *Phys. Rev. A*, 13:2123, 1976.

[135] H. J. Kimble, M. Dagenais, and L. Mandel. Photon antibunching in resonance fluorescence. *Phys. Rev. Lett.*, 39:691, 1977.

[136] S. Kiravittaya, R. Songmuang, A. Rastelli, H. Heidemeyer, and O. G. Schmidt. Multi-scale ordering of self-assembled InAs/GaAs(001) quantum dots. *Nanoscale Research Letters*, 1:1, 2006.

[137] E. Knill, R. Laflamme, and G. J. Milburn. A scheme for efficient quantum computation with linear optics. *Nature*, 409(6816):46–52, 2001.

[138] L. Knöll and G. Weber. Theory of n-fold time-resolved correlation spectroscopy and its application to resonance fluorescence radiation. *J. Phys. B.: At. Mol. Phys.*, 19:2817, 1986.

[139] M. Koch, C. Sames, M. Balbach, H. Chibani, A. Kubanek, K. Murr, T. Wilk, and G. Rempe. Three-photon correlations in a strongly driven atom-cavity system. *Phys. Rev. Lett.*, 107:023601, 2011.

[140] A. Kress, F. Hofbauer, N. Reinelt, M. Kaniber, H. J. Krenner, R. Meyer, G. Böhm, and J. J. Finley. Manipulation of the spontaneous emission dynamics of quantum dots in two-dimensional photonic crystals. *Phys. Rev. B*, 71:241304, 2005.

[141] A. Kubanek, A. Ourjoumtsev, I. Schuster, M. Koch, P. W. H. Pinkse, K. Murr, and G. Rempe. Two-photon gateway in one-atom cavity quantum electrodynamics. *Phys. Rev. Lett.*, 101:203602, 2008.

[142] A. Kuzmich, W. P. Bowen, A. D. Boozer, A. Boca, C. W. Chou, L.-M. Duan, and H. J. Kimble. Generation of nonclassical photon pairs for scalable quantum communication with atomic ensembles. *Nature*, 423: 731, 2003.

[143] P. G. Kwiat, K. Mattle, H. Weinfurter, A. Zeilinger, A. V. Sergienko, and Y. Shih. New high-intensity source of polarization-entangled photon pairs. *Phys. Rev. Lett.*, 75:4337, 1995.

[144] Wang L, A. Rastelli, and O. G. Schmidt. Structural and optical properties of in (ga) as/ gaas quantum dots treated by partial capping and annealing. *Journal of Applied Physics*, 100(6):064313, 2006.

[145] L. Lanco, S. Ducci, J.-P. Likforman, X. Marcadet, J. A. W. van Houwelingen, H. Zbinden, G. Leo, and V. Berger. Semiconductor waveguide source of counterpropagating twin photons. *Phys. Rev. Lett.*, 97:173901, 2006.

[146] B. P. Lanyon, J. D. Whitfield, G.G. Gillett, M. E. Goggin, M. P. Almeida, I. Kassal, J. D. Biamonte, M. Mohseni, B. J. Powell, M. Barbieri, A. Aspuru-Guzik, and A. G. White. Towards quantum chemistry on a quantum computer. *Nat. Chem.*, 2:106, 2010.

[147] A. Laucht, F. Hofbauer, N. Hauke, J. Angele, S. Stobbe, M. Kaniber, G. Böhm, P. Lodahl, M.-C. Amann, and J. J. Finley. Electrical control of spontaneous emission and strong coupling for a single quantum dot. *New J. Phys.*, 11:023034, 2009.

[148] A. Laucht, S. Pütz, T. Günthner, N. Hauke, R. Saive, S. Frédérick, M. Bichler, M. C. Amann, A. W. Holleitner, M. Kaniber, and J. J. Finley. A waveguide-coupled on-chip single-photon source. *Phys. Rev. X*, 2: 011014, 2012.

[149] F. P. Laussy, E. del Valle, and C. Tejedor. Strong coupling of quantum dots in microcavities. *Phys. Rev. Lett.*, 101:083601, 2008.

[150] F. P. Laussy, E. del Valle, and C. Tejedor. Luminescence spectra of quantum dots in microcavities. I. Bosons. *Phys. Rev. B*, 79:235325, 2009.

[151] F. P. Laussy, E. del Valle, and J.J. Finley. Universal signatures of lasing in the strong coupling regime. *Proc. SPIE*, 8255:82551G, 2012.

[152] F. P. Laussy, E. del Valle, M. Schrapp, A. Laucht, and J. J. Finley. Climbing the Jaynes–Cummings ladder by photon counting. *J. Nanophoton.*, 6:061803, 2012.

[153] F.P. Laussy. *Exciton-polaritons in microcavities*, volume 172, chapter 1. Quantum Dynamics of Polariton Condensates, pages 1–42. Springer Berlin Heidelberg, 2012. ISBN 978-3-642-24186-4.

[154] P. Lodahl, S. Mahmoodian, and S. Stobbe. Interfacing single photons and single quantum dots with photonic nanostructures. *Rev. Mod. Phys.*, 87:347, 2015.

[155] A. Löffler, J. P. Reithmaier, G. Sek, C. Hofmann, S. Reitzenstein, M. Kamp, and A. Forchel. Semiconductor quantum dot microcavity pillars with high-quality factors and enlarged dot dimensions. *Appl. Phys. Lett.*, 86:111105, 2005.

[156] R. Loudon. Non-classical effects in the statistical properties of light. *Rep. Prog. Phys.*, 43:913, 1980.

[157] R. Loudon. *The quantum theory of light*. Oxford Science Publications, 2000.

[158] A. P. D. Love, D. N. Krizhanovskii, D. M. Whittaker, R. Bouchekioua, D. Sanvitto, S. Al Rizeiqi, R. Bradley, M. S. Skolnick, P. R. Eastham, R. André, and Le Si Dang. Intrinsic decoherence mechanisms in the microcavity polariton condensate. *Phys. Rev. Lett.*, 101:067404, 2008.

[159] L. Martinez Maestro, E. Martin Rodriguez, F. S. Rodriguez, M. C. Iglesias de la Cruz, A. Juarranz, R. Naccache, F. Vetrone, D. Jaque, J. A. Capobianco, and J. Garcia Solé. Cdse quantum dots for two-photon fluorescence thermal imaging. *Nano Letters*, 10:5109, 2010.

[160] L. Mandel and E. Wolf. *Optical coherence and quantum optics*. Cambridge Univ. Press, 1995.

[161] I. Marcikic, H. De Riedmatten, W. Tittel, H. Zbinden, and N. Gisin. Long-distance teleportation of qubits at telecommunication wavelengths. *Nature*, 421:509, 2003.

[162] A. M. Marino, V. Boyer, and P. D. Lett. Violation of the Cauchy-Schwarz inequality in the macroscopic regime. *Phys. Rev. Lett.*, 100: 233601, 2008.

[163] G. Meurant. A review on the inverse of symmetric tridiagonal and block tridiagonal matrices. *SIAM Journal on Matrix Analysis and Applications*, 13:707, 1992.

[164] D. A. B. Miller. Are optical transistors the logical next step? *Nat. Photon.*, 4:3, 2010.

[165] B. R. Mollow. Power spectrum of light scattered by two-level systems. *Phys. Rev.*, 188:1969, 1969.

[166] K. Mølmer. Correlation functions and the quantum regression theorem. *http://owww.phys.au.dk/quantop/kvanteoptik/qrtnote.pdf*, 2010.

[167] A. Muller, W. Fang, J. Lawall, and G. S. Solomon. Emission spectrum of a dressed exciton-biexciton complex in a semiconductor quantum dot. *Phys. Rev. Lett.*, 101:027401, 2008.

[168] K. Müller, A. Rundquist, K. A. Fischer, T. Sarmiento, K. G. Lagoudakis, Y. A. Kelaita, C. Sánchez Muñoz, E. del Valle, F. P. Laussy, and J. Vučković. Coherent generation of nonclassical light on chip via detuned photon blockade. *Phys. Rev. Lett.*, 114:233601, 2015.

[169] M. Müller, S. Bounouar, K. D. Jöns, M. Glässl, and P. Michler. On-demand generation of indistinguishable polarization-entangled photon pairs. *Nat. Photon.*, 8(3):224–228, 2014.

[170] D. S. Naik, C. G. Peterson, A. G. White, A. J. Berglund, and P. G. Kwiat. Entangled state quantum cryptography: Eavesdropping on the ekert protocol. *Phys. Rev. Lett.*, 84:4733, 2000.

[171] C. Navarrete-Benlloch. Open systems dynamics: Simulating master equations in the computer. *arXiv:1504.05266*, 2015.

[172] R. Centeno Neelen, D. M. Boersma, M. P. van Exter, G. Nienhuis, and J. P. Woerdman. Spectral filtering within the Schawlow-Townes linewidth of a semiconductor laser. *Phys. Rev. Lett.*, 69:593, 1992.

[173] M. A. Nielsen and I. L. Chuang. *Quantum computation and quantum information*. Cambridge Univ. Press, 2000.

[174] T. R. Nielsen, P. Gartner, and F. Jahnke. Many-body theory of carrier capture and relaxation in semiconductor quantum-dot lasers. *Phys. Rev. B*, 69:235314, 2004.

[175] T. Niemczyk, F. Deppe, H. Huebl, E. P. Menzel, F. Hocke, M. J. Schwarz, J. J. Garcia-Ripoll, D. Zueco, T. Hummer, E. Solano, A. Marx, and R. Gross. Circuit quantum electrodynamics in the ultrastrong-coupling regime. *Nature Phys.*, 6:772, 2010.

[176] G. Nienhuis. Spectral correlations in resonance fluorescence. *Phys. Rev. A*, 47:510, 1993.

[177] G. Nogues, A. Rauschenbeutel, S. Osnaghi, M. Brune, J. M. Raimond, and S. Haroche. Seeing a single photon without destroying it. *Nature*, 400:239, 1999.

[178] J. L. O'Brien, A. Furusawa, and J. Vuckovic. Photonic quantum technologies. *Nat. Phys.*, 3:687, 2009.

[179] R. Ohta, Y. Ota, M. Nomura, N. Kumagai, S. Ishida, S. Iwamoto, and Y. Arakawa. Strong coupling between a photonic crystal nanobeam cavity and a single quantum dot. *Appl. Phys. Lett.*, 98:173104, 2011.

[180] I. S. Osad'ko. Photon distribution functions of fluorescence photons from single nanoparticles: Three different photon counting methods. *Opt. Spectrosc.*, 107(6):948, 2009.

[181] Y. Ota, S. Iwamoto, N. Kumagai, and Y. Arakawa. Spontaneous two-photon emission from a single quantum dot. *Phys. Rev. Lett.*, 107: 233602, 2011.

[182] Z. Y. Ou, S. F. Pereira, H. J. Kimble, and K. C. Peng. Realization of the einstein-podolsky-rosen paradox for continuous variables. *Phys. Rev. Lett.*, 68:3663, 1992.

[183] J.-W. Pan, D. Bouwmeester, H. Weinfurter, and A. Zeilinger. Experimental entanglement swapping: Entangling photons that never interacted. *Phys. Rev. Lett.*, 80:3891, 1998.

[184] J.-W. Pan, Z.-B. Chen, C.-Y. Lu, H. Weinfurter, A. Zeilinger, and M. Zukowski. Multiphoton entanglement and interferometry. *Rev. Mod. Phys.*, 84:777, 2012.

[185] F. Pearle. Wavefunction collapse and conservation laws. *Found. Phys.*, 30:1145, 2000.

[186] M. Peiris, B. Petrak, K. Konthasinghe, Y. Yu, Z. C. Niu, and A. Muller. Two-color photon correlations of the light scattered by a quantum dot. *Phys. Rev. B*, 91:195125, 2015.

[187] R. Penrose. *The road to reality: A compelte guide to the laws of the Universe.* Alfred A. Knopf, 2004.

[188] A. Peruzzo, M. Lobino, J. CF Matthews, N. Matsuda, A. Politi, K. Poulios, X. Zhou, Y. Lahini, N. Ismail, K. Wörhoff, Y. Bromberg, Y. Silberberg, M. G. Thompson, and J. L. OBrien. Quantum walks of correlated photons. *Science*, 329:1500, 2010.

[189] E. Peter, P. Senellart, D. Martrou, A. Lemaître, J. Hours, J. M. Gérard, and J. Bloch. Exciton-photon strong-coupling regime for a single quantum dot embedded in a microcavity. *Phys. Rev. Lett.*, 95:067401, 2005.

[190] M. B. Plenio and P. L. Knight. The quantum-jump approach to dissipative dynamics in quantum optics. *Rev. Mod. Phys.*, 70:101, 1998.

[191] E. M. Purcell. The question of correlation between photons in coherent light rays. *Nature*, 178:1449, 1956.

[192] M. D. Reid and D. F. Walls. Violations of classical inequalities in quantum optics. *Phys. Rev. A*, 34:1260, 1986.

[193] A. Reinhard, T. Volz, M. Winger, A. Badolato, K. J. Hennessy, E. L. Hu, and A. Ĭmamoğlu. Strongly correlated photons on a chip. *Nat. Photon.*, 6:93, 2012.

[194] G. Reithmaier, M. Kaniber, F. Flassing, S. Lichtmannecker, K. Muller, A. Andrejew, J. Vuckovik, R. Gross, and J. J. Finley. On-chip generation, routing, and detection of resonance fluorescence. *Nano Lett.*, 15:5208, 2015.

[195] J. P. Reithmaier, G. Sek, A. Löffler, C. Hofmann, S. Kuhn, S. Reitzenstein, L. V. Keldysh, V. D. Kulakovskii, T. L. Reinecker, and A. Forchel. Strong coupling in a single quantum dot–semiconductor microcavity system. *Nature*, 432:197, 2004.

[196] A. Ridolfo, M. Leib, S. Savasta, and M. J. Hartmann. Photon blockade in the ultrastrong coupling regime. *Phys. Rev. Lett.*, 109:193602, 2012.

[197] M. A. Rowe, D. Kielpinski, V. Meyer, C. A. Sackett, W. M. Itano, C. Monroe, and D. J. Wineland. Experimental violation of a Bell's inequality with efficient detection. *Nature*, 409:791, 2001.

[198] H. Sakai, T. Saito, T. Ikeda, K. Itoh, T. Kawabata, H. Kuboki, Y. Maeda, N. Matsui, C. Rangacharyulu, M. Sasano, Y. Satou, K. Sekiguchi, K. Suda, A. Tamii, T. Uesaka, and K. Yako. Spin correlations of strongly interacting massive fermion pairs as a test of bell's inequality. *Phys. Rev. Lett.*, 97:150405, 2006.

[199] G. Sallen, A. Tribu, T. Aichele, R. André, L. Besombes, C. Bougerol, M. Richard, S. Tatarenko, K. Kheng, and J.-Ph. Poizat. Subnanosecond spectral diffusion measurement using photon correlation. *Nat. Photon.*, 4:696, 2010.

[200] C. Sánchez Muñoz, E. del Valle, C. Tejedor, and F. P. Laussy. Violation of classical inequalities by photon frequency filtering. *Phys. Rev. A*, 90:052111, 2014.

[201] C. Sánchez Muñoz, E. del Valle, A. González Tudela, K. Müller, S. Lichtmannecker, M. Kaniber, C. Tejedor, J.J. Finley, and F.P. Laussy. Emitters of N-photon bundles. *Nat. Photon.*, 8:550, 2014.

[202] C. Sánchez Muñoz, F. P. Laussy, C. Tejedor, and E. del Valle. Enhanced two-photon emission from a dressed biexciton. *New J. Phys.*, 17:123021, 2015.

[203] V. Scarani, H. De Riedmatten, I. Marcikic, H. Zbinden, and N. Gisin. Four-photon correction in two-photon bell experiments. *The European Physical Journal D-Atomic, Molecular, Optical and Plasma Physics*, 32:129, 2005.

[204] A. L. Schawlow and C. H. Townes. Infrared and optical masers. *Phys. Rev.*, 112:1940, 1958.

[205] C. A. Schrama, G. Nienhuis, H. A. Dijkerman, C. Steijsiger, and H. G. M. Heideman. Intensity correlations between the components of the resonance fluorescence triplet. *Phys. Rev. A*, 45:8045, 1992. doi: doi:10.1103/PhysRevA.45.8045.

[206] S. Schumacher, J. Förstner, A. Zrenner, M. Florian, C. Gies, P. Gartner, and F. Jahnke. Cavity-assisted emission of polarization-entangled photons from biexcitons in quantum dots with fine-structure splitting. *Opt. Express*, 20:5335, 2012.

[207] I. Schuster, A. Kubanek, A. Fuhrmanek, T. Puppe, P. W. H. Pinkse, K. Murr, and G. Rempe. Nonlinear spectroscopy of photons bound to one atom. *Nat. Phys.*, 4:382, 2008.

[208] M. Schwartz, U. Rengstl, T. Herzog, M. Paul, J. Kettler, S. L. Portalupi, M. Jetter, and P. Michler. Generation, guiding and splitting of triggered single photons from a resonantly excited quantum dot in a photonic circuit. *Opt. Express*, 24:3089, 2016.

[209] M. O. Scully and M. S. Zubairy. *Quantum optics*. Cambridge University Press, 2002.

[210] B. Silva, C. Sánchez Muñoz, D. Ballarini, A. González Tudela, M. de Giorgi, G. Gigli, K. W. West, L. Pfeiffer, E. del Valle, D. Sanvitto, and F. P. Laussy. The colored hanbury brown–twiss effect. *arXiv:1406.0964*, 2014.

[211] B. Silva, C. Sánchez Muñoz, D. Ballarini, A. González Tudela, M. de Giorgi, G. Gigli, K. W. West, L. Pfeiffer, E. del Valle, D. Sanvitto, and F. P. Laussy. The colored hanbury brown–twiss effect. *Scientific Report*, 6:37980, 2016.

[212] Mark P. Silverman. *Quantum superposition: counterintuitive consequences of coherence, entanglement, and interference*. Springer, 2008.

[213] N. Sim, M. F. Cheng, D. Bessarab, C. M. Jones, and L. A. Krivitsky. Measurement of photon statistics with live photoreceptor cells. *Phys. Rev. Lett.*, 109:113601, 2012.

[214] C. Simon, H. de Riedmatten, M. Afzelius, N. Sangouard, H. Zbinden, and N. Gisin. Quantum repeaters with photon pair sources and multimode memories. *Phys. Rev. Lett.*, 98:190503, 2007.

[215] N. Somaschi, V. Giesz, L. De Santis, J. C. Loredo, M. P. Almeida, G. Hornecker, S. L. Portalupi, T. Grange, C. Anton, J. Demory, C. Gomez, I. Sagnes, N. D. Lanzillotti-Kimura, A. Lemaitre, A. Auffeves, A. G. White, L. Lanco, and P. Senellart. Near-optimal single-photon sources in the solid state. *Nat. Photon.*, 10:340, 2016.

[216] M. D. Srinivas and E. B. Davies. Photon counting probabilities in quantum optics. *Opt. Acta*, 28(7):981, 1981.

[217] K. Srinivasan and O. Painter. Linear and nonlinear optical spectroscopy of a strongly coupled microdisk–quantum dot system. *Nature*, 450:862, 2007.

[218] B. Srivathsan, G. Kaur Gulati, B. Chng, G. Maslennikov, D. Matsukevich, and C. Kurtsiefer. Narrow band source of transform-limited photon pairs via four-wave mixing in a cold atomic ensemble. *Phys. Rev. Lett.*, 111:123602, 2013.

[219] R. M. Stevenson, R. J. Young, P. Atkinson, K. Cooper, D. A. Ritchie, and A. J. Shields. A semiconductor source of triggered entangled photon pairs. *Nature*, 439:179, 2006.

[220] C. Stroud. *A Jewel In The Crown: Essays In Honor Of The 75th Anniversary Of The Institute Of Optics.* Univ of Rochester Pr, 2004.

[221] S. Stufler, P. Machnikowski, P. Ester, M. Bichler, V. M. Axt, T. Kuhn, and A. Zrenner. Two-photon Rabi oscillations in a single $In_xGa_{1-x}As$/GaAs quantum dot. *Phys. Rev. B*, 73:125304, 2006.

[222] J. K. Thompson, J. Simon, H. Loh, and V. Vuletić. A high-brightness source of narrowband, identical-photon pairs. *Science*, 313:74, 2006.

[223] R. J. Thompson, G. Rempe, and H. J. Kimble. Observation of normal-mode splitting for an atom in an optical cavity. *Phys. Rev. Lett.*, 68: 1132, 1992.

[224] Y. Todorov, A. M. Andrews, R. Colombelli, S. De Liberato, C. Ciuti, P. Klang, G. Strasser, and C. Sirtori. Ultrastrong light-matter coupling regime with polariton dots. *Phys. Rev. Lett.*, 105:196402, 2010.

[225] F. Troiani. Entanglement swapping with energy-polarization-entangled photons from quantum dot cascade decay. *Phys. Rev. B*, 90: 245419, 2014.

[226] F. Troiani, J. I. Perea, and C. Tejedor. Cavity-assisted generation of entangled photon pairs by quantum dot cascade decay. *Phys. Rev. B*, 74:235310, 2006.

[227] A. Ulhaq, S. Weiler, S. M. Ulrich, R. Roßbach, M. Jetter, and P. Michler. Cascaded single-photon emission from the Mollow triplet sidebands of a quantum dot. *Nat. Photon.*, 6:238, 2012.

[228] L. Upton, M. Harpham, O. Suzer, M. Richter, S. Mukamel, and T. Goodson III. Optically excited entangled states in organic molecules illuminate the dark. *The Journal of Physical Chemistry Letters*, 4:2046–2052, 2013.

[229] W. Vogel and D.-G. Welsch. *Quantum Optics*. Wiley-VCH, 3, 2006.

[230] T. Volz, A. Reinhard, M. Winger, A. Badolato, D. J. Hennessy, E. L. Hu, and A. Imamoglu. Ultrafast all-optical switching by single photons. *Nat. Photon.*, 6:605, 2012.

[231] A. Wallraff, D. I. Schuster, A. Blais, L. Frunzio, R.-S. Huang, J. Majer, S. Kumar, S. M. Girvin, and R. J. Schoelkopf. Strong coupling of a single photon to a superconducting qubit using circuit quantum electrodynamics. *Nature*, 431:162, 2004.

[232] D. F. Walls and G. J. Milburn. *Quantum Optics*. Springer-Verlag, 1994.

[233] H. Walther, B. T H Varcoe, B.-. Englert, and T. Becker. Cavity quantum electrodynamics. *Rep. Prog. Phys.*, 69:1325, 2006.

[234] T. C. Wei, K. Nemoto, P. M. Goldbart, P. G. Kwiat, W. J. Munro, and F. Verstraete. Maximal entanglement versus entropy for mixed quantum states. *Phys. Rev. A*, 67:022110, 2003.

[235] N. Wiener. Generalized harmonic analysis. *Acta Mathematica*, 55:117, 1930.

[236] J. Wiersig, C. Gies, F. Jahnke, M. Aßmann, T. Berstermann, M. Bayer, C. Kistner, S. Reitzenstein, C. Schneider, S. Höfling, A. Forchel, C. Kruse, J. Kalden, and D. Homme. Direct observation of correlations between individual photon emission events of a microcavity laser. *Nature*, 460:245, 2009.

[237] H. M. Wiseman and G. J. Milburn. *Quantum Measurement and Control*. Cambridge Univ. Press, 2010.

[238] W. K. Wootters. Entanglement of formation of an arbitrary state of two qubits. *Phys. Rev. Lett.*, 80:2245, 1998.

[239] T. Yoshie, A. Scherer, J. Heindrickson, G. Khitrova, H. M. Gibbs, G. Rupper, C. Ell, O. B. Shchekin, and D. G. Deppe. Vacuum Rabi splitting with a single quantum dot in a photonic crystal nanocavity. *Nature*, 432:200, 2004.

[240] J.Q. You and F. Nori. Superconducting circuits and quantum information. *Physics Today*, 58:42, 2005.

[241] J. Zakrzewski, M. Lewenstein, and T. W. Mossberg. Theory of dressed-state lasers. I. effective hamiltonians and stability properties. *Phys. Rev. A*, 44:7717, 1991.

[242] W. R. Zipfel, R. M. Williams, and W. W. Webb. Nonlinear magic: multiphoton microscopy in the biosciences. *Nature Biotechnology*, 21:1369, 2003.

[243] P. Zoller, M. Marte, and D. F. Walls. Quantum jumps in actomic systems. *Phys. Rev. A*, 3(1):198, 1986.